

H.V.M. Hamelers

A Mathematical Model
for
Composting Kinetics

CENTRALE LANDBOUCATALOGUS



0000 0872 2981

Promotoren:

Prof. dr. ir. W.H. Rulkens

Hoogleraar in de Milieutechnologie

Prof. dr. ir. G. van Straten

Hoogleraar in de Meet-, regel- en systeemtechniek

Samenstelling promotiecommissie:

Prof. dr. ir. G. P. A. Bot, Wageningen Universiteit.

Prof. dr. ir. G. Lettinga, Wageningen Universiteit.

Prof. dr. ir. J. Grasman, Wageningen Universiteit.

Dr. T.L. Richard, Iowa State University.

Dr. ir. A. Rinzema, Wageningen Universiteit.

Hubertus Victor Marie Hamelers

Wageningen, 30/6/2001

A Mathematical Model for Composting Kinetics

Proefschrift

ter verkrijging van de graad van doctor
op gezag van de rector magnificus
van Wageningen Universiteit,
prof. dr. ir. L. Speelman,
in het openbaar te verdedigen
op woensdag 27 juni 2001
des ochtends te elf uur in de Aula

15/6/2001

CIP-DATA KONINKLIJKE BIBLIOTHEEK, DEN HAAG

Hamelers, H.V.M.

A mathematical model for composting kinetics

Thesis Wageningen University, Wageningen, the Netherlands – With ref.-With summary

ISBN: 90-5808-445-0

Subject headings: composting/mathematical model/kinetics/waste treatment

Table of Contents

Abstract	
Chapter 1	
Introduction	1
Chapter 2	
Dimensional analysis and parameter identifiability of state space models	31
Chapter 3	
A theoretical model of a single composting particle: development and simulation	67
Chapter 4	
An analytical approximate solution of the OUR	113
Chapter 5	
Experimental validation of the single particle model	167
Chapter 6	
Development of the distributed OUR model	197
Chapter 7	
Validation of the distributed OUR model	227
Chapter 8	
Significance of the new distributed OUR model for composting reactor design	247
Summary (in English and Dutch)	277
Dankwoord	293
Curriculum Vitae	295

Abstract

Hamelers, H.V.M. (2000) A mathematical model for composting kinetics. *Doctoral Thesis*, Wageningen University, Wageningen, The Netherlands.

Composting plays an important role in waste management schemes and organic farming, as the compost produced enables reuse of organic matter and nutrients. Modern composting plants must comply with strict environmental regulations, including gas emissions such as nuisance odors.

Designing composting plants to meet these requirements using current trial-and-error strategies is too costly and time consuming and poor performance and failure are too often the result.

Mathematical reactor models can serve as an essential tool for faster and better process designs, system analysis, and operational guidance.

However, all reactor models developed so far are based on empirical kinetic formulations, restricting the generality and thus applicability of the results. To achieve greater generality for design and analysis, a mechanistic model for composting kinetics is needed. Any mechanistic model is based on a number of assumptions and must be validated against experiments. To make validation possible, all model parameters must be identifiable. A parameter is identifiable if one can uniquely determine its value from the data at hand. The objective of this thesis is to develop a mechanistic kinetic model of the composting process whose parameters are all identifiable.

This thesis has been structured in three main parts.

The first part, "dimensional identifiability analysis," is concerned with the use of dimensional analysis of parameter identifiability. Together with a proposed modified deductive modeling strategy, this part of the thesis is a methodological contribution to modeling of relatively complex systems with limited available measurements.

The second part, "the single particle model," is focuses on the development and validation of a theoretical model for the aerobic degradation of a single waste particle. This theoretical model gives insight into the processes occurring within a composting waste particle. An analytical solution of this model, containing only identifiable parameters, is both derived and validated.

The third part of the thesis, "the distributed model," deals with the development, validation and application of a kinetic model for a waste consisting of a distributed range of waste particle sizes. The model is based on a distribution function describing the particle size distribution and the previously developed analytical solution to the identifiable single particle model. The distributed model is validated and is used to analyze aeration requirements, compost quality and compost quantity for a new composting reactor concept. This model application shows the advantages of the distributed model relative to previous first order models for reactor design and analysis.

1. INTRODUCTION	2
1.1. COMPOSTING OBJECTIVES	2
1.2. THE COMPOSTING PROCESS.....	3
1.3. THE COMPOSTING PLANT	5
1.4. MODELLING CONCEPTS.....	10
1.4.1. <i>Some definitions</i>	10
1.4.2. <i>Model building strategy</i>	10
1.4.3. <i>State concept</i>	13
1.5. COMPOSTING KINETICS	15
1.6. DEDUCTIVE MODELLING: MERITS AND LIMITATIONS	18
1.7. THESIS OBJECTIVE.....	19
1.8. THESIS STRUCTURE	24
1.9. REFERENCES	26

1. Introduction

1.1. Composting Objectives

Composting plays an important role in waste management schemes and organic farming, as it enables reuse of organic matter and nutrients. In organic farming compost is considered as an essential element for enhancing soil health [1] and disease suppressiveness [2].

Compost is generally produced from different types of organic waste like manure and the organic fraction of household waste. The primary objective of a compost plant is to produce compost conforming to specific product standards with minimal emissions to the environment. The quality of the product compost has to be guaranteed, to secure stable marketing of the compost.

The quality of compost is determined by a number of product properties depending on the application. Typical applications are production of a soil amendment in field agriculture or an ingredient for potting mixes. Each application sets its specified quality criteria. Although criteria differ strongly from country to country and application to application, they have some aspects in common. These common aspects are:

- Stabilisation [3]

Stabilisation refers to the oxygen consumption rate of the compost, a low oxygen consumption rate implies a high stability. Application of compost with a high oxygen consumption rate may cause oxygen depletion for plant roots, resulting in plant damage. Compost is considered sufficiently stable, if the oxygen consumption under standardized conditions is below a specific level.

- Pathogens level[4]

Human pathogens are an important topic if the waste contains faecal matter, such as materials containing raw sewage sludge or night soil. Human pathogens present in the compost may cause disease in humans handling the compost. Also crops grown on the compost may be contaminated, endangering the health of the consumer. Plant pathogens can be present in the waste if it contains infected plants or plant parts. Plants grown on compost or in a soil amended with plant disease contaminated compost can get damaged after infection.

Both human and plant pathogens are rapidly killed if the temperature is sufficiently high. Temperature induced decay and other decay mechanisms are operating during composting. A sufficiently long residence time of the waste at a certain temperature level is often used to

guarantee pathogen reduction. This criterion can be easily checked as temperature is relatively simply recorded.

- Dry matter content

In practice a dry matter content in the range of 60-70% is often preferred. At this dry matter content the material can be easily handled, it is no longer sticky and transport costs are minimised. If the dry matter content becomes too high, dust problems may occur during handling of the compost.

The main obstacle for public acceptance of a composting plant is the (expected) odour emission. A composting plant is only acceptable if the odour emissions are well controlled [5, 6]. This has led to the application of so-called closed systems, enabling the collection and treatment of off-gasses. These closed systems have higher investment cost and are therefore only feasible if the residence time of the waste within the system is minimized.

A composting plant should thus produce sufficiently stable, pathogen free and sufficiently dry compost with minimal odor emissions. To make this possible within economic constraints a well-designed operated composting operation is necessary.

1.2. The composting process

The biological oxidation of organic matter in solid waste to carbon dioxide, water and heat is generally used as an overall representation of the composting process. The microbial population in the waste catalyses this oxidation reaction, yielding new biomass. The produced heat accumulates in the solid waste, giving rise to a significant temperature ascent.

The composting rate is a result of the microbial activity inside the waste, and is influenced by a number of factors. Biomass, oxygen, temperature, organic matter, moisture and waste structure are considered as the most important factors influencing the composting rate [7-15].

- Temperature[10, 11, 14, 16-19]

A temperature increase within the range of ambient up to $55 \pm 5^{\circ}\text{C}$ is considered beneficial for the process rate. Above this level a further temperature climb will lead to inactivation of the micro-organisms and consequently a decrease in process rate, a process referred to as microbial suicide. Therefore, compost mass has to be aerated sufficiently to remove excess heat, preventing too high temperatures.

- Biomass[20, 21]

Although the microbial biomass catalyses the organic matter conversion, seeding or

inoculating the process has no major effect on the rate. The composition of the microbial population changes strongly during the composing process as a result of changing conditions within the composting material.

- Moisture[19, 22-24]

Drying of the composting waste leads to a lower composting rate in which case addition of water is beneficial. However, if the moisture content becomes too high a different limitation of the composting rate will occur as the aeration is hindered. A moisture content of 40-60% is generally considered optimal.

- Oxygen[19, 25, 26]

Oxygen is needed as a reactant and must be sufficiently supplied by aeration. If oxygen supply is too low to meet the demand, the oxygen shortage will result in a lower process rate and the production of odours. The effect of the oxygen level on the process rate is not yet fully documented, however a level of 10 vol.% in the gas phase is considered sufficient.

- Organic matter[27-30]

The composition of organic matter influences the degradation rate. Soluble components are in general degraded faster than insoluble components. Within the group of insoluble components differences exist, especially lignin and ligno-cellulose are relatively slowly degraded. These components are only degraded aerobically at a substantial rate by white-rot fungi.

- Porosity[23]

A certain air porosity of the waste is needed, to ensure sufficient permeability. If permeability is too low more aeration energy is needed to overcome the pressure gradient over the waste bed.

- Particle size[14]

A smaller particle size is assumed to enhance the degradation rate, although the experimental evidence is limited. A smaller particle size is beneficial as the surface for hydrolysis is increased or the transport of oxygen is enhanced. A too small particle size may lead to a low porosity.

- C/N ratio[31]

The C/N ratio is often used as a nutrient status of the waste, if the C/N ratio is too high N-limitation of the composting rate is encountered. A value of 25 is considered sufficient. If the C/N ratio is too low excess N may lead to a volatilisation of ammonia.

1.3. The composting plant

Under normal operating conditions a composting plant should produce the desired product quality. The type of process and waste determine the potential compost quality. The actual quality is determined by more factors, notably the operation of the plant. Figure 1.1 shows a schematic representation of a typical state-of-the-art composting plant. Apart from the gas treatment all operations will be described sequentially starting with the waste acceptance.

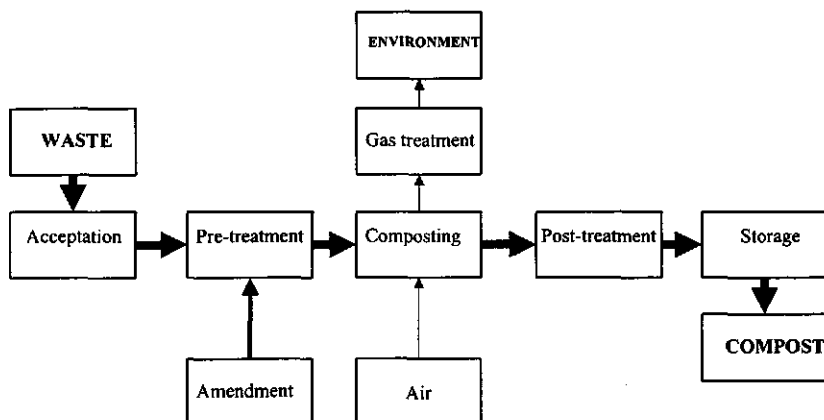


Figure 1.1: Schematic overview of composting plant

Waste acceptance

Acceptance of the waste is important for those quality aspects that can not, or only at high cost, be influenced by plant operations. Examples of such aspects are glass and heavy metals content. For safety and esthetical reasons glass may be present only at low levels. As glass is difficult to separate selectively, only acceptance of waste with low glass levels is a solution to the problem. The same applies to heavy metals, if these can not be removed at acceptable cost, only wastes with low levels of heavy metals are accepted. In this thesis the emphasis lies on composting technology, and the matter of waste acceptance will not be further discussed.

Pre-treatment[32]

The waste is pre-treated to obtain a good starting material for the subsequent composting process. If the starting material is not optimal, the limited process rate will give insufficiently stabilized compost, given the fixed residence time in closed composting systems. Water content, energy content, waste permeability, and particle size all are important aspects to consider.

- Energy content

The energy content of the waste can be too low; in that case insufficient heat is produced during the process to evaporate the water. This problem can occur in the case of waste material with a high water or ash content. Use of an energy rich amendment can solve the problem. This will in general not be compost as compost has a low energy content due to the stabilisation. An amendment from outside like sawdust or bark is necessary.

- Water content

A low water content limits the degradation rate and adding water to the waste is necessary. A possible source of water can be the condense from off-gas cooling. A high water content results in poor air permeability of the waste and consequently in poor aeration. Mixing with a dry amendment can solve this problem. The amendment can be a solid waste stream, such as coarse screenings from the post treatment, compost or may originate from outside. Too high a water content thus may cause two problems simultaneously, a poor permeability and a low energy content. In such cases an amendment is needed that increases the permeability and adds sufficient energy. Such an amendment often will consist of a mixture of compost and an energy rich material from outside.

- Waste permeability

Apart from the water content, waste air permeability is also effected by the waste compressibility. Upon piling the waste, it will experience a mechanical pressure depending on the position within the heap. The material at the bottom will encounter the highest mechanical pressure. As a result of the mechanical pressure the material will be compressed and the permeability will decrease. A high compressibility can be adjusted by using an amendment with a low compressibility.

- Particle size

Shredding can reduce particle size. A too small particle size may however increase the compressibility of the waste. The particle size distribution is important, as large particles tend to form air channels leading to preferential flow. An uneven air distribution leads to a retardation of the process rate, since in poorly aerated areas oxygen depletion may occur. Size distribution can be influenced by selectively shredding of big particles.

Composting reactor[10]

The composting reactor is that part of the compost plant where the waste is actually biologically transformed into compost. In intensive composting systems, the reactor is not only the container of the waste but also includes the aeration, mixing, control facilities etc. In

the composting reactor the pre-treated waste is piled on a perforated floor structure. The floor structure should enable an even aeration of the waste. The pile is confined within walls to prevent air leakage from the pile to the environment and to improve air distribution. Forced aeration is necessary, as otherwise a temperature inhibition of the process will occur. Continuous mixing of the waste is rarely applied and without loss of generality the composting process may be regarded as a static batch process. This so-called static pile forced aerated composting operation is therefore the basic composting operation considered in this thesis. This composting operation is representative for a typical modern composting plant, and most reactor research is aimed at this type of system.

As a result of the forced aeration the composting material tends to dry. The material can become too dry to sustain a satisfactory process rate, and moistening will be necessary to reach stabilisation. For an uniform remoistening, mixing of the waste is necessary. In the case of remoistening the whole composting operation must consequently be described as a series of static pile forced aerated operations.

Figure 1.2 shows the conceptual framework of this sequencing batch operation as a series of three reactors. This configuration makes it possible to control temperature, oxygen and moisture level. Before waste enters the first reactor water might be added to achieve a suitable moisture level. The reactor is filled and aeration switched on. As a result of the air supply, oxidation will start, heat produced and temperature will rise. To prevent a too high temperature and an oxygen limitation in the pile, sufficient air must be supplied. A simple process control is based on controlling the level of the temperature of the material at a certain location within the reactor. If the measured temperature exceeds the set level, the temperature-control unit will increase aeration. Once the temperature is maintained at its set level, oxygen supply will be sufficient and separate control of the oxygen level is not necessary.

A minimum flow should however be set to prevent oxygen depletion during start-up and at the end of the process.

Within the pile a temperature gradient will develop. The lowest temperatures will predominate at the flow entrance point while the highest temperatures will be recorded at the flow exit point. Between entrance and exit locations temperature differences up to 50 °C are not uncommon. [33-35] This temperature gradient can be made smaller or even eliminated, by using air recirculation. By mixing the off-gases with the cooler air entering the system a more uniform temperature distribution through the pile is accomplished. This strategy is widely

employed in mushroom substrate preparation. [36]

Controlling at a constant temperature implies that the produced heat must be removed from the pile. The main mechanism of heat removal is evaporation of water and removal of this water vapor with the aeration flow. This causes drying of the material to such a point that the process rate may be limited. Mixing and remoistening can take away this limitation. Mixing and remoistening is generally done on a fixed time basis and care should be taken to supply the right amount of water. After mixing and remoistening the reactor can be filled again and the process is continued.

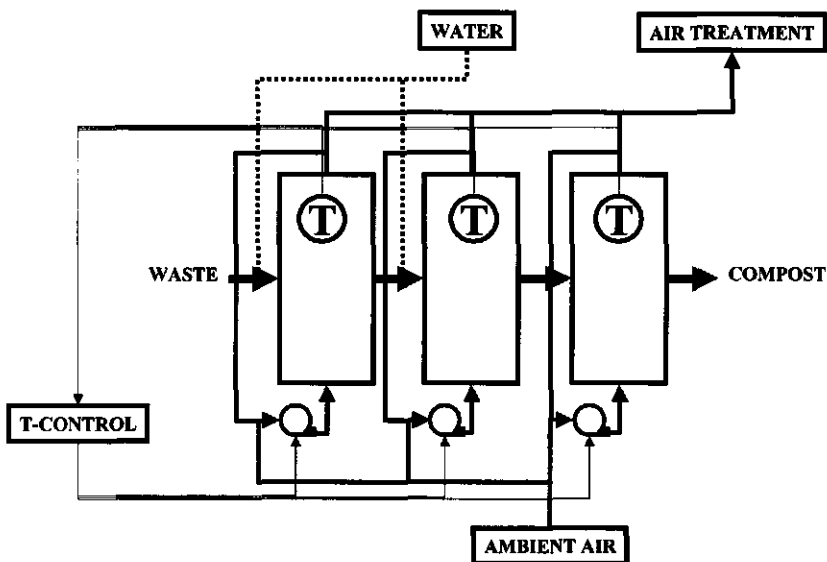


Figure 1.2: Schematic overview of composting reactor.

Gas-treatment

The off-gases are collected and will be emitted to the atmosphere after cleaning. Odour treatment is necessary in almost all cases as odour represents the biggest emission problem in composting. A high odour level is the biggest obstacle for public acceptance of the process. Composting of materials with a low C/N ratio like animal manure may have problems with a high ammonia emission [37]. Gas cleaning can be performed with physical-chemical as well as with biological methods. If a biofilter is used, cooling of the off-gases is necessary to prevent overheating of the biofilter. The cooling will produce condense that might be recovered and used for moistening of the waste.

Post-treatment

The composted material is further refined in the post-treatment step. Sieving is commonly used to obtain certain size fractions. The minimum quality standards can however hardly be influenced during this stage[38]. Water addition is sometimes applied, although only in the case of a too dry material. However excessive drying is an indication of sub-optimal process and should not be standard practice.

Storage

After the post-treatment step the product is either directly sold or stored. Storage requirements should always be considered, as the product might not be used on a regular base around the year. For instance compost use in field agriculture is almost absent during winter and has a peak in the early spring.

The performance of the composting reactor largely determines the quality of the product. Of course proper operation of the other steps is important. However as they serve to optimize the performance of the composting reactor, they can be understood as secondary to the composting operation.

It follows directly that proper design and operation of the composting reactor is necessary to guarantee a good compost quality and reduced emissions. As composting is primary a microbial process, the main function of the composting reactor will be realisation of optimal environmental conditions for the microbial population. To define these optimal conditions the dependence of the composting rate on environmental conditions, i.e. composting kinetics should be known.

Knowledge of the kinetic optimum is not sufficient. Assume that for a specific waste the optimal composting temperature is determined as 45 °C. For pathogen reduction an elevated temperature well above 45 °C is necessary. These demands for the operational composting temperature obviously conflict, and a temperature level has to be chosen such that pathogen reduction is assured while the composting process rate is not too much hampered. In composting engineering a trade-off always has to be made between different conflicting objectives. Knowledge of the optimum alone is therefore not sufficient and the explicit dependence of the composting rate in a broad range of the environmental factors should be known. This allows better optimisation through calculation. The best way to achieve this is via proper modelling of the process. This motivates the efforts in this thesis to develop a suitable and useful composting model.

1.4. Modelling concepts

Before discussing composting kinetics modelling in more detail some general notions on the model cycle and state space models will be introduced to facilitate the discussion.

1.4.1. Some definitions

In this thesis the term model is always used to mean a mathematical model. Aris defines a mathematical model concisely as “any set of equations that under certain conditions and for a certain purpose provide an adequate description of a physical system”[39]. A physical system is an outlined part of reality whose properties one seeks to understand, in this thesis the composting rate of a waste sample. A model contains basically two types of quantities, parameters that are constant in time and variables that vary in time. An input variable is a variable that is not affected by other quantities within the model and that can be freely chosen (to some extent) or is imposed by the outside world. The output is a variable that is observed. All remaining variables are called internal variables in this thesis. Composting kinetics is a dynamic process as its output depends not only on the current input but also all earlier inputs, for instance the composting rate is dependent on the temperature history of the sample, not only on the current temperature.

1.4.2. Model building strategy

A model building strategy describes the steps needed to build an adequate model for a given process. A model building strategy is no strict methodology, it is more a set of guidelines that have proven useful. In literature many different sets of guidelines can be found, see for example [40-47]. Figure 1.3 gives a schematic representation of the model building process based on the work of Heij and Eykhoff. The figure is structured around the starting points and outcome that are underlined in the text.

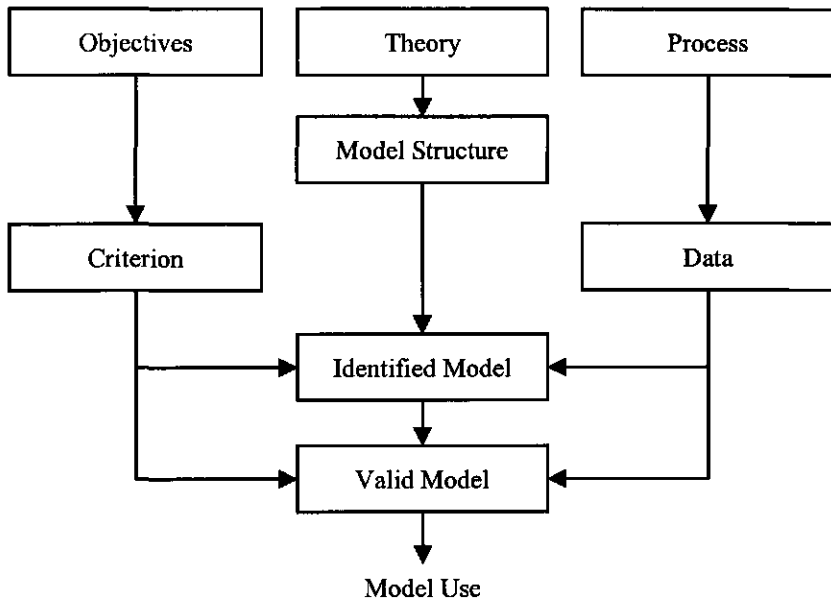


Figure 1.3: The model building process.

The starting point of the strategy lies in the phenomenon or process of interest, the theory about the process and the objectives of the modelling exercise. Modeling objectives influence modelling process during all phases. Typical modelling objectives are understanding, describing, predicting, controlling or optimising the process. For instance, in modelling a composting process it is important to know whether one wants to have a model that just describes the rate of a specific waste or one wants to understand the processes that are occurring. In the case of describing the rate one might use an empirical model, while for understanding how various factors affect the rate one uses a mechanistic model. Objectives are especially important when evaluating the resulting model.

The process of interest in this thesis is composting kinetics. Associated with this process is a body of more or less well developed theory that describes and explains the phenomenon. Theory if available leads to a set of a priori concepts about the process. For instance, realising that composting is a microbial process leads to inclusion of the concept “microbial biomass” into the model. The choice for concepts is also influenced by the model objective. Based on the a priori concepts a model structure is defined, i.e. a collection of feasible models is constructed. The strategy of deriving a model structure from theory is called the deductive strategy (classical modelling, white box modelling), where the theory takes a central place.

However theory is not always available, or theory is deemed less relevant, in such a case a so-called inductive strategy (black box modelling) is followed. Instead of deducting a model from first principles, a flexible model family (e.g. linear regression, difference equations with flexible order, etc.) is chosen as the model structure. The inductive approach tries to find the relationship between output and input.

From studying the phenomenon through experimentation data are obtained. These data are used to identify the model that best describes the data. From the theory is it sometimes possible to partly specify the parameter values. However parameter values for the specific process are often not sufficiently accurately known and parameter estimation is necessary from data. The parameter values are estimated by selecting those parameter values that give the best correspondence between the model outcome and data. To evaluate the correspondence between data and prediction a criterion is needed, that ideally is based on the modelling objective. In the inductive strategy model identification is broader in the sense that also changes in the model structure can be investigated. Based on the data decisions are made on what terms to retain in, add to, or remove from the model. The distinction between parameter estimation sec and model identification in a broader sense is not so clear cut, if parameter estimation yields zero for a certain parameter value, this might induce a change in the model structure. As a result of the model identification an identified model results.

After having identified the model the validity of the result should be assessed. Model validation might be loosely defined as assessing the quality of the model i.e. determining whether the model will be adequate for its intended use. As validity is not a clearly defined property, it is not surprising there are no universal tools to measure validity. However, a number of elements may be distinguished [47].

Before validating the model first the extent to which the model can describe the data is evaluated. This is a not an element of model validation, as during model development the parameter values have been chosen such that the data and model prediction correspond best. If this correspondence is poor the model validity may be doubted, but if there is a good correspondence this does not necessarily mean that the model is good. A faulty model containing sufficient parameters may well be able to describe the data very well.

A first element of model validation is to compare the model prediction with new data, i.e. data that have not been used for parameter estimation. Although this test is better than using the data used for parameter estimation it still does not tell whether the model represents the underlying structure of the process [48].

A second element is to investigate to what extent the model structure corresponds to what is known about the process. Elements of this step are comparing parameter values and the output development to what is known or expected. This is not a step that can be put rigorously in a statistical framework like the first element. However it does give information on how good the model represents the underlying structure of the process. This latter step makes sense only for the deductive modelling strategy.

Iteration (not shown in figure) is an important step in modelling process. If at some stage of the modelling process the outcome is not satisfactory, this stage or some previous stage has to be repeated.

The inductive and deductive strategy can be viewed as the extremes of a continuum of modelling strategies. Intermediate strategies, using both theoretical elements and empirical functions are sometimes called grey box modelling. These grey-box modelling strategies are commonly used, however this concept needs the concepts of inductive and deductive modelling for definition and tools.

1.4.3. State concept

The state is a vector of variables that are assumed to sufficiently accurately represent the process at some point of time. Variables are called state variables if knowledge of the current state and the future inputs completely describes the future development of the process, i.e. it is not required to know the history of the process. Using the state concept a dynamic process is conventionally [45] represented as:

$$\text{eq. 1-1} \quad \frac{dx(t)}{dt} = f(x(t), u(t), \theta)$$

$$\text{eq. 1-2} \quad y(t) = g(x(t), u(t), \theta)$$

t : time

x(t) : n-dimensional state vector

u(t) : m-dimensional input

θ : q-dimensional parameter vector

y(t) : p-dimensional output vector

f,g : vector valued functions

A vector expression is natural as in most cases more than one state variable is involved. The following elements can be distinguished in a state-space representation:

State variables

The state variables are assumed to represent the essential aspects of the process under study. Typical state variables in composting would be temperature, oxygen, moisture content etc. A state variable generally shows a spatial and temporal development in response to the influence of other state variables and/or the environment. An important application of models is predicting the trajectory of the state variables in time and space.

Constitutive relationships

The state variables are linked to each other via a number of relations and some or all state variables are linked to an input. If the model is meant to reflect a physical reality, such a linkage represents some physical, chemical or biological interaction. These equations are derived from chemistry, physics and biology, for instance the Monod-relationship describing the growth rate of a bacterium as function of substrate concentration.

Parameters

Parameters are part of equations describing the constitutive relationships. Parameters are typically constant and independent of the state variables. Parameters are generally not directly measurable and must be inferred from some type of experiment. If the relationships reflect some well accepted principle it is often possible to relate the unknown parameters to results of other research.

Input

The input describes the influence of the environment on the process. Typical examples in composting are airflow rate, mixing, etc. The initial state of the state vector can also be viewed as an input, but because it is a constant vector it is often useful to consider it part of the parameters. The input sometimes can not be observed, for instance the initial biomass concentration in composting. In such a case the unknown initial state can be treated as a unknown parameter.

Output

The output describes which part of the process is observed. This can be a direct observation of the state variables or some other derived measures as a conversion rate. Once the model is available, also other quantities of interest for which no observations are available can be

computed. These are sometimes called “performance outputs”.

A specific state-space representation without the specified parameter values is often referred to as a model structure in systems science literature. However to fully characterise a process not only a model structure but also a specific set of parameter values is needed. In control theory a model is often defined as a model structure together with a specific set of parameters. The same model structure with a different set of parameter values is in this view a different model. This may be confusing as in the engineering literature usually the term “model” refers to the model structure only, e.g. the Monod-model. In this thesis we will use model to refer to the structure, and a model with a set of specific parameter values will be referred to as calibrated or identified model.

1.5. Composting kinetics

Composting kinetics is defined in this thesis as a comprehensive set of equations (mathematical model) that describes the dependence of the composting rate on environmental factors over a range of practical interest. The kinetic model to be developed should be able to predict the process rate in relation to the (actual) composition of the waste and (actual) conditions to which this waste is exposed in the reactor.

The process rate is preferably expressed on the basis of a unit amount of waste and not of the total amount of the waste. Keener [49] discusses this matter in more detail and proposes the following first order model:

$$\text{eq. 1-3} \quad \frac{dm}{dt} = -k(x_1, x_2, \dots x_n)[m - m_e]$$

m	: Composting mass	[kg]
k	: Composting process rate constant	[h ⁻¹]
x _i	: Environmental factor e.g. temperature, oxygen, moisture, etc	
t	: Time	[h]
m _e	: Equilibrium mass, i.e. the residual mass after infinite composting time	[kg]

If the environmental factors remain constant in time, integration of the above equation directly leads to

$$eq. \ 1-4 \quad R = \frac{m - m_e}{m_0 - m_e} = e^{-k(x_1, x_2, \dots, x_n)t}$$

R : Compost mass ratio

[1]

The compost mass ratio changes from 1 at $t=0$ to 0 at $t=\infty$ and is a useful measure for process progress and consequently compost stability. In case of chicken manure the data of Keener [49] show that this model is applicable over a short time period (approx. 3 days), after such a period the k-value had to be updated, to reflect the changes in waste composition. In the case of yard waste the model is applicable over a much longer period once the peak activity has been reached [50]. The value of the first-order constant depends on the type of waste. A number of kinetic models have been published in the literature about the dependence of the first order rate constant on environmental factors [4, 13, 16, 23, 24, 51-55]. These models share the following multiplicative structure:

$$eq. \ 1-5 \quad k(x_1, x_2, \dots, x_n) = k_s \cdot f_1(x_1) \cdot f_2(x_2) \cdots f_n(x_n)$$

k_s : Composting process rate constant under standard environmental conditions [h^{-1}]

n : Number of environmental factors

f_1, f_2 : Environmental factor effect function

The functions f describe the effect of a specific rate determining factor on the process rate constant. If the process rate is measured under standard conditions all functions have the value 1. The most extensive model is still the kinetic model proposed by Haug. This model runs as:

$$eq. \ 1-6 \quad R_a(T, O_2, M, BVS, FAS) = k_s \cdot BVS \cdot f_1(T) \cdot f_2(M) \cdot f_3(O_2) \cdot f_4(FAS)$$

R_a : Absolute degradation rate [$kg \cdot hr^{-1}$]

BVS : biological degradable volatile solids [kg]

k_s : Standard rate constant [hr^{-1}]

T : Temperature [$^{\circ}C$]

O_2 : Gas phase oxygen content [% vol.]

M	: Moisture content waste	[kg water.(kg waste) ⁻¹]
FAS	: Free air space	[m ³ air.(m ³ bulk waste) ⁻¹]

An important assumption underlying the multiplicative model is the independence of the effects of the different environmental factors involved. However, Richard [18, 26] has shown that depending on moisture content, oxygen content and material, the optimal temperature varied from 52 °C to 64 °C. The effect also depends on the extent of organic matter degradation, thus not only do environmental factors influence each other but also the changing composition of the waste influences the effect. Compared to the factors oxygen, moisture and temperature, the dependence of the rate on the waste composition has received little attention. A distinct feature of the models used to date is that they are inductive models i.e. they try to relate directly the input (e.g. temperature) to the output, the composting rate. Although these models give a good description of the observed kinetic dependencies, it is expected that the data-oriented approach will not yield a comprehensive kinetic model i.e. a model that embraces all major environmental factors including waste composition. The following justification is given to substantiate this statement.

1. To investigate all environmental factors and their possible interactions a big experimental effort is needed. This is especially so because the heterogeneity of the waste calls for numerous replications. For instance to determine the effect of oxygen and moisture on the optimal temperature Richard performed the experiments at three moisture levels, three oxygen levels and four temperatures. To achieve sufficient accuracy each combination was measured three times, yielding a total of 108 experiments. Trying to include two additional factors like pH and porosity in this scheme would give 3x3x108 experiments, which gives a total of 972 experiments.
2. A number of factors (biomass, particle size) are expected to be important but can not be measured. For instance biomass can not be measured as no techniques are available for quantitative measurement in an organic waste matrix [56]. This makes it impossible to come up with an inductive model for these factors. As these factors tend to be variable, they constitute a source of variability when measuring the effect of other factors.

None of the aforementioned objections is of a principal nature, i.e. with sufficient effort and smart measurement techniques they could be overcome. Nevertheless taking into account the

current measurement standards in composting the inductive approach seems to have reached its practical limit.

The lack of a theoretical framework for composting kinetics thus seems to be the main obstacle for further development of kinetics and hence a deductive model approach is needed to achieve further progress.

1.6. Deductive modelling: merits and limitations

In the previous section it has been argued that the empirical approach has been developed to its limit of practicality. Further progress is not expected because of limits in measurement techniques and the resources needed to perform all experiments needed.

In contrast, mechanistic models exploit not only the data but also a priori information from the laws of physics, chemistry, etc. The deductive strategy is expected to lead to models with fewer parameters, as no parameters are needed to describe what is already known. As a mechanistic model reflects the structure of the process it is expected to yield better extrapolations [45].

However in the field of environmental and ecological modelling the deductive methodology does not always yield adequate models [41, 46, 57-60], and in particular the predictive power is low [48]. As the composting process can be considered as a microbial ecological process, the problems encountered in the field of ecological modelling may be expected to also occur in modelling of composting kinetics.

The basic problem can be made clear by considering the state space representation. Assuming the model to have a solution $x(t)=H(x_0, u(t), \theta)$ and substituting this relationship in the output function shows that the output function can also be considered as a function of the parameter vector, input and the initial value vector.

$$\text{eq. 1-7} \quad y = G(x_0, u(t), \theta)$$

If we consider the initial states as parameters that need to be estimated, one may write the following model:

$$\text{eq. 1-8} \quad y = G(u(t), \Theta)$$

Θ : Extended parameter vector

This model will be called the conceptual input-output (I/O) model, as it describes the output of the system as function of the input and a number of parameters, based on the conceptual model. It is important to note that an inductive model has a similar nature, i.e. it tries to relate the output to the input using some parameterized relationships.

If the state space model is made more complex by incorporating more state variables, the conceptual I/O model will contain more parameters. The number of (unknown) initial values and the number of parameters of the constitutive relationships generally increase. It is obvious that if the number of states introduced in the model increases while the number of inputs and outputs remain the same at some point the number of parameters needed for deductive modelling will be larger than needed for the inductive model derived from the same input output set. The larger number of parameters often show to be unidentifiable as non-identifiability can occur already in relatively simple models [60]. In this situation the advantage of a good predictability attributed to deductive modelling might be lost, as numerous sets of parameters are able to describe the data set. In this way an increase in the number of parameters may lead to an increase in the uncertainty of the prediction. The crux of the problem is that what one assumes about the system is much more complex than what one observes from the system. [41].

The problems of inadequate theory and incomplete measurements are related. If sufficient measurements were available, probably more complete and well accepted theory would be available. Incomplete measurements are thus a problem both in inductive and deductive modelling. Either strategy tends to obscure the problem. The inductive strategy discards the theory and thus has no way of knowing that measurements might be lacking. The deductive modelling often tacitly assumed that there exists a well-established quantitative theory of the phenomenon of interest. This is however not always the case. Neglecting the status of the a priori concepts would lead to overconfidence in the predictive power of the model [46].

1.7. Thesis objective

In section 1.5 it has been argued that the inductive approach seems to have reached its limit of practicability in the field of composting kinetics and a more deductive approach would seem in place. As discussed in section 1.6 it shows that in the field of ecological and environmental modelling to which composting belongs, the deductive approach also is limited. Due to a lack

of sufficient data and adequate theory, deductive models tend to be overparameterized and parameters are often unidentifiable. The problem is made worse because experimentation with environmental systems is restricted. Although in composting kinetics, experimentation is more accessible the basic problem of insufficient data and inadequate theory is definitely present. In such a case deductive modelling might yield models with unidentifiable parameters.

The challenge would seem to lie in developing a deductive model with yet identifiable parameters. To meet this challenge the so-called identifiability analysis is introduced as an important additional step in the deductive modelling strategy. Identifiability analysis is concerned with the question whether and under which circumstance parameters are identifiable. Consequently the objective of the thesis is:

To develop and test a theoretical framework for the composting kinetics that serves as a basis for the development of a comprehensive, yet identifiable kinetic model. The development of the kinetic model is performed using a deductive modelling incorporating identifiability analysis.

To prevent that the deductive strategy yields an overparametrized model, an additional modelling step is introduced, namely specification of an identifiable conceptual I/O model. The modified strategy is depicted in figure 1.4, the differences with the general modelling strategy as depicted in figure 1.3 will be discussed.

The main change is the introduction of two types of related models, the conceptual model and the conceptual I/O model. Based on theory and the model objective a qualitative conceptual will be set up first. The qualitative model is a kind of picture of the process of interest. This qualitative model is based on a number of notions and assumptions with different degrees of credibility. The credibility may range from well established laws like the principle of mass and energy conservation, up to pure hypothesis for instance on the structure of waste. The model objectives influence the conceptual model via the selection of boundaries and the level of sophistication. The qualitative model will next be transformed into a set of equations. In this thesis the state space representation is used. This type of model is a natural choice as it is based on a number of balance equations describing the fate of the different components present within the composting particle. The result of this step is the so-called conceptual (state space) model, as represented in eq. 1-1 and eq. 1-2.

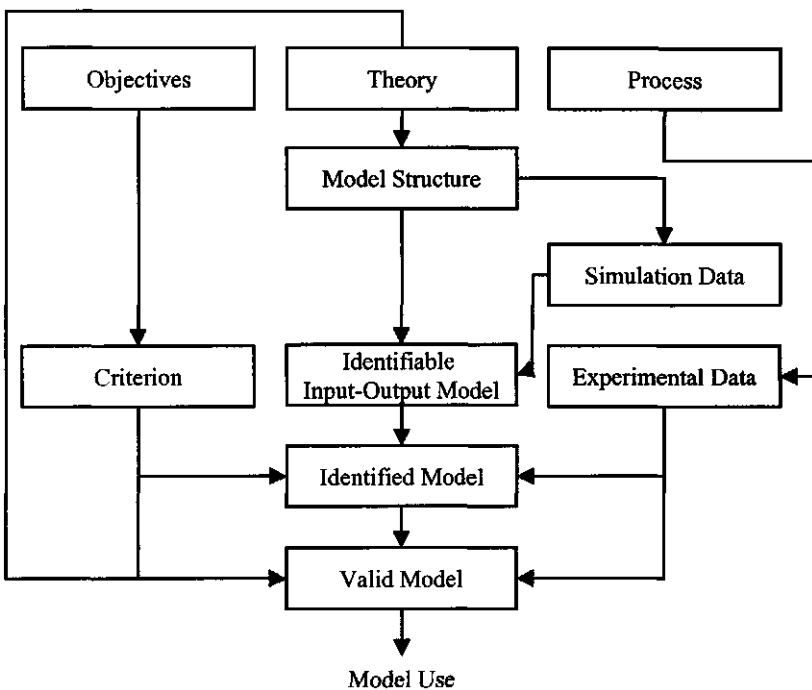


Figure 1.4: The modified model building process.

As a first step the conceptual I/O model will be set up, i.e. the function relating the input to the output without reference to the state variables, as represented in eq. 1-8. In this thesis an analytical solution is sought as this improves the insight in the process. To arrive at an analytical I/O model it will be necessary to use a number of simplifying assumption during the derivation. In this thesis two main techniques will be employed.

1. State aggregation

By reducing the number of states the number of initial values is reduced. The aggregation of states implies also aggregation of the associated constitutive relationships, and consequently leads to a reduced number of parameters. It depends on the nature of these relationships whether acceptable approximations can be achieved or not.

2. Separation of time constants

A state model often introduces different sub processes like microbial growth, diffusion and mixing. If the sub processes have a considerable faster or slower dynamics, they can be represented either as pseudo-steady state descriptions (fast, e.g. pH equilibrium) or as constants (slow, dissolution of inert materials).

As a limited amount of measurements is available, probably the parameters in the conceptual I/O model will be unidentifiable. Therefore if the conceptual I/O model is unidentifiable, a new conceptual I/O model will be derived, one that contains only identifiable parameters. In this thesis two techniques will be mainly used.

1 Dimensional analysis

In this thesis it will be shown that dimensional analysis is also a very useful tool in identifiability analysis. It offers a simple way to convert part of the unidentifiable parameters into groups of identifiable parameters.

2 Practical identifiability analysis

Practical identifiability analysis makes it possible to investigate the experimental conditions under which the I/O model is identifiable. In this thesis the main experimental condition taken into account the duration of the experiments. For the practical identifiability analysis and the experimental set-up simulation data are used that are generated by the conceptual model.

In this way a new conceptual I/O model arises, with identifiable parameters. Because this identifiable I/O model finds its starting point in the conceptual model, a relationship between the parameters in the original conceptual I/O model and the identifiable can be established. This relationship gives some insight in the physical basis of unidentifiability. The parameter in the conceptual model will be referred to as basic parameter while the parameter in the identifiable I/O model will be called aggregated parameter, as they often are a function of a number of basic parameter.

For model validation, it is important to note that one is dealing with two types of models, the conceptual model that parameterises the whole process, and the identifiable input-output model that parameterises the relationship between input and output as implied by the conceptual model. Although both models are related, the nature of their validation differs. The identifiable conceptual I/O model can be primarily treated as a model relating input and output. The capability of the model to do such is the essential test. As the parameters are estimated minimising the prediction error, bias and variance of the prediction error are useful statistics to assess the model performance.

Validation of the conceptual model must be considered in a different fashion. From the reduction it has become clear that it is often not the full model but only part of it is that is validated. Validation of the identifiable conceptual I/O model is thus a necessary but not a sufficient condition for validation of the full model. If the estimated parameter values are in

accordance with current knowledge, it may be assumed that the right hypotheses have been made, which gives an enhanced credibility to the conceptual model.

The credibility of the conceptual model can also be assessed using a comparison of alternative conceptual models. Comparing a number conceptual models means comparing the associated identifiable I/O models. The conceptual model that has the identifiable conceptual I/O model that best describes the data has the highest credibility. If the identifiable conceptual I/O models describe both the data well, the only way to distinguish between them is by applying additional different inputs to the process. Only those models consistent with these new stimuli will be retained.

Distinction between the conceptual model and the I/O model is thus also helpful for model validation. The identifiable I/O model can be validated against data in a stricter manner, while the conceptual model can be only checked for credibility.

Using the modified modelling approach in this thesis a theoretical model with an associated identifiable I/O model is developed. This combination of models makes it possible to:

1. link existing knowledge on kinetics to more general theory on microbial kinetics. For instance if it is possible to incorporate the parameters microbial yield and growth rate in the model, values of these parameters from the literature can be used. This makes more information available for modelling.
2. get more insight into the structure of the composting process. This insight is a result of the fact that a theoretical interpretation is given to the data. This is not only of scientific interest but might also open up new ways for process improvement.
3. make a more efficient use of the relative scarce data. As it is practically impossible to obtain the combined effects of all relevant environmental factors (temperature etc.) for the same type of waste, it is not surprising that different inductive models have been put forward for the effect of the same factor [13]. However these different data could be interpreted and used in a more coherent way, by a conceptual identifiable I/O model as the interactions are accounted for in the aggregated parameters as they are based on the conceptual model.
4. extrapolate the results to some extent. The objective of the kinetic model is to correctly predict the composting rate under the condition prevailing in a composting reactor. In a composting reactor many different combinations of factors will occur and prediction outside the measurement range (time, temperature, type of waste, moisture etc) will probably always occur. As has been argued in section 1.5, this is because it is practically

impossible to measure all potential combinations of factors. Extrapolation outside the realm of measurement is risky if the model is based on data solely. However if one has a model that is structurally valid, it is expected that extrapolation still makes sense.

1.8. Thesis structure

In chapter 2 the dimensional analysis is introduced as a new tool to investigate parameter identifiability. Dimensional analysis is used to prove a new necessary condition for parameter identifiability and gives a simple tool to construct the maximum number of parameter groups that are identifiable. Dimensional analysis also plays a role in facilitating further identifiability analysis by reducing the number of parameters involved.

In chapter 3 the so-called conceptual model is developed based on theoretical knowledge. This model represents the structure to the best of our knowledge. Use has been made of lumped variables to prevent the model from becoming unwieldy.

In chapter 4 an analytical conceptual I/O model is developed for the OUR time course. The analytical model is an approximation of the conceptual model. The quality of the analytical model is based on a comparison of the behaviour of the conceptual and the analytical model.

In chapter 5 the analytical conceptual model is validated. The identifiability of the parameters in the analytical model is first studied, together with the experimental design. This identifiability will be mainly based on dimensional analysis and a local identifiability analysis. A transformation will be performed to get an analytical identifiable conceptual I/O model for the OUR time course. Experiments with a so-called flat plate system are described that give the data needed for the parameter estimation. Where possible the aggregated parameter of the identified models will be compared to the basic parameters in the conceptual model.

In chapter 6 a distributed model will be developed. This is done in two steps. First an appropriate distribution function is chosen based on an extension of the conceptual model developed in chapter 3. Combining this distribution function with a slightly simplified version of the identifiable model developed in chapter 5 will yield a new model describing a set of distributed parameters.

In chapter 7 the distributed model will be investigated for its practical identifiability, again with a local identifiability analysis. Validation of the distributed model takes place by comparing the response of a distributed model system with the response of the flat plate system

In chapter 8 the predictive capability of the new kinetic model is compared to that of the generally used first order model. To do so a comparison of the both models capability to predict the OUR time course at a low gas phase oxygen content is made.

1.9. References

1. Wells, A.T., K.Y. Chan, and P.S. Cornish, *Comparison of conventional and alternative farming systems on the properties of a yellow earth in New South Wales*. Agriculture, Ecosystems and Environment, 2000. **80**: p. 47-60.
2. Hoitink, H.A.J., M.J. Boehm, and Y. Hadar. *Mechanisms of suppression of soilborn plant pathogens in compost amended substrates*. in *Proceedings of the International Composting Research Symposium*. 1992. Columbus OH: Renaissance Publications.
3. Inbar, Y., et al., *New Approaches to compost maturity*. Biocycle, 1990(December): p. 64-69.
4. Haug, R.T., *Compost Engineering: Principles and Practice*. 1980, Ann Arbor: Ann Arbor Science.
5. Finstein, M.S. and J.A. Hogan. *Integration of Composting Process Microbiology, Facility Structure and Decision-making*. in *Proceedings of the International Composting Research Symposium*. 1992. Columbus OH: Renaissance Publications.
6. Van Durme, G.P., B.F. McNamara, and C.M. McGinley, *Bench-scale Removal of odor and volatile organic compounds at a composting facility*. Water Environment Research, 1992. **64**(1): p. 19-27.
7. Cardenas, R.R., *Recent developments in composting processes*. Advances In Environmental Science And Engineering Vol1, 1979.
8. de Bertoldi, M.G., M.G. Vallini, and A. Pera, *The biology of composting: a review*. Waste Management & Research, 1983. **1**: p. 157-176.
9. Finstein, M.S. and M.L. Morris, *Microbiology of municipal solid waste composting*. Applied Microbiology, 1975. **19**: p. 113-151.
10. Finstein, M.S., et al., *Composting ecosystem management for waste treatment*. Bio/Technology, 1983. **1**: p. 347-353.
11. Golueke, C.G. and L.F. Diaz, *Composting and the limiting factor principle*. Biocycle, 1987: p. 22-25.
12. Poincelot, R.P. *The biochemistry of composting*. in *National conference on Composting of Municipal Residues and Sludges*. 1977: Information Transfer Inc.
13. Richard, T.L., *The kinetics of solid-state aerobic biodegradation*. 1997, Cornell University.

14. Gray, K.R., K. Sherman, and A.J. Biddlestone, *Review of composting part 1. Process Biochemistry*, 1971. 6(6): p. 32-36.
15. Gray, K.R., K. Sherman, and A.J. Biddlestone, *Review of composting part 2. Process Biochemistry*, 1971. 6(10): p. 22-28.
16. Cathcart, T.P., F.W. Wheaton, and R.B. Brinsfiled, *Optimizing variables affecting composting of blue crab scrap*. Agricultural Wastes, 1986. 15: p. 269-286.
17. Nakasaki, K., M. Shoda, and H. Kubota, *Effect of temperature on composting of sewage sludge*. Applied and Environmental Microbiology, 1985. 50(6): p. 1526-1530.
18. Richard, T.L. and L.P. Walker, *Temperature kinetics of aerobic solid-state biodegradation*. Proceedings of the IBE, 1998. 1: p. A10-A30.
19. Suler, D.J. and M.S. Finstein, *Effect of Temperature, Aeration, and Moisture on CO₂ Formation in Bench-Scale, Continuously Thermophilic Composting of Solid Waste*. Applied and Environmental Microbiology, 1977. 33(2): p. 345-350.
20. Nakasaki, K. and T. Akiyama, *Effects of seeding on thermophilic Composting of Household Organic Waste*. Journal of Fermentation Technology, 1988. 66(1): p. 37-42.
21. Nakasaki, K., et al., *Effect of seeding during thermophilic composting of sewage sludge*. Applied And Environmental Microbiology, 1985. 49: p. 724-726.
22. Bakshi, M.P.S., V.K. Gupta, and P.N. Langar, *Effect of moisture lever on the chemical compostion and nutritive value of fermented straw*. Biological Wastes, 1987. 21: p. 283-290.
23. Jeris, J.S. and R.W. Regan, *Controlling environmental parameters for optimum composting II: moisture, free air space and recycle*. Compost Science, 1973. 14(2): p. 8-15.
24. Schulze, K.L., *Relationship between moisture content and activity of finished compost*. Compost Science, 1961. 2(2): p. 32-34.
25. Nakasaki, K., et al., *Oxygen diffusion and microbial activity in the composting of dehydrated sewage sludge cakes*. Journal of Fermentation Technology, 1987. 56(1): p. 43-48.
26. Richard, T.L., L.P. Walker, and J.M. Gosset, *The effects of oxygen on solid-state biodegradation kinetics*. Proceedings of the IBE, 1999. 2: p. A22-A39.

27. Finstein, M.S., F.C. Miller, and P.F. Strom, eds. *Waste treatment composting as a controlled system*. Biotechnology: a comprehensive treatise, ed. H.J. Rehm and G. Reed. Vol. 8. 1985, VCH: Weinheim. 363-398.
28. Waksman, S.A., T.C. Cordon, and N. Hulpoi, *Influence of temperature upon the microbiological population and decomposition processes in compots and stable manure*. Soil Science, 1939. 47: p. 37-61.
29. Godden, B., et al., *Evolution of enzyme activities and microbial populations during composting of cattle manure*. European Journal Of Applied Microbiology And Biotechnology, 1983. 17: p. 306-310.
30. Godden, B. and M. Penninckx, *Biochemistry of manure composting: lignin biotransformation and humification*. Compost: Production Quality And Use,Pg, 1987.
31. Morisaki, N., et al., *Nitrogen Transformation during Thermophilic Composting*. Journal of Fermentation and Bioengineering, 1989. 67(1): p. 57-61.
32. Haug, R.T., *Composting process design criteria: part i-feed conditioning*. Biocycle, 1986: p. 38-43.
33. Atchley, S.H. and J.B. Clark, *Variability of Temperature, Ph, and Moisture in an Aerobic Composting Process*. Applied And Environmental Microbiology, 1979. 38(6): p. 1040-1044.
34. Kuter, G.F., H.A.J. Hoitink, and L.A. Rossman, *Effects of aeration and temeprature on composting of municipal sludge in a full-scale system*. Journal Water Pollution Control Federation, 1985. 57(4): p. 309-315.
35. MacGregor, S.T., et al., *Composting Process Control Based on Interaction Between Microbial Heat Output and Temperature*. Applied and Environmental Microbiology, 1981. 41(6): p. 1321-1330.
36. van Griensven, L., *The Cultivation of Mushrooms*. 1988, Horst, the Netherlands: Proefstation Champignonteelt.
37. Keener, H.M., et al. *Remix Frequency of Compost based on Moisture Control*. in ASAE-meeting. 1994. Kansas.
38. Richard, T.L., *Municipal solid waste composting: physical and biological processing*. Biomass and Bioenergy, 1992. 3(3-4): p. 163-180.
39. Aris, R., *Mathematical modelling techniques*. 1978, London: Pitman.
40. Beck, M.B., *Model structure identification from experimental data*. 1980, Laxenburg, Austria: IIASA.

41. Beck, M.B., *Construction and Evaluation of Models of Environmental Systems*, in *Modelling Change in Environmental systems*, A.J. Jakeman, M.B. Beck, and M.J. McAleer, Editors. 1993, John Wiley & Sons.
42. Eykhoff, P., *System Identification*. 1974: John Wiley & Sons.
43. Heij, C. and J.C. Willems, *A deterministic approach to approximate modelling*, in *From data to model*, J.C. Willems, Editor.
44. Keesman, K.J., *A set-membership approach to the identification and prediction of ill-defined systems: application to a water quality system*. 1989, Twente.
45. Ljung, L. and T. Glad, *Modeling of dynamic systems*. 1994, Prentice Hall: New Jersey.
46. Reichert, P. and M. Omlin, *On the usefulness of overparametrized ecological models*. Ecological Modelling, 1997. **95**: p. 289-299.
47. Spriet, J.A. and G.C. Vansteenkiste, *Computer-aided modelling and simulation*. 1982, London: John Wiley & Sons.
48. van Straten, G., *Models for Water Quality Management: The Problem of Structural change*. Water Science and Technology, 1998. **37**(3): p. 103-111.
49. Keener, H.M., et al. *Optimizing the efficiency of the composting process*. in *Proceedings of the International Composting Research Symposium*. 1992. Columbus OH: Renaissance Publications.
50. Marugg, C., et al., *A kinetic model of the yard waste composting process*. Compost Science & Utilization, 1993. **1**(1): p. 38-51.
51. Jeris, J.S. and R.W. Regan, *Controlling environmental parameters for optimum composting III*. Compost Science, 1973. **14**(3): p. 16-22.
52. Nakasaki, K., et al., *A New Composting Model and Assessment of Optimum Operation for effective Drying of Composting Material*. Journal of Fermentation Technology, 1987. **65**(4): p. 441-447.
53. Finger, S.M., R.T. Hatch, and T.M. Regan, *Aerobic microbial growth in semisolid matrices: heat and mass transfer limitation*. Biotechnology and Bioengineering, 1976. **18**: p. 1193-1218.
54. Stombaugh and Nokes, *Development of a biologically based aerobic composting simulation model*. Transactions of the ASEA, 1996. **39**(1): p. 239-250.
55. Whang, D.S. and G.F. Meenaghan, *Kinetic model of composting process*. Compost Science, 1980(May/June): p. 44-46.

56. Mitchell, D.A. and B.K. Lonsane, *Definition, Characteristics and potential*, in *Solid Substrate Cultivation*, H.W. Doelle, D.A. Mitchell, and C.E. Rolz, Editors. 1992, Elsevier Applied Science: London.
57. Beck, M.B. *Understanding environmental systems*. in *Predictability and Nonlinear Modelling in Natural Sciences and Economics*. 1994. Wageningen: Kluwer.
58. Harremoes, P. and H. Madsen, *Fiction and Reality in the Modelling World- Balance between Simplicity and Complexity, Calibration and Identifiability, Verification and Falsification*. Water Science and Technology, 1999. 39(9): p. 1-8.
59. Hauhs, M., et al., *Summary of a workshop on ecosystem modelling: The end of an era?* The Science of the Total Environment, 1996. 183(1-2): p. 1-5.
60. Schulze, K., K. Beven, and B. Huwe, *Equifinality and the Problem of Robust Calibration in Nitrogen Budget Simulations*. Soil Sci. Soc.Am., 1999. 63: p. 1934-1941.

2. DIMENSIONAL ANALYSIS AND PARAMETER IDENTIFIABILITY OF STATE SPACE MODELS.....	32
2.1 INTRODUCTION	32
2.2 BASIC CONCEPTS.....	34
2.2.1 <i>Units, measures and dimension</i>	34
2.2.2 <i>Dimensional homogeneity</i>	36
2.2.3 <i>The II-theorem and dimensional analysis</i>	38
2.2.4 <i>State space models and estimation</i>	40
2.2.5 <i>Identifiability</i>	43
2.3 DIMENSIONAL PARAMETER IDENTIFIABILITY ANALYSIS.....	47
2.3.1 <i>Single parameter identifiability</i>	47
2.3.2 <i>Unobserved dimensions free representation</i>	49
2.4 EXAMPLES: BATCH MICROBIAL GROWTH.....	51
2.4.1 <i>Basic model equations</i>	51
2.4.2 <i>Model M0</i>	53
2.4.3 <i>Model M1</i>	53
2.4.4 <i>Model M2</i>	55
2.4.5 <i>Model M3</i>	56
2.4.6 <i>Model similarity and global identifiability</i>	56
2.4.7 <i>Practical identifiability model M2.</i>	59
2.5 DISCUSSION	62
2.6 REFERENCES	64

2. Dimensional analysis and parameter identifiability of state space models

2.1 Introduction

Dimensional analysis is widely applied in mathematical modeling of physical systems and is primarily used as a guide line in setting up models and model analysis [1, 2]. Dimensional analysis is based on the principle of dimensional homogeneity that states that a relationship or model should be conceptually valid irrespective of the choice of the system of units involved [3]. Application of dimensional analysis leads to a reduction of the number of variables and parameters involved in a certain model structure. This reduction is achieved by transforming the original model structure to a dimensionless model structure via the famous Π -theorem [4]. The result is an equivalent model structure with dimensionless groups that are combinations of variables and parameters of the original model.

Theoretical mathematical models of physical systems contain physically interpretable parameters i.e. parameters that have a specific meaning. In many cases the parameter values are (partly) unknown and experiments are performed to arrive at the correct parameter values. An input is given to the system and the output is monitored. From these measurements knowledge about parameter values is extracted. These measurements are in general not dimensionless, they will have some associated unit.

Making a model structure dimensionless causes difficulties for parameter estimation purposes. The dimensionless groups will contain both measured variables as well as parameters that are yet unknown. Parameter estimation is thus not possible with the transformed dimensionless measurements, as the parameters needed for transformation are not known beforehand. This makes a straight application of the Π -theorem in the field of parameter estimation difficult.

This does not mean, however, that in parameter estimation dimensional analysis can not play a useful role. This chapter is intended to show the usefulness of dimensional analysis in the field of parameter estimation, more specifically in parameter identifiability analysis.

A parameter estimation routine fed with data will aim to generate a parameters vector that describes the data best in some sense. If there exist more parameter vectors that describe the same data set equally well the following problems may arise:

- The parameters do not give a unique physical representation of the system. This is a

problem when the model is going to be used for extrapolation or prediction. If the description is not unique, one may end up with different extrapolations depending on the parameter vector used for prediction.

- A non-unique parameter vector might yield an ill-posed identification problem, i.e. the parameter estimation routine might fail.

It is thus important that the experiment is designed such that a unique parameter set is identified. Identifiability analysis is trying to answer the question whether the results of an intended experiment will yield a unique parameter estimate. A parameter that can be uniquely determined is called identifiable. Identifiability analysis has been introduced by Bellman and Astrom [5]. Since then a large body of papers has been published on this issue, see for a review [6].

Basically two approaches might be distinguished for identifiability analysis, the so-called structural or theoretical identifiability analysis and the so-called practical identifiability analysis. The theoretical identifiability analysis aims at determining which parameters can be uniquely identified from the data at all. The practical identifiability analysis is involved with the question whether the data and the model structure allow a sufficiently accurate parameter estimation. Even if a parameter can theoretically be uniquely determined it still might be the case that several values for this parameter give nearly the same data set. In such a case the unique parameter vector is hard to resolve. A parameter should thus not only be theoretically but also practically identifiable.

There exist methods to assess theoretical and practical identifiability for both linear and non-linear models [7]. Especially for non-linear these methods require extensive symbolic manipulation and extensive calculations, probably hampering a more widespread use of these methods [8].

In this paper the usefulness of dimensional analysis in the field of parameter identifiability analysis will be investigated. It will be shown that by dimensional analysis a (partial) simplification is sometimes possible. This partial simplification reduces the complexity of the theoretical identifiability analysis and shows connections with model structures with known identifiability properties.

When studying practical identifiability it is common to use some kind of scalar identifiability measure [9]. By optimizing this measure in relation to the experimental input an optimal experimental design is sought. It will be shown that by applying dimensional analysis a less

complicated optimization problem can be constructed.

This paper is application oriented and its primary goal is to show the usefulness of applying dimensional analysis to the area of parameter identifiability. All ideas are applied to the parameter estimation from batch culture data. To make the paper self-contained first some concepts linked to dimensional analysis, parameter identifiability and microbial growth models will be introduced.

2.2 Basic concepts

2.2.1 Units, measures and dimension

Engineering literature often equates dimensional analysis with the famous Buckingham Π -theorem. As this theorem is very powerful and useful it often hinders a broader view on the theory of physical dimensions. The major notions and theorems on dimensional analysis are as follows.

To a *physical quantity* Q a value can be assigned by means of a suitable *measurement*. Performing a measurement consists of two steps, selecting the *appropriate unit* U and carrying out the *comparison* of the physical quantity with the chosen unit.

The result of the measurement is a numerical value *the measure*, expressing the ratio of Q to U . The measurement result thus consists of a numerical value (the measure) and a unit associated with the measurement. Take as an example, the measurement of the distance between two points. The distance is the physical quantity, one uses a measuring stick with a length of 1 m, which is adopted as the unit. Comparing the length of the distance with the measuring stick gives as a result the ratio distance: measuring stick = the measure.

After accepting the meter as a basic unit one can start to define the unit for area. The choice of a unit is to some extent arbitrary and one might use for instance the hectare as the area unit. Accepting meter as length unit and the hectare as the area unit, the equation for the area of a rectangle runs as:

$$\text{eq. 2-1} \quad A = 1/10,000 L_x \cdot L_y$$

A : Area of rectangle [ha]

L_x, L_y : Length of rectangle sides [m]

The constant 1/10,000 is only introduced to account for the difference in length and area unit. If one would change the basic length unit from m to mm, one had to change the constant in eq. 2-1. This type of constant is called an *arbitrary constant* as it is used for unit conversion only, it reflects no physical relationship[10].

The common standard area unit is the area of a square with unit length, the area unit thus being m^2 . Using the m^2 area unit the area of a rectangle can be calculated as:

$$\text{eq. 2-2} \quad A = L_x \cdot L_y. \quad [m^2]$$

A : Area of rectangle

This equation does not change upon a change in the distance unit. The m^2 area is a so called derived unit. A derived unit is composed of *basic* units, according to some definition relationship. Use of derived units makes it possible to arrive at *consistent* set of units. A set of units is consistent if the use of this set does not lead to *arbitrary constants* in the physical relationships. Basic units are also referred to as *primary* or *fundamental* units. Basic units are independent, they can not be derived from each other. The basic units together form the unit system.

The derived unit of a physical quantity Q can be generally represented as:

$$\text{eq. 2-3} \quad \{Q\} = \prod_{i=1}^k U_i^{d_i}$$

$\{Q\}$: Unit of Q

$U_1 \dots U_k$: k Fundamental units

d_i : Dimensional exponents with respect to basic unit i.

The measure of a physical quantity depends on the system of units used. Whenever we are setting up or manipulating an equation describing some physical reality, we do not worry about the specific units chosen. The only requirement is that the same system of basic units is used throughout and that the derived units are consistent with these basic units. In such a case the variable coincides with the measure.

Sometimes in the text we are considering more than one system of basic units and we have to

refer explicitly to the dependence of the measure on the system of basic units. In such a case we denote the measure as $[Q|U]$, in which U denotes the specific system of basic units used.

Even a set of consistent basic units is to some extent arbitrary, for instance the physical quantity length can be measured with different basic units as m, cm, mm, km, foot, yard etc. These units have in common that they can measure each other, they can be compared to each other, expressed in some ratio. Changing a basic unit will likely influence the measure. Consider a new unit of length with a measure L expressed in the original length unit. The new consistent unit of area will have a measure of L^2 expressed in the original length unit. L^2 is called the *measure formula* and is the mathematical expression for the measure of the new consistent unit expressed in terms of the original consistent unit. This expression is by convention also referred to as the physical dimension, i.e. independent of a specific set of basic units [11]. The physical dimension can be considered as a variable that describes all potential units that can be compared to each other. The variable L thus stands for all potential length units (m, cm, mm, km, foot, yard etc). In the sequel a dimension will be indicated with a bold capital letter (L = length, T = time). The dimension of a single physical entity can therefore be represented by the dimensional vector $[Q]$

$$\text{eq. 2-4} \quad [Q] = \begin{pmatrix} d_1 \\ d_2 \\ \vdots \\ d_k \end{pmatrix}$$

i.e the vector of the dimensional exponents of the fundamental units U (see eq. 2-3). It should be noted that this vector is independent of the set of basic units and it only depends on the definition of the dimensions.

2.2.2 Dimensional homogeneity

Consider a relationship between a (dependent) physical quantity Q_i and some (independent) physical quantities $Q_2 \dots Q_n$, $Q_i = f(Q_2 \dots Q_n)$. If this relationship is a sound physical description the equation(s) should be invariant for the choice of the basic units. Would this property not hold, then the result of a relationship would depend on the system of units chosen. This is certainly an unwanted situation, as two observers would see a different reality only because

they were using different unit systems. A meaningful physical relationship between physical entities should thus be independent of the choice of the system of units. The relationship should be such that if the system of fundamental units is changed the outcome of the relationship using the new measures should be the original outcome expressed in the new system of units. A relationship holding this property is called dimensional homogenous. A relationship is thus dimensionally homogeneous if the relationship,

$$\text{eq. 2-5} \quad \|Q_1|U\| = f(\|Q_2|U\|, \|Q_3|U\|, \dots, \|Q_n|U\|)$$

holds for any consistent set of basic units.

The property of dimensional homogeneity can be studied with an algebraic framework of which Langhaar gives an excellent overview [3]. Central in this framework is the dimensional matrix. The dimensional matrix is formed by aligning the dimensional vectors of all physical quantities involved. The rows indicate the dimensions involved, while the columns stand for specific quantities.

$$\text{eq. 2-6} \quad [Q_1, Q_2, \dots, Q_n] = \begin{pmatrix} d_{1,1} & d_{1,2} & \cdots & \cdots & \cdots & d_{1,n} \\ \cdots & \cdots & \cdots & \cdots & \cdots & \cdots \\ d_{i,1} & d_{i,2} & \cdots & d_{i,j} & \cdots & d_{i,n} \\ \cdots & \cdots & \cdots & \cdots & \cdots & \cdots \\ d_{k,1} & d_{k,2} & \cdots & \cdots & \cdots & d_{k,n} \end{pmatrix}$$

A central issue in dimensional analysis is the question whether a specific relationship is dimensionally homogenous. To test dimensional homogeneity two theorems can be employed, the Rank-theorem and the Differential theorem. Both theorems are described by Langhaar and express a necessary and sufficient condition for a dimensionally homogenous relationship. The first is a straightforward combination of the theorems 6 and 7 of Langhaar [3].

Rank (R)- theorem

The relationship $Q_1 = f(Q_2, \dots, Q_n)$ is dimensionally homogeneous if and only if the dimensional

matrix $[Q_2 \dots Q_n]$ has the same rank as the dimensional matrix $[Q_1 Q_2 \dots Q_n]$.

Differential Equation (D)-Theorem

A differentiable function $Q_i = f(Q_1 \dots Q_n)$ is dimensionally homogeneous if and only if it is a solution of the (set of) differential equation(s):

$$\text{eq. 2-7} \quad [Q_1, Q_2, \dots, Q_n] \cdot \begin{pmatrix} 0 \\ Q_2 \cdot \frac{\partial Q_1}{\partial Q_2} \\ \vdots \\ Q_n \cdot \frac{\partial Q_1}{\partial Q_n} \end{pmatrix} = \begin{pmatrix} 0 \\ 0 \\ \vdots \\ 0 \end{pmatrix}$$

Of course the dimensional homogeneity of a given relationship can be simply checked by hand. The interesting aspect of these theorems is that the functional relationship need not be known, as only a list of physical quantities involved suffices to check the dimensional homogeneity.

2.2.3 The Π -theorem and dimensional analysis

The Π -theorem describes how a dimensional relationship can be transformed into similar relationship containing only dimensionless variables. These dimensionless variables are products of the original dimensional variables. The number of dimensionless groups is in general smaller than the number of original variables. The Π -theorem states:

Π -Theorem

Every relationship $F(Q_1 \dots Q_n) = 0$ between n physical quantities can be reduced to an equivalent dimensionless form between k dimensionless groups Π_i , $F(\Pi_1, \dots, \Pi_k) = 0$, $k \leq n$. The value of k equals $n - m$, in which m is the rank of the dimensional matrix $[Q_1 \dots Q_n]$.

Application of the Π -theorem has a number of advantages [2]:

- (i) The number of physical quantities that enter the relationship is reduced which makes it easier to treat the problem at hand. This is true when solving equations, but also when performing experiments. A reduction of variables is even possible if the exact functional relationship is not known yet.
- (ii) Seemingly different models may appear to be similar when put in dimensionless form. This may make it possible to use results already derived from other systems.
- (iii) Dimensionless numbers give insight in scaling. Scaling is only physically meaningful if two quantities have the same dimension. Dimensionless numbers make scaling possible when more dimensions are involved.

The dimensionless groups can be constructed from the dimensional matrix of the physical quantities involved. In most practical situations the number of physical quantities involved (n) will be larger than the number of basic dimensions involved (k). To find the dimensionless groups the dimensional matrix (see eq. 2-8) is separated in a left side identity matrix and a right side residual matrix. This separation can be achieved by applying Gaussian reduction.

$$\text{eq. 2-8} \quad [Q_1, Q_2, \dots, Q_n]_R = \left(\begin{array}{cccc|cccc|c} 1 & 0 & 0 & \cdots & 0 & d_{1,k+1} & \cdots & \cdots & d_{1,n} \\ \cdots & 1 & \cdots \\ 0 & 0 & 1 & 0 & 0 & d_{i,k+1} & \cdots & \cdots & d_{i,n} \\ \cdots & \cdots & \cdots & 1 & \cdots & \cdots & \cdots & \cdots & \cdots \\ 0 & 0 & 0 & \cdots & 1 & d_{k,k+1} & \cdots & \cdots & d_{k,n} \end{array} \right)$$

$[Q_1, Q_2, \dots, Q_n]_R$ Reduced dimensional matrix

Left of the dashed line the first k columns form the identity matrix, right of the dashed line the remaining $n-k$ columns form the residual matrix. From this reduced dimensional matrix the $n-k$ dimensional groups can be constructed as [4]:

eq. 2-9

$$\Pi_j = Q_{j+k} \cdot \prod_{i=1}^k Q_i^{-d_{i,j+k}}$$

- k : Rank of dimensional matrix.
- n : Number of physical entities
- j : j lies in the range $1..n-k$
- i : i lies in the range $1..k$
- d_{ij} : Element i,j of reduced dimensional matrix.
- Π_j : Dimensionless number j

In this way a set of mutually independent dimensionless numbers is constructed. It should however be noted that there are more ways to construct these sets depending on the choice of the physical quantities making up the identity matrix.

2.2.4 State space models and estimation

Continuous dynamic systems can be conveniently represented in state space form as:

eq. 2-10

$$\begin{aligned}\frac{dx(t)}{dt} &= f(x(t), u(t), \theta) \\ x(0) &= x_0\end{aligned}$$

eq. 2-11

$$y(t) = g(x(t), u(t), \theta)$$

- x : State vector, $x(t) \in \mathbb{R}^n$
- x_0 : Initial values
- Ω : Admissible parameter space
- θ : Parameter vector, $\theta \in \Omega \subset \mathbb{R}^q$
- $[0, T]$: Time interval considered
- t : Time, $t \in [0, T]$
- $u(t)$: Input vector, $u(t) \in \mathbb{R}^m$
- f : Vector valued state function
- g : Vector valued output function

y : Output vector, $y(t) \in \mathbb{R}^p$

The state space model representation is widely used to model phenomena in natural sciences. In engineering state space models are derived from the mass and energy balances describing the phenomenon at hand. The state variables x describe together the state of the system under study. The input describes the influence of the environment on the system. The interaction of the state variables with the input and the interaction between the state variables determine the development of the system over time. These interactions are described by the state vector function f , containing the parameter θ . Here only state space models with parameters that have a physical interpretation will be considered, where the parameter value quantifies the relationship between state variables. The output y describes the information obtained from the system through some kind of measurement.

Knowledge of input, initial values and parameters make it possible to predict the behavior of the system, i.e. calculate the trajectories in time (and space) of the state variables, irrespective of the previous history.

In most practical cases not all information is available and experiments have to be performed to obtain the missing information. In an experiment one applies an input to the system, observes the output and tries to deduce the parameter values from the results thus obtained. For the estimation of the parameters a (vector valued) function is needed that relates the input to the output. In this so-called input output (I/O) function the state variables as such play no role. The state variables are auxiliary signals of the system that are not measured, but only used to represent the system [12]. This can be illustrated in the following way. An obvious prerequisite for the model 2-10 is of course that the model has a solution, i.e one can write

eq. 2-12
$$x(t) = F(t, x_0, \theta, u(t))$$

F : Solution to function f

Substitution of this solution into the output equation (eq. 2-11) gives:

eq. 2-13
$$y(t) = g(F(t, x_0, \theta, u(t)), \theta, u(t))$$

This shows that the output is only linked to the parameter vector, input and initial values, and the state variables as such play no role. In (environmental engineering) practice often only limited measurements are possible because reliable affordable sensors are lacking [9]. This means that in practice initial values are unknown or are controlled by a known momentary input. The unknown initial values will be treated as a parameter, and an extended parameter vector q is defined that contains the proper parameters and the unknown initial values. An extended input vector is defined which contains the proper input and the controlled initial values. Without loss of generalization the input-output relation can thus be formally written as:

$$\text{eq. 2-14} \quad y(t) = h(q, z(t))$$

- $y(t)$: Estimated output
- q : Extended parameter vector
- z : Extended input
- h : Vector valued I/O function.

The parameter vector q is estimated by finding that parameter vector that gives the closest match between the predicted and measured output. Conventionally the parameters are found by minimizing a quadratic objective function J :

$$\text{eq. 2-15} \quad J(q) = \int (y_m(t) - h(q, z(t)))^2 dt$$

- J : Objective function
- $y_m(t)$: Measured output at time t

As already noted, in (environmental engineering) practice limited measurements are often available. This makes the question whether the estimation procedure will lead to a unique value of q particularly meaningful. Parameter uniqueness is a desirable property as it prevents ambiguity in interpretation of data and predictions.

2.2.5 Identifiability

If a parameter has the property that it can be uniquely estimated it is called identifiable. Identifiability analysis is concerned with the techniques needed to assess the existence of this property. Identifiability can be investigated by determining whether output obtained with different parameter values can be distinguished one from another, independent of the value of other parameters. Only if this is the case a parameter can be uniquely identified. The problem of distinguishing between parameters can thus be replaced by the problem of distinguishing between outputs [13]. There are a number of different closely related definitions of identifiability. In this chapter the definition as proposed by Walter [7] will be used.

Parameter identifiability definition

Consider a model $y = h(q, z(t))$ as defined before. (eq. 2-14). Consider two parameter vectors r and q . The parameter q_i is said to be identifiable if $h(q, z(t)) = h(r, z(t))$ implies that $q_i = r_i$.

It should be noted that the property is defined for a specific parameter. This property needs not to hold for all model parameters, some parameters may be identifiable while others are not. If this property holds for all parameters in the model, it is said that the model is identifiable. Both definitions have a local analog, local identifiability is defined over the neighborhood of a specific parameter value. The main question is how to determine these properties. There is a large amount of literature on identifiability for linear systems but few methods exist for nonlinear models. Some methods will be specifically mentioned as use is made of them.

Local identifiability

Local identifiability is a necessary condition for global identifiability. Local identifiability analysis is more frequently applied in the literature than global identifiability analysis as it is easier to use. If the parameter values are approximately known a local identifiability analysis might give sufficient information. An important tool to study local parameter identifiability is the sensitivity function. The sensitivity function is defined as the first derivative of h with respect to a specific parameter. The sensitivity function shows the effect of a small parameter change on the response of the system.

$$\text{eq. 2-16} \quad s_i(t) = \frac{\partial h(q, z(t))}{\partial q_i}$$

s_i : Sensitivity function of function h for parameter i

Sensitivity functions are used for sensitivity analysis and local identifiability analysis. In sensitivity analysis the sensitivity coefficients are used to quantify the effect of a parameter on the output of the model. Beck and Arnold state that parameters are identifiable, if the sensitivity coefficients are linearly independent over the range of observations. They derive this criterion from studying the prerequisites that guarantee the existence of a minimum of a generalized least squares sum. The sensitivities are expressed by means of the sensitivity matrix K , given by:

$$\text{eq. 2-17} \quad K(q) = \begin{pmatrix} \frac{\partial h(q, z_1)}{\partial q_1} & \dots & \frac{\partial h(q, z_1)}{\partial q_p} \\ \frac{\partial h(q, z_i)}{\partial q_1} & \dots & \frac{\partial h(q, z_i)}{\partial q_p} \\ \frac{\partial h(q, z_n)}{\partial q_1} & \dots & \frac{\partial h(q, z_n)}{\partial q_p} \end{pmatrix}$$

$K(q)$: Sensitivity matrix

z_i : Input $z(t)$ at $t = t_i$

If the rank of this matrix equals the number of unknown parameters then the parameters are identifiable [7]. This criterion is equivalent to the linear independence of the sensitivities [14]. This criterion can also be used to investigate the presence of structural identifiability i.e. irrespective of the estimation method used [7].

Global identifiability

There are several methods to investigate global identifiability for dynamic systems [15]. In this paper the power series expansion method according to Pojanpahlo [16] will be used. The method is based on expanding the output function as a Taylor series. The series and thus the output function is only distinguishable if the different derivative terms are unique.

Consider an input-output function $y(t) = h(q, z(t))$ as in eq.2-14. It is sufficient for the identifiability of the system that the set of equations

$$\text{eq. 2-18} \quad h^k(q, z(0)) = h^k(r, z(0)) \quad k = 0 \dots \infty$$

in which :

h^k : k-th Time derivative of the output function at $t=0$

q, r : Parameter vectors

implies that $q=r$.

Three main steps can be distinguished when using the procedure. For a general nonlinear system the procedure involves three main steps[17].

1. Successive differentiation of $h(q, z)$.
2. Evaluation of $h^k(q, z(0))$ by substitution of quantities already known from lower derivatives
3. Solving q as a function of r , and checking the uniqueness of the solution.

Practical identifiability

If the model is correct and the measurements are error-free, a perfect match can be found, so the lowest possible value of the objective function J will be zero. In the error-free case, the parameter vector for which $J(q)=0$ will be called the nominal parameter vector q_n . However, in practice measurements are always corrupted and the minimal value of J will be larger than zero. If the measurement error variance ρ^2 is considered additive one can write for the (expectation) of the objective function using experimental data:

$$\text{eq. 2-19} \quad J_{\text{exp}}(q) = J(q) + \rho^2$$

$J(q)$: Objective function using error-free data, i.e. model error.

$J_{\text{exp}}(q)$: Objective function using experimental data, i.e. containing an error

ρ^2 : Error variance

Consider a parameter vector \mathbf{q} in the neighborhood of the nominal parameter set \mathbf{q}_n . For the nominal parameter set $J(\mathbf{q}_n)=0$ and thus the value of the objective function using experimental data is expected to be: $J_{exp}(\mathbf{q}_n) = \rho^2$. For any $\mathbf{q} \neq \mathbf{q}_n$ this means that $J_{exp}(\mathbf{q}) - J_{exp}(\mathbf{q}_n) = J(\mathbf{q}) > 0$. Thus in presence of an additive error, the parameter are also identifiable. However if $\rho^2 \gg J(\mathbf{q})$ then $J_{exp}(\mathbf{q})$ and $J_{exp}(\mathbf{q}_n)$ are practically the same and it is practically impossible to identify \mathbf{q}_n as a unique estimate. Thus we would like $J_{exp}(\mathbf{q}) - J_{exp}(\mathbf{q}_n)$ to be maximized. This is what optimal experimental design wants to achieve, optimizing the experimental input such that the practical identifiability is maximized.

Along these lines an identifiability measure has been developed by Reich. The principle of the method [18] is as follows. Given the input and assuming the model to be correct a measure for practical identifiability can be obtained by studying the correlation-like matrix \mathbf{R}_{θ} :

$$eq. 2-20 \quad \mathbf{R}_{\theta} = \mathbf{D}^{-1} \cdot \mathbf{M}_{\theta} \cdot \mathbf{D}^{-1}$$

in which the matrix \mathbf{D} equals the diagonal matrix:

$$eq. 2-21 \quad \mathbf{D} = diag\left(\sqrt{m_{1,1}}, \sqrt{m_{2,2}}, \dots, \sqrt{m_{p,p}}\right)$$

where \mathbf{M}_{θ} is the symmetric matrix with elements m_{ij} defined by:

$$eq. 2-22 \quad m_{i,j} = \frac{1}{n} \cdot \sum_{k=1}^n \frac{dh((\mathbf{q}, z(t_k)))}{dq_i} \cdot \frac{dh((\mathbf{q}, z(t_k)))}{dq_j}$$

n : Number of observations

The elements of \mathbf{D} represent the sensitivities of the individual parameters while the matrix \mathbf{R}_{θ} represents the redundancy of the parameter. The value of the inverse of the determinant of \mathbf{R}_{θ} , $|\mathbf{R}_{\theta}|^{-1}$ is used as the identifiability measure. Reich states that if $|\mathbf{R}_{\theta}|^{-1} > 10^4$ the parameter will be not practically identifiable.

2.3 Dimensional parameter identifiability analysis

2.3.1 Single parameter identifiability

Parameter identifiability implies that each (potentially) observed error-free trajectory can be associated with a single value of the identifiable parameter. This property is a direct consequence of the identifiability definition. If two values of the same parameter would give rise to the same data set, the parameter is not identifiable by definition. This means that for each identifiable parameter there will exist a parameter identification function such that:

$$\text{eq. 2-23} \quad q_i = d_i(y, z)$$

q_i :parameter i

d_i :parameter estimation function belonging to parameter i

Essential for application of dimensional analysis is the question whether this relationship is dimensionally homogenous. As estimation is concerned with a realistic physical situation, it is expected that this parameter identification function should be dimensionally homogenous. To prove this conjecture we start by assuming that the parameter is identifiable and that the parameter identification function is not dimensionally homogenous. It will be shown that these assumptions lead to a contradiction, proving that parameter identifiability implies dimensional homogeneity of the parameter identification function. The proof runs as follows:

- (i) The input-output relationship under study $y = h(z, q)$ is dimensionally homogenous. This assumption is valid as the input-output relationship describes a physical reality.
- (ii) The parameter q_i is an identifiable parameter and consequently has an estimation function d_i such that $q_i = d_i(y, z)$. This follows directly from the definition of identifiability.
- (iii) The estimation function d_i is not dimensionally homogenous by assumption.
- (iv) From the R-theorem it follows that if the rank of the dimensional matrix $[q_i, y, z]$ equals the rank of $[y, z]$, than the parameter identification d_i function would be dimensionally homogenous. As assumption (iii) states that parameter identification d_i is not dimensionally homogenous it follows directly that $r([q_i, y, z]) > r([y, z])$. As addition of a single column to a matrix can lead at most to an increase of the rank by one it follows that

$r([q_i, y, z]) = r([y, z]) + 1$. Here the notation of $r(A)$ as rank of matrix A is introduced

- (v) As the dimensional matrix $[y, z, q_1, \dots, q_n]$ has more columns than $r([q_i, y, z])$ it follows directly that $r([y, z, q_1, \dots, q_n]) \geq r([q_i, y, z])$ and in combination with (iv) that $r([y, z, q_1, \dots, q_n]) \geq r([y, z]) + 1$.
- (vi) The dimensional homogeneity of the input-output relation (i) implies that there exists a reduced dimensional matrix. As $r([y, z, q_1, \dots, q_n]) \geq r([y, z]) + 1$ (v) at least one column representing the dimensional exponents of a parameter is needed for the construction of the identity matrix part of the reduced dimensional matrix. The parameter q_i can be used for this purpose as $r([q_i, y, z]) = r([y, z]) + 1$ (iv). The reduced dimensional matrix can thus be based on the ordering of the physical quantities as: $[y, z, q_1, \dots, q_{j-1}, \dots, q_{j+1}, \dots, q_n]$, $j = 1..n, j \neq i$.
- (vii) As the input-output relationship is dimensionally homogenous it follows directly that the input-output relation is a solution of the vector of differential equations given by D-theorem. The differential equation at position $i = r([y, z]) + 1$ runs as:

$$\text{eq. 2-24} \quad \sum_{j=1}^n q_j \cdot \frac{\partial h(y, z, q)}{\partial q_j} \cdot d_{i,j} = 0$$

This equation holds as the elements $d_{i,j}$ of the reduced dimensional matrix are zero for $i < r[y, z] + 1$ and $j = r[y, z] + 1$.

- (viii) From (vii) it follows directly that the parameter q_i is locally not identifiable, and thus also not globally. This proves that the assumption of identifiability implies that the parameter estimation function is dimensionally homogenous
- (ix) Combining the R-theorem with the result (viii) gives the

Dimensional non-identifiability theorem (DI-theorem).

A parameter q_i is non-identifiable if the rank of the dimensional matrix $[y, z]$ i.e. of the observed quantities is smaller than the rank of the dimensional matrix $[y, z, q_i]$ i.e. of the observed quantities together with the parameter q_i .

A parameter that is detected to be unidentifiable with this criterion will be called *dimensionally-non-identifiable*. Any parameter for which the rank of the dimensional matrix $[y, z]$ equals the rank of the dimensional matrix $[y, z, q]$ is potentially identifiable. It will be said

that such a parameter is *not dimensionally-non-identifiable*. This somewhat cumbersome expression arises from the fact that the DI-theorem is a necessary but not sufficient condition for parameter identifiability. A direct consequence of this theorem is that a dimensionless parameter is always not dimensionally-non-identifiable.

2.3.2 Unobserved dimensions free representation

Dimensional analysis is able to detect whether a parameter is dimensionally unidentifiable. The presence of a non-identifiable parameter makes parameter estimation troublesome. The parameter estimation routine may fail, and interpretation of parameter values is difficult. In the following it will be shown that if a model is dimensionally non-identifiable, it is possible to transform this model into a model that:

- contains fewer parameters
 - contains only dimensionally-identifiable parameters
 - has an output function that is indistinguishable from the original.
- (i) The starting point is an output-input relationship $y=h(z,q)$, as has been defined before which is dimensionally homogenous, i.e. $r[y,z,q] = r[z,q]$. The parameter vector q contains p parameters. Let n be the total number of dependent and independent variables.
- (ii) The number of dependent and independent variables equals the rank of the dimensional matrix $[y,z]=n$. This means each measured variable represents a basic dimension. Addition of another measured variable with the same dimension adds no new information from the point of view of dimensional analysis. It is therefore perfectly valid to neglect additional measurements with the same dimension.
- (iii) If the I/O model is dimensionally non-identifiable, there is at least one parameter that is not identifiable. As a consequence of the DI-theorem this means that $r[y,z,q]=v > r[y,z]$.
- (iv) If the I/O model is dimensionally homogenous, then according to the II-theorem there does exist an equivalent dimensionless representation with at most $m=n+p-v$ dimensionless groups.
- (v) As m is the upper bound on the number of dimensionless groups that are needed to describe the I/O-relation, then m is also the upper bound on the number of identifiable parameter (combinations).
- (vi) According to the DI-theorem the m dimensionless groups are all not dimensionally-non-

identifiable. Together with (v) this implies that there exists an equivalent representation of the I/O-relationship that contains no dimensionally-non-identifiable parameters. However, this equivalent relationship describes the data in a dimensionless framework. This is theoretically fine, but when performing actual measurements and parameter estimation, the data can not be made dimensionless, as the parameters needed for rendering the dimensionless parameters are not known yet.

- (vii) To apply dimensional analysis to parameter estimation one needs to construct a representation free of *unobserved dimensions*. The unobserved dimensions are those dimensions that are part of the dimension of a parameter but not part of the dimension of the observations. The unobserved dimensions are represented by the rows $i > n$. As an example see the reduced dimensional matrix for 4 dimensions.

$$\text{eq. 2-25} \quad \left(\begin{array}{c|cc|cccc|c} 1 & 0 & 0 & 0 & d_{1,4} & \cdots & \cdots & \cdots & d_{1,n+p} \\ 0 & 1 & 0 & 0 & d_{2,4} & \cdots & \cdots & \cdots & d_{2,n+p} \\ \hline 0 & 0 & 1 & 0 & d_{3,4} & \cdots & d_{i,j} & \cdots & d_{3,n+p} \\ 0 & 0 & 0 & 1 & d_{4,4} & \cdots & \cdots & \cdots & d_{4,n+p} \end{array} \right)$$

Above the horizontal line are the observed dimensions, below the line the unobserved dimensions. Left of the vertical dashed lines are the columns representing the dimensional vector of the input and output. Left of the second uninterrupted line are the columns representing the dimensional vector of the physical quantities that make up the basis for making the relationship dimensionless.

- (viii) Similar to the construction of dimensionless groups parameter groups (eq. 2-9) can be constructed that are free of unobserved dimensions. These parameter combination that are free from unobserved dimensions can be constructed as:

$$\text{eq. 2-26} \quad q_j^{\text{udf}} = q_{j+n} \prod_{i=n+1}^v q_i^{-d_{ij}}$$

$i:$	$n+1 \dots v$
$j:$	$1 \dots m$

q_j^{udf} : Unobserved-dimensions-free-parameter combination j

It easily checked with the DI-theorem that these m groups are not dimensionally-non-identifiable.

- (ix) The I/O function that is transformed with these parameters contains only observed dimensions, thus only parameters that are not dimensionally-non-identifiable. The number of these parameters is $m = n + p - r[y, z, q]$. The I/O function obtained in this way has the same equivalent dimensionless representation as the original I/O model and is thus equivalent to the original.
- (x) Although the dimensional transformation of the I/O function leads to an equivalent function, the solution of the I/O function is often not known. In these cases the parameters are estimated from a numerical integration of the original model. To achieve the same result in the simulated I/O function, the original state space model can be dimensionally transformed to the representation free of unobserved dimensions.

These findings can be summarized as:

Unobserved Dimension Free representation (UDF) theorem

If the rank of the dimensional matrix $[y, z, q] = v$ and the rank of the dimensional matrix of the observations $[y, z]$ equals n then the maximum number of identifiable parameter combinations equals $p + n - v$. If $n < v$ then there are at least $v + 1 - n$ (original) parameters that are dimensionally non-identifiable. The identifiable parameter combinations can be found by gaussian reduction of the dimensional matrix $[y, z, q]$. The identifiable groups are constructed from this reduced matrix according to eq 2-26

2.4 Examples: Batch microbial growth

2.4.1 Basic model equations

In a batch reactor the growth of a heterotrophic organism oxidizing an organic compound is often described by the Monod-equation:

$$\text{eq. 2-27} \quad \frac{dX}{dt} = \mu_m \cdot \frac{S}{K_s + S} \cdot X$$

$$t = 0, \quad X = X_0$$

eq. 2-28

$$\frac{dS}{dt} = -\frac{1}{Y_s} \cdot \frac{dX}{dt}$$

$$t = 0, \quad S = S_0$$

X	: Microbial biomass density	[X.L ⁻³]
S	: Growth-limiting substrate	[S.L ⁻³]
t	: Time	[T]
μ_m	: Maximum growth rate	[T ⁻¹]
K _s	: Half-saturation constant	[S.L ⁻³]
Y _s	: Microbial yield on substrate	[X.S ⁻¹]

These two equations that together describe the batch growth dynamics are the starting point for the identifiability analysis. Apart from the biomass and substrate concentration, sometimes the so-called oxygen uptake rate (OUR) is measured by respirometry. The OUR is the amount of oxygen consumed per unit time and per unit volume. The OUR is described by:

eq. 2-29

$$OUR = \frac{\mu_m}{Y_{O_2}} \cdot \frac{S}{K_s + S} \cdot X$$

OUR : Oxygen uptake rate

[O₂.T⁻¹.L⁻³]Y_{O₂} : microbial yield on oxygen[X.O₂⁻¹]

Instead of the usual indication of units, the dimensions are indicated as X for biomass amount, S for substrate amount, L for distance and T for time. This convention is adopted to stress once more the difference between a unit and a dimension. Substrate and biomass have different dimensions, as they indicate the amount of a substance. According to the SI convention (1998), the preferred expression is mole of substance. Of course one can express both the substrate and biomass in kg per m³. Although the unit is then seemingly the same, the dimension isn't!

The identifiability of the parameters in the basic model i.e. Y_s, μ_m , K_s, S₀, X₀ will be studied in dependence on the type of measurement available; The case that both substrate and

biomass are measured is the basic model M0. However, in practice it is not always possible to measure both substrate and biomass concentration. Three different cases will be discussed in which only one type of measurement is available. The case that only substrate is measured is called M1. M2 is the case in which the oxygen uptake rate (OUR) is measured. This model contains an additional parameter Y_{O_2} . Model M3 is characterized by the measurement of only the biomass concentration.

2.4.2 Model M0

Both the substrate and biomass concentration are a function of the parameter, initial values and the time. The dimensional matrix can be set up using the dimensions T, S, X and L for the consecutive rows 1 to 4. The column sequence of the matrix is similar to the ordering of the dimensional exponents S, t, X, Y_S , μ_m , K_S , S_0 , X_0 . The dimensional matrix has been set up and transformed into an identity matrix with the associated left residual matrix. This operation gives as a result that none of the parameters are dimensionally non-identifiable. This is not surprising as all state variables are directly measured and therefore the matrices are not explicitly presented.

2.4.3 Model M1

In case of the substrate measurement only the I/O model can be described as $S = h(t, Y_S, \mu_m, K_S, S_0, X_0)$. The dimensional matrix can be set up using the following dimensions T, S, X and L for the consecutive rows 1 to 4. The column sequence of the matrix is similar to the ordering of the quantities in the I/O function, i.e. are formed by the dimensional exponents S, t, Y_S , μ_m , K_S , S_0 , X_0 . Setting up the dimensional matrix gives as a result:

$$\text{eq. 2-30} \quad \begin{pmatrix} 0 & 1 & 0 & -1 & 0 & 0 & 0 \\ 1 & 0 & -1 & 0 & 1 & 1 & 0 \\ 0 & 0 & 1 & 0 & 0 & 0 & 1 \\ -3 & 0 & 0 & 0 & -3 & -3 & -3 \end{pmatrix}$$

This matrix is transformed into the right identity matrix and the left residual matrix. This gives as a result:

eq. 2-31

$$\left(\begin{array}{ccc|cccc} 1 & 0 & 0 & 0 & 1 & 1 & 1 \\ 0 & 1 & 0 & -1 & 0 & 0 & 0 \\ \hline 0 & 0 & 1 & 0 & 0 & 0 & 1 \\ \hline 0 & 0 & 0 & 0 & 0 & 0 & 0 \end{array} \right)$$

Although four dimensions are distinguished, the rank of the dimensional matrix $[S, t, Y_s, \mu_m, K_s, S_0, X_0]$ is 3. This is reflected in the reduced dimensional matrix as the fourth row consists of zeros only. This means that the distance dimension (L) is superfluous, the S and X concentration can in this case be considered as a basic dimension in their own right. The rank of the dimensional matrix of the observations, i.e. $r[S, t] = 2$. According to the UDF-theorem this means that a maximum of $5+2-3 = 4$ parameter groups can be identified, while at least $5-4+1=2$ parameters will be dimensionally non-identifiable.

The first two rows reflect the dimensional exponents associated with the observed dimensions T and S . The third row reflects the unobserved dimension X . The parameters μ_m, K_s, S_0 are not dimensionally non-identifiable, none of them have non-zero dimensional exponent in the third row. The parameters Y_s and X_0 are dimensionally non-identifiable, as they contain a non-observed dimension. This can be seen from the presence of non-zero dimensional exponent in the third row. The parameter combination X_0/Y_s however is not dimensionally non-identifiable.

As an explicit solution for the I/O function is not known, the original model will be transformed such that only not dimensionally non-identifiable parameters remain. This can be done by using the transformation $Z=X/Y_s$. This gives the following modified model:

eq. 2-32

$$\frac{dZ}{dt} = \mu_m \cdot \frac{S}{K_s + S} \cdot Z$$

$$t = 0, \quad Z = Z_0$$

eq. 2-33

$$\frac{dS}{dt} = -\frac{dZ}{dt}$$

$$t = 0, \quad S = S_0$$

The effect of the transformation is that the parameters Y_s , and X_0 have been replaced by a single new parameter Z_0 . This representation can be used for numerical integration, needed for the parameter estimation.

2.4.4 Model M2

The I/O function is $OUR = f(t, Y_{O2}, Y_s, \mu_m, K_s, X_0, S_0)$ and contains 6 parameters. The rows of the dimensional matrix are ordered according to the dimensions T, O_2, S, X . The distance dimension is left out, as incorporation would show it to be superfluous again. The columns are ordered according to the listing of the quantities of the I/O function. Constructing again the reduced dimensional matrix $[OUR, t, Y_{O2}, Y_s, \mu_m, K_s, X_0, S_0]$ gives as a result:

$$eq. 2-34 \quad \left(\begin{array}{cccc|cccc} 1 & 0 & 0 & 0 & 0 & 1 & 1 & 1 \\ 0 & 1 & 0 & 0 & -1 & 1 & 1 & 1 \\ \hline 0 & 0 & 1 & 0 & 0 & 1 & 1 & 1 \\ 0 & 0 & 0 & 1 & 0 & -1 & 0 & -1 \end{array} \right)$$

The rank of the dimensional matrix $[OUR, t, Y_{O2}, Y_s, \mu_m, K_s, X_0, S_0] = 4$, while the rank of $[OUR, t] = 2$. This implies (UDF-theorem) that the I/O function contains maximally $6+2-4 = 4$ parameters or parameter combinations that are not dimensionally non-identifiable. There are at least $6-4+1 = 3$ original parameters dimensionally non-identifiable.

Looking at the rows under the horizontal dashed line indicates that the parameters Y_s , Y_{O2} , X_0 and S_0 are not identifiable. The parameter (combinations) μ_m , K_s , Y_s/Y_{O2} , X_0/Y_{O2} and $S_0/Y_s/Y_{O2}$ are all not dimensionally non-identifiable. The original model can be transformed into a system with only parameters that are not dimensionally non-identifiable ($Z_1 = X/X_0$, $Z_2 = S.Y_s/Y_{O2}$, $K_{ox} = K_s.Y_s/Y_{O2}$):

$$eq. 2-35 \quad \frac{dZ_1}{dt} = \mu_m \cdot \frac{Z_2}{K_{ox} + Z_2} \cdot Z_1$$

$$t = 0, \quad Z_1 = Z_{1,0}$$

$$\frac{dZ_2}{dt} = -\frac{dZ_1}{dt}$$

eq. 2-36

$$t = 0, \quad Z_2 = Z_{2,0}$$

$$OUR = \mu_m \cdot \frac{Z_2}{K_{ox} + Z_2} \cdot Z_1$$

eq. 2-37

2.4.5 Model M3

This model can be treated along similar lines as for substrate M1. The main result is that the following parameters are not dimensionally non-identifiable; μ_m , $K_s \cdot Y_s$, X_0 , $S_0 \cdot Y_s$. Using the transformation $Z = S \cdot Y_s$, $Z_0 = S_0 \cdot Y_s$ and $K_x = K_s \cdot Y_s$, the following transformed model is obtained:

$$\frac{dX}{dt} = \mu_m \cdot \frac{Z}{K_x + Z} \cdot X$$

eq. 2-38

$$t = 0, \quad X = X_0$$

$$\frac{dZ}{dt} = -\frac{dX}{dt}$$

eq. 2-39

$$t = 0, \quad Z = Z_0$$

2.4.6 Model similarity and global identifiability

An important advantage of dimensional analysis is that it brings the model to its structural essential, it might connect models that might otherwise look seemingly different. This will be illustrated by application to the study of the global identifiability properties of the models M0..M3. Holmberg [19] studied the global identifiability of the model M0 extended with an additional biomass decay term. This model proved to be identifiable. However, this does not imply that the model M0 will be identifiable, as removing one term might make a model non-identifiable [6].

It must be realized that if a parameter has been shown to be identifiable in the framework of a certain model structure, this result is independent of the units of the physical quantities involved. This is the principle of dimensional homogeneity applied to identifiability. This means that the result of the analysis is independent of the units attributed to the different state

variables, as long as the model structure is not changed.

To better show the similarity between the models some variables are renamed, and the output is written in terms of the new variable names. The results of this operation are shown in table 2.1.

Table 2-1: Overview of M0..M3 expressed with similar variable names

Model	Rename	Equation	Output
M0	$X = Z_1$ $S = Z_2$	$\frac{dZ_1}{dt} = \mu_m \cdot \frac{Z_2}{K_s + Z_2} \cdot Z_1$ $t = 0, \quad Z_1 = Z_{1,0}$ $\frac{dZ_2}{dt} = -\frac{1}{Y_s} \cdot \frac{dZ_1}{dt}$ $t = 0, \quad Z_2 = Z_{2,0}$	$y = \begin{pmatrix} Z_1 \\ Z_2 \end{pmatrix}$
M1	$Z = Z_1$ $S = Z_2$	$\frac{dZ_1}{dt} = \mu_m \cdot \frac{S}{K_s + S} \cdot Z_1$ $t = 0, \quad Z_1 = Z_{1,0}$	$y = \begin{pmatrix} Z_1 - Z_{1,0} \\ Z_2 \end{pmatrix}$
M2		$\frac{dZ_2}{dt} = -\frac{dZ_1}{dt}$	$y = \begin{pmatrix} Z_1 - Z_{1,0} \\ Z_2 - Z_{2,0} \end{pmatrix}$
M3	$X = Z_1$ $Z = Z_2$	$t = 0, \quad Z_2 = Z_{2,0}$	$y = \begin{pmatrix} Z_1 \\ Z_2 - Z_{2,0} \end{pmatrix}$

This table shows that the model M1, M2 and M3 are identical, while M0 only differs through the presence of the yield coefficient Y_s . The models M1, M2 and M3 are thus special cases of the original model M0 with $Y_s = 1$.

The main difference between the models is the type of output, M0 has two outputs X and S while the other models have a single output. However for the models M1, M2 and M3 two outputs can be reconstructed. For model M1 it follows directly from eq. 2-28 that $Z - Z_0 = S_0 - S$. This means that from the measurements of S a second output $Z - Z_0$ can be reconstructed. To obtain a similar output for model M2 one has to consider that:

$$eq. 2-40 \quad OVR = \frac{dZ_1}{dt} = -\frac{dZ_2}{dt}$$

From this it follows straightforwardly:

$$\text{eq. 2-41} \quad \begin{aligned} Z_1 - Z_{1,0} &= \int_0^t \text{OUR}(\tau) d\tau \\ Z_2 - Z_{2,0} &= - \int_0^t \text{OUR}(\tau) d\tau \end{aligned}$$

This means these two outputs similar to S and X in the model M0 can be constructed from the output OUR. The output for M3 can be constructed in the same fashion as for M1. All outputs are tabulated in table 1 using the new variable names.

As first step in investigating the global identifiability of all models M2 has been investigated. The result of the analysis is that the model is identifiable, i.e. all parameters are identifiable. The details of the analysis are not shown, they showed analogous to the analysis of Holmberg [19], with the difference that in our analysis an additional time derivative had to be taken into account.

With this result the of the other models M0,M1 and M3 can be easily checked using the following outcome of the power series expansion theorem (eq. 2-18). If $y(t) = h(q, z(t))$, with all parameters identifiable and the initial value $y(0)$ equals zero then parameter q is than also identifiable for a modified output $y'(t)$ equalling $y(t)+g(q)$.

(i) The first equation of the system of equations generated according to eq. 2-18 for the original output $y(t)$ runs as: $0=0$ and gives thus no information on identifiability.

(ii) As the parameters are identifiable this means that the subsequent equations imply: $q=r$.

(iii) The first equation of the system for the modified output $y'(t)$ runs as: $q_0+g(q)=r_0+g(r)$.

(iv) The remaining equations for the modified output $y'(t)$ are the same as for the $y(t)$ as

$$\frac{dg(q)}{dt} = 0.$$

(v) Results iii and iv together show that the subsequent equations imply $q=r$ and thus that the model equations are also identifiable for the modified output.

As model M2 has a zero initial output for both output, it follows directly that M1 and M3 are also globally identifiable. For model M0 the identifiability of M1 implies that the parameter μ , K_S and $Z_{1,0}=X_0/Y_S$, can be identified. However as X_0 is measured, Y_S can be directly found from $Z_{1,0}$ and all parameters are identifiable.

2.4.7 Practical identifiability model M2.

The practical identifiability of the estimation of the Monod parameters from a batch culture with only substrate measurement (model M2) will be studied using dimensional analysis. The main aim is to show the usefulness of the application of dimensional analysis. The practical identifiability measure $|R_0|^{-1}$ as defined before will be used. The most informative experiment can be designed by looking for the optimal value of this identifiability measure in relation to the experimental input. In case of Monod kinetics this is an essential step, as has been shown by Holmberg for a batch culture [19]. In a batch culture depending on the chosen initial substrate level the variance of the estimated maximal growth rate constant can range between 5% and 700%.

The practical identifiability measure should preferably be dimensionless. The measure is then independent of the choice of units. The measure $|R_0|^{-1}$ as discussed before is indeed dimensionless as the inspection of the matrix R quickly reveals.

The practical identifiability measure $|R_0|^{-1}$ depends on:

- the parameters μ_m , K_s , S_0 , X_0/Y_s

It must be noted that the two parameters S_0 , X_0/Y_s are assumed to be under experimental control. The initial substrate concentration can be freely chosen and measured. Although the biomass concentration can not be measured it is assumed that the initial biomass concentration can be influenced by the amount of seed.

- the measuring frequency f_M

The measuring frequency describes the number of observation per time unit. In general a higher measuring frequency will lead to better practical identifiability as more information is obtained. In this thesis we are mostly interested in on-line measurements and we will analyze the situation that the frequency is sufficiently high.

- the cultivation time.

Holmberg showed that with an increasing experimental time the practical identifiability increased. With insufficient culture time the substrate concentration at the end of the experiment is still much higher than K_s . This means that during the experiment the parameter K_s does not influence the output and thus is not identifiable. Consequently instead of the experimental time the substrate concentration at the end of the experiment (S_e) will be used as a measure of the cultivation time.

Accepting this list of relevant quantities it is clear that there exist a relation between the practical identifiability measure $|R_0|^{-1}$ and the listed quantities.

$$\text{eq. 2-42} \quad |R_0|^{-1} = f(S_E, f_M, \mu_m K_S, S_0, X_0/Y_S)$$

Applying the Π -theorem to this relationship gives the dimensionless relationship

$$\text{eq. 2-43} \quad |R_0|^{-1} = f(\Pi_1, \Pi_2, \Pi_3, \Pi_4)$$

in which,

$$\begin{aligned} \text{eq. 2-44} \quad \Pi_1 &= \frac{K_S}{S_0} \\ \Pi_2 &= \frac{X_0}{S_0 \cdot Y_S} \\ \Pi_3 &= \frac{S_E}{S_0} \\ \Pi_4 &= \frac{f_M}{\mu_m} \end{aligned}$$

Assuming that Π_4 is so large that a further increase no longer gives a substantial improvement of the practical identifiability, it may be concluded that the practical identifiability is in essence only influenced by the three dimensionless groups Π_1 , Π_2 and Π_3 . The number of influencing variables to be optimized is reduced by two, the number of observed dimensions. This makes the optimization less complicated, as fewer variables need to be taken into account.

Figure 2-1 shows the results for the effect of Π_1 , Π_2 on the identifiability measure $|R_0|^{-1}$. The dimensionless parameter Π_3 has a value of 10^4 . Based on experimental times listed in literature this is a realistic value. The X-axis shows the log value of Π_1 , the Y-axis the log value of Π_2 . The value of $\log(|R_0|^{-1})$ is shown as contour lines. The figure has two distinct minima expressed as log values around (-1.4, -0.9) and at (-4, -0.9). The last minimum is clearly lower and would be the preferable experimental set up.

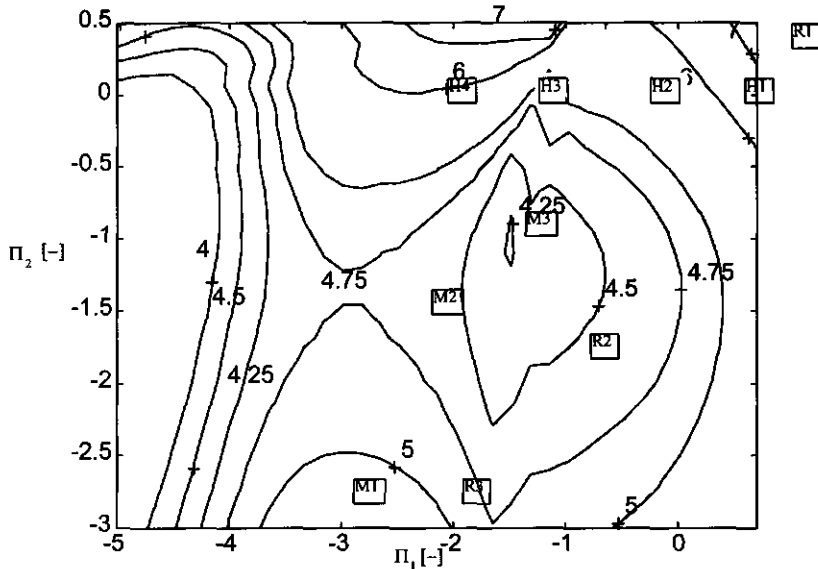


Figure 2.1: Contourplot of $|R_\theta|^{-1}$ as a function of Π_1 and Π_2 . Note the logarithmic scale of the X and Y-axis. The numbers denote $\log(|R_\theta|^{-1})$ values.

Practical identifiability of the Monod model in batch culture has been previously investigated in literature. Holmberg investigated the effect of the ratio $K_s/S_0 = \Pi_1$ by lowering the K_s value. This gives a number of points parallel to the horizontal axes (H1,H2,H3,H4). Holmberg found the point H3 to be the optimal experimental design.

Yoo [20] proposed a sequential design based on the Fischer information index. The points M1, M2 and M3 represent sequential improvements of the estimation. It shows nicely that indeed their approach leads to an improved estimate. Robinson [21] investigated the identifiability with a visual inspection of the sensitivity functions, and studied the points R1, R2 and R3. They found the point R2 to be optimal.

It is interesting to note that the results of these studies conform with this figure. This is clearly a good indication of the soundness of this approach. It also shows the advantage of this approach. The optimal location can be directly read from one curve.

It is also clear that all these previous studies missed the existence of a better minimum. This is probably due to the fact that in all studies the initial biomass concentration was fixed.

2.5 Discussion

Dimensional analysis is a tool widely used in mathematical modelling. It's strength lies in the fact that is an easy technique that may simplify the model under study. This simplification will save work and effort in subsequent modelling steps.

In parameter estimation straight application of the Π -theorem is not possible, as the parameters needed for construction of dimensionless groups are unknown. The essence of this chapter is that a meaningful application of dimensional analysis is possible by looking at the *unobserved dimension free representation*. This means one aims not at removing all dimensions (dimensionless representation) but at removing those dimensions that are not part of the dimensions of the observations. In this way information on what is observed is incorporated in the dimensional analysis. With this in mind it was shown to be beneficial to apply dimensional analysis to the problem of theoretical and practical identifiability.

Theoretical identifiability

One type of non-identifiability can be assessed with the dimensional method developed in this paper (DI-theorem). The source of the non-identifiability is the incomplete observation of all the fundamental dimensions involved. In this way the method gives more insight into the nature of the problem of parameter non-identifiability.

Using the reduced dimensional matrix it is possible to transform the model such that the parameters remaining have only observed dimensions. This technique is very useful as it can be used without specific knowledge of the functional relationship between observations and parameters. In this way any dimensionally non-identifiable parameters are removed from the model structure.

Dimensional analysis is not a replacement for formal theoretical identifiability proofs. It is more a tool to be applied before embarking on a more formal method. The gain to be expected is that if dimensional non-identifiability occurs this can be removed, and a simpler transformed model can be used as a starting point for the formal method. This has been illustrated with an example of Monod kinetics during batch cultivation.

Practical identifiability analysis

If a practical identifiability measure is used that is dimensionless, application of the Π -theorem leads to a substantial reduction of the influencing factors. In this way it is easier to define an optimal experimental design. This has been done for the model M1, and indeed showed to give a good insight in the design of an optimal experiment.

Dimensional analysis can thus profitably be applied both for theoretical and practical identifiability analysis. Depending on the model, using the dimensional analysis might:

- (i) Give insight into the presence of source of non-identifiability
- (ii) Remove this source of non-identifiability
- (iii) Give a model with a smaller number of parameters for identifiability analysis.
- (iv) Show a relation between identifiability of parameters of related models.
- (v) Give a better insight in the optimal experimental design.

Dimensional analysis alone is not a sufficient tool for theoretical or practical identifiability analysis. Other formal tools are yet needed, however, applying dimensional analysis prior to formal identifiability analysis reduces the complexity of the problem at hand. It is concluded that dimensional analysis is a powerful and easy method that merits wider application in parameter estimation.

2.6 References

1. Aris, R., *Mathematical modelling techniques*. 1978, London: Pitman.
2. Astarita, G., *Dimensional analysis, scaling and orders of magnitude*. Chemical engineering Science, 1997. **52**(24): p. 4681-4698.
3. Langhaar, H.L., *Dimensional Analysis and the Theory of Models*. 1951, New York: John Wiley & Sons.
4. Zlokarnik, M., *Dimensional Analysis and Scale-up in Chemical Engineering*. 1991, Berlin: Springer.
5. Bellman, R. and K.J. Astrom, *On Structural Identifiability*. Mathematical Biosciences, 1970. **7**: p. 329-339.
6. Walter, E. and L. Pronzato, *Qualitative and Quantitative Experiment Design for Phenomenological Models- A Survey*. Automatica, 1990. **26**(2): p. 195-213.
7. Walter, E., *Identifiability of State Space Models*. 1982, Berlin: Springer.
8. Zheng, Q., *Computer Algebra is indispensable in some problems of mathematical biology*. Mathematical Biosciences, 1998. **151**: p. 219-225.
9. VanRolleghem, P.A., M. van Daele, and D. Dochain, *Practical Identifiability of a Biokinetic Model of Activated Sludge Respiration*. Water Research, 1995. **29**(11): p. 2561-2570.
10. Duncan, W.J., *Physical similarity and dimensional analysis*. 1953, London: Arnold & Co.
11. Focken, C.M., *Dimensional methods and their application*. 1953, London: Arnold & Co.
12. Ljung, L. and T. Glad, *Modeling of dynamic systems*. 1994, Prentice Hall: New Jersey.
13. Grewal, M.S. and K. Glover, *Identifiability of Linear and Nonlinear Dynamical Systems*. IEEE Transactions on Automatic Control, 1976: p. 833-837.
14. Beck, J.V. and K.J. Arnold, *Parameter estimation in Engineering and Science*. 1977, New York: John Wiley and Sons.
15. Walter, E. and L. Pronzato, *On the identifiability and distinguishability of nonlinear parameteric models*. Mathematics and Computers in Simulation, 1996. **42**: p. 125-134.

16. Pohjanpalo, H., *System Identifiability Based on the Power Series Expansion of the Solution*. Mathematical Biosciences, 1978. **41**: p. 21-33.
17. Chappell, M.J., K.R. Godfrey, and S. Vajda, *Global Identifiability of the Parameters of Nonlinear Systems with Specified Inputs: A comparison of methods*. Mathematical Biosciences, 1990. **102**: p. 41-73.
18. Seber, G.A.F. and C.J. Wild, *Nonlinear regression*. 1989, New York: John Wiley & Sons.
19. Holmberg, A., *On the Practical Identifiability of Microbial Growth Models Incorporating Michaelis-Menten Type Nonlinearities*. Mathematical Biosciences, 1982. **62**: p. 23-43.
20. Yoo, J.Y., et al., *Experimental Design for Parameter Estimation from Batch Culture*. Biotechnology and Bioengineering, 1986. **XXVIII**: p. 836-841.
21. Robinson, J.A. and J.M. Tiedje, *Nonlinear Estimation of Monod Growth Kinetic Parameters from a Single Substrate Depletion Curve*. Applied and Environmental Microbiology, 1983. **45**(5): p. 1453-1458.

3. A THEORETICAL MODEL OF A SINGLE COMPOSTING PARTICLE: DEVELOPMENT AND SIMULATION	68
3.1 INTRODUCTION	68
3.2 MODEL DEVELOPMENT	69
3.2.1 <i>Introduction</i>	69
3.2.2 <i>Geometric structure</i>	72
3.2.3 <i>State variables</i>	73
3.2.4 <i>Conversion reactions</i>	74
3.2.5 <i>Diffusional mass transport</i>	77
3.2.6 <i>Convective mass transport</i>	78
3.2.7 <i>Model equations</i>	82
3.3 MODEL BEHAVIOR	85
3.3.1 <i>Model input and output</i>	85
3.3.2 <i>OUR and state variables</i>	88
3.3.3 <i>State variable profiles</i>	90
3.3.4 <i>OUR sensitivity analysis</i>	93
3.3.5 <i>Waste characteristic analysis</i>	96
3.4 MODEL COMPARISON	100
3.4.1 <i>Effect of an anaerobic period</i>	102
3.4.2 <i>Combined effect of oxygen and moisture</i>	103
3.4.3 <i>Pseudo effect of high temperature</i>	105
3.5 DISCUSSION AND CONCLUSIONS.....	106
3.6 REFERENCES	110

3. A theoretical model of a single composting particle: development and simulation

3.1 *Introduction*

The Oxygen Uptake Rate (OUR) is the amount of oxygen that is taken up by a unit sample of waste in a unit period of time. It is the most important composting process rate indicator as it is directly linked to the composting reaction[1], it is linearly linked to heat production independent of molecular substrate composition [2, 3]and it is a direct measure of compost stability[4]. The OUR depends strongly on the state of the waste, e.g. temperature and moisture content influence the OUR [5-7].

To predict the OUR a kinetic model is needed that relates the rate determining factors to the OUR. Kinetic models developed so far are empirical multiplicative models [1]. Multiplicative models have the following structure:

$$\text{eq. 3-1} \quad \text{OUR}(x_1, x_2, \dots, x_n) = \text{OUR}_s \cdot f_1(x_1) \cdot f_2(x_2) \cdots f_n(x_n)$$

OUR	: Oxygen Uptake Rate	[mol O ₂ .m ⁻³ .s ⁻¹]
OUR _s	: Oxygen Uptake Rate under standard conditions	[mol O ₂ .m ⁻³ .s ⁻¹]
x _i	: Rate determining factor i, i=1..n	
n	: Number of rate determining factors	
f _i	: Function describing the effect of rate determining factor factor i	

The functions f_i describe the effect of a specific rate determining factor on the OUR. If the OUR is measured under standard conditions all functions have the value 1. Two questionable assumptions are implied by the use of multiplicative models. The first is that the rate determining factor are supposed to act independent of each other. This is an assumption that requires further investigation, as during composting the waste composition and structure strongly changes. The second is that the waste is treated as a kind of homogenous matter, the distributed nature of the waste composition is not taken into account. As a waste sample

contains many different particles accepting this assumption without further examination is doubtful.

A theoretical model is proposed representing the main biological and transport processes occurring in a single composting particle. The theoretical model is synthesized on the basis of principles from microbiology, mass transfer and biotechnology. This approach enables use of scientific knowledge already available and relates phenomena in composting to more general biotechnological principles. The model is based on seven state variables: particle size, insoluble substrate, soluble substrate, dissolved oxygen, biomass, inert material and water. The model describes the temporal development and if necessary the spatial development of the state variables. The processes of microbial growth, microbial decay, microbial hydrolysis, diffusion and volumetric change are included. Such models are up to now lacking for composting. A first approach to a state-space model for composting kinetics was presented in a previous publication [8]. In this chapter the model is extended in the sense that the role of water is further elaborated

The main application of the model is to predict the Oxygen Uptake Rate (OUR) of a composting particle in relation to the particle state. The development of in time of the OUR and main state variables was studied in detail for the so-called nominal parameters. The nominal parameters set describes the composting of chicken manure under thermophilic conditions. A parameter sensitivity analysis was performed for the OUR. The effect of the waste characteristics on the OUR was further studied by changing the corresponding parameter values. All information obtained in this way allows an understanding of the sequence of processes occurring in the particle.

Analysis of the theoretical model shows that the main assumptions underlying the use empirical multiplicative models are not justified. Multiplicative models will thus not suffice to describe composting kinetics, this will be shown by some examples from literature. The theoretical model, in contrary to multiplicative models, can explain these examples. Some comments will be made on the steps necessary to develop a practical model from the theoretical model.

3.2 Model development

3.2.1 Introduction

The volume of a waste particle is made up of four components, water, insoluble substrate,

inert matter and aerobic biomass. Although these components are not pure, the four components have distinct physical, chemical and biological properties. Except for water these components are treated as solid phases existing in tiny lumps. The solid phases interact only via the water phase that is present everywhere within the particle. The tiny particles form together a porous matrix, of which the pores are filled with water. The boundary of the waste particle is the interface with the gas phase, by definition a waste particle thus contains no gas. The water contains soluble substrate that is produced by microbial hydrolysis from insoluble substrate. This soluble substrate is oxidised by aerobic micro-organisms, transforming the soluble organic matter into carbon dioxide and new micro-organisms, while producing heat. This reaction, called the composting reaction, is the basis of the whole composting process. The waste particle is exposed to a gas phase that serves as the source of oxygen needed for the composting reaction. From the gas-waste particle interface the oxygen will diffuse via the water phase into the particle. The concentration gradient necessary to induce diffusion is created by the oxygen consumption by the aerobic biomass.

A typical penetration depth of oxygen within the particle is estimated to be in the order of magnitude of 50 µm [8]. This limited penetration is due to diffusion transport resistance inside the particle, and not by a mass transfer limitation at the gas phase side. Due to the limited penetration of oxygen the core of the waste particle can be anaerobic. Figure 3.1 shows a schematic representation of the particle.

Within the anaerobic core the particle insoluble inorganic material will be converted into soluble substrate by microbial hydrolysis. The hydrolysis reaction is brought about by exoenzymes excreted by anaerobic micro-organisms. Within the anaerobic region the hydrolysis products will be rapidly transformed by fermentative organisms into different fermentation products, mainly volatile fatty acids as acetic acid and propionic acid. The energy gained by the organisms from the hydrolysis and fermentation reactions is small compared to the energy gained from oxidation of these compounds. The energy and the anaerobic biomass produced by these reactions is consequently neglected. The rate of the fermentation reactions is in general much higher than the hydrolysis rate. The chain of reactions occurring under anaerobic conditions can thus be replaced by a single reaction converting insoluble organic material into soluble fermentation products. The rate of this lumped solubilisation reaction is determined by the hydrolysis rate while the products composition is determined by the fermentation reactions and the composition of the original insoluble organic matter.

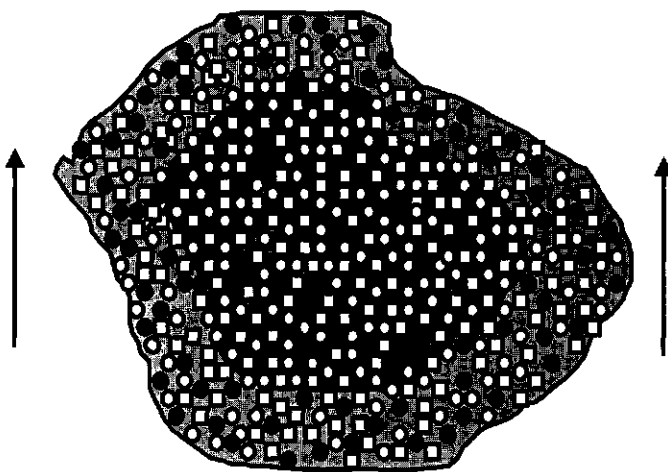


Figure 3.1: Schematic representation of a waste particle, the outer thick black line indicates the boundary between the gas phase and the particle. The gas phase is flushed with a gas stream (arrows). The white squares indicate the insoluble substrate, the white circles the inert matter, the black circles the aerobic biomass. The tiny lumps of the solid components form a matrix of which the pores are water filled. The gray area between the tiny particles indicates the water phase. The water in the outer part of the particle contains dissolved oxygen (light gray), the water in the inner region (dark gray) is anaerobic, due to oxygen depletion by the aerobic biomass.

Carbon dioxide will diffuse to the edge of the particle and be removed with the gas flow. Carbon dioxide is assumed not to influence transport and conversion processes and will no longer be considered. Other mineralization products like ammonia and sulphate will not be considered for similar reasons. Nutrients are assumed to be sufficiently present. During practical composting the temperature of the material usually increases because of the heat produced and a gradient of temperature within a composting pile is observed. Because of the small size of the particles almost no temperature gradient exists within the particle. [8]. Therefore the temperature gradient over the particle may be neglected. In most modern composting operations a temperature control is employed, resulting in a fairly stable temperature over time. This means that individual particles will be exposed to a constant temperature in time. In this paper therefore only particles with a homogenous temperature in space and time are considered.

Summarising a waste particle is a water filled porous matrix, consisting of two regions, a thin outer aerobic layer and a larger inner anaerobic region. The anaerobic region serves as a

substrate base for the aerobic layer. Insoluble material is hydrolysed and the soluble products are subsequently transported by diffusion to the aerobic layer. Within the aerobic region the population of aerobic micro-organisms oxidises the soluble substrate and new aerobic biomass is formed. Decay of the aerobic biomass again leads to the production of new insoluble material. The OUR is a measure of the actual microbial reaction rate. The diffusional transport rate of oxygen, the diffusional transport rate of the soluble substrate and the solubilisation rate may limit the microbial reaction rate. It depends on the state of the system which process or combination of processes will be determining the overall composting rate, a mathematical model is needed to find out which process is rate determining.

3.2.2 Geometric structure

The geometric structure of the composting particle is represented as a two-sided flat plate (Fig 3.2). The left side is the centre of the plate where no net flux occurs. At the right side the particle is bounded by the gas phase interface. The flat plate representation can be used to model other geometry's also as long as they have the same specific surface area [9, 10] and the conversion takes place in a small layer of the particle next to the gas interface. As the penetration depth of oxygen is small this approach seems valid. For most regular bodies the specific surface area can be written as:

$$\text{eq. 3-2} \quad A_s = \frac{\alpha}{L_c}$$

As	: Specific area	$[\text{m}^2 \cdot \text{m}^{-3}]$
α	: Body specific constant	$[-]$
L_c	: Characteristic size measure of the body	$[\text{m}]$

In the case of a sphere $\alpha = 3$ and L_c equals the radius of the sphere, in case of a cylinder $\alpha = 2$ and L_c equals the radius of the cylinder, in case of a two-sided flat plate $\alpha = 1$ and L_c is half of the plate thickness. As a two-sided flat plate represents the geometry of the waste particle, the specific surface area of a particle is determined by the half-plate thickness. This measure is called the characteristic particle size, and will be used to characterise the surface area of the waste particle.

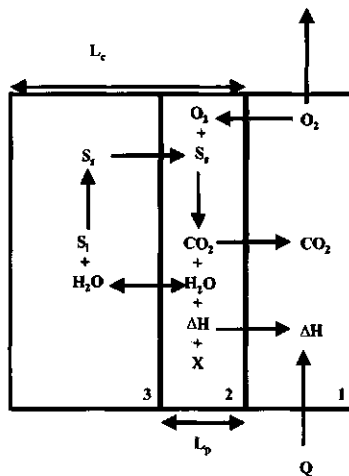


Figure 3.2: Flat plate representation of the waste particle. The rectangle 1 indicates the gas phase, that is flushed with a gas flow Q and acts as a source of oxygen (O_2) and as sink for carbon dioxide (CO_2) and heat (ΔH). As the whole system is isothermal and the gas phase is assumed to be saturated with water vapor no removal of water takes place. The transport rate of oxygen between the gas phase and the particle is determined by the rate of diffusion inside the particle. The area 2 indicates the aerobic segment. Here soluble substrate (S_s) is oxidized yielding carbon dioxide, heat, water and new biomass (X). In the anaerobic core, area 3 the soluble substrate is produced from insoluble substrate (S_i). This soluble substrate is transported by diffusion to the aerobic region. The decay of microbial biomass is not indicated.

3.2.3 State variables

The state variables describe all relevant properties of the waste particle under consideration. Based on the previous description the following variables are taken into account: the aerobic biomass concentration X , the dissolved oxygen concentration O_2 , the soluble substrate concentration S_s , the insoluble substrate concentration S_i , the insoluble inert material concentration I and the water content W . The tiny lumps of inert material and insoluble substrate are considered impermeable and water is retained only at the surface of these lumps via adhesive forces. The behaviour of the biomass colonies with respect to water is more complex. The water is partly retained within the cell and partly in the pores between the cells inside the colony. These water retaining forces inside the microbial colony are considered to

be much bigger than those of the other two insoluble components. That is why water is divided in two separate phase the colony bounded water and the remaining free water. The water content therefor refers to the free water i.e. the water not retained in the colony and will be expressed as volume fraction ε_w . If not otherwise mentioned, water will refer to the free water. All other components are expressed as concentrations i.e. as the amount of the component per particle volume. This definition eases the structuring of the mass balances, however it lacks a thermodynamical meaning. This has to be considered for the dissolved species when their influence on kinetics is described. The size of the lumps of insoluble compounds is assumed to be so small, that the system can be described as a continuum.

3.2.4 Conversion reactions

Three conversion reactions are distinguished, growth and decay of aerobic biomass and the solubilisation of the insoluble substrate. The aerobic biomass growth is modeled with a Monod-type of growth model. The growth of the aerobic biomass is modeled with an explicit dependence on oxygen and soluble substrate.

$$\text{eq. 3-3} \quad R_G = \mu_m \cdot \frac{S_s}{K_s \cdot \varepsilon_w + S_s} \cdot \frac{O_2}{K_{O_2} \cdot \varepsilon_w + O_2} \cdot X$$

R_G	: Growth rate of biomass	$[\text{mol X.m}^{-3}.\text{s}^{-1}]$
X	: Biomass concentration	$[\text{mol X.m}^{-3}]$
O_2	: Oxygen concentration	$[\text{mol O}_2.\text{m}^{-3}]$
S_s	: Soluble substrate concentration	$[\text{mol S}_s.\text{m}^{-3}]$
μ_m	: Maximal conditional growth rate	$[\text{s}^{-1}]$
ε_w	: Free water fraction	$[-]$
K_{O_2}	: Half saturation constant oxygen	$[\text{mol O}_2.\text{m}^{-3}]$
K_s	: Half saturation constant soluble substrate	$[\text{mol S}_s.\text{m}^{-3}]$

In case no other factors limits the specific growth rate, the half-saturation constant denotes that concentration at which the growth rate reaches half of its maximum value. As growth takes generally place in the aqueous phase, the half-saturation constant expresses the activity (concentration) of the limiting substance in the water phase. As mentioned earlier concentrations are however expressed on the total particle volume. Therefore the half-

saturation constants need to be expressed on the particle volume basis and not on basis of the water phase. This is accomplished by the multiplication with ε_w . The biomass decay rate R_d is given by:

$$\text{eq. 3-4} \quad R_d = b \cdot X$$

R_d : Biomass decay rate [mol X.m⁻³.s⁻¹]

b : Biomass decay rate constant [s⁻¹]

This means that the net production rate of biomass R_x can be written as:

$$\text{eq. 3-5} \quad R_x = R_G - R_d$$

R_x : Net biomass production rate [mol X.m⁻³.s⁻¹]

The consumption rate of oxygen R_{O_2} is linearly related to the production rate of the aerobic biomass and is expressed as:

$$\text{eq. 3-6} \quad R_{O_2} = \frac{R_G}{Y_{O_2}}$$

R_{O_2} : Consumption rate of oxygen [mol O₂.m⁻³.s⁻¹]

Y_{O_2} : Biomass yield on oxygen [mol X.mol O₂⁻¹]

The hydrolysis rate of insoluble substrate R_h is described by:

$$\text{eq. 3-7} \quad R_h = k_h \cdot S_i$$

S_i : Insoluble substrate concentration [mol S_i.m⁻³]

R_h : Hydrolysis rate [mol S_i.m⁻³.s⁻¹]

k_h : Hydrolysis rate constant [s⁻¹]

The net production of soluble substrate is both influenced by the hydrolysis rate and the

soluble substrate consumption rate. The net production of soluble substrate R_{S_s} can thus be written as:

$$\text{eq. 3-8} \quad R_{S_s} = R_h - \frac{R_G}{Y_{S_s}}$$

R_{S_s}	: Net production rate of soluble substrate	[mol S _s .m ⁻³ .s ⁻¹]
Y_{S_s}	: Biomass yield on soluble substrate	[mol X.mol S _s ⁻¹]

The net production rate of insoluble substrate R_{S_i} is given by:

$$\text{eq. 3-9} \quad R_{S_i} = -R_h + \frac{R_d}{Y_{S_i}}$$

R_{S_i}	: Net production rate of insoluble substrate	[mol S _i .s ⁻¹]
Y_{S_i}	: Biomass yield on insoluble substrate	[mol X.mol S _i ⁻¹]

The second term describes the conversion of dead biomass into insoluble substrate, the stoichiometric coefficient is given as a biomass yield. This somewhat counter intuitive representation has been selected to get a consequent notation of the stoichiometric coefficients.

During the oxidation of soluble substrate water is formed, however water is also needed for the construction of new cells as the largest part of a cell consists of water. Microbial culturing is generally performed in aqueous culture and the amount needed for new cells is small compared to the amount present. Therefor the amount of water needed for new cells is not considered in aqueous cultures. In composting however the amount needed for the construction of new cells may locally be considerable compared to the amount locally present and should therefore be considered. The amount of water needed for hydrolysis is neglected.

The net water production rate R_w may therefor be written as:

$$\text{eq. 3-10} \quad R_w = -\Psi \cdot R_x + \frac{R_G}{Y_w}$$

R_w	: Net production rate of water	[mol W.s ⁻¹]
Ψ	: Biomass water content	[mol W.mol X ⁻¹]
Y_w	: Biomass yield expressed on water	[mol X.mole W ⁻¹]

3.2.5 Diffusional mass transport

As water is fluid and interacts with solid surfaces it moves as a result of a water content gradient within the particle. Such a gradient can develop as a result of drying or spatial differences in degradation of insoluble substrate. Although this transport has no common physical background with diffusion of dissolved species, its transport rate is often treated as being linearly related to the water content gradient, giving diffusion like behaviour. The colonies have the strongest binding force with respect to water and are therefore assumed to have constant water content irrespective of the amount of free water remaining. The remaining free water is attached through the action of surface adhesive forces to the surface of the other insoluble particles. These forces tend to bring the water distribution to an equilibrium condition in which each insoluble tiny lump of insoluble substrate and inert material is surrounded by the same equilibrium amount of water. It is assumed that this equilibrium is always instantaneously reached. These assumptions imply a spatially constant volumetric free water fraction ε_f based on the total volume excluding the biomass. This exclusion is because of the strong water binding inside the colony. The ε_f will be expressed as:

$$\text{eq. 3-11} \quad \varepsilon_f = \frac{V_{p,w}}{A.L_c - V_{p,X}}$$

$V_{p,w}$: Total free water volume within the particle	[m ³]
$V_{p,X}$: Total biomass volume within the particle	[m ³]
ε_f	: Equilibrium free water filled porosity	[\cdot]

These assumption with respect to the distribution of water are quite strong, however insufficient information is available to refine the assumptions. It is important to note that the equilibrium free water fraction is different from the free water fraction ε_w . This variable has been introduced previously as a conversion factor from water based concentration to particle

volume based concentrations. Although in practice the difference between these two variables will be very small as the biomass volume is relatively small, they need to be distinguished for a further coherent development of the model.

The soluble substrate and oxygen are transported via diffusion in the water phase. This diffusion is hindered due to the presence of impenetrable particles of insoluble and inert material. The biomass colonies represent also a barrier to diffusion, however this obstruction is only partial as diffusion is still possible within a biomass colony, as the biomass colonies contains pores with water. As the transport distance is also increased due to the increased tortuosity the effective diffusion coefficient will decrease. The effective diffusion coefficient is calculated as:

$$\text{eq. 3-12} \quad D_{i,\text{eff}} = D_i \cdot \varepsilon_w^2$$

$D_{i,\text{eff}}$: Effective diffusion coefficient of compound i $[\text{m}^2 \cdot \text{s}^{-1}]$
 D_i : Diffusion coefficient of compound i in pure water $[\text{m}^2 \cdot \text{s}^{-1}]$

Of course this represents again a simplification, however this type of relationship is widely used in modelling sediments and soils [11, 12]. Insoluble components diffusion transport is excluded due to their grain size.

3.2.6 Convective mass transport

As the amount of components present in the waste particle is changing during composting the particle as a whole is expected to undergo volume changes. Assuming the particle to retain its integrity, i.e. it does not break or crack, a change in particle volume is equivalent to a change in particle size. Models that take volume changes of the system itself into account are relatively scarce compared to models with constant volume systems, therefore this point will be more in detail discussed.

Figure 3.3 shows a schematic representation of a certain particle volume V_p at time t with an area A and a characteristic particle size L_c . The components in the volume V_p fill this volume up and the total component volume equals the volume V_p . Within a certain time step Δt the volume $V_p(t)$ has increased and has become the volume $V_p(t+\Delta t)$. This increase of the volume

V_p leads to an outward mass flow, as the newly produced material can not be contained within the volume $V_p(t)$. Material leaves (in case of net volume production) or enters (in the case of net breakdown of volume) the volume V_p at $z=L_c$ as the boundary at $z=0$ has been chosen as a reference point. This means that at L_c at time t a volumetric mass flow with a velocity u occurs that equals:

$$\text{eq. 3-13} \quad u(t) \approx \frac{1}{A} \frac{V_p(t + \Delta t) - V_p(t)}{\Delta t}$$

A	: Total surface area of the particle	[m ²]
V_p	: Particle volume	[m ³]
t	: Time	[s]
Δt	: Small time increment	[s]
u	: convective velocity	[m.s ⁻¹]

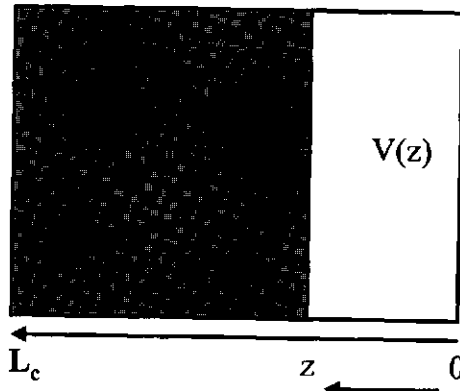


Figure 3.3: Occurrence of a convective flow u within the waste particle as a result of change of the volume of the components contained in volume $V(z)$. u is the convective flow at location z . A is the total cross-sectional area of the flat plate system considered. $V(z)$ is the volume from the particle-gas boundary until the specific depth z . At the right side the particle is assumed fixed, the left side represents the center of the particle.

The exact value of the convective velocity can be found by having Δt approach zero. This limit yields straightforwardly:

$$\text{eq. 3-14} \quad u(t) = \frac{dV_p(t)}{dt}$$

It is important to note the same type of movement will occur within the particle at each depth z . The reasoning above yielding eq 3-14 is valid for each component volume V that exist within the particle. Associated with each location z within the particle is the total components volume V between 0 and z , equalling:

$$\text{eq. 3-15} \quad V(z) = z \cdot A \quad z \leq L_c$$

z : Distance from gas-particle interface [m]

This implies that at each location z there is an associated convective flow $u(z)$.

$$\text{eq. 3-16} \quad u(z) = \frac{1}{A} \cdot \frac{dV(z)}{dt}$$

The volume $V(z)$ can be divided in the volume of the water phase and the insoluble compounds.

$$\text{eq. 3-17} \quad V(z) = V_{S_i}(z) + V_I(z) + V_X(z) + V_w(z)$$

V_{S_i} : Volume of insoluble substrate between 0 and z [m³]

V_I : Volume of inert material between 0 and z [m³]

V_X : Volume of biomass between 0 and z [m³]

V_w : Volume of free water between 0 and z [m³]

Consequently the rate of change of the components volume can be written as:

$$\text{eq. 3-18} \quad \frac{dV(z)}{dt} = \frac{dV_{S_i}(z)}{dt} + \frac{dV_I(z)}{dt} + \frac{dV_X(z)}{dz} + \frac{dV_w(z)}{dz}$$

The volume change of the insoluble species S_i, X and I is a result of the production rate of the insoluble species and can be calculated as:

$$\text{eq. 3-19} \quad \begin{aligned} \frac{dV_{S_i}(z)}{dt} &= A \int_0^z \frac{R_{S_i}(\zeta)}{\rho_{S_i}} d\zeta \\ \frac{dV_X(z)}{dt} &= A \int_0^z \frac{R_X(\zeta)}{X_m} d\zeta \\ \frac{dV_I(z)}{dt} &= 0 \end{aligned}$$

ρ_{S_i}	: Specific density of insoluble substrate	[mol S _i .m ⁻³]
X_m	: Maximal density of biomass	[mol X.m ⁻³]
ζ	: Integration variable	[m]

The volume change of the water phase is not a result of the local production of water alone as it is the case with the insoluble species above. Water is assumed to redistribute instantaneously over the whole particle. The volume of (free) water within a specific volume V(z) is thus determined by the equilibrium free water fraction ε_f at that instance. It follows directly from the definition of the equilibrium free water that:

$$\text{eq. 3-20} \quad \frac{dV_w(z)}{dt} = \frac{d\varepsilon_f(V(z)-V_X(z))}{dt}$$

Applying the chain rule gives:

$$\text{eq. 3-21} \quad \frac{dV_w(z)}{dt} = \varepsilon_f \cdot \frac{d(V(z)-V_X(z))}{dt} + (V(z)-V_X(z)) \frac{d\varepsilon_f}{dt}$$

Substituting eq. 3-18 and using the knowledge that the inert material is not converted gives the following result:

$$\text{eq. 3-22} \quad (1-\varepsilon_f) \frac{dV(z)}{dt} = \frac{dV_{S_i}(z)}{dt} + (1-\varepsilon_f) \frac{dV_X(z)}{dz} + (V(z) - V_X(z)) \frac{d\varepsilon_f}{dt}$$

By substituting eq. 3-22 and eq. 3-19 in eq. 3-16 gives the following result for the convective velocity.

$$\text{eq. 3-23} \quad u(z) = \left(\frac{z - \int_0^z \frac{X}{\rho_X} d\zeta}{1-\varepsilon_f} \right) \cdot \frac{d\varepsilon_f}{dt} + \int_0^z \left(\frac{R_X}{X_m} + \frac{1}{(1-\varepsilon_f)} \frac{R_{S_i}}{\rho_{S_i}} \right) d\zeta$$

This result shows clearly that the convective velocity is determined by the global change in the equilibrium free water content (first right hand term term) and the local conversion of biomass and insoluble substrate (second right hand term). The net production rate of water does not enter this equation directly as it is accounted for via the first global term.

3.2.7 Model equations

The balance equations for all state variables are listed. They are formed combining all process descriptions according to the model description given up to this point.

Oxygen

$$\text{eq. 3-24} \quad \frac{\partial O_2}{\partial z} = \frac{\mathcal{D}_{O_2,\text{eff}} \cdot \frac{\partial O_2}{\partial z}}{\rho} - \frac{\partial u(z) O_2}{\partial z} + R_{O_2}$$

$t = 0$	$0 < z \leq L_c$	$O_2 = 0$
$t > 0$	$z = 0$	$O_2 = O_{2,i}$
$t > 0$	$z = L_c$	$\frac{\partial O_2}{\partial z} = 0$

$D_{O_2,\text{eff}}$: Effective diffusion coefficient of oxygen $[m^2 \cdot s^{-1}]$

$O_{2,i}$: Dissolved oxygen content at gas side interface $[\text{mol } O_2 \cdot m^{-3}]$

The dissolved oxygen content at the gas side interface $O_{2,i}$ is assumed to be in equilibrium with the oxygen content of the gas phase.

Soluble substrate

eq. 3-25

$$\frac{\partial S_s}{\partial t} = \frac{\partial D_{S_s, \text{eff}}}{\partial z} \frac{\partial S_s}{\partial z} - \frac{\partial u(z) S_s}{\partial z} + R_{S_s}$$

$t = 0$	$0 < z \leq L_c$	$S_s = S_{s,0}$
$t > 0$	$z = 0$	$\frac{\partial S_s}{\partial z} = 0$
$t > 0$	$z = L_c$	$\frac{\partial S_s}{\partial z} = 0$

$D_{S_s, \text{eff}}$: Effective diffusion coefficient of soluble substrate [m².s⁻¹]
 $S_{s,0}$: Initial soluble substrate concentration [mol S_s.m⁻³]

Biomass

eq. 3-26

$$\frac{\partial X}{\partial t} = - \frac{\partial u(z) X}{\partial z} + R_X$$

$t = 0$	$0 < z \leq L_c$	$X = X_0$
$t > 0$	$z = 0$	$\frac{\partial X}{\partial z} = 0$
$t > 0$	$z = L_c$	$\frac{\partial X}{\partial z} = 0$

X_0 : Initial biomass concentration [mol X.m⁻³]

Insoluble substrate

eq. 3-27

$$\frac{\partial S_i}{\partial t} = - \frac{\partial u(z) S_i}{\partial z} + R_{S_i}$$

$t = 0$	$0 < z \leq L_c$	$S_i = S_{i,0}$
$t > 0$	$z = 0$	$\frac{\partial S_i}{\partial z} = 0$
$t > 0$	$z = L_c$	$\frac{\partial S_i}{\partial z} = 0$

$S_{i,0}$: Initial insoluble substrate concentration [mol S_i.m⁻³]

Inert material

eq. 3-28

$$\frac{\partial I}{\partial z} = -\frac{\partial u(z)I}{\partial z}$$

$t = 0$	$0 < z \leq L_c$	$I = I_0$
$t > 0$	$z = 0$	$\frac{\partial I}{\partial z} = 0$
	$z = L_c$	$\frac{\partial I}{\partial z} = 0$

I_0 : Initial inert material concentration [mol L⁻³]

Water

The equation for the equilibrium free water fraction can be derived from the water balance over the whole particle and runs as:

eq. 3-29

$$\frac{d\varepsilon_f}{dt} = \frac{1}{L_c} \left(\int_0^{L_c} \frac{R_w(\zeta)}{\rho_w} d\zeta - \varepsilon_f \cdot \frac{dL_c}{dt} \right)$$

$$\varepsilon_f = \varepsilon_{f,0} \quad t = 0$$

$\varepsilon_{f,0}$: Initial equilibrium free water content [-]

Particle size

The change in particle size can be found by considering the overall volume balance and shows that the particle size is influenced by all three net production rates. The resulting equation runs as:

eq. 3-30

$$\frac{dL_c}{dt} = \int_0^{L_c} \left(\frac{R_w(\zeta)}{\rho_w} + \frac{R_x(\zeta)}{\rho_x} + \frac{R_{S_i}(\zeta)}{\rho_{S_i}} \right) d\zeta$$

$$L_c = L_{c,0} \quad t = 0$$

$L_{c,0}$: Initial particle size [m]

The resulting model contains 5 partial differential equations and two ordinary differential equations. All equations contain non-linear kinetic expressions, making that this model can not be solved analytically. The model has been solved numerically, by discretization both in time and space. The resulting discretized equations have been integrated via an implicit algorithm. (Press et. all.)

The equations for the non-dissolved components (inert matter, organic insoluble matter, free water, biomass) are linked via the prerequisite that their partial volume take up the total volume. One equation of a non-dissolved component could therefore be omitted, however in the calculations this is not done as an error-check would then be lost.

3.3 Model behavior

3.3.1 Model input and output

The model input and output describe together the interaction of the system under study with its environment. The output are the measurements that can (potentially) be made on the system. The input are the means to influence the system. Input and output are the handles available to check whether the proposed model is justified. Model output consists of the following elements:

The OUR is the rate at which a sample of waste consumes oxygen. The OUR is calculated as the oxygen flux at the gas interface of the particle.

eq. 3-31

$$OUR(t) = -\frac{1}{L_{c,0}} \cdot D_{O_2,eff} \cdot \left. \frac{\partial O_2}{\partial z} \right|_{z=0}$$

The OUR is defined based on the initial volume, as measured values of the OUR are all based on some initial measure of the composting material.

The state variables X , S_i , S_s and O_2 are all a function of time and location within the particle. They all exhibit a spatial profiles within the particle, that influences the OUR. These profiles are therefore important output of the model. They are directly obtained from the numerical solution of the model equations.

The average state variables $X(t)$, $S_i(t)$ and $S_s(t)$ are found by integrating the calculated values

of the corresponding state variables as follows:

$$eq. 3-32 \quad X(t) = \frac{1}{L_c} \cdot \int_0^{L_c} X(t, z) dz$$

X(t) : Spatially averaged biomass concentration [mol X.m⁻³]

The average values of the insoluble substrate S_i(t) and soluble substrate S_s(t) are calculated in the same way. The state variables ε_i(t) and L_c(t) are directly derived from the solution of the model equations.

The model input consists of the following elements, the initial states of the state variables (7) and the interfacial dissolved oxygen concentration. As the model input consist mainly of waste characteristics, the model input will be referred to as waste characteristics, an important topic for plant design.

Model calculations are performed for composting of chicken manure at 55 °C and an oxygen content of 18% in the gas phase. The chosen conditions represent a typical optimal situation [13]. Chicken manure is the main type of waste used in this research. The specific values used in the simulation are given in table 1.

The development in time of the OUR and averaged state variables will be first studied. In the development of the OUR four phenomenological phases will be distinguished. These phases are used throughout this paper to structure the development of the output in general. Secondly the gradients of the main state variables will be studied. The spatial gradients will be compared at four points of time, typical for each phenomenological phase. Thirdly for each period the dominant OUR limiting process (growth, decay, hydrolysis, oxygen diffusion, substrate diffusion) is identified via a parameter and input sensitivity analysis. Such an analysis gives information on which parameters and inputs are influential at a certain point of time. If the parameters and inputs associated with a certain process are influential at a certain point of time it is supposed that the associated process is rate determining.

Fourthly the effect of the waste characteristics on the OUR time course is studied. Waste characteristics can vary strongly, understanding the effect of these factors might show how general the phenomenological division of the OUR time series is.

Table 3.1: Nominal parameter values.

	Symbol	Name	value	unit	Reference
Kinetic	μ_{\max}	Maximum biomass growth rate	$2 \cdot 10^{-4}$	s ⁻¹	[14]
	B	Biomass decay constant	$3.8 \cdot 10^{-5}$	s ⁴	[14]
	K_h	Hydrolysis constant	$4.9 \cdot 10^{-7}$	s ⁻¹	[15]
	K_s	Substrate saturation constant	0.31	mol C.m ⁻³	[14]
	K_{O_2}	Oxygen saturation constant	$3.4 \cdot 10^{-4}$	mol O ₂ .m ⁻³	[16]
Yield	Y_{O_2}	Biomass yield on oxygen	1.12	mol C.mol ⁻¹ O ₂	[17]
	Y_s	Biomass yield on soluble substrate	0.53	mol C.mol C ⁻¹	[17]
	Y_w	Biomass yield on water	1.34	mol C.mol ⁻¹ H ₂ O	Based on oxygen
	Y_p	Biomass yield on polymeric substrate	1.0	mol C.mol ⁻¹ C	Assumption
Physical chemical	D_{O_2}	Oxygen diffusion constant	$1.8 \cdot 10^{-9}$	m ^{2.s⁻¹}	[18]
	D_{Ss}	Soluble substrate diffusion constant	$1.1 \cdot 10^{-9}$	m ^{2.s⁻¹}	[18]
	ρ_{Si}	Insoluble substrate density	23000	mol C.m ⁻³	[19]
	ρ_w	Water density	55000	mole H ₂ O.m ⁻³	[20]
	X_m	Biomass density	8000	mole C .m ⁻³	[21]
	ρ_i	Inert material density	46000	mol C.m ⁻³	[19]
	Ψ	Biomass water content	5	mol H ₂ O .mole C ⁻¹	Assumption 20 % DM
Waste characteristics	$L_{e,0}$	Particle thickness	0.0025	m	Assumption
	S_{s0}	Initial soluble substrate concentration	1420	mole C.m ⁻³	[22]
	S_{p0}	Initial polymeric substrate concentration	4750	mole C.m ⁻³	[22]
	X_0	Initial biomass concentration	1.5	mole C.m ⁻³	Assumption
	$\epsilon_{w,0}$	Initial water content	0.83	[\cdot]	[22]
	I_0	Initial inert concentration	450	mole I.m ⁻³	[22]
	O_{20}	Initial oxygen concentration	0	mol O ₂ .m ⁻³	Assumption
	O_{2b}	Interfacial oxygen concentration	0.18	mol O ₂ .m ⁻³	[23]

3.3.2 OUR and state variables.

Figure 3.4 show the time series of the OUR, divided into four period, indicated A, B, C and D. During the first period A the OUR clearly increases until it reaches a maximal level at approximately twenty-two hours. During the second period B the OUR remains at a steady maximum level, that lasts until 46 hours. The OUR declines sharply during the third period C, within 10 hours. the OUR drops to another, albeit lower, nearly constant level. During the fourth period D the OUR decreases very slowly.

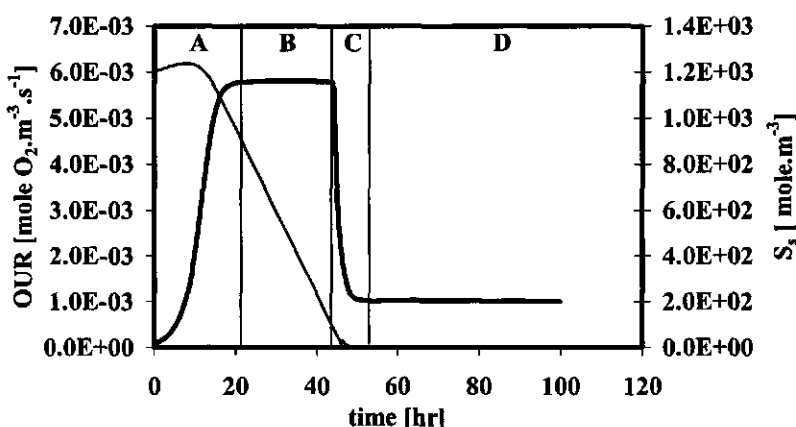


Figure 3.4: Course of the oxygen uptake rate (OUR, left Y-axis, thick line) and the spatially averaged soluble substrate concentration ($S_i(t)$, right Y-axis, thin line) in time(X-axis). Capital characters indicate the distinguished process phases (see text).

The soluble substrate concentration (Figure 3.4) reaches in period A an initial peak at 8 hr, after which the soluble substrate concentration decreases. During period B this decrease occurs nearly linear until the end of period B. At the start of period C the substrate is nearly depleted and the soluble concentration decreases more slowly. From 53 hours onward the soluble substrate concentration is negligible.

The soluble substrate concentration (Figure 3.4) reaches in period A an initial peak at 8 hr, after which the soluble substrate concentration decreases. During period B this decrease occurs nearly linear until the end of period B. At the start of period C the substrate is nearly depleted and the soluble concentration decreases more slowly. From 53 hours onward the

soluble substrate concentration is negligible.

The biomass concentration (Figure 3.5) strongly increases during period A, during period B the increase rate levels off and the biomass concentration reaches a maximum at the end of period B. At the start of period C there occurs a relative steep drop in the biomass concentration. During period D a nearly constant level is reached.

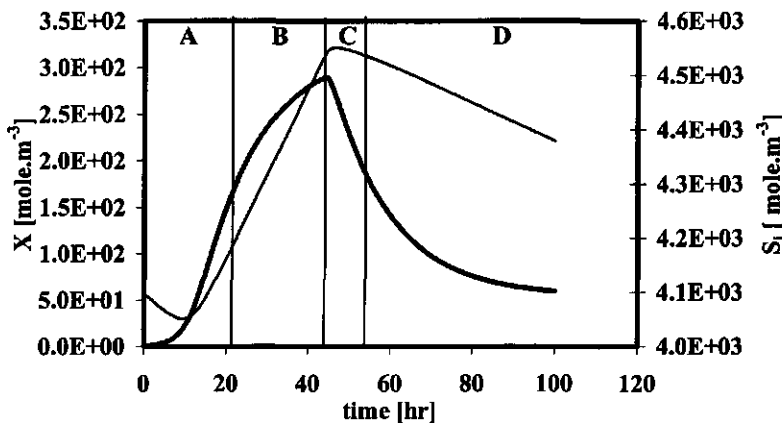


Figure 3.5: Course of the spatially averaged biomass concentration ($X(t)$, left Y-axis, thick line) and the spatially averaged insoluble substrate concentration ($S_i(t)$, right Y-axis, thin line) over time (X-axis).

The insoluble substrate concentration (Figure 3.5) decreases initially during period A. However soon the level increases again until the end of period B. During period B and C there is a slow decrease in insoluble substrate concentration.

The free water fraction ϵ_f (Figure 3.6) is relatively constant during the period considered. There is initially a small decrease during the first two periods, followed by a slow increase during period C and D.

The particle size (Figure 3.6) shows at the start of period A an initial decrease shortly, after which it starts to increase until the end of period B when it reaches its maximum. The particle size decreases from this point on during period C and D.

Although the inert material is not converted in any way, the inert concentration still shows some variation. However, this variation is solely a result of changes in particle volume and therefore only the development of the particle size has been shown.

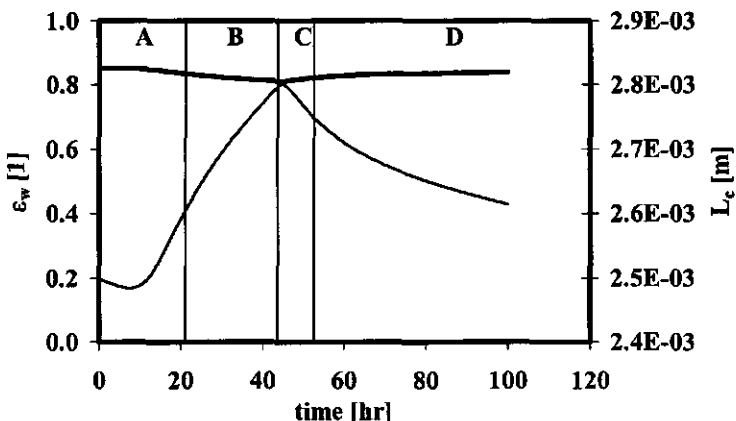


Figure 3.6: Course of the free water fraction (ϵ_f , left Y-axis, thick line) and the particle size (L_c , right Y-axis, thin line) over time (X-axis). Capital characters indicate the distinguished process phases (see text)

3.3.3 State variable profiles

State variables having a distinct gradient will be shown at the following points of time; at $t=10$ hr characteristic for period A, at $t=35$ hr characteristic for period B, at $t=45$ hr characteristic for period C and at $t=100$ hr characteristic for period D. As the inert material is not subject to any reaction, and its concentration can be calculated from the other components, this gradient will not be discussed.

Figure 3.7 shows that oxygen has only a limited penetration within the particle. Going from case $t=10$ hr to case $t=35$ hr the penetration depth decreases. At $t=45$ hr and $t=100$ hr the penetration depth has increased again. In all cases only a small fraction of the particle is oxygenated.

Figure 3.8 shows the development of the gradients of the soluble substrate. The soluble substrate has at $t=10$ hr a high level and nearly no gradient can be distinguished over the whole particle. At $t=35$ hr the level has lowered and no clear gradient has developed. At $t=45$ hr and at $t=100$ hr a clear gradient has developed with basically a zero concentration at the gas side interval.

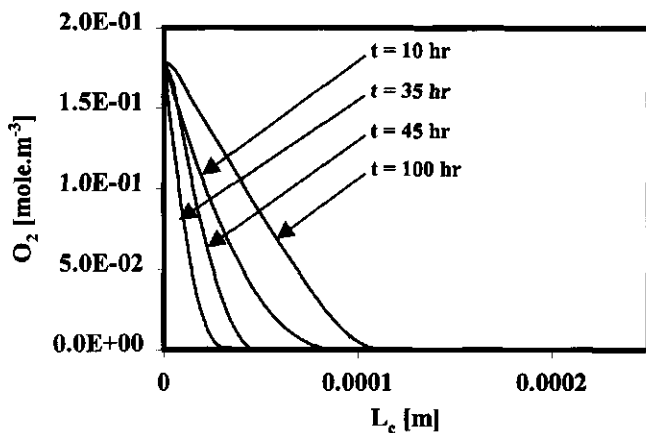


Figure 3.7: Dissolved oxygen profiles (O_2 , Y-axis) at four points of time. The X-axis denotes the distance [m] from the particle-gas phase interface, note the partial scale with respect to the particle size($L_{c,0} = 0.0025 \text{ m}$). The Y-axis denotes the oxygen concentration [mole.m^{-3}].

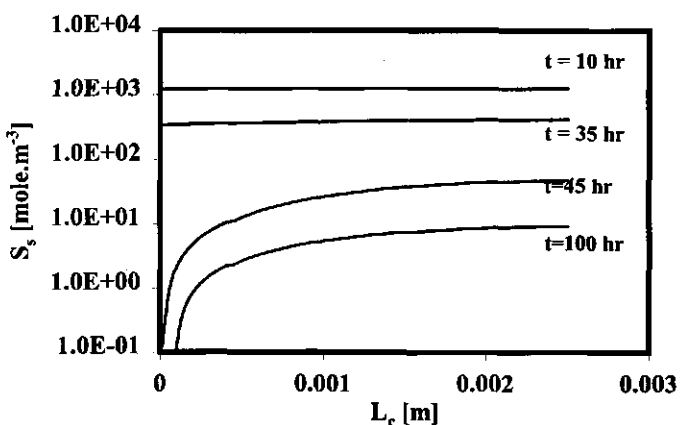


Figure 3.8: Soluble substrate concentration (S_s) profiles at four points of time. The X-axis denotes the distance [m] from the particle-gas phase interface. The Y-axis denotes the soluble substrate concentration [mole.m^{-3}], note the logarithmic scale.

The biomass profiles (Figure 3.9) show at $t = 10$ hr and $t = 35$ hr the same shape, maximal at the gas-side interface and from this location slowly decreasing. The depth over which the biomass concentration is flat at the gas side interface coincides with the oxygen penetration depth. The overall biomass level is much higher at $t = 35$ hr. At $t = 100$ hr a clear peak in biomass density has developed, the peak coinciding with oxygen penetration depth. The biomass profile at $t = 45$ hr is a kind of transitional profile.

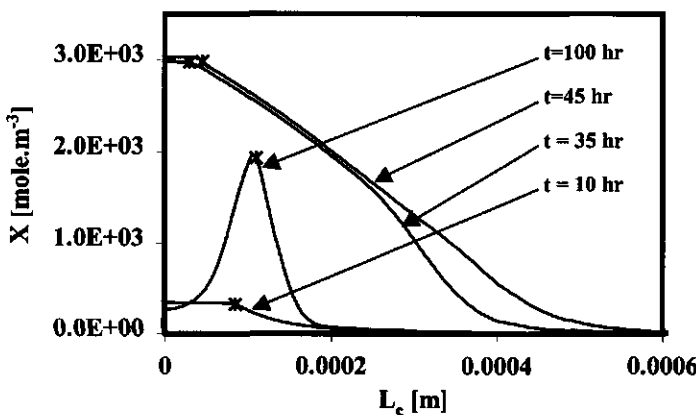


Figure 3.9 : Biomass concentration (X , Y-axis) profiles at four points of time. The X-axis denotes the distance [m] from the particle-gas phase interface. Note the partial scale with respect to the particle size ($L_{c,0} = 0.0025$ m).

The insoluble substrate profile (Figure 3.10) is nearly flat at $t = 10$ hr, there is only a slight depression at the gas side interface. This depression however has deepened at $t = 35$ hr. At $t = 45$ hours the insoluble substrate concentration rises again at the gas side interface, and a small peak emerges. At $t = 100$ hr the picture becomes more complex as two peaks have emerged. The insoluble substrate profile is mirror image of the biomass profiles.

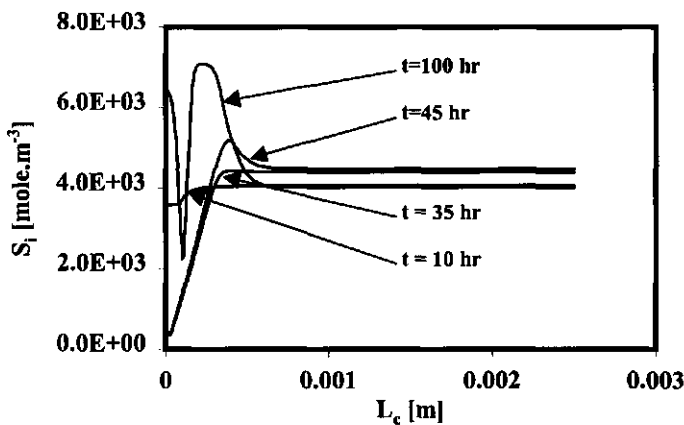


Figure 3.10: Insoluble substrate concentration (S_i , Y-axis) profiles at four points of time. The X-axis denotes the distance [m] from the particle-gas phase interface.

3.3.4 OUR sensitivity analysis

Understanding the importance of the parameters gives insight in the nature of the rate determining processes and might give a direction for further model simplification. The sensitivity function is defined as:

$$\text{eq. 3-33} \quad S(p,t) = \frac{p}{\text{OUR}(t)} \frac{\partial \text{OUR}(t)}{\partial p}$$

p : Parameter of interest

$S(p,t)$: OUR sensitivity for parameter p at time t.

[1]

The sensitivity function is dimensionless as it is scaled with respect to the OUR and the parameter. The absolute value of a sensitivity function is a measure of the influence of the associated parameter at that specific point of time and is called the absolute sensitivity. A parameter is defined as influential if its absolute sensitivity is at least 10% of the maximum of all absolute sensitivities. (at that specific point of time). For each period (A, B, C and D) the average values of the sensitivities over each period are compared. The sensitivity functions

and their average are determined numerically.

Table 3.2 lists for each period the influential parameter. The yield on oxygen is influential during the whole process. The maximal growth rate, the oxygen diffusion coefficient, particle size, interfacial oxygen level are influential during the first three periods. The biomass decay factor and the initial biomass concentration are only important during the first period. The maximal biomass density is important during the second and third period. The yield on substrate, hydrolysis rate, initial soluble substrate, and initial insoluble substrate are important during the third and fourth period. The other parameter show to be of minor importance with respect to the course of the OUR.

Table 3.2: The averaged scaled sensitivities of the influential parameter of the model. Parameters that are not mentioned have no significant effect in any period. The symbol – indicates that the parameter has no significant effect in the associated period.

	Period A	Period B	Period C	Period D
Y_{O_2}	-0.21	-0.49	-0.50	-0.76
μ_m	1.0	0.57	-0.82	--
D_{O_2}	0.21	0.5	-0.35	--
$L_{e,0}$	-0.42	-1.0	0.83	--
$O_{2,i}$	0.24	0.53	-0.47	--
b	-0.16	--	--	--
X_0	0.14	--	--	--
X_m	--	0.45	-0.30	--
K_h	--	--	0.35	0.86
Y_{Ss}	--	--	1.0	1.0
$S_{S,0}$	--	--	0.74	0.17
$S_{i,0}$			0.29	0.72

Period A will be referred to as the biomass growth limited period. The increase of the OUR during period A is mainly determined by the biomass growth. The parameters describing the biomass growth (μ_m , b , X_0) are all influential during this period. Also the diffusion of oxygen

is already of importance, (D_{O_2} , $L_{c,0}$, $O_{2,i}$) however the process of biomass growth is more important as the maximal growth is the dominant parameter.

Period B is the biofilm-limited period. The parameters associated with the diffusion of oxygen are more important than during the first period. As the simulation indicates there has been a development of a biofilm at the gas-side interface. As oxygen is the main limiting substrate and has a low saturation constant, it is interesting to compare these results with the equation given by Harremoes [24] for the oxygen flux of a steady-state biofilm with zero-order kinetics. Dividing this flux by the particle size give the following relationship for the OUR:

$$\text{eq. 3-34} \quad \text{OUR} = \frac{1}{L_c} \sqrt{2.D_{O_2,\text{eff}} \cdot O_{2,i} \cdot \frac{\mu_m \cdot X_m}{Y_{O_2}}}$$

The values of the calculated sensitivities compare well to the sensitivities as predicted by the formula above, -1 for L_c , $-1/2$ for Y_{O_2} , and $1/2$ for $D_{O_2,\text{eff}}$, $O_{2,i}$, μ_m , X_m .

During period D, the hydrolysis-limited period the OUR is determined by the hydrolysis rate. The S_{s0} and k_h are the dominant parameter. The fact that S_{s0} also influences the hydrolysis rate is due to the conversion of soluble substrate to biomass. This biomass forms insoluble substrate after biomass decay.

Period C can be characterized as a transition period. The balance between soluble substrate consumption and production shift during period C. In the first two period sufficient soluble substrate is present and the soluble substrate consumption rate is determined by the OUR. In the last period the soluble substrate production rate determines the OUR. The transition period is very short and is characterized by the influential position of soluble substrate concentration. The initial soluble substrate concentration determines the length of the period A and B, however not the rate itself, as is shown by the low sensitivity during period A and B. This explains why the parameter sensitivities of $L_{c,0}$, Y_{O_2} , $D_{O_2,\text{eff}}$, $O_{2,i}$, μ_m , and X_m have nearly the negative value of period B during period C. If the OUR in period B is lower it will take longer to achieve soluble substrate depletion. This means that the OUR during period C will increase. Also if the hydrolysis is faster more soluble substrate will be produced during period A and B and depletion will occur later.

3.3.5 Waste characteristic analysis

The following waste characteristics are studied, particle size, interfacial oxygen concentration, initial soluble substrate, initial insoluble substrate, initial ash and initial biomass. The waste characteristics are changed one by one, by multiplication of the nominal values with the factors 0.25, 0.5, 2 and 4. A change in one component is in all cases compensated by an opposite change in the water content.

Moisture influences the particle size within a pile, as with increasing moisture content more and more small pores are filled. (Miller) Filling small pores is equivalent to reducing specific surface area and thus increasing the particle size. This effect of moisture can thus not be fully incorporated with a model that takes into account a single particle. Water content as such is therefore not studied at this point. The results for inert material are not shown as this showed to have a negligible effect both on the OUR and the average soluble substrate concentration.

Initial biomass concentration

The initial biomass concentration (Figure 3.11) has only a minor effect on the OUR time course. Period A becomes somewhat shorter, the rest of the behavior remains basically the same. This finding is in accordance with the sensitivity analysis, only during period A biomass is an influential factor. The initial biomass density is in literature generally accepted to have a small effect. Nakasaki studied the effect of inoculation on sewage sludge composting [25] and household waste [26]. The inoculum was compost from the thermophilic composting phase. The composting rate was measured as the carbon dioxide production rate at a constant oxygen level and temperature. They studied mixtures consisting of a seed and either sewage sludge or household waste. As a control a mixture with sterilized compost was used. This makes their study special as they are able to discriminate between the effect of adding (thermophilic) biomass and other effects induced by the material itself. The studied the inoculum at three levels, their result was in good accordance with the model predictions. The peak in activity occurred earlier in time with increased inoculation, however the maximum composting rate was not influenced. The same effect in the case of household waste was more pronounced as the waste itself contained fewer organisms than sewage sludge.

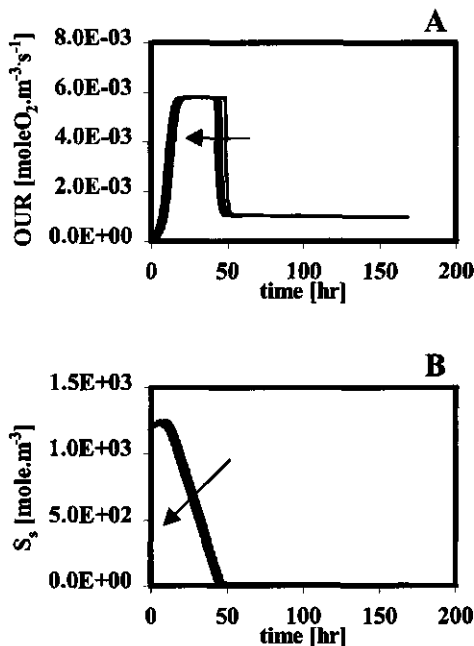


Figure 3.11: The effect of a change in initial biomass concentration (X_0) on the course of the OUR (A, Y-axis) and soluble substrate concentration S_s (B, Y-axis). The X-axis denotes the time in hours. The time course of OUR and S_s are shown for five different values of X_0 , specifically 2, 2, 2, 1, 1, 2 and 4 times the nominal value. A thick line indicates the time course of the nominal value. The arrow indicates the time courses for increasing values of X_0 .

The initial insoluble substrate

The initial insoluble substrate concentration (Figure 3.12) has only a slight influence on the rate during periods A and B, the main effect is an extension of period B. There is a small effect on the maximal oxygen uptake rate, however this effect is small as compared to the effect of particle size and interfacial oxygen concentration. During period D the OUR increases clearly with an increasing insoluble substrate concentration, which is in accordance with the sensitivity analysis. The effect of the initial insoluble substrate on the average soluble substrate concentration is twofold, the peak increases and it takes longer to achieve the soluble substrate depletion.

Initial soluble substrate

The initial soluble substrate concentration (fig 3.13) has no effect on the OUR during period A. The duration of period B is extended, however, the maximum rate is not influenced. At the lowest value of the initial substrate concentration it seems that period A is not completed and period B is absent. Period C and D are only slightly influenced. The soluble substrate concentration course is of course strongly influenced by its initial value, however, the shape of

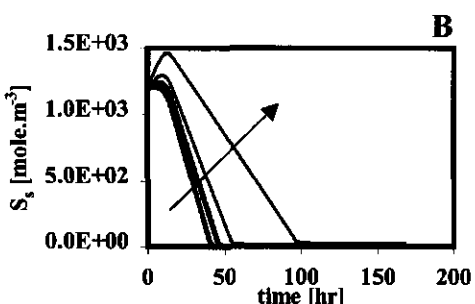
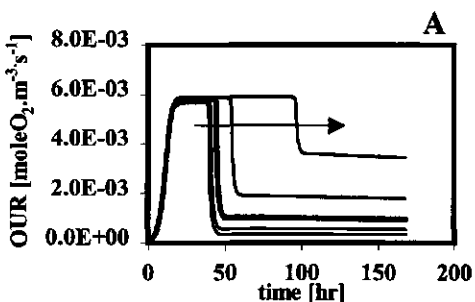


Figure 3.12: The effect of a change in initial soluble concentration ($S_{s,0}$) on the time course of the OUR (A) and spatially averaged soluble substrate concentration $S_s(t)$. (B) The X-axis denotes the time in hours. The time course of OUR and S_s are shown for five different values of $S_{s,0}$, specifically $2^{-2}, 2^{-1}, 1, 2$ and 4 times the nominal value. A thick line indicates the time course of the nominal value. The arrow indicates the time courses for increasing values of $S_{s,0}$.

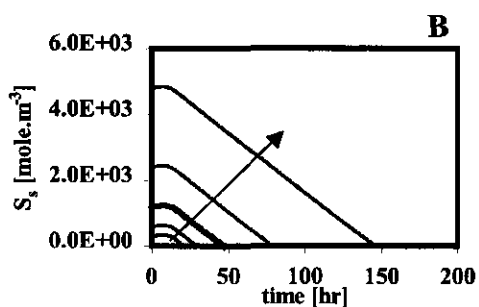
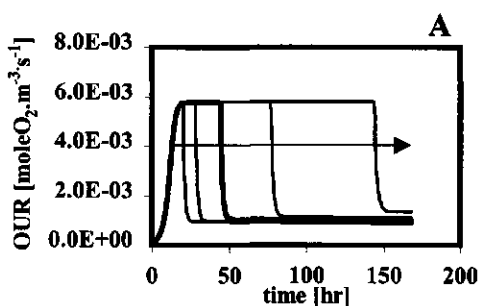


Figure 3.13: The effect of a change in initial insoluble concentration ($S_{i,0}$) on the time course of the OUR (A) and spatially averaged soluble substrate concentration $S_s(t)$ (B). The X-axis denotes the time in hours. The time course of OUR and S_s are shown for five different values of $S_{i,0}$, specifically $2^{-2}, 2^{-1}, 1, 2$ and 4 times the nominal value. A thick line indicates the time course of the nominal value. The arrow indicates the time courses for increasing values of $S_{i,0}$.

the curves remain comparable. The main difference is that with increasing initial soluble substrate it takes longer before the soluble substrate is depleted.

Interfacial oxygen concentration

The interfacial oxygen concentration (Figure 3.14) strongly influences the OUR during period A and B. During period A the rate increases with increasing interfacial oxygen concentration, the duration of the period seems to increase slightly. With increasing interfacial oxygen concentration the maximum OUR during period B increases and the duration of the period decreases. There seems to be no strong effect on period C and period D. With an increasing interfacial oxygen concentration the period for complete depletion of the soluble substrate decreases.

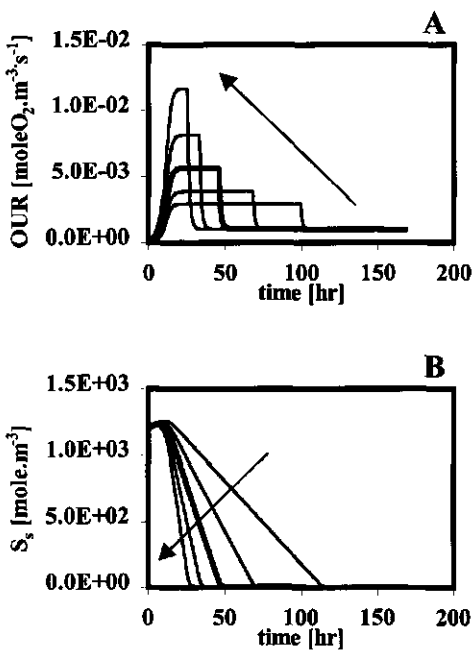


Figure 3.14: The effect of a change in the interfacial oxygen concentration ($O_{2,i}$) on the time course of the OUR (A) and spatially averaged soluble substrate concentration $S_s(t)$ (B). The X-axis denotes the time in hours. The time course of OUR and S_s are shown for five different values of $O_{2,i}$, specifically $2^{-2}, 2^{-1}, 1, 2$ and 4 times the nominal value. A thick line indicates the time course of the nominal value. The arrow indicates the time courses for increasing values of $O_{2,i}$.

Initial Particle size

With increasing particle size the OUR drastically decreases during both period A, B and C (Figure 3.15). The particle size has no effect on the duration of period A, the duration of period B and C however increases. The rate during period D is independent from the particle size. With increasing particle size it shows that it takes longer for the soluble substrate to

become depleted. The behavior of the soluble substrate concentration is thus following the changes of the OUR.

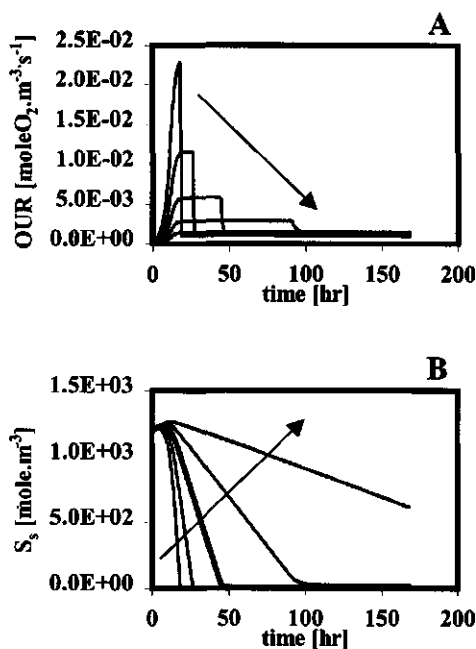


Figure 3.15: The effect of a change in the particle size ($L_{c,0}$) on the time course of the OUR (A) and spatially averaged soluble substrate concentration $S_s(t)$ (B). The X-axis denotes the time in hours. The time course of OUR and S_s are shown for five different values of $L_{c,0}$, specifically 2^{-2} , 2^{-1} , 1, 2 and 4 times the nominal value. A thick line indicates the time course of the nominal value. The arrow indicates the time courses for increasing values of $L_{c,0}$.

3.4 Model Comparison

The theoretical model will be compared to current empirical models for composting kinetics. The comparison will focus on the effect of oxygen level on composting kinetics. Oxygen has been chosen because suitable data and empirical models are available. For other model inputs either good data or empirical models are not available.

Empirical models use the Monod model to describe the effect of the oxygen level in the gas phase on the OUR. The actual OUR is calculated as a function of oxygen level and the OUR measured at optimal reference conditions.

$$\text{eq. 3-35} \quad \text{OUR}(t, pO_2) = \frac{pO_2}{K_{O_2} + pO_2} \cdot \text{OUR}(t, pO_{2,\text{ref}})$$

pO_2 : Oxygen level of the gas phase

[vol. % O₂]

$pO_{2,\text{ref}}$: Reference oxygen level of the gas phase

[vol. % O₂]

In experimental studies the oxygen content of the gas phase is used as a measure for the dissolved interfacial oxygen concentration. In the oxygen pressure range used in composting the linear relation between oxygen level and dissolved oxygen concentration is valid and the Henry relationship can be used. However it should be kept in mind that the Henry coefficient changes strongly as a function of temperature, at a higher temperature oxygen solubility will be lower[23]. The Henry coefficient may also change as a result of a change in dissolved components [27]. The oxygen gas phase content is generally measured after removal of water vapor. Compared to the measurements the actual oxygen content of the gas inside the composting matrix gas phase is lower due to the presence of water vapor. As the water vapor content increases with temperature, the actual oxygen content will decrease. This means that care should be exerted when comparing K_{O_2} values from different situation with respect to temperature and waste composition.

In many studies on composting kinetics the so-called Cumulative Oxygen Uptake (COU) is used as a composting process rate measure. The cumulative oxygen uptake is defined as:

$$\text{eq. 3-36} \quad COU(t_{low}, t_{upper}) = \int_{t_{low}}^{t_{upper}} OUR(\tau) d\tau$$

COU	: Cumulative Oxygen Uptake	[mol O ₂ .m ⁻³]
t _{low}	: Lower value of time period	[s]
t _{upper}	: Upper value of time period	[s]

If the oxygen content remains constant over time, the oxygen correction factor can be directly used as a correction factor for the oxygen dependence of the COU.

$$\text{eq. 3-37} \quad COU(t_{lower}, t_{upper}, O_2) = \frac{O_2}{K_{O_2} + O_2} \cdot COU(t_{lower}, t_{upper}, O_{2,ref})$$

In models studies different values of K_{O_2} are used ranging from 1 to 6 vol.-% of oxygen (Richards).In some studies the so-called Cumulative Carbon dioxide Production or CCP is used as composting rate measure. The CCP and COU are linearly correlated [19, 28].

There are relatively few studies on the effect of oxygen level where a constant oxygen level is maintained while oxygen is consumed. All studies to be discussed support the use of the Monod relationship, i.e a saturation level is found. However in all of these controlled studies results are reported that hamper the use of a multiplicative model. It will be investigated to what extent the theoretical model is able to explain these discrepancies.

3.4.1 Effect of an anaerobic period

Anaerobic periods occur frequently in practical processes as a result of equipment malfunction. Van Ginkel [19] studied the effect of an anaerobic period on the heat production of a sample of a mixture of manure and straw. The process rate was amongst others measured as the oxygen uptake rate. The process rate was determined at 37 °C, the oxygen level was kept at 20 vol.%. The batch of material was first 5 days run at a oxygen level of 20% subsequently two days at 0% and then for another period of nearly 3 days at 20% again.

This oxygen level input sequence was simulated. To account for the effect of temperature the maximum growth rate was reduced by a factor 2 compared to the nominal parameter set [29]. Moisture content, inert content, soluble and insoluble substrate concentrations have been changed according to the mixture composition. Other parameters were the same as in the nominal situation.

Figure 3.16 shows the calculated course of the OUR. The first five days the OUR shows the normal development. When the oxygen level drops to zero no oxygen uptake occurs. At the moment the oxygen level is increased again there is nearly immediate increase in OUR, however the maximum level is kept only for a short period and the OUR drops again to the stable level from the previous aerated period. The calculated and measured OUR (not shown) time series agree satisfactorily, the maximum levels are in reasonable agreement. Both calculations and measurements show the rapid OUR increase after the anaerobic period. The explanation suggested by the theoretical model is that during the anaerobic period, the hydrolysis goes on and the soluble hydrolysis products will accumulate. After the oxygen level has restored again, this leads to an increased activity. The response is rapid compared to the start up as the biomass is already available from the previous period and needs not to grow as during start up. Such a behavior can not be modelled by a multiplicative model, this would predict the same level directly after as before the anaerobic period. The distinct peak could not have been modelled let alone be predicted, as is the case for the theoretical model.

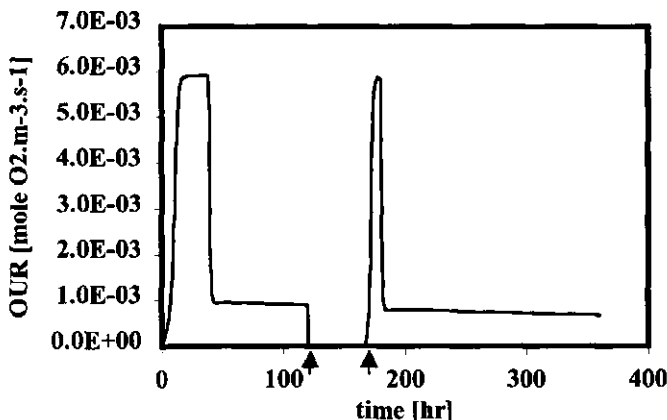


Figure 3.16: Effect of an aerobic period on the time (X-axis) course of the OUR (Y-axis). Arrows indicate the beginning and ending of the anaerobic period.

3.4.2 Combined effect of oxygen and moisture

Suler [30] investigated the effect of oxygen level concentration on composting rate under different temperature and moisture conditions. The composting rate was expressed as the cumulative amount of carbon dioxide evolved over a 96-hour production CCP(0-96). The relationship was tested at different temperatures (48, 52, 56, 60, 64, 68 and 72 °C) at a moisture content of 60 %. At all temperatures the CCP(0-96) was measured at oxygen levels of 2%, 10%, 18%. At 52 °C the CCP(0-96) was also studied at 25 and 35 % O₂. The findings with respect to the effect of oxygen were at all temperatures the same. Only the CCP(0-96) at 2% was significant lower, from 10% onward no significant increase in CCP(0-96) was found. The same oxygen dependency was found at a moisture content of 50% and a temperature of 56 °C. At the same temperature, however, the oxygen dependency changed drastically at moisture content of 70%. At this moisture content a clear overall decrease in process rate was found and up to 18% oxygen a clear positive effect was found.

To understand this change in oxygen dependence the experiments at moisture content of 60 and 70% and temperature of 56 °C were simulated. The nominal parameter set was used a starting point. The waste characteristics were changed to account for the dry matter and organic matter content. The particle size was adjusted to account for the observed maximum carbon dioxide production rate. At 70% moisture this maximum production rate was significantly lower. This can be attributed to the fact that at a higher moisture content more

pores in the waste bed are filled with water. The surface area in the bed will be lower and thus particle size will be bigger. The OUR time course was simulated over 96 hours, summation of the OUR results gave the simulated COU values. This exercise was performed for oxygen levels of 2%, 4%, 8%, 16% and 32%.

Figure 3.17 shows the simulated relation between COU and oxygen level. For both simulated situations the calculated values give the same pattern as the measured value. At 60% moisture there is no effect of oxygen from 10% onward, however for the experiment at 70% moisture a distinct relationship can be seen up to 20%.

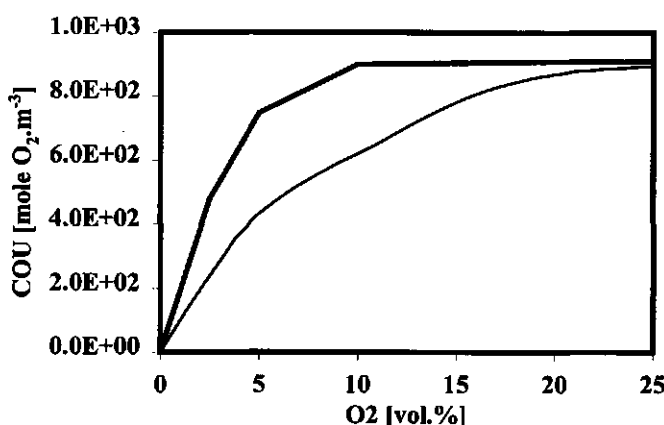


Figure 3.17: The simulated $\text{COU}(0,96)$ (Y-axis) as a function of gas phase oxygen level (X-axis) for two different moisture levels (60% thick line, 70% thin line).

This effect of the moisture content is a result of the change induced in the maximum OUR achieved during the biofilm limited period. If the activity of the biomass is such that all soluble substrate is consumed during the COU measurement period, the COU will be solely determined by the amount of available soluble substrate. This means that if the soluble substrate is depleted within the measurement period no longer any effect of the oxygen level on the substrate saturated phase can be detected by the COU. Any further increase of the oxygen level in this situation might lead to a more rapid degradation of the initially soluble substrate, but this effect is not reflected in the COU.

This situation changes if the OUR is lowered to such an extent that the substrate is no longer depleted at the end of the measurement period. At the 60% moisture content this occurs at an oxygen level smaller than 10%. Below this value any further decrease of the oxygen level will be reflected in the COU as the availability of soluble substrate is no longer limiting.

At 70% moisture soluble substrate is still available at the end of the measurement period at an oxygen level of 20%. This is because the OUR is smaller due to the larger particle size and it takes longer to deplete the soluble substrate. If soluble substrate is still present a change in oxygen will reflect in the COU.

3.4.3 Effect of high temperature.

Richard [31] investigated the effects of the oxygen level on the composting rate. The materials tested were a synthetic food waste mixed with wood chips and sewage sludge mixed with wood chips. The material was composted in a rotating drum reactor of 1500 l. From the reactor at regular intervals a sample was taken. This sample was divided over 36 one liter micro-reactors. These reactors were able to control the temperature and air oxygen level. The composting rate of the material could in this way be measured at different temperatures (35,45,55 and 65 °C) and at different oxygen levels (2%, 4% and 21%). The composting rate was measured as the CCP measured between 12 to 36 hours, after filling the micro-reactors.

Richards compared different models to account for the observed effect of oxygen and found the Monod to be the best model, to describe the data. To account for the observed dependency of the K_{O_2} -parameter on temperature and moisture content, this parameter was presented as a linear function of temperature and moisture. The observed dependency on sampling time was not accounted for.

The positive effect of moisture i.e. with an increasing moisture content a higher K_{O_2} -parameter is found can be explained along the same line as for the work of Suler. The most striking feature was the occurrence of negative K_{O_2} -parameter values at high temperature values. This indicates an inverse relationship, i.e with increasing oxygen content a lowering of the CCP was found until a stable level was reached. This type of behavior was observed at 65 °C and sometimes at 55 °C.

To understand this unusual behavior the experimental set up has been simulated with the theoretical model. To do so the two steps had to be simulated, first the composting in the rotating drum reactor and secondly the measurement in the micro-reactors. To simulate the

composting period, the OUR was simulated for nine days with constant conditions of oxygen (20 vol. %) and constant temperature of 55 °C. After simulation of the nine days reactor period the average waste composition was calculated. This mimics the mixing of the material before filling the micro-reactors. This average composition is used as starting conditions for the simulation of the micro-reactors. The mixed material has a lower soluble substrate and a higher biomass density, compared to the nominal input set. The OUR is simulated for 36 hours and the COU is based on the 12-36 hour period.

Figure 3-18 B shows the simulated COU dependence of the oxygen content. The figure shows the characteristic inverse effect. In this case a K_{O_2} value of -2.3 was found. This is in the same range as indicated by Richards. The reason for this inverse behavior lies in the choice of the 12-36 period. Figure 3-18 A shows the COU(0,36) and COU(0,12). The upper line shows the COU(0,36), this line shows the behavior as in the case of the study of Suler. This shows a saturation level starting from 4 vol.% of oxygen. This saturation level is again a result of the soluble substrate depletion. The lower line shows COU(0,12), this shows a strong dependence on the oxygen level as sufficient soluble substrate is present. The difference between these curves gives the COU(12,36). This value increases with decreasing oxygen not as a result of some microbial stimulation but as a result of the increased availability of soluble substrate in the 12-36 hrs period. The higher COU in this period is thus a result of an oxygen limitation, however due to the experimental set up is interpreted as a stimulation of the process.

That this phenomenon is mainly seen at higher temperatures is a result of the fact that the growth rate is than higher and the amount of soluble substrate consumed in the first 12 hours is bigger, and thus differences are bigger. A second point that can be explained is that the inverse behavior was mainly seen in the nine day samples, while it was nearly absent at the 31-day samples. After such a long time the initial soluble substrate will be zero and the 12-36 period will be substrate depleted in all cases.

3.5 Discussion and Conclusions

A mathematical model based on mechanistic assumptions has been developed for a composting particle. The model analysis showed that the composting process must be understood as a sequence of four phases during which different sub-processes determine the overall process rate. During the first period biomass growth is the most important rate determining process. Soon however also the diffusion rate of oxygen starts to influence the

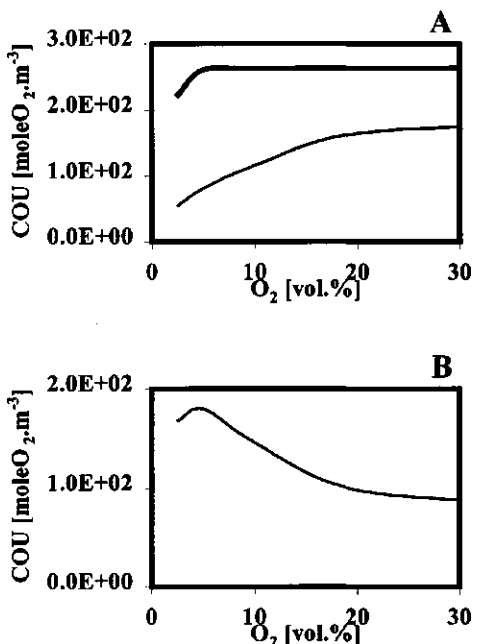


Figure 3.18: Explanation of the observed inverse oxygen effect. The $\text{COU}(0,36)$ (Y-axis, Thick line) and the $\text{COU}(0,12)$ are shown in panel A as a function of the gas phase oxygen level (X-axis). Panel B shows the $\text{COU}(12,36)$ (Y-axis) as a function of the gas phase oxygen level (X-axis).

overall process rate as a biofilm emerges at the surface of the particle. The overall process rate during this second period may be described by biofilm kinetics. Once the soluble substrate is depleted the third period starts. This is a short transition period during which the OUR drops sharply and becomes at its end solely hydrolysis limited. At this point starts the forth period, the hydrolysis limited period. Analysis of the effect of the waste characteristic on the OUR development showed that this view is valid for a large range of different characteristics. Only if the amount of soluble substrate initially present is very low the biofilm period is not present. Oxygen level dependence of the composting rate reported in literature have been evaluated. The calculations show that the theoretical model also predicts a saturation level with respect to the oxygen level. Application of the Monod relationship to the calculated oxygen dependence gives K_{O_2} -parameter values that are much higher than the one used to describe the microbial kinetics, indicating the importance of mass transfer limitation of oxygen. The K_{O_2} -parameter values based on the theoretical model are in the same range as reported by Richard [31]. Examination of the data also revealed the inadequacy of the assumption of independence of rate determining factors. The work of Richard showed that the K_{O_2} -parameter was not constant but differed depending on the conditions of the waste (temperature, moisture)[1]. Also Suler [30] found that the oxygen dependence was depending on the moisture content.

Van Ginkel [19] clearly showed that an anaerobic period influenced the oxygen dependency. All these findings can be simulated and explained by the theoretical model. This shows that the assumptions underlying the theoretical model, seem to be reasonable at least with respect to oxygen.

This dependence of the oxygen dependency on the state of the particle has two consequences. The first is that the assumption of a single constant K_{O_2} value underlying empirical models, is not warranted. This value is depending on the state of the waste, notably the soluble substrate concentration. This implies that in the context of an empirical model the K_{O_2} is a function of the state variables. As some of these variables can not be easily measured, this means that a restriction for the development of an adequate empirical model. The second consequence is that the COU is not the most suitable measure to monitor oxygen dependence. The dependence of the K_{O_2} on the soluble substrate concentration makes that statements on the effect of oxygen are strictly speaking only valid for the COU and can not be generalized. This dependency makes that a result of the integration step as in eq. 3-36 is invalid, and that the COU is not a proper measure to asses the effect of oxygen on the composting rate. These considerations imply that conclusions based on COU/CCP measurement should be extrapolated very carefully, their validity is restricted to the observation period, measurement conditions and waste type. However experimental data are readily generalized to statements as "10% oxygen is sufficient". Such statements might be true but need not to be, as they depend on the period and the phenomena of interest.

It seems to be fair to conclude that the theoretical model is a powerful tool to get insight in the composting process. The theoretical model explains and describes phenomena that are not handled by current empirical models like the interactions between rate determining factors, like oxygen. The model describes the OUR development as a process with distinct phases, and it would be almost accidental if the effect of some input would have the same effect on the output during all phases. The interfacial oxygen level gives a clear example of this. The parameter sensitivity analysis showed oxygen to be only influential when soluble substrate is not depleted, but even then with different degrees. A function accounting for the effect of oxygen on OUR should thus take into account the soluble substrate concentration. This undermines the assumption of independence underlying current empirical models.

The multiplicative empirical model has shown to have such major limitations that other types of models are needed to acquire reliable reactor models. The theoretical model is a natural

candidate for such new type of model, however it needs some major adjustment to be of practical use. For reactor applications, and parameter estimation the model is too complicated and a reduced model is needed.

3.6 REFERENCES

1. Richard, T.L., *The kinetics of solid-state aerobic biodegradation*. 1997, Cornell University.
2. Cooney, C.L., D.I. Wang, and R.I. Materles, *Measurement of heat evolution and correlation with oxygen consumption during microbial growth*. Biotechnology and Bioengineering, 1968. 11: p. 269-281.
3. Luong, J.H.T. and B. Volesky, *Heat evolution during microbial process - estimation, measurement, and applications*. Advances In Biochemical Engineering/Biotechnology, 1983. 28: p. 1-40.
4. Inbar, Y., et al., *New Approaches to compost maturity*. Biocycle, 1990(December): p. 64-69.
5. Jeris, J.S. and R.W. Regan, *Controlling environmental parameters for optimum composting I: experimental procedures and temperature*. Compost Science, 1973. 14(1): p. 10-15.
6. Jeris, J.S. and R.W. Regan, *Controlling environmental parameters for optimum composting II: moisture, free air space and recycle*. Compost Science, 1973. 14(2): p. 8-15.
7. Jeris, J.S. and R.W. Regan, *Controlling environmental parameters for optimum composting III*. Compost Science, 1973. 14(3): p. 16-22.
8. Hamelers, H.V.M. *A Theoretical Model of Composting Kinetics*. in *Proceedings of the International Composting Research Symposium*. 1992. Columbus OH: Renaissance Publications.
9. Aris, R., *Mathematical modelling techniques*. 1978, London: Pitman.
10. Rappoldt, C., *The application of diffusion models to an aggregated soil*. Soil Science, 1997. 150(3): p. 645-661.
11. Revsbech, N.P., *Diffusion characteristics of microbial communities determined by use of oxygen microsensors*. Journal of Microbiological Methods, 1989. 9: p. 111-122.
12. Griffin, D.M. and E.J. Luard. *Water stress and microbial ecology*. in *Strategies Of Microbial Life In Extreme Environments*. 1979. Berlin.
13. Hansen, R.C., et al. *Composting of poultry manure*. in *Proceedings of the International Composting Research Symposium*. 1992. Columbus OH: Renaissance Publications.

14. Sonnleitner, B., *Biotechnology of thermophilic bacteria- growth, products and application*. Advances In Biochemical Engineering/ Biotechnology, 1983.
15. Cooney, C.L. and D.L. Wise, *Thermophilic Anaerobic Digestion of Solid Waste for Fuel Gas Production*. Biotechnology and Bioengineering, 1975. XVII: p. 1119-1135.
16. Bodelier, P.L. and H.J. Laanbroek, *Oxygen uptake kinetics of Pseudomonas chlororaphis grown in glucose- or glutamate-limited continuous cultures*. Archives Microbiology, 1997. 167: p. 392-395.
17. Heijnen, J.J. and J.A. Roele, *A macroscopic model describing yield and maintenance relationship in aerobic fermentation processes*. Biotechnology And Bioengineering, 1981. 23: p. 739-763.
18. Bird, R.D., W.E. Stewart, and E.N. Lightfoot, *Transport phenomena*. 1960, New York: John wiley & sons.
19. van Ginkel, J.T., *Physical and biochemical processes in composting material*. 1996, Wageningen Agricultural University: Wageningen.
20. Bolze, R. and G. Tuve, *CRC Handbook of Tables for applied Engineering Science*. 1973: CRC Press.
21. Alphenaar, A., *Anaerobic granular sludge*. 1994, Wageningen Agricultural University: Wageningen.
22. Koornneef, E., *Composting van kippemest*, in *Environmental Technology*. 1988, Wageningen Agricultural University: Wageningen.
23. Wilhelm, E., R. Battino, and R.J. Wilcock, *Low-Pressure Solubilities of Gases in Liquid Water*. Chemical Reviews, 1977. 77(2): p. 219-262.
24. Harremoes, P., *Biofilm kinetics*, in *Water Pollution Microbiology vol.2*, R. Mitchell, Editor. 1978, John Wiley & Sons: New York.
25. Nakasaki, K., et al., *Effect of seeding during thermophilic composting of sewage sludge*. Applied And Environmental Microbiology, 1985. 49: p. 724-726.
26. Nakasaki, K. and T. Akiyama, *Effects of seeding on thermophilic Composting of Household Organic Waste*. Journal of Fermentation Technology, 1988. 66(1): p. 37-42.
27. Schumper, A., G. Quicker, and W. Deckwer, *Gas Solubilities in Microbial Culture Media*. Advances In Biochemical Engineering, 1979. 24.

28. Richard, T.L. and L.P. Walker, *Temperature kinetics of aerobic solid-state biodegradation*. Proceedings of the IBE, 1998. 1: p. A10-A30.
29. Characklis, W.G. and W. Gujer. *Temperature dependency of microbial reactions*. in *Kinetics Of Water Waste Treatment*. 1975. Copenhagen.
30. Suler, D.J. and M.S. Finstein, *Effect of Temperature, Aeration, and Moisture on CO₂ Formation in Bench-Scale, Continuously Thermophilic Composting of Solid Waste*. Applied and Environmental Microbiology, 1977. 33(2): p. 345-350.
31. Richard, T.L., L.P. Walker, and J.M. Gosset, *The effects of oxygen on solid-state biodegradation kinetics*. Proceedings of the IBE, 1999. 2: p. A22-A39.

4. AN ANALYTICAL APPROXIMATE SOLUTION OF THE OUR	114
4.1. INTRODUCTION	114
4.2. APPROXIMATE MODEL	115
4.2.1. <i>Conceptual model outline</i>	115
4.2.2. <i>Simplifying assumptions</i>	118
4.2.3. <i>Balance equations</i>	122
4.2.4. <i>Solution strategy</i>	125
4.3. SUBSTRATE SATURATED STAGE SOLUTION	125
4.3.1. <i>OUR</i>	125
4.3.2. <i>Soluble substrate</i>	133
4.3.3. <i>Total insoluble substrate</i>	134
4.3.4. <i>Switch time</i>	137
4.4. SUBSTRATE LIMITED STAGE SOLUTION	139
4.4.1. <i>Total insoluble substrate</i>	139
4.4.2. <i>OUR</i>	139
4.4.3. <i>Soluble substrate</i>	140
4.5. PREDICTION BIAS.....	142
4.5.1. <i>Comparison for the nominal parameter set</i>	142
4.5.2. <i>Comparison over a parameter range</i>	147
DISCUSSION.....	151
4.6.1. <i>Evaluation</i>	151
4.6.2. <i>Implications</i>	153
4.7. REFERENCES	155

4. An analytical approximate solution of the OUR.

4.1. Introduction

To understand the composting process and to develop better composting systems knowledge of the composting kinetics is paramount. The Oxygen Uptake Rate (OUR) is the most important composting process rate measure (chapter 3). In chapter 3 a theoretical model was constructed for the composting kinetics of equally sized particles. The theoretical model showed to explain the effect of oxygen on the OUR dynamics better than conventional empirical models.

Although the theoretical model seems to be a good starting point for process design, the numerical solution however requires a big computational effort. As a process design involves many process evaluations, direct practical application of the theoretical model seems limited. To increase the potential for practical application of the theoretical model an analytical approximate solution of the theoretical model will be developed in this chapter. Modern composting plants operate at constant process conditions (temperature, oxygen) by using feedback control. Therefore the analytical model aims at describing the OUR time course under constant process conditions.

Apart from practical application as such, an analytical solution has the additional advantage of giving more insight into the relations between the basic processes determining the OUR. Otherwise insight in the theoretical model may only be obtained by numerical approximation e.g. a sensitivity analysis. The results of such an analysis always depend on the specific values of the parameters used for the simulation. An analytical model however can be understood with little or no knowledge of the parameter values involved.

For composting, at the moment no analytical solutions are present for the OUR time course other than a first-order model [1]. This model is only valid over a specific time period and does not handle the initial higg rate period well [2]. In the field of solid state fermentation the logistic function is used as a description of the OUR[3]. However this function is also empirical and lacks a mechanistic background to relate the model parameters to environmental conditions. The logistic model has been used only to model a much shorter fermentation period than is conventionally needed for composting.

This chapter focuses on an analytical approximation of the OUR, other state variables are only taken into account if this is necessary to arrive at the solution for the OUR. In this way an approximate analytical expression for the development in time for soluble substrate, insoluble substrate, biomass and oxygen is obtained as a function of the initial particle conditions water content, particle size, interfacial oxygen concentration. The analytical approximation is based on a simplification of the mass balances underlying the theoretical model. These simplifications cause a deviation between the numerical results of the theoretical model and the analytical approximation. The analytical approximation is only valuable if this deviation may be neglected. The deviation of the analytical approximation will therefore be investigated for different situations.

4.2. Approximate model

4.2.1. Conceptual model outline

The conceptual model used in this chapter is based on the conceptual model presented in chapter 3. Chapter 3 describes in more detail the assumptions underlying the conceptual model. The basic model assumption is the particulate nature of the waste. The waste is assumed to exist in separate particles that are influenced only via the gas phase surrounding the particles. The particle volume is made up of water, inert material, insoluble substrate and aerobic microbial biomass. Soluble substrate and oxygen are dissolved within the water. The primary reaction occurring in the particle is the oxidation of soluble substrate. This reaction produces water, carbon dioxide, heat and new biomass. The reaction is performed by the aerobic biomass and the rate is influenced by the concentration of biomass, oxygen and soluble substrate. Carbon dioxide and heat are assumed to be removed without influencing the process.

The oxygen needed for oxidation originates from the gas phase that is assumed to have a constant oxygen content. The gas phase and the particle have the same constant temperature. The gas phase is saturated with water and thus no water loss from the particle occurs. As oxygen is directly consumed within the particle, oxygen penetrates the particle only over a short distance. Oxygen is transported by diffusion in the water phase because of an oxygen profile induced by the oxygen consumption. As only the outer region of the particle is aerobic, the remaining inner region of the particle will be anaerobic.

Insoluble substrate is converted into soluble substrate via microbial hydrolysis. This process occurs both in the aerobic and the anaerobic region. Soluble substrate is only degraded in the aerobic layer of the particle and thus a concentration profile within the particle will build up. As a result of the profile, soluble substrate will diffuse from the anaerobic into the aerobic region.

Water is either free water that can migrate under the action of a water potential difference or is associated with biomass. The associated water is attached to extracellular polymeric substances or is contained within the cell membrane. As water is a main constituent of biomass, biomass growth is accompanied by an appreciable water uptake. As biomass growth takes place only in the aerobic region a free water profile will arise. It is assumed that the water transport induced by this free water profile is so fast that an instantaneous redistribution of water within the particle occurs.

Biomass growth, insoluble substrate degradation and water redistribution cause a convective mass transport within the particle. As biomass only grows within the aerobic region the main volume increase takes place in this region. This volume increase induces a convective material transport toward the anaerobic region.

Material balances, accounting for conversion reactions, diffusion transport and convective transport were set up as described in chapter 3. Computer simulation gave the characteristic OUR time course shown in figure 4.1. Initially the OUR shows a strong increase and reaches a maximum plateau. At a certain point of time the OUR suddenly drops sharply. This sharp drop is followed by a slow decrease in the OUR. A parameter sensitivity analysis gives an explanation for this characteristic behavior, schematically shown in figure 4.2. Initially sufficient soluble substrate is present and the OUR is only determined by the penetration depth of oxygen and the biomass concentration (Fig. 4.2A). Growth of biomass occurs only within the aerobic region. As a result of the biomass increase the OUR will increase and consequently the penetration depth of oxygen will decrease. At a certain point of time the biomass concentration has reached its maximum level (Fig. 4.2B). As long as sufficient substrate is available, the maximum conversion rate will be maintained. The produced biomass is expelled by the convective mass transport, which velocity is maximal during this phase. As a result of the soluble substrate conversion in the aerobic phase, a concentration profile has developed (Fig. 4.2A/B).

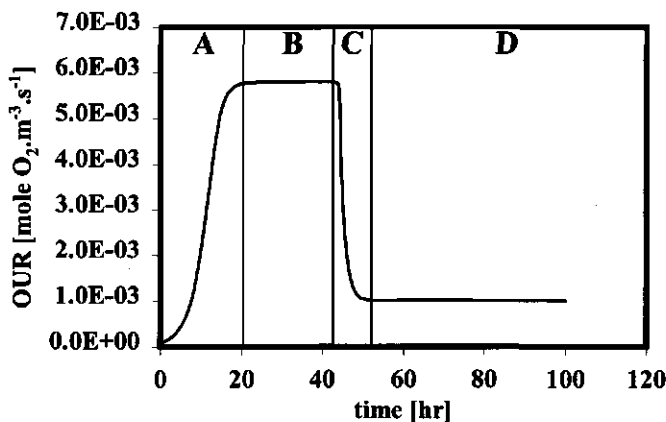


Figure 4.1: The characteristic development in time of the OUR. Four different periods are distinguished. A: OUR increase due to biomass growth; B: plateau of maximum OUR due to biofilm limitation; C: fast decrease due to limited soluble substrate availability; D: slow decrease due to hydrolysis of insoluble substrate. The periods A and B form together the substrate saturated stage. The periods C and D form together the substrate limited stage.

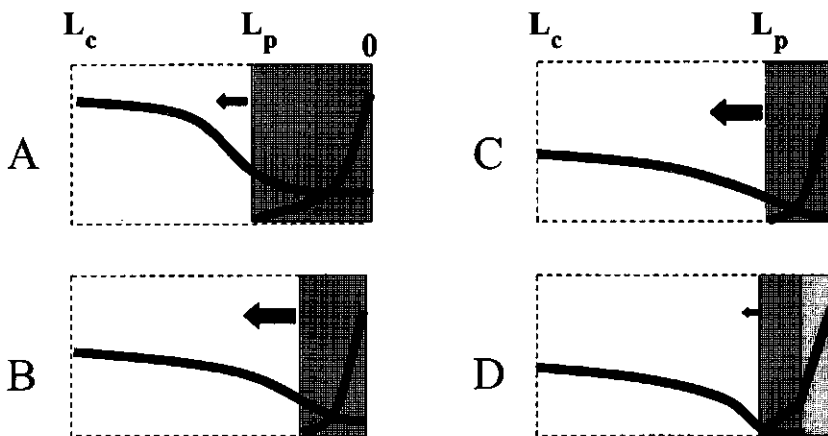


Figure 4.2: Schematic representation of the development in time of the main processes. The four situations are representative for the periods enumerated in figure 4.1. The left side is the interior of the particle, the right side is the gas side interface. The gray area is the area where the aerobic microbial activity takes place. The black line indicates the soluble substrate profile, the dashed line the oxygen profile. The arrow indicates the direction and importance of the inward directed convective mass transport. L_c is the characteristic particle size and L_p is the penetration depth of oxygen within the particle.

After some time the soluble substrate becomes rate limiting. The biomass within the aerobic region is no longer fully saturated with substrate. This situation arises at the moment that the soluble substrate concentration is zero at the gas particle interface. (Fig. 4.2C)

From this moment on an ever-increasing part of the biomass will be substrate limited (Fig. 4.2D). Oxygen supply is no longer limiting. The conversion initially takes place in a small region next to the gas interface as biomass is abundantly present there. The OUR in this situation is determined by the flux of soluble substrate into the biomass region next to the gas interface. At first this flux is determined by the diffusional transport rate and the OUR decreases quickly. Soon the flux is solely determined by hydrolysis, and the OUR decreases only slowly.

4.2.2. Simplifying assumptions

The approximate analytical solution is based on a modified model, resulting from simplifying the theoretical model as presented in chapter 3. The following simplifying assumptions are used:

- The conversion processes are approximated.

In chapter 3 a biomass decay coefficient b was introduced that described the death of biomass. The dead biomass was incorporated into the insoluble substrate using a conversion constant Y_{Sd} . The sensitivity analysis showed this conversion constant unimportant, implying that this process might be simplified. The same applies for the dependence of the growth rate on soluble substrate and oxygen. The parameters describing this dependency showed no significant effect in the sensitivity analysis. The following simplified description of the conversion reactions is therefore proposed. The aerobic microbial growth process rate (R_g) consists of three sub processes, all first order in biomass. The maximum growth rate (μ_m) describes the growth as a result of the conversion of soluble substrate. The decay rate constant (b) describes the auto oxidation of the organism needed for its maintenance requirement. This is a different interpretation of the biomass decay factor, such that no dead biomass is produced but the apparent yield remains the same. With respect to oxygen and soluble substrate these processes are zero-order. Hydrolysis of all biomass is introduced to allow degradation of the produced biomass on the long term. Otherwise, the biomass would accumulate, as no

degradation of biomass at all would take place. If oxygen and soluble substrate are present, hardly any effect can be seen on the growth rate as $k_h \ll \mu_m$.

$$R_X = (\mu_m - b)X - k_h X = \mu_n X \quad O_2 > 0 \wedge S_s > 0$$

eq. 4-1

$$R_X = -k_h X \quad O_2 = 0 \vee S_s = 0$$

X	: Biomass concentration	[mol X.m ⁻³]
O ₂	: Oxygen concentration	[mol O ₂ .m ⁻³]
S _s	: Soluble substrate concentration	[mol S _s .m ⁻³]
R _X	: Aerobic microbial growth rate	[mol X.m ⁻³ .s ⁻¹]
μ_n	: Net growth rate constant	[s ⁻¹]
μ_m	: Maximal growth rate constant	[s ⁻¹]
b	: Biomass decay constant	[s ⁻¹]
k _h	: Hydrolysis rate constant	[s ⁻¹]

Associated with the microbial growth is the soluble substrate consumption. This conversion rate equals:

eq. 4-2

$$R_{S_s} = \frac{\mu_m}{Y_{S_s}} X = \frac{1}{Y_{S_s}} \frac{\mu_m}{\mu_n} R_X$$

R _{Ss}	: Consumption rate of soluble substrate	[mol S _s .m ⁻³ .s ⁻¹]
Y _{Ss}	: Biomass yield on soluble substrate	[mol X.mol S _s ⁻¹]

It is important to note that the soluble substrate consumption is determined by the maximum growth rate constant, as soluble substrate is consumed both for net growth and maintenance. For the consumption rate of oxygen (R_{O₂}) a relationship similar to the soluble substrate consumption rate can be set up using the biomass yield on oxygen (Y_{O₂}).

$$\text{eq. 4-3} \quad R_{O_2} = \frac{1}{Y_{O_2}} \frac{\mu_m}{\mu_n} R_X$$

R_{O_2} : Consumption rate of oxygen [mol O₂.m⁻³.s⁻¹]

Y_{O_2} : Biomass yield on oxygen [mol X.mol O₂⁻¹]

As both the insoluble substrate and biomass act as a source of soluble substrate it makes sense to lump these two variables together to a new variable, called total insoluble substrate. ($S_{i,t}$)

$$\text{eq. 4-4} \quad S_{i,t} = S_i + \frac{X}{Y_{S_i}}$$

Y_{S_i} : Biomass yield on insoluble substrate [mol X.mol S_i⁻¹]

S_i : "Genuine" insoluble substrate concentration [mole S_i.m⁻³]

$S_{i,t}$: Total insoluble substrate concentration [mole S_{i,t}.m⁻³]

This lumping is also practically meaningful, because as a rule, biomass and insoluble substrate can not be separated from each other when present in waste. The hydrolysis rate of the total insoluble substrate can be described by a first-order approximation.

$$\text{eq. 4-5} \quad R_{S_i} = k_h \cdot S_{i,t}$$

R_{S_i} : Hydrolysis rate of total insoluble substrate [mol S_{i,t}.m⁻³.s⁻¹]

- The particle size is assumed constant.

As the simulation in chapter 3 with the theoretical model revealed that the particle size showed only a moderate change, the particle size L_c is assumed constant, at any time L_c equals the initial particle size $L_{c,0}$. Particle size constancy can be considered as a different interpretation of the average state variables, their concentration being now based on the initial volume and not on the actual volume. This agrees with composting (research) practice where as a rule measured amounts are related to some initial amount or volume. The reason for this is the difficulty to measure frequently amounts of different components accurately.

- Convective mass transport

Convective mass transport is of importance only during the first phase of the process, when significant amounts of biomass are produced. Particle size constancy implies that at any time the overall volume changes must cancel. The volume changes of water and biomass are considered. The volume change of insoluble substrate may be neglected over the first part of the process, as it is a relatively slow process.

- Water

The particle size is assumed constant and the total particle volume consequently does not change. As only the biomass volume and water volume changes are taken into account, the change in water volume and thus amount is determined by biomass growth. Hence the balance equation for water needs not be evaluated explicitly, and will no longer be considered.

Diffusion of soluble compounds takes place only in the water phase. The effective diffusion coefficient of oxygen is determined according to :

$$\text{eq. 4-6} \quad D_{O_2} = \varepsilon_{w,0}^2 \cdot D_{O_2,w}$$

D_{O_2} : Effective diffusion coefficient of oxygen $[m^2.s^{-1}]$

$D_{O_2,w}$: Diffusion coefficient in pure water $[m^2.s^{-1}]$

$\varepsilon_{w,0}$: Initial volumetric water fraction $[-]$

The effective diffusion coefficient for soluble substrate is determined in the same way.

$$\text{eq. 4-7} \quad D_{S_s} = \varepsilon_{w,0}^2 \cdot D_{S_s,w}$$

D_{S_s} : Effective diffusion coefficient of soluble substrate $[m^2.s^{-1}]$

$D_{S_s,w}$: Diffusion coefficient of soluble substrate in pure water $[m^2.s^{-1}]$

As inert material is not converted and the particle size is fixed, the average concentration will not change over time. The inert material is therefore not longer taken into account.

4.2.3. Balance equations

From the previous discussion it has become clear that the state variables biomass, oxygen, soluble and insoluble substrate are taken explicitly into account. The balances are based on the balances derived in chapter 3, however they are sometimes altered to correspond with the simplifying additional assumptions listed before. The dependency of the state variables on space and time is not explicitly represented to simplify the notation. This holds for the following variables, X , S_s , S_i , O_2 , R_X , R_{O_2} , R_{S_s} , R_{S_i} and the convective velocity u .

Biomass, X

eq. 4-8

$$\frac{\partial X}{\partial t} = - \frac{\partial u \cdot X}{\partial z} + R_X$$

$$\begin{array}{lll} t = 0 & z > 0 & X = X_0 \\ t > 0 & z = 0 & \frac{\partial X}{\partial z} = 0 \\ t > 0 & z = L_c & \frac{\partial X}{\partial z} = 0 \end{array}$$

z	: Spatial coordinate	[m]
X_0	: Initial biomass concentration	[mol $\text{X} \cdot \text{m}^{-3}$]
L_c	: Characteristic particle size	[m]
$u(z)$: Convective velocity	[$\text{m} \cdot \text{s}^{-1}$]
t	: Time	[s]

The first term of the balance eq. 4-8 reflects the convective transport rate while the second term denotes the microbial growth rate

Oxygen, O₂

eq. 4-9

$$\frac{\partial O_2}{\partial t} = D_{O_2} \cdot \frac{\partial^2 O_2}{\partial z^2} - R_{O_2}$$

$$t = 0 \quad 0 < z \leq L_c \quad O_2 = O_{2,i}$$

$$t > 0 \quad z = 0 \quad O_2 = O_{2,i}$$

$$t > 0 \quad \begin{cases} z = L_p = L_c \quad \frac{\partial O_2}{\partial z} = 0 \quad \text{or} \\ z = L_p < L_c \quad \frac{\partial O_2}{\partial z} = 0 \wedge O_2 = 0 \end{cases}$$

L_p : Penetration depth of oxygen [m]

O_{2,i} : Oxygen concentration at the gas side interface [mol O₂.m⁻³]

The same balance is used as in the theoretical model, except that the convective mass transport is neglected. The first term in the balance denotes the diffusion term. The diffusion coefficient is assumed constant and thus no longer makes part of the derivative term. The second term describes the oxygen consumption rate. The boundary condition at the gas interface side (z=0) describes that the oxygen concentration there is constant, i.e. determined by a constant gas phase oxygen content. Two situations must be however considered for the other boundary condition. If the particle is fully penetrated the boundary condition at z=L_c becomes the zero flux condition. However if the particle is not fully penetrated a new variable the oxygen penetration depth (L_p) enters into the problem. This new variable describes the depth within the particle where the oxygen has just been depleted. The equation can in this case be solved by using two conditions at z=L_p both the oxygen concentration and the oxygen flux are zero.

The choice of the initial condition is somewhat arbitrary. However it will show that this is not a matter of great importance as a pseudo-steady state is rapidly attained, i.e. the initial condition is no longer relevant.

Soluble substrate balance, S_s

eq. 4-10

$$\frac{\partial S_s}{\partial t} = D_{S_s} \cdot \frac{\partial^2 S_s}{\partial z^2} + R_{S_s} - R_{S_s}$$

$$t = 0 \quad 0 < z \leq L_c \quad S_s = S_{s,0}$$

$$t > 0 \quad z = 0 \quad \frac{\partial S_s}{\partial z} = 0$$

$$t > 0 \quad z = L_c \quad \frac{\partial S_s}{\partial z} = 0$$

$S_{s,0}$: Initial soluble substrate concentration

[mol $S_s \cdot m^{-3}$]

Apart from the omission of the convective transport term the same balance equation has been used as for the theoretical model. The first term of the balance again denotes the diffusion term, again with a constant diffusion coefficient. The second term is the production of soluble substrate through hydrolysis, while the third term denotes the consumption of soluble substrate by microbial oxidation.

Total Insoluble substrate, $S_{i,t}$

eq. 4-11

$$\frac{dS_{i,t}}{dt} = -k_h \cdot S_{i,t} + \frac{R_X}{Y_{S_i}}$$

eq. 4-12

$$t = 0 \quad 0 \leq z \leq L_c \quad S_{i,t} = S_{i,t,0}$$

$S_{i,t,0}$: Initial insoluble substrate concentration

[mol $S_{i,t} \cdot m^{-3}$]

The spatial distribution of the insoluble substrate has been neglected. The balance can therefore be expressed as an ordinary differential equation. The first term denotes the degradation of insoluble substrate due to hydrolysis, while the second term denotes the production of new total insoluble substrate due to growth of biomass.

4.2.4. Solution strategy

The previous paragraph presented the balance equations that need to be solved to obtain an expression for the OUR as a function of time, initial states and the constant process conditions. The strategy used to solve these balances is based on the presence of the two distinct process stages, the substrate saturated and the substrate limited stage. In the first stage sufficient soluble substrate is present and the OUR is determined by the penetration depth of oxygen and the specific volumetric conversion rate within this region (Fig. 2A+2B). A solution of the oxygen and biomass balance is needed to solve for the OUR.

During the subsequent substrate limited stage the OUR is determined by the availability of soluble substrate to the biomass (Fig 2D). The OUR can be determined by solving the soluble substrate balance.

The point of time at which the transition from the substrate saturated to the substrate limited stage occurs is called the switch time (t_s). The solution is only complete if the switch time is known. The switch time can be found by the condition that at the switch time the soluble substrate concentration at the gas interface has just become zero (Fig 2C). To obtain a solution for the switch time the soluble substrate balance during the substrate saturated stage needs to be solved.

The main interest lies in a typical OUR time course i.e. the process development of particles with such properties as can be expected to exist in practice. This allows sometimes further simplifications because solutions irrelevant for practice need no consideration.

4.3. Substrate saturated stage solution

4.3.1. OUR

All equations under this heading are valid if time is smaller than or equal to the switch time $t \leq t_s$. This condition will not be explicitly mentioned with each equation. The biomass balance will be considered first. The OUR is determined by the active biomass i.e. the biomass inside aerobic region. The aerobic region is determined by the penetration depth of oxygen within the particle (L_p), i.e. the distance at which the oxygen concentration has become zero. Through differentiation eq. 4-8 can be written as:

$$\text{eq. 4-13} \quad \frac{\partial X}{\partial z} = -X \cdot \frac{\partial u}{\partial z} - u \cdot \frac{\partial X}{\partial z} + R_x \quad z \leq L_p$$

It is assumed that initially the biomass concentration is homogeneously distributed. As the biomass growth takes place at the same rate within the aerobic region, the biomass concentration will remain homogeneously distributed, and therefore the term $u \cdot \frac{\partial X}{\partial z}$ in eq. 4-13 vanishes.

Biomass and free water are the only two components that undergo an appreciable volume change. This means that the convective velocity can be calculated as: (see chapter 3: eq3-16, 3-17 and 3-18):

$$\text{eq. 4-14} \quad u(z) = \frac{1}{A} \cdot \frac{dV(z)}{dt} = \frac{1}{A} \cdot \left(\frac{dV_x(z)}{dt} + \frac{dV_w(z)}{dt} \right)$$

$V(z)$: Volume of all components going from 0 to z	[m ³]
$V_x(z)$: Cumulative biomass volume going from 0 to z	[m ³]
$V_w(z)$: Cumulative water volume going from 0 to z	[m ³]
A	: Specific surface area of particle	[m ²]

The free water is defined as the water that does not make part of the microbial colonies within the waste particle. At any time the free water is assumed evenly distributed over the inert and insoluble lumps within the whole waste particle. This assumption implies that a volumetric free water fraction ϵ_f may be defined that everywhere within the particle has the same value. The volumetric free water fraction may change in time due to microbial growth.

$$\text{eq. 4-15} \quad \epsilon_f = \frac{V_w(L_c)}{V(L_c) - V_x(L_c)}$$

ϵ_f	: Free water fraction on biomass free volume	[-]
--------------	--	-----

As the total particle size is assumed constant in time the following relation holds:

eq. 4-16

$$dV_x(L_c) = -dV_w(L_c)$$

This equation expresses that a change in biomass volume is compensated by an opposite change in water volume. This is a realistic assumption as the biomass volume is mainly made up of water and the degradation of insoluble substrate is relatively small during the substrate saturated stage. The local water volume is changing due to the local production of biomass and the change in the volumetric free water content ε_f .

eq. 4-17

$$\frac{dV_w(z)}{dt} = \frac{d\varepsilon_f(V(z) - V_x(z))}{dt}$$

The change of the free water fraction ε_f can be found by considering the total particle volume.

eq. 4-18

$$\frac{d\varepsilon_f}{dt} = \frac{d\left(\frac{V_w(L_c)}{V(L_c) - V_x(L_c)}\right)}{dt}$$

The change of biomass volume is a result of biomass growth and one can write:

eq. 4-19

$$V_x(z) = A \int_0^z \left(\frac{X}{X_m} \right) d\zeta$$

$$\frac{dV_x(z)}{dt} = A \int_0^z \left(\frac{R_X}{X_m} \right) d\zeta$$

ζ : Spatial coordinate [m]

X_m : Maximal biomass density [mol X.m⁻³]

Upon substitution eq. 4-15, eq. 4-16, eq. 4-19 in eq. 4-18 and some manipulation the following relationship for the temporal change in the free water content is found:

eq. 4-20

$$\frac{1}{1-\varepsilon_f} \frac{d\varepsilon_f}{dt} = \frac{1}{L_c - \int_0^{L_c} \frac{X}{X_m} d\zeta} \cdot \int_0^{L_c} \frac{R_X}{X_m} d\zeta$$

Combining eq 4-14, 4-17 and 4-19 gives the following result for the convective velocity:

$$eq. \ 4-21 \quad u(z) = -\frac{z - \int_0^z \frac{X}{X_m} d\zeta}{1 - \varepsilon_f} \cdot \frac{d\varepsilon_f}{dt} + \int_0^z \frac{R_X}{X_m} d\zeta$$

Combining eq. 4-20 and 4-21, eliminating ε_f , gives the following relationship for the convective velocity $u(z)$:

$$eq. \ 4-22 \quad u(z) = -\frac{z - \int_0^z \frac{X}{X_m} d\zeta}{L_c - \int_0^{L_c} \frac{X}{X_m} d\zeta} \cdot \int_0^{L_c} \frac{R_X}{X_m} d\zeta + \int_0^z \frac{R_X}{X_m} d\zeta$$

For the biomass balance the first derivative of the convective velocity with respect to z (eq. 4-13) is needed. Two additional relationships are used to derive this derivative. The first relation (4-23) is an approximation and expresses that the biomass expelled into the anaerobic region is not taken into account when evaluating the integral over the whole particle. This introduces no substantial error as this biomass fraction is very small anyhow and thus its omission only influences the convective velocity marginal.

$$eq. \ 4-23 \quad \int_0^{L_c} \frac{X}{X_m} d\zeta = L_p(t) \frac{X_a(t)}{X_m}$$

$X_a(t)$: Biomass concentration within the aerobic region [mol X.m⁻³]

A new biomass variable has been introduced for the sake of clarity. X_a represents the biomass concentration within the aerobic region, this biomass concentration is everywhere the same within this region, and is therefore represented as a function of time only.

The second relation (4-24) is exact as biomass growth takes place only within the aerobic region.

$$\text{eq. 4-24} \quad \int_0^{L_c} \frac{R_X}{X_m} d\zeta = L_p(t) \frac{R_X(t)}{X_m}$$

Combining the biomass balance (4-13) with the appropriate rate term (4-1), the convective velocity equation (4-22) and the additional relationships (4-23,4-24) gives after some manipulation the following equation describing biomass growth within the aerobic segment:

$$\text{eq. 4-25} \quad \frac{dX_a(t)}{dt} = \frac{R_X}{1 - \frac{X_a(t)L_p(t)}{X_m L_c}} \left(1 - \frac{X_a(t)}{X_m} \right)$$

This equation can not be directly solved, as the penetration depth is a yet unknown function of time. However ahead of the treatment of the oxygen balance it will be assumed here that the penetration depth is inversely proportional to square root of the biomass concentration. The penetration depth reaches its minimum when the biomass concentration $X_a(t)$ reaches its maximum value.

$$\text{eq. 4-26} \quad L_p(t) = L_{p,\min} \cdot \sqrt{\frac{X_m}{X_a(t)}}$$

$L_{p,\min}$: Minimum penetration depth of oxygen [m]

Substituting eq 4-26 in eq. 4-25 gives a differential equation that can be solved.

$$\text{eq. 4-27} \quad \frac{dX_a(t)}{dt} = \frac{\mu_n \cdot X_a(t)}{1 - \frac{L_{p,\min}}{L_c} \sqrt{\frac{X_a(t)}{X_m}}} \left(1 - \frac{X_a(t)}{X_m} \right)$$

$t = 0 \quad X_a = X_0$

This equation can be solved by separating the variables and has as a solution:

eq. 4-28

$$\mu_n \cdot t = \ln \left(\frac{X_a(t)}{X_m - X_a(t)} \cdot \frac{X_m - X_0}{X_0} \right) + \frac{L_{p,\min}}{L_c} \cdot \ln \left(\frac{X_m + X_a(t) - 2\sqrt{X_m \cdot X_a(t)}}{X_m - X_a(t)} \cdot \frac{X_m - X_0}{X_m + X_0 - 2\sqrt{X_m \cdot X_0}} \right)$$

The biomass concentration can not be expressed as an explicit function of t . However in case that the minimal penetration depth is much smaller than the particle size, the second term on the right side of equation 4-28 may be neglected. This can be seen by solving eq. 4-27 for $L_{p,\min}=0$. The biomass concentration can than be expressed as an explicit function of t , i.e. the logistic function.

$$X_a(t) = \frac{\beta}{\beta + e^{-\mu_n \cdot t}} \cdot X_m \quad \text{eq. 4-29}$$

β : Dimensionless initial biomass concentration

[1]

In this function β equals:

$$\beta = \frac{X_0}{X_m - X_0} \quad \text{eq. 4-30}$$

In case that the factor $\lambda_{p,\min} = L_{p,\min}/L_c$ may not be neglected the logistic function can still be used for approximation. In this case the parameter μ_n and β need to be adjusted in the following way. At the point of time that $X=0.5$, the first time derivative of the logistic function reaches its maximum. The parameter values for μ_n and β for the approximating logistic function (4-29) are chosen such that $X=0.5$ is reached at the same point of time as the general solution (4-28) and has the same value of the first time derivative at this point. The resulting approximating solution runs as:

$$X(t) = \frac{\beta_{\text{eff}}}{\beta_{\text{eff}} + e^{\mu_{\text{eff}} \cdot t}} \cdot X_m \quad \text{eq. 4-31}$$

β_{eff} : Effective dimensionless initial biomass concentration

[-]

μ_{eff} : Effective growth rate constant

[s⁻¹]

$$\text{eq. 4-32} \quad \mu_{\text{eff}} = \mu_n \cdot \frac{1}{1 - \lambda_{p,\min} \cdot \sqrt{\frac{1}{2}}}$$

$\lambda_{p,\min}$: Dimensionless minimal penetration depth [-]

It is interesting to note that this result implies that the effective growth rate depends on the particle size. Of course this is only an apparent growth rate constant, the true constant remains the same at the time. The effective initial biomass concentration runs as:

$$\text{eq. 4-33} \quad \beta_{\text{eff}} = \beta^{\frac{1}{1 - \lambda_{p,\min} \cdot \sqrt{\frac{1}{2}}}} \cdot \left(\frac{\sqrt{\beta + 1} + \sqrt{\beta}}{\sqrt{\beta + 1} - \sqrt{\beta}} \cdot \frac{2 - \sqrt{2}}{2 + \sqrt{2}} \right)^{\frac{-\lambda_{p,\min}}{1 - \lambda_{p,\min} \cdot \sqrt{\frac{1}{2}}}}$$

This approximation works well if $\lambda_{p,\min} = \frac{L_{p,\min}}{L_c} \ll 1$ and becomes exact if $\lambda_{p,\min} = 0$.

For larger particles when $\lambda_{p,\min}$ is small the effective constants coincide with the "true" constants, however as $\lambda_{p,\min}$ increases the effective growth rate constant increases. To understand this phenomenon, consider a nearly fully penetrated particle, biomass growth and OUR increase will then be almost exponential. However the situation is described by a logistic function that predicts an ever decreasing specific growth rate in time. To use the logistic curve in such a situation the growth rate constant needs to be increased. A similar explanation can be given for the initial dimensionless biomass density.

The penetration depth of oxygen can be found by solving the oxygen balance. As shown in appendix A-2 the solution of the oxygen profile can after a short initial period be described as:

$$\text{eq. 4-34} \quad O_2 = O_{2,i} - \frac{\rho_m \cdot \mu_m}{Y_{O_2} \cdot D_{O_2}} \cdot \frac{\beta_{\text{eff}}}{\beta_{\text{eff}} + e^{-\mu_{\text{eff}} \cdot t}} \left(z - \frac{z^2}{2L_p} \right) L_p$$

From eq 4-34 and the condition that the oxygen concentration is zero at the penetration depth, the penetration depth can be calculated as:

$$\text{eq. 4-35} \quad L_p(t) = \sqrt{2 \cdot D_{O_2} \cdot O_{2,i} \frac{Y_{O_2}}{X_a(t) \mu_m}}$$

This equation shows that the assumptions made about the penetration depth earlier to solve the biomass balance are warranted (eq. 4-26) and the minimum penetration depth $L_{p,\min}$ can be expressed as :

$$\text{eq. 4-36} \quad L_{p,\min} = \sqrt{2 \cdot D_{O_2} \cdot O_{2,b} \frac{Y_{O_2}}{\rho_x \cdot \mu_m}}$$

The OUR is determined by the penetration depth and the conversion rate within the aerobic region.

$$\text{eq. 4-37} \quad \text{OUR}(t) = L_p(t) \frac{\mu_m}{Y_{O_2}} \cdot \frac{\beta_{\text{eff}}}{\beta_{\text{eff}} + e^{-\mu_{\text{eff}} \cdot t}} \cdot X_m$$

Substituting eq. 4-35 and eq. 4-31 in this relationship (4-37) gives the time dependence of the OUR during the substrate saturated stage.

$$\text{eq. 4-38} \quad \text{OUR}(t) = \sqrt{\frac{\beta_{\text{eff}}}{\beta_{\text{eff}} + e^{-\mu_{\text{eff}} \cdot t}}} \cdot \text{OUR}_m$$

OUR_m : maximally attainable OUR [mol O₂.m⁻³.s⁻¹]

The OUR_m is a new parameter and describes the OUR reached at maximal biomass density given the interfacial oxygen concentration and particle size. The parameter OUR_m equals:

$$\text{eq. 4-39} \quad \text{OUR}_m = \frac{I}{L_c} \sqrt{2 \cdot D_{O_2} \cdot O_{2,i} \cdot \frac{X_m \cdot \mu_m}{Y_{O_2}}}$$

A second variable of importance is the cumulative oxygen uptake. By integration over time of the OUR function the COU can be calculated as:

$$eq. 4-40 \quad COU(t) = \left(\ln \left(\frac{2.\beta_{eff} + e^{-\mu_{eff}.t} + 2.\sqrt{\beta_{eff} \cdot (\beta_{eff} + e^{-\mu_{eff}.t})}}{2.\beta_{eff} + 1 + 2.\sqrt{\beta_{eff} \cdot (\beta_{eff} + 1)}} \right) + \mu_{eff}.t \right) \cdot \frac{OUR_m}{\mu_{eff}}$$

4.3.2. Soluble substrate

The solution of the soluble substrate can be found by applying the method of variation of parameters as described in appendix (A-3). The solution runs as:

eq. 4-41

$$S_s(t, z) = S_{s,0} + \int_0^t k_h \cdot S_{i,t}(\tau) d\tau - \frac{Y_{O_2}}{Y_{S_s}} \int_0^t OUR(\tau) d\tau - \frac{Y_{O_2}}{Y_{S_s}} \frac{OUR(t)}{D_{S_s}} \sum_{n=1}^{\infty} \frac{2}{(n\pi)^2} \cdot \frac{L_c}{n\pi L_p(t)} \sin \left(n\pi \cdot \frac{L_p(t)}{L_c} \right) \left(1 - e^{-\lambda_n \cdot D_{S_s} \cdot t} \right) \cos(z \cdot \sqrt{\lambda_n})$$

λ_n : eigenvalue n (see appendix) [-]

$$eq. 4-42 \quad \lambda_n = \left(\frac{n\pi}{L_c} \right)^2$$

The first term of the solution 4-42 is the initial soluble substrate concentration, the second term is the amount of soluble substrate produced and the third term represents the amount of oxidized soluble substrate. The first three terms together represent the time course of the average soluble substrate concentration. The fourth term describes the shape of the soluble substrate profile in the particle. It is clear that at $t=0$ this term is zero due to the exponential term. After some time the exponential term has completely decayed and the steepness of the profile depends strongly on the current OUR, with a higher OUR the profile will be steeper. The profile will be also steeper with an increasing particle size and a decreasing diffusion coefficient D_{S_s} .

4.3.3. Total insoluble substrate

A solution for the total insoluble substrate development during the substrate limited period is needed to estimate the amount of soluble substrate produced during this period. This information is needed to obtain the switch time. The biomass production is linearly linked to the oxygen uptake rate as the transient term has been neglected in the solution of the oxygen balance. The total insoluble substrate balance may than be written as:

$$\text{eq. 4-43} \quad \frac{dS_{i,t}}{dt} = -k_h \cdot S_{i,t} + \frac{Y_{O_2}}{Y_{S_i}} \cdot \text{OUR}(t)$$

$$\text{eq. 4-44} \quad t = 0 \quad 0 < z \leq L_c \quad S_{i,t} = S_{i,t,0}$$

The general solution to this equation is given as:

$$\text{eq. 4-45} \quad S_{i,t} = S_{i,t,0} e^{-k_h t} + e^{-k_h t} \cdot \int_0^t \frac{Y_{O_2}}{Y_{S_i}} \cdot \frac{\text{OUR}(\tau)}{e^{-k_h \tau}} d\tau$$

$\text{OUR}(\tau)$

As no solution to the integral in 4-45 could be found, the solution was approximated in the following way. After some time the OUR approaches its maximum value OUR_m and the OUR is almost independent t . In case the OUR is constant the solution to eq. 4-45 can be directly found. Therefore we split the substrate saturated in two periods, one during which the OUR clearly changes over time and during which the OUR is nearly constant. The main thus focuses on the period during which the OUR has not yet sufficiently approached it's maximum. This period starts at $t=0$ and ends a certain time t_a , the saturation time. At this point of time the OUR equals $\alpha \cdot \text{OUR}_m$. These parameters are defined as:

$$\text{eq. 4-46} \quad \alpha = \frac{\text{OUR}(t)}{\text{OUR}_m} = \sqrt{\frac{\beta_{\text{eff}}}{\beta_{\text{eff}} + e^{-\mu_{\text{eff}} \cdot t_a}}}$$

t_a : saturation time

[s]

α : saturation level

[-]

From this equation t_α may be expressed as a function β_{eff} , μ_{eff} and the chosen parameter α as:

$$\text{eq. 4-47} \quad t_\alpha = \frac{1}{\mu_{\text{eff}}} \ln \left(\frac{\alpha^2}{\beta \cdot (1 - \alpha^2)} \right)$$

The attention is of course focused to the integral in eq 4-45. Using partial integration it can be shown that the following inequality is valid.

$$\text{eq. 4-48} \quad e^{-k_h t} \cdot \int_0^t \text{OUR}(\tau) d\tau < e^{-k_h t} \cdot \int_0^t \frac{\text{OUR}(\tau)}{e^{-k_h \tau}} d\tau < \int_0^t \text{OUR}(\tau) d\tau$$

This means that the solution lies between the boundaries:

$$\text{eq. 4-49} \quad S_{i,t,0} \cdot e^{-k_h t} + e^{-k_h t} \cdot \frac{Y_{O_2}}{Y_{S_i}} \text{COU}(t) < S_{i,t} < S_{i,t,0} \cdot e^{-k_h t} + \frac{Y_{O_2}}{Y_{S_i}} \text{COU}(t)$$

By either choosing the lower or upper boundary the maximum error introduced is smaller than the difference between upper and lower bound. Expressing the difference between upper and lower bound as a fraction of the initial total insoluble substrate gives:

$$\text{eq. 4-50} \quad \varepsilon \leq \frac{Y_{O_2}}{Y_{S_i}} (1 - e^{-k_h t}) \frac{\text{COU}(t)}{S_{i,t,0}}$$

ε : Approximation error [~]

As $k_h t_\alpha \ll 1$ and $\text{COU}(t_\alpha) \ll S_{i,t,0}$, eq. 4-50 shows that the approximate solution will have a small error relative to the total amount of consumed oxygen. In case of the nominal parameter set the error is less than 0.1%. The lower boundary will be used as a solution for the total insoluble substrate ($t \leq t_\alpha$):

$$\text{eq. 4-51} \quad S_{i,t}(t) = \left(S_{i,t,0} + \frac{Y_{O_2}}{Y_{S_i}} COU(t) \right) e^{-k_h t}$$

By substituting the relationship t_a in eq 4-51- the following relation is obtained for $S_{i,t}$ at t_a .

$$\text{eq. 4-52} \quad S_{i,t}(t_a) = \left(S_{i,t,0} + \frac{Y_{O_2}}{Y_{S_i}} \frac{OUR_m}{\mu_{eff}} \cdot \ln\left(\frac{1+\alpha}{(1-\alpha)}\right) \right) e^{-k_h t_a}$$

Now if $t > t_a$ the relationship for the $S_{i,t}$ is easily found from eq. 4-45 and 4-51 and runs as:

$$\text{eq. 4-53} \quad S_{i,t}(t) = \left(S_{i,t,0} + \frac{Y_{O_2}}{Y_{S_i}} \cdot COU(t_a) \right) e^{-k_h t_a} + \frac{Y_{O_2}}{Y_{S_i}} \cdot \frac{OUR_m}{k_h} \cdot (1 - e^{-k_h(t-t_a)})$$

The solution for the total insoluble substrate within the substrate-saturated period can be summarised as:

$$\text{eq. 4-54} \quad S_{i,t}(t) = \begin{cases} \left(S_{i,t,0} + \frac{Y_{O_2}}{Y_{S_i}} \cdot COU(t_a) \right) e^{-k_h t} & t \leq t_a \\ \left(S_{i,t,0} + \frac{Y_{O_2}}{Y_{S_i}} \cdot COU(t_a) \right) e^{-k_h t} + \frac{Y_{O_2}}{Y_{S_i}} \cdot \frac{OUR_m}{k_h} \cdot (1 - e^{-k_h(t-t_a)}) & t > t_a \end{cases}$$

The following result can be used for the amount of soluble substrate produced during the substrate saturated period.

eq. 4-55

$$\int_0^t k_h \cdot S_{i,t}(\tau) d\tau = \left(S_{i,t,0} + \frac{Y_{O_2}}{Y_{S_i}} \frac{OUR_m}{\mu_{eff}} \cdot \ln\left(\frac{1+\alpha}{(1-\alpha)}\right) \right) \left(1 - e^{-k_h t} \right) + \frac{Y_{O_2}}{Y_{S_i}} \frac{OUR_m}{k_h} \left((t - t_a) - \frac{1}{k_h} (1 - e^{-k_h(t-t_a)}) \right)$$

This solution can be used for the whole substrate limited period for $t > t_a$. For $t < t_a$, the second term should be set to zero.

4.3.4. Switch time

The substrate limited stage starts when the biomass within the aerobic region gets insufficient substrate. This situation starts when the soluble substrate concentration at the gas interface becomes zero. From this point of time on a small segment next to gas interface will be substrate limited. The switch time can be derived from the solution of the soluble substrate balance. The solution as given in eq. 4-41 is not very easily to interpret, but can be further simplified if $\frac{L_p(t_s)}{L_c} \ll 1$ (see Appendix A-3). This is a realistic assumption as at t_s the biomass concentration will be high due to growth, and the penetration depth will be consequently small. The result runs as:

$$\text{eq. 4-56} \quad S_s(t,0) = S_s(0) + \int_0^t k_h S_{i,r}(\tau) d\tau - \frac{Y_{O_2}}{Y_{S_s}} \int_0^t OUR(\tau) d\tau - \frac{1}{3} \frac{Y_{O_2}}{Y_{S_s}} \frac{OUR(t)}{\frac{D_{S_s}}{L_c^2}}$$

The switch time can be obtained from this equation via the condition that at the switch time the soluble substrate concentration at the gas side interface becomes zero. The equation can be solved for the switch time analytically, if the following assumptions hold:

$\beta_{eff} \ll 1 \wedge \mu_{eff} t_s \gg 1 \wedge k_h t_s \ll 1$. Together with the previous mentioned condition

$\frac{L_p(t_s)}{L_c} \ll 1$, these conditions express that at switch time:

- The penetration depth of oxygen should be small compared to the particle size.
- The initial biomass density should be clearly smaller than the maximum biomass density
- The switch time should be appreciably bigger than the biomass generation time.
- The switch time should be so small that no appreciable fraction of the total insoluble substrate is degraded.

It is sustained that these conditions will be met under practical circumstances. The first two conditions are not strictly necessary to obtain an analytical solution. Leaving these conditions out gives however an expression that is more cumbersome. If one of other two conditions is not met a numerical solution should be found for equation 4-56. The simplified analytical form will be used to show the meaning of the different factors influencing the switch time.

$$\text{eq. 4-57} \quad t_s = \left(1 - \frac{k_h \cdot \left(\frac{Y_{S_i}}{Y_{O_2}} \cdot S_{i,t,0} + COU(t_a) \right)}{OUR_m} \right)^{-1} \cdot \left[\frac{Y_{S_i}}{Y_{O_2}} \frac{S_{s,0}}{OUR_m} - \frac{\ln(4\beta_{eff})}{\mu_{eff}} - \frac{L_c^2}{3D_{S_i}} \right]$$

t_s : Switch time [s]

Equation 4-57 expresses the main factors influencing the switch time. The switch time is the product of two terms between brackets. The first of these terms is dimensionless and describes the effect of the ratio between the production of soluble substrate through hydrolysis and the consumption of soluble substrate through oxidation. This term will in practice be near one

as $OUR_m > k_h \cdot \frac{Y_{S_i}}{Y_{O_2}} S_{i,t}$, it is interesting to note that if the OUR_m becomes smaller the switch

time will increase. This makes sense because if the maximum consumption capacity equals the production capacity, the point where the substrate will be depleted never will be reached. The first term might be considered as the inverse of the fraction of the consumption capacity left after the hydrolyzed soluble substrate has been consumed.

The second term has time as dimensions and consists of three sub-terms that describe the factors that influence the degradation time of the initial soluble substrate. The first sub-term denotes the time needed to degrade the initial soluble substrate at maximum consumption capacity. This is of course an underestimate of the actual time needed as the initial consumption capacity is smaller than the maximum. This is corrected by the second sub-term. As β is smaller than one the term will be negative and thus the switch time will increase. At switch time a soluble substrate profile is present in the particle. This implies that not all initially substrate present needs to be degraded at switch time. The time needed to degrade this remainder is given by the third sub-term.

4.4. Substrate limited stage solution

This phase starts at the switch time t_s , the state of the system at the end of the substrate saturated stage determines the initial state for the substrate limited stage. The solutions will therefore be presented with the status at switch time as the initial state.

4.4.1. Total insoluble substrate.

First an overall approximate solution is sought for the insoluble substrate balance. The approximate solution is chosen such that it is expected to be exact on the long run. Therefore first the hydrolysis limited stage is considered, when the average soluble substrate concentration is in a steady state at low value. The biomass production rate will then be solely determined by the soluble substrate production rate i.e. by the hydrolysis rate. Under these circumstance the total insoluble substrate balance equation can be written as:

$$\frac{dS_{i,t}}{dt} = -k_h S_{i,t} + \frac{Y_s}{Y_{S_i}} k_h S_{i,t} = -k_n S_{i,t} \quad t \geq t_s$$

eq. 4-58

$$k_n = k_h \left(1 - \frac{Y_s}{Y_{S_i}}\right)$$

k_n : net hydrolysis rate [s⁻¹]

The initial condition at $t=t_s$ is given by $S_{i,t}(t_s)$ as calculated by 4-54. The first term in the total insoluble substrate balance is the proper hydrolysis rate, i.e. the amount of soluble substrate produced. The second term represents the biomass related insoluble substrate that is produced from the hydrolysed insoluble substrate. The solution for the total insoluble substrate runs as:

$$S_{i,t} = S_{i,t}(t_s) e^{-k_n(t-t_s)} \quad eq. 4-59$$

4.4.2. OUR

Both in the substrate saturated and limited stage the same set of equations describe the soluble substrate balance. However, there is a difference. In the substrate saturated stage the OUR is determined by oxygen and biomass concentration and the OUR can be solved without knowledge of the soluble substrate balance. In the substrate limited stage the OUR is

determined by the availability of soluble substrate and the OUR needs to be solved from the soluble substrate balance.

As the soluble substrate balance is the same for both the substrate limited and substrate saturated stage, eq. 4-41 will also serve as a solution. For the substrate limited period the OUR can be obtained from this solution from the prerequisite that the substrate concentration at $z=0$ remains zero. Now starting from the simplified solution for the soluble substrate at $z=0$ (see Appendix A-3):

eq. 4-60

$$S_s(t,0) = 0 = S_s(t_s) + \int_{t_s}^t k_{h,i} S_{i,i}(\tau) d\tau - \frac{Y_{O_2}}{Y_{S_s}} \int_{t_s}^t OUR(\tau) d\tau - \frac{1}{3} \frac{Y_{O_2}}{Y_{S_s}} \frac{OUR(t)}{\frac{D_{S_s}}{L^2}}$$

To solve this equation for OUR the equation is differentiated with respect to time to obtain the following ordinary differential equation:

$$\text{eq. 4-61} \quad \frac{dOUR(t)}{dt} = \frac{3 \cdot D_{S_s}}{L_c^2} \left(\frac{Y_{S_s}}{Y_{O_2}} k_h S_{i,t}(t) - OUR(t) \right) \quad t \geq t_s$$

$t = t_s \quad OUR = OUR(t_s)$

The initial condition $OUR(t)$ can be obtained from eq. 4-38. Substituting the result of the insoluble substrate eq. 4-60 gives an expression that can be solved. The solution runs as: eq. 4-62

$$OUR(t) = \left(OUR(t_s) - \frac{Y_{S_s}}{Y_{O_2}} S_{i,t}(t_s) \frac{k_h \cdot \frac{3.D_{S_s}}{L_c^2}}{\frac{3.D_{S_s}}{L_c^2} - k_n} \right) e^{-\frac{3.D_{S_s}}{L_c^2} \cdot (t-t_s)} + \frac{Y_{S_s}}{Y_{O_2}} S_{i,t}(t_s) \frac{k_h \cdot \frac{3.D_{S_s}}{L_c^2}}{\frac{3.D_{S_s}}{L_c^2} - k_n} \cdot e^{-k_n \cdot (t-t_s)}$$

4.4.3. Soluble substrate

The average soluble substrate concentration can be easily found once the OUR is determined. The average soluble substrate concentration $S_s(t)$ can be found by integrating the soluble substrate balance eq. 4-10 over z, giving :

eq. 4-63

$$S_s(t) = S_s(t_s) + \int_{t_s}^t k_h \cdot S_{i,t}(\tau) d\tau - \frac{Y_{O_2}}{Y_{S_s}} \int_{t_s}^t OUR(\tau) d\tau$$

After substitution of eq 4-63, evaluation of the integrals and after some manipulation of these results the following equation is derived.

eq. 4-64

$$S_s(t) = S_s(t_s) + S_{i,t}(t_s) \left(1 - \frac{\frac{3 \cdot D_{S_s}}{L_c^2}}{\frac{3 \cdot D_{S_s}}{L_c^2} - k_n} \right) (1 - e^{-k_n(t-t_s)}) - \left(\frac{Y_{O_2}}{Y_{S_s}} \cdot \frac{OUR(t_s)}{\frac{3 \cdot D_{S_s}}{L_c^2}} - \frac{k_h}{\frac{3 \cdot D_{S_s}}{L_c^2} - k_n} S_{i,t}(t_s) \right) (1 - e^{-k_n(t-t_s)})$$

Now from eq. 4-61 it becomes clear that at $t=t_s$ the following relationship is valid:

eq. 4-65

$$S_s(t_s) = \frac{1}{3} \frac{Y_{O_2}}{Y_{S_s}} \frac{OUR(t_s)}{\frac{D_{S_s}}{L_c^2}}$$

Substituting eq. 4-66 in eq. 4-65 then yields the final result for the soluble substrate concentration:

eq. 4-66

$$S_s(t) = S_{i,t}(t_s) \left(1 - \frac{\frac{3 \cdot D_{S_s}}{L_c^2}}{\frac{3 \cdot D_{S_s}}{L_c^2} - k_n} \right) (1 - e^{-k_n(t-t_s)}) + \frac{k_h}{\frac{3 \cdot D_{S_s}}{L_c^2} - k_n} S_{i,t}(t_s) (1 - e^{-k_n(t-t_s)}) - \frac{Y_{O_2}}{Y_{S_s}} \cdot \frac{OUR(t_s)}{\frac{3 \cdot D_{S_s}}{L_c^2}} \cdot e^{-k_n(t-t_s)}$$

4.5. Prediction Bias

Simplification of the theoretical model was necessary to obtain an analytical approximate solution. Model simplification is however expected to introduce a prediction bias i.e. the OUR prediction of the approximate solution will differ from the theoretical model prediction.

Although the primary interest lies in the OUR, evaluation of the prediction bias of some other model outputs is necessary. For some state variables (oxygen, soluble substrate, average insoluble substrate) an analytical approximation was needed to arrive at the analytical OUR approximation. As good approximation of the OUR does not guarantee a good representation of the underlying processes, the approximated variables will be assessed. If the essential behavior of the underlying processes is correctly reproduced the analytical approximation can also be considered as a sound representation of the mechanistic model basis.

The extent and importance of the prediction bias will be studied for a nominal parameter set and for a larger parameter range. For the nominal parameter set (as defined in the previous chapter) both the OUR and the approximated state variables will be investigated. For the parameter range only the bias in the OUR prediction will be studied. The prediction bias is quantified by the conventional multiple correlation coefficient R^2 and the median relative error e_m .

4.5.1. Comparison for the nominal parameter set

The nominal parameter set as listed in chapter 3 describes the composting of chicken manure at 55 °C. The same parameter set will be used to investigate the performance of the analytical model. The bias in the following predictions is investigated, the OUR time course, the average soluble substrate concentration time course, the average total insoluble substrate time course, the soluble substrate concentration and the spatial profile of the oxygen concentration. The bias is expressed as the absolute relative error defined as:

$$eq. \ 4-67 \quad e_i = \frac{|OUR_I(t_i) - OUR_H(t_i)|}{OUR_I(t_i)}$$

e_i : Relative error of observation i [-]

t_i : Time instant of observation i. [s]

$OUR_I(t_i)$: Prediction with the theoretical model at t_i [$\text{mol O}_2 \cdot \text{m}^{-3} \cdot \text{s}^{-1}$]

$\text{OUR}_{\text{II}}(t_i)$: Prediction with analytical approximation at t_i [mol O₂.m⁻³.s⁻¹]

The relative error measures the bias at one point of time. To measure the overall bias two measures will be used, the conventional multiple coefficient of variation R^2 between $\text{OUR}_i(t_i)$ and $\text{OUR}_{\text{II}}(t_i)$ and the median e_m of the relative error e_i , both calculated over the a period running from 0 to 100 hr with a time interval of 0.25 hr. The median relative error is less sensitive to the outliers than the average.

Figure 4.3 compares the OUR as calculated by the theoretical model and the analytical approximation. The two curves are the same with respect to the main features, the initial growth phase ending in plateau and the subsequent sharp drop followed by a low plateau, which has a gentle slope. The prediction by the analytical approximation of a two hour longer substrate saturated stage represents the main difference.

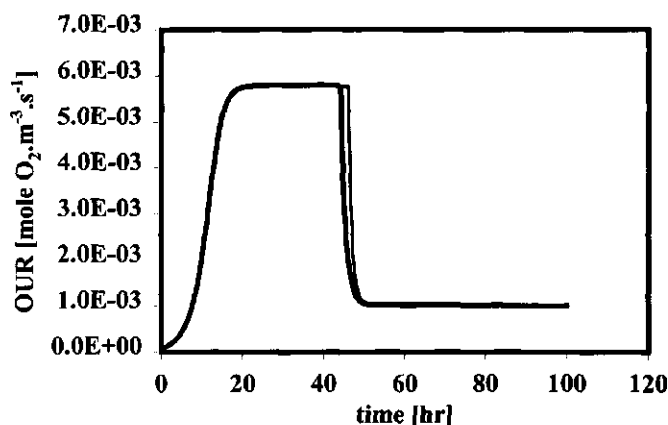


Figure 4.3: The time course of the OUR as predicted by the theoretical model (thick line) and as predicted by the analytical approximation (thin line).

Figure 4.4 shows the relative error as a function of time together with the time course of the OUR. There are two distinct peaks in the relative error, one during the initial OUR increase and one at the end of the substrate saturated period. These peaks occur as a result of small shift in time of one curve relative to the other. At place where the OUR curve is steep a relative large error will occur. The second peak represents the largest contribution to the overall error. Leaving out this second peak gives an increase of R^2 from 0.967 to 0.991. The

average relative error gives a decrease from 2.1 % to 0.7%. In the sequel the median relative error e_m is used as this is in both cases 0.72%

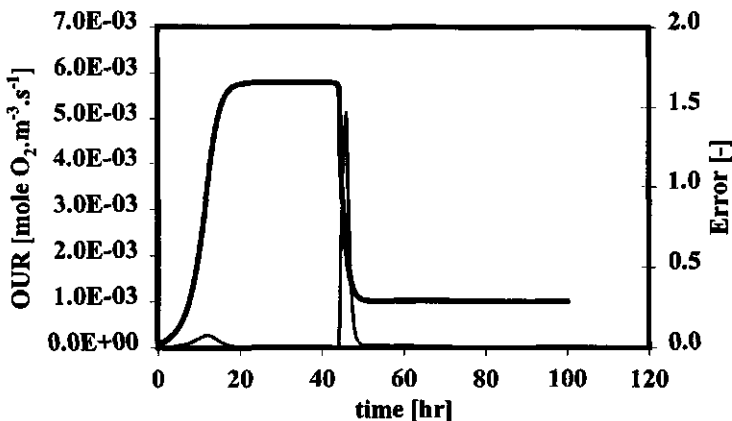


Figure 4.4: The time course of the OUR as predicted by the theoretical model (thick line) and the relative error e of the analytical approximation (thin line).

Figure 4.5 ($R^2 = 0.998$) shows that for the time course of the average soluble substrate no clear differences can be noted. The analytical approximation predicts a somewhat higher soluble substrate concentration (15 mole.m^{-3}), during the substrate saturated period. This increased level can explain the prolonged substrate saturated stage.

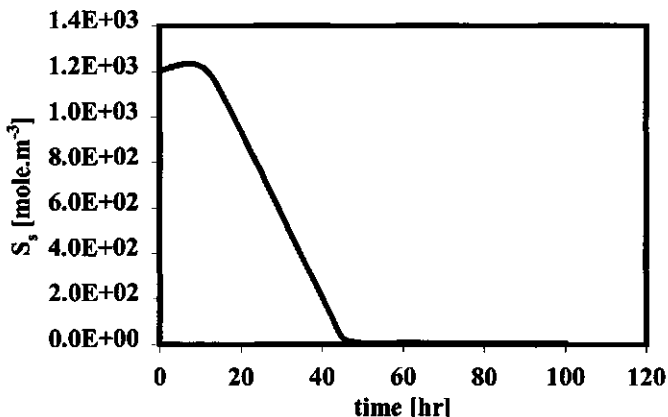


Figure 4.5: The time course of the average soluble substrate concentration as predicted by the theoretical model and as predicted by the analytical approximation. The lines almost completely coincide.

Figure 4.6 ($R^2 = 0.995$) shows the time course of the average insoluble substrate. Both curves show an initial decrease of the total insoluble substrate, followed by an increase to a maximum at $t=47$ hrs, after which a steady decline takes place. There is a small difference at the maximum concentration, the analytical solution predicts a somewhat higher concentration. This difference can account for the increased soluble substrate production that leads to an extended substrate saturated stage.

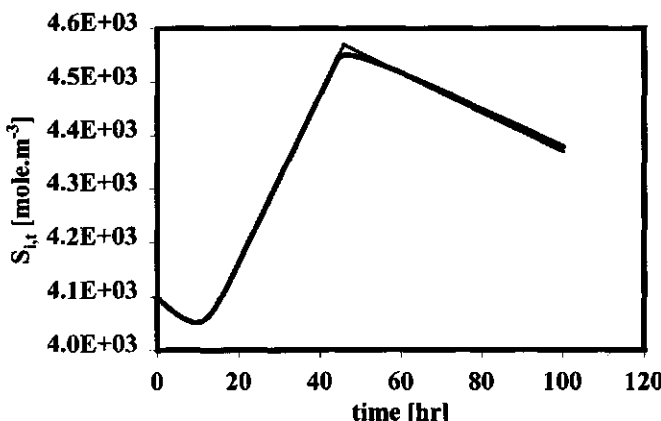


Figure 4.6: The time course of the average insoluble substrate concentration as predicted by the theoretical model (thick line) and as predicted by the analytical approximation (thin line).

Figure 4.7 ($R^2 = 0.994$) shows the oxygen gradient at $t= 10$ hr and at $t= 35$ hr. The analytical approximation follows the curves according to theoretical model well, both models predict a small penetration depth. At $t= 35$ hr the penetration depth has decreased due to an increase of the OUR, which is predicted well by both models.

Figure 4.8A ($R^2 = 0.994, 0.99, 0.99$) shows the soluble substrate gradients at three different points of time. The curves at $t= 10$ hr do coincide, both models predict the actual increase of the soluble substrate. At $t= 35$ hr the concentration has become lower the gradient of both profiles has become steeper. A small difference between the curves is observed. As the multiple correlation coefficient is still very high this indicates that this difference is the same at each location, again indicating that the difference is caused by the higher predicted solubilization of insoluble substrate. At $t=45$ hr the soluble substrate is nearly depleted as predicted by both models. Figure 4.8B shows that there remains a difference in the soluble substrate profiles at $t= 45$. It is now clearer seen that the analytical profile still has not reached

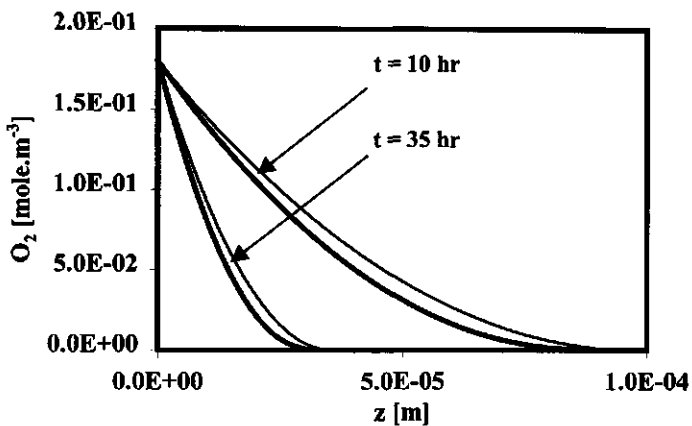


Figure 4.7: Comparison between the oxygen profile as predicted by the theoretical model (thick line) and the analytical approximation (thin line) at two point of time. The full particle size L_c is 0.0025 m.

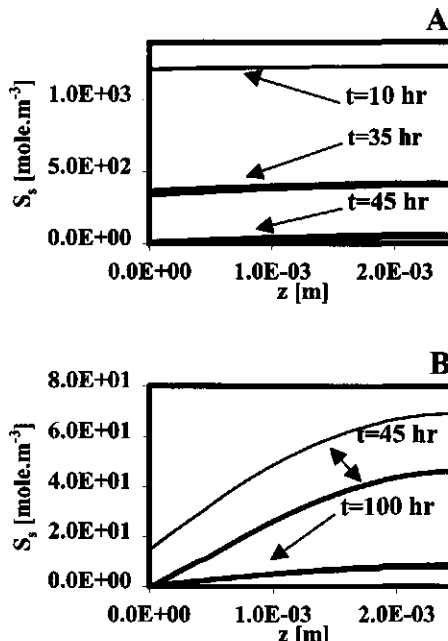


Figure 4.8: The profile of the average soluble substrate concentration as predicted by the theoretical model (thick line) and as predicted by the analytical approximation (thin line). The profiles are shown at different points of time characteristic for the OUR time course. The lines coincide at $t=10$ hr.

a zero concentration at the gas side interface while the numerically calculated profile already has. Later on at $t=100$ hr the profile nearly coincide again, indicating that the solubilization rate is accurately approximated analytically.

4.5.2. Comparison over a parameter range

The OUR time course is investigated over a larger parameter space (including initial conditions), to see whether at different parameter sets the analytical approximation works also well. For each different parameter set the OUR time course calculated with the theoretical (numerical) model and with the analytical approximation are compared. This makes it possible to see whether the effect of a change in a certain waste characteristic is reflected in the analytical solution. As the waste characteristics (particle size, interfacial oxygen concentration, initial ash concentration, initial insoluble substrate concentration, initial biomass concentration and initial soluble substrate concentration) are expected to have the largest variance they are examined. The nominal parameter set is chosen as the reference point and the waste characteristic parameters are changed by factors 2^{-2} , 2^{-1} , 2 and 2^2 . Parameters are changed one-by-one and the multiple correlation coefficient is calculated and the median of the relative error e_m is calculated for each parameter set. The results are presented in table 4.1, only the results for the minimum and maximum parameter value are shown in graphs.

Table 4.1: The relative median error (error) and the multiple correlation coefficient (R^2) for different values of the main waste characteristics. The top line indicates the waste characteristics investigated. The factor indicates the multiplication factor of the nominal parameter value.

Factor	L_c		$O_{2,i}$		S_{i,t_0}		$S_{s,0}$	
	Error [%]	R^2	Error [%]	R^2	Error [%]	R^2	Error [%]	R^2
2^{-2}	0.9	0.88	1.0	0.98	0.5	0.97	0.8	0.97
2^{-1}	0.9	0.95	0.9	0.97	0.5	0.97	0.7	0.97
1	0.7	0.97	0.7	0.97	0.7	0.97	0.7	0.97
2	0.5	0.96	0.5	0.97	0.6	0.96	0.9	0.95
4	0.1	1.00	0.5	0.96	0.5	0.93	1.0	0.80

Figure 4.9 shows that both for the small (4.9B) and the big particle size (4.9A) the approximate solution comes very near the theoretical OUR. Table 1 it shows that with increasing particle size the analytical approximation has a smaller median error and an

increasing R^2 , however in all cases the error remains small. When the period between the theoretical switch time and the analytically determined switch time is left out the multiple correlation coefficient becomes in all cases >0.99 . This explains also why with decreasing particle size the error somewhat increases, a small particle gives a high OUR_m and thus a larger error when the OUR drops after the switch time

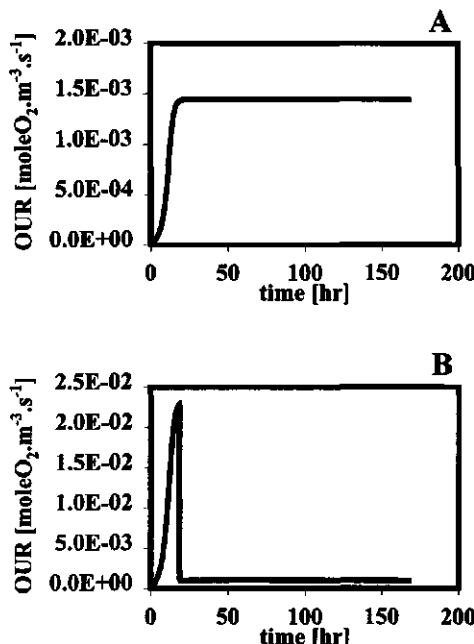


Figure 4.9: The time course of the OUR as predicted by the theoretical model and as predicted by the analytical approximation for the maximum particle size (A) and the minimum particle size (B). In both cases the lines coincide.

Figure 4.10 shows that with increasing S_s the switch time increases. The approximate solution shows the same behaviour. As with increasing S_s there is an increase in the switch time, a bigger difference in the approximated and theoretical switch time is expected. This results in an increasing error and decreasing R^2 .

Figure 4.11 shows that with an increasing interfacial oxygen concentration the maximum OUR increases and the switch time decreases. This effect is very well mimicked by the approximate solution. Table 4.1 indicates that with a decreasing oxygen concentration the error increases. As the same behaviour is not detected in the R^2 this could be a result of the fact that the average OUR value decreases, increasing in this way the relative error.

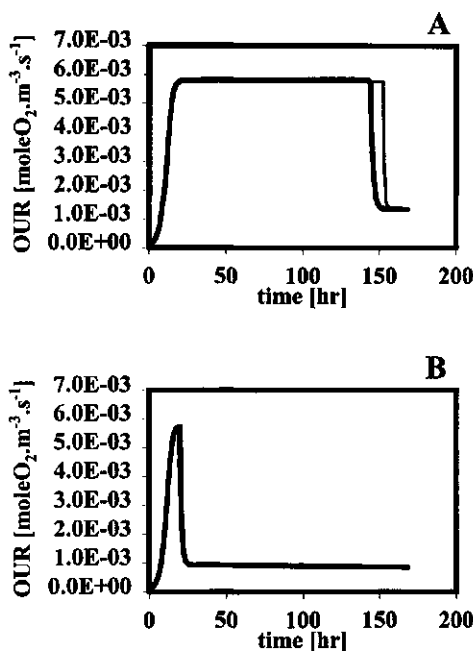


Figure 4.10: The time course of the OUR as predicted by the theoretical model (black line) and as predicted by the analytical approximation (gray line) for the maximum value (A) and the minimum value (B) of the initial soluble substrate concentration. In case B the curves nearly coincide

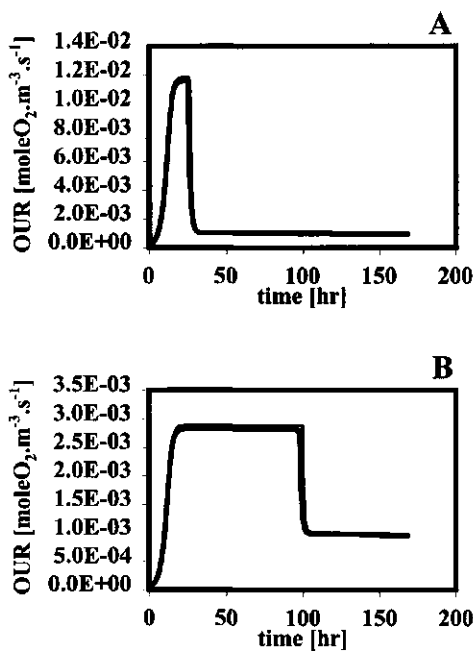


Figure 4.11: The time course of the OUR as predicted by the theoretical model (thick line) and as predicted by the analytical approximation (thin line) for the maximum value (A) and the minimum value (B) of the interfacial oxygen concentration. In both cases the curves nearly coincide.

Figure 4.12 shows that with increasing S, the switch time and the hydrolytic activity both increases. The approximate solution is again nearly the same in both cases. With increasing S, there is a small decrease in R^2 , probably as a result of the increasing switch time. The relative error shows no systematic change.

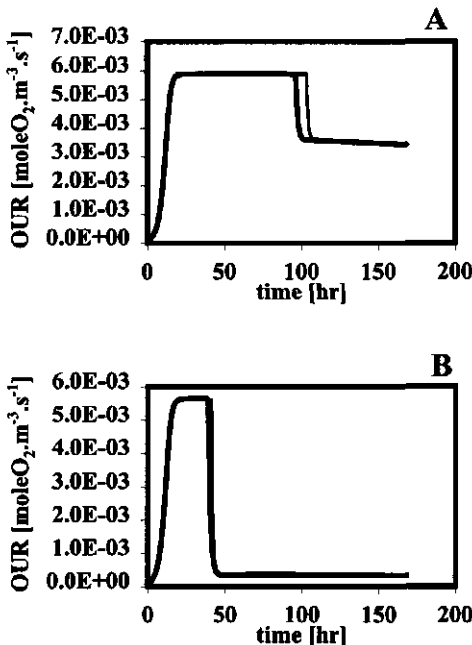


Figure 4.12: The time course of the OUR as predicted by the theoretical model (thick line) and as predicted by the analytical approximation (thin line) for the maximum value (A) and the minimum value (B) of the initial insoluble substrate concentration. In case B the curves nearly coincide.

In all cases it seems that the main deviation between theoretical model and analytical approximation is the overestimation of the switch time. Figure 4.13 shows the analytical prediction of the switch time plotted as a function of the prediction by the theoretical model. The latter value was determined as the first point of time after reaching the maximum OUR where the OUR has dropped to 99.5% of the maximum OUR. Linear regression analysis with a zero intercept shows that the switch is overestimated on the average by 5.7%. If a period of 5 hrs before and after the switch time is omitted from the calculation the R^2 is in all cases >0.99 while the median error < 0.2%.

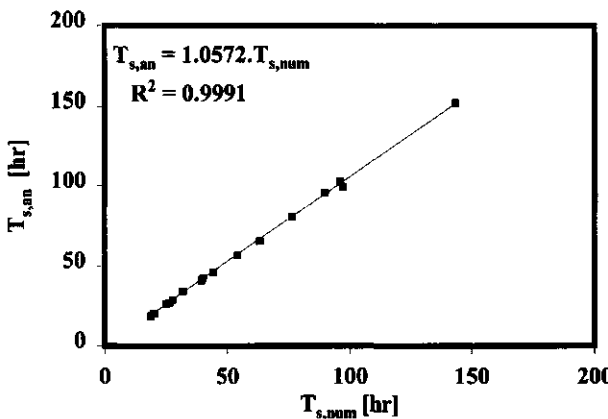


Figure 4.13: The switch time as estimated by the analytical approximation $T_{s,an}$ as a function of the switch time estimated by the theoretical model $T_{s,num}$. The line gives the best linear fit with a zero intercept included.

4.6. Discussion

4.6.1. Evaluation

An analytical approximation for the theoretical model has been developed. The bias of this analytical approximation is compared to the theoretical model. There is a trade-off between the complexity of the model and its accuracy. If a model is simplified, some phenomena will no longer be taken into account and the prediction error of the simplified model will increase. In the present case the prediction error introduced by the approximation yields a median error of less than 1%. Whether this value is critical depends largely on the intended use of the model, no general statements can be made in this respect. The advantage of using the analytical solution has to be weighted against the drawback of the prediction error. This will be done in the following for some applications of the analytical model:

- Prediction of the OUR

The analytical model can be used for predicting the OUR, e.g. predicting the rate in a reactor model. Use of the analytical approximation gives an increase of the prediction error, whether this increase is substantial depends on the size of other sources of prediction error. An important source of variance is the variance of the waste characteristics. This variance is intrinsic to most types of waste and is not a sampling error that can be restored by getting larger samples. For instance Veeken [4] found that biowaste had a large size distribution, 25-

35% had a radius bigger than 5 and 15-20% has a size smaller than 0.05 mm. Such a large span of radius causes of course an effect far outweighing the variance induced by the use of the approximate solution.

- Obtaining analytical understanding

Analysis of the nominal parameter set showed that the analytical approximation describes very well the main features as predicted by the theoretical model. The analytical model thus reflects very well the underlying processes. This is definitely an advantage of the analytical approximation it gives an analytical understanding of the process, while the numerical approximation only gives a quantitative knowledge of the system. For instance the effect of particle size on the time course of the OUR time course can be understood without further calculations.

- Parameter estimation

In nearly all cases the parameter describing the composting process of a specific waste are fully or partly unknown, implying that parameters have to be estimated from experiments. Non-linear parameter estimation needs many evaluations of the model equations. The analytically approximation is well suited for this application as it needs only a small computational effort. One simulation over a period of 100 hr takes 20 minutes while the analytical approximation takes 0.3 seconds (PENTIUM II 350 MHz) Using the simplified model would introduce only a slight bias in the parameter estimates. For instance in case of the nominal case, decreasing the soluble substrate concentration by 0.9% already gives a perfect fit of the theoretical and approximate model.

- Checking the numerical approximation

The prediction bias measures the difference in behavior resulting from the simplification of the model structure. It is assumed that if the prediction bias is small that the simplified model structures is equivalent to the original model structure. This approach however needs access to the model behavior of the original model. The theoretical model behavior is acquired from a numerical approximation of the model. The error introduced by this numerical approximation is unknown.

The fact that both approximations are so near is a good indication that both the numerical and analytical approximation gives a good representation of the underlying model equations.

Ascribing the prediction bias solely to the analytical approximation in a sense is an arbitrary

choice, as there is no knowledge on the numerical error. It even can not be ruled out that the analytical solution is a better representation than the numerical approximation.

From the discussion it becomes clear that in most applications the analytical approximation is the method of choice as it combines a lower computational burden with analytical insight and introduces a small nearly negligible prediction error for practical purposes. The numerical approximation is needed when new situations are investigated that do not comply with the additional assumptions underlying the analytical approximation.

4.6.2. Implications

Accepting the analytical approximation some more general conclusions to be drawn on the time course of the OUR.

1. The root-logistic relationship.

Based on the presented derivation the root-logistic relationship emerges as a analytical model for the OUR time course during the substrate saturated stage. The model identifies the limited aerated zone at the surface of the waste particle as the growth limiting factor. The penetration depth of oxygen determines the extent of the aerated space. Biomass produced in excess over the amount needed to fill up this limited aerated space is removed via a convective flow directed at the aerobic core of the particle.

In solid state fermentation the OUR is often described by the logistic growth, i.e. the same model however neglecting the square root. The logistic growth model is considered an empirical equation, i.e. a relationship with a good data-fit but without a mechanistic background. These two relationships are hard to distinguish if the data have some variance. If the data are generated by a root logistic rate equation with a growth rate μ_{eff} it can be shown that a logistic relationship with a growth rate constant 72% of μ_{eff} describes the data also well. The growth rate measured in food solid state fermentation is usually lower then measured in submerged culture [5]. This analysis would show that the growth rate of biomass is not lower but only the growth rate of the aerobic biomass activity is lower.

2. Maximum oxygen uptake rate

The analytical solution shows that the maximum oxygen uptake rate OUR_m is determined by a number of parameters, among which the particle size is the dominant parameter. Contrary to the wide spread assumption in composting literature the maximum oxygen uptake rate is not determined by the soluble substrate concentration. The soluble substrate is very important in

explaining the duration of the high rate phase. The analysis indicates that a clear distinction must be made between the value of the maximum rate and the period that the OUR stays at this maximum value. Such a distinction is often not made because most studies are focused at cumulative indexes that average the rate.

3. The soluble substrate diffusion coefficient.

The sharp drop in the OUR at the beginning of the substrate limited stage is modelled as being determined by the substrate diffusion rate. This might seem odd as the sensitivity analysis of the theoretical model in the previous chapter showed D_{ss} to be of minor importance. The fact that the soluble substrate diffusion coefficient is not detected in the sensitivity analysis lies in the extreme sensitivity of the switch time. There are many parameters that influence the switch time. A small change in such a parameter shifts the switch time strongly and thus influences the activity in the transient phase stronger than the substrate diffusion coefficient does.

4. The net hydrolysis rate

The apparent hydrolysis is smaller than the actual hydrolysis rate, the reason being that part of the solubilized substrate is again converted to insoluble substrate in the form of biomass. This observation is interesting as the hydrolysis rate of the aerobic process would be lower than of complete anaerobic process, as methanogens have a much lower biomass yield. This might explain why anaerobic processes are operated at somewhat lower retention times than the aerobic processes [6]. This conclusion is only valid if the insoluble substrate is anaerobically hydrolyzed. Lignin and cellulose connected to it is hardly degradable during anaerobic processes but may be degraded aerobically. For such components this conclusion is not valid.

These implications show the advantage of having analytical insight in the composting process. Insight is obtained that is independent of the exact value of the parameter used. On the other hand care must be taken to keep in mind the assumption underlying the derivation of the analytical assumption. The numerical approximation can however always be used to investigate the extent of a possible deviation.

The analytical solution approximates the theoretical model well and gives more insight in the processes occurring in a composting particle. It will be used in the following chapters as the preferred model as it enables to introduce a size distribution.

4.7. References

1. Keener, H.M., et al. *Optimizing the efficiency of the composting process.* in *Proceedings of the International Composting Research Symposium.* 1992. Columbus OH: Renaissance Publications.
2. Marugg, C., et al., *A kinetic model of the yard waste composting process.* Compost Science & Utilization, 1993. 1(1): p. 38-51.
3. Oriol, E., et al., *Solid-State Culture of Aspergillus niger on Support.* Journal of Fermentation Technology, 1988. 66(1): p. 57-62.
4. Veeken, A.H.M., *Removal of heavy metals from biowaste,* in *Environmental Technology.* 1998, Wageningen Aricultural University: Wageningen.
5. de Reu, J.C., *Solid-State Fermentation of Soya Bean to Tempe.* 1995, Wageningen Agricultural University: Wageningen.
6. Cecchi, F. and J. Mata-Alvarez, *Anaerobic digestion of municipal solid waste, an up-to-date review,* in *Solid substrate cultivation,* H.W. Doelle, D.A. Mitchell, and C.E. Rolz, Editors. 1992, Elsevier: London.

A Appendix

The function of the appendices is to clarify some steps with respect to the solution the partial differential equations describing the O₂ and S_s balance. Both equations are solved by the method of variation of parameters. Although this is a standard method it is shortly generally introduced (A.1) to simplify the treatment of the individual balances. In this way more insight in the validity of some additional simplifications is obtained. In appendix A.1 the general solution for a partial differential equation with homogenous boundary conditions is described [Berg, 1978 #135]. The solution of the O₂ balance (A.2) and S_s balance (A3) follows similar lines. First the partial differential equation is transformed into an equation with homogenous boundary conditions. For the specific equation that arises in this way the solution can then be directly derived from the general solution described in A.1.

A.1 *The method of variation of parameters*

The method of variation of parameters is used to solve the partial differential equations resulting from the different material balances from chapter 3. This method is shortly introduced to simplify the treatment of the subsequent balances.

For the sake of brevity the notation has been changed e.g. subscript t denotes the partial derivative with respect to t, z the first partial derivative with respect to z, zz the second partial derivative with respect to z. The first step is to transform the problem at hand to an inhomogeneous equation with homogenous boundary conditions. The resulting transformed problem can be written as:

$$\text{eq. A-1} \quad w_t - k \cdot w_{zz} = Q(z, t) \quad 0 < z < L \quad 0 < t$$

w : variable of interest e.g. O₂

z : spatial coordinate

t : time

Q : source function

k : constant

L : left boundary

The boundary conditions are represented as:

$$\text{eq. A-2} \quad w_z(0, t) = 0 \quad t > 0$$

$$\text{eq. A-3} \quad w(L, t) = 0 \quad t > 0$$

The initial condition is represented by the function $f(z)$ as:

$$\text{eq. A-4} \quad w(z, 0) = f(z)$$

The nature of the boundary conditions may differ depending on the nature of the original problem. The solution of the homogeneous problem has eigenvalues λ_n and eigenfunctions $\varphi_n(z)$. The general solution to the problem is given by:

$$\text{eq. A-5} \quad w(z, t) = \sum_{n=0}^{\infty} \left[c_n e^{-\lambda_n k t} + \int_0^t e^{-\lambda_n k(t-\tau)} q_n(\tau) d\tau \right] \varphi_n(z)$$

In this general solution the constant c_n is given by:

$$\text{eq. A-6} \quad c_n = \frac{2}{L} \int_0^L f(z) \varphi_n(z) dz$$

In this equation the factor $2/L$ is the normalizing constant of the eigenfunctions, which may differ, depending on the eigenfunctions. The constant c_n in combination with the exponential term $c_n e^{-\lambda_n k t}$ describes a transient part of the solution if $\lambda_n > 0$. These transient functions will be neglected if the product $\lambda_n k t > 5$ at the time of interest.

In the general solution q_n is given by:

$$\text{eq. A-7} \quad q_n(t) = \frac{2}{L} \int_0^L Q(z, t) \varphi_n(z) dz$$

In the general solution q_n forms with an exponential term the (convolution) integral $\int e^{-\lambda_n k(t-\tau)} \cdot q_n(\tau) d\tau$. This integral describes the combined effect of the source term and the boundary conditions. This integral can be considered as a weighted time average of the function q_n , the importance of the function values further back in time diminishes. It is clear that if the exponential term drops sharply compared to the change in q_n this convolution integral can be well approximated by:

$$\text{eq. A-8} \quad \int_0^t e^{-\lambda_n k(t-\tau)} \cdot q_n(\tau) d\tau = \int_0^t e^{-\lambda_n k(t-\tau)} \cdot q_n(t) d\tau = \frac{q_n(t)}{\lambda_n k} \left(1 - e^{-\lambda_n k t}\right)$$

Again if $\lambda_n k t > 5$ the exponential term in the result above will be omitted. The validity of the approximation of the convolution integral is considered for the logistic function as this is the driving function during the substrate saturated phase. The analytical approximation is compared to a numerical approximation to find out under which conditions a good approximation is obtained. The logistic function is given by:

$$\text{eq. A-9} \quad g(t) = \frac{1}{1 + e^{-\mu \left(t - \frac{1}{\mu} \ln \left(\frac{1}{\beta}\right)\right)}}$$

- | | | |
|---------|---|-----------------------|
| μ | : growth rate constant | [time ⁻¹] |
| β | : initial dimensionless biomass β | [time] |

The logistic function is presented in this way to emphasize the property of β as inducing a mere time shift in the logistic function. By now considering the θ the dimensionless time (μt), the convolution integral can be represented as:

$$\text{eq. A-10} \quad \int_0^\theta e^{-\nu(\theta-\tau)} \cdot \frac{1}{1 + e^{-\tau-\ln(\beta)}} d\tau$$

- | | | |
|----------|------------------------------|-----|
| θ | : Dimensionless time μt | [1] |
|----------|------------------------------|-----|

In this equation v is the ratio between the two time constants involved:

eq. A-11

$$v = \frac{\lambda_n k}{\mu}$$

v : time constant ratio

[1]

Figure A-1 shows the numerically calculated integral and the analytical approximation for $\ln(\beta^{-1})=3$ (fig A-1A) and $\ln(\beta^{-1})=6$ (fig A-1B). In both graphs the curves for $v=1$ and $v=5$ are shown. The numerical approximation and the show that at a ratio of 5 the curves nearly coincide, while at $v=1$ the curves coincide at higher values of θ . The parameter β has no effect on these conclusions as it represents mainly a shift in time of the curve.

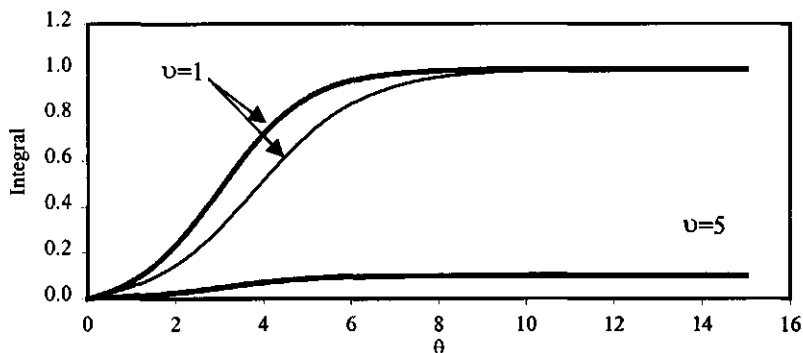


Figure A-1 The numerically calculated integral I (eq. A-10) (thin line) and its analytical approximation (thick line) for $\ln(\beta^{-1}) = 3$ for two different values of v .

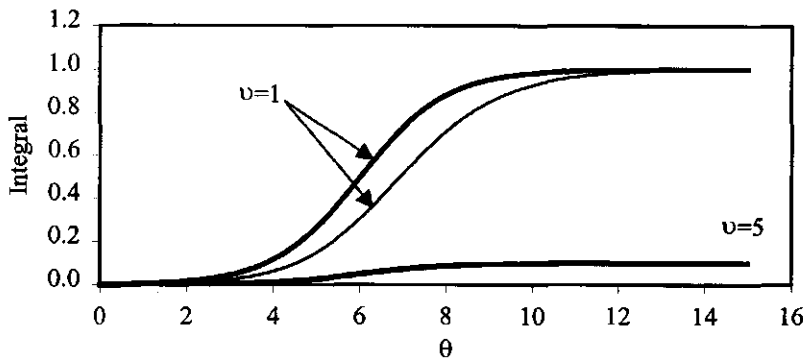


Figure A-1B The numerically calculated integral I (eq. A-10) (gray thick line) and its analytical approximation (black thin line) for $\ln(\beta^{-1}) = 6$ for two different values of v .

A.2 Oxygen balance during the substrate saturated phase

The balance equation is given in table 1 of chapter 3. The following transformation is used to obtain a problem with homogeneous boundary conditions.

$$\text{eq. A-12} \quad u = O_2 - O_{2,i}$$

This gives the general form with:

$$\text{eq. A-13} \quad Q(t) = -\frac{\mu_n}{Y_{O_2}} \cdot \frac{\beta_{\text{eff}}}{\beta_{\text{eff}} + e^{-\mu_{\text{eff}} \cdot t}} \cdot X_n$$

$$\text{eq. A-14} \quad f(z) = -O_{2,i}$$

The associated eigenfunctions and eigenvalues are:

$$\text{eq. A-15} \quad \varphi_n = \sin(\sqrt{\lambda_n} \cdot z)$$

$$\text{eq. A-16} \quad \lambda_n = \left[\frac{\left(n + \frac{1}{2} \right) \pi}{L_p} \right]^2$$

It should be noted that L_p denotes the still unknown penetration depth of oxygen and not the particle size L_c . As $f(z)$ is zero, the values of c_n are zero. The functions q_n can be easily found as Q is only a function of time:

$$\text{eq. A-17} \quad q_n = \frac{2}{\left(n + \frac{1}{2} \right) \pi} \cdot \frac{\mu_n}{Y_{O_2}} \cdot \frac{\beta_{eff}}{\beta_{eff} + e^{-\mu_{eff} \cdot t}} \cdot X_m$$

The convolution integral in the general solution given by A-5 can be written as:

$$\text{eq. A-18} \quad \int e^{-\lambda_n D(t-\tau)} \cdot \frac{2}{\left(n + \frac{1}{2} \right) \pi} \cdot \frac{\mu_n}{Y_{O_2}} \cdot \frac{\beta_{eff}}{\beta_{eff} + e^{-\mu_{eff} \cdot \tau}} \cdot X_m d\tau$$

This integral may be approximated by the following integral.

$$\text{eq. A-19} \quad \int e^{-\lambda_n D(t-\tau)} \cdot \frac{2}{\left(n + \frac{1}{2} \right) \pi} \cdot \frac{\mu_n}{Y_{O_2}} \cdot \frac{\beta_{eff}}{\beta_{eff} + e^{-\mu_{eff} \cdot \tau}} \cdot X_m d\tau$$

This approximation is acceptable if the value of $\lambda_n D$ is much bigger than μ_{eff} in which case the exponential term decays very rapidly compared to the decay of the logistic term. The effect of the initial condition on the solution will also decay very rapidly, and thus may be neglected. This approximating integral can be solved and gives as a general solution:

$$\text{eq. A-20} \quad O_2 = O_{2,i} + \frac{\mu_n}{D_{O_2} Y_{O_2}} \cdot \frac{\beta_{eff}}{\beta_{eff} + e^{-\mu_{eff} \cdot t}} \cdot X_m \cdot \sum_{n=0}^{\infty} \frac{2 L_p^2}{\left[\left(n + \frac{1}{2} \right) \pi \right]^3} \sin \left(\frac{\left(n + \frac{1}{2} \right) \pi}{L_p} \cdot z \right)$$

The sin series can be replaced by a quadratic term in z, which gives the following solution:

$$\text{eq.A-21} \quad O_2 = O_{2,i} - \frac{X_m \cdot \mu_n}{Y_{O_2} \cdot D_{O_2}} \cdot \frac{\beta_{\text{eff}}}{\beta_{\text{eff}} + e^{-\mu_{\text{eff}} \cdot t}} \cdot \left(z - \frac{z^2}{2 \cdot L_p} \right) \cdot L_p$$

As at L_p the oxygen concentration is zero the following result can be deduced for the penetration depth.

$$\text{eq.A-22} \quad L_p(t) = \sqrt{2 \cdot O_{2,i} \cdot \frac{Y_{O_2} \cdot D_{O_2} \cdot \beta_{\text{eff}} + e^{-\mu_{\text{eff}} \cdot t}}{X_m \cdot \mu_n \cdot \beta_{\text{eff}}}}$$

A.3 Soluble substrate balance during the substrate saturated phase

The equation has to be solved to obtain the soluble substrate gradient at the end of the substrate saturated phase. This specific gradient is needed then as it constitutes the initial condition for the soluble substrate balance during the substrate limited period. The equation is given in table 1 of chapter 3. The conversion term can be written as:

$$\text{eq. A-23} \quad R_{S_s} = \begin{cases} \frac{\mu_m}{Y_{S_s}} \cdot g(t) \cdot X_m & z \leq L_p \\ 0 & z > L_p \end{cases}$$

$$g(t) = \frac{\beta_{\text{eff}}}{\beta_{\text{eff}} + e^{-\mu_{\text{eff}} \cdot t}}$$

The balance equation of the soluble substrate equation can be transformed to the standard set of equations by using the following transformation:

$$\text{eq. A-24} \quad S_s(t, z) = w + \int_0^t k_h \cdot S_{s,i}(\tau) d\tau + S_s(0)$$

The integral represents the amount of soluble substrate that is produced up to time t. As the total insoluble substrate is not considered as a function of spatial coordinate, it is not

necessary to have an explicit solution at this point. This gives the following function Q and f.

$$\text{eq. A-25} \quad Q(z,t) = R_s,$$

$$\text{eq. A-26} \quad f(z) = 0$$

The associated eigenfunctions and eigenvalues are:

$$\text{eq. A-27} \quad \varphi_n = \cos(\sqrt{\lambda_n} z)$$

$$\text{eq. A-28} \quad \lambda_n = \left[\frac{n\pi}{L_c} \right]^2$$

The values of c_n are zero as $f(z)=0$ as can be seen by considering the integral given in eq.A-6.

The functions q_n can be found by considering the integral A-7. This results in:

$$\begin{aligned} \text{eq. A-29} \quad q_0 &= -\frac{\mu_m}{Y_{S_s}} \cdot \frac{L_p(t)}{L_c} \cdot X_m \cdot g(t) \\ q_n &= -\frac{\mu_m}{Y_{S_s}} \cdot \frac{2}{n\pi} \cdot g(t) \cdot X_m \cdot \sin\left(n\pi \cdot \frac{L_p(t)}{L_c}\right) \quad n > 0 \end{aligned}$$

The general solution for u can thus be written as:

$$\text{eq. A-30}$$

$$w = -\frac{1}{L_c} \cdot \int_0^t L_p(t) g(\tau) \frac{\mu_m}{Y_{S_s}} \cdot X_m d\tau - \left[\sum_{n=1}^{\infty} \int_0^t e^{-\lambda_n D_{S_s}(t-\tau)} \frac{2}{n\pi} \frac{\mu_m}{Y_{S_s}} \cdot X_m \cdot g(t) \cdot \sin\left(n\pi \cdot \frac{L_p(t)}{L_c}\right) d\tau \right] \cos(\sqrt{\lambda_n} z)$$

As stated earlier the soluble substrate balance is needed to determine the switch time. At this point of time generally the biofilm will be well developed and $g(t)$ and $L_p(t)$ will only change slowly. This allows the following approximation:

eq. A-31

$$\begin{aligned} & \int_0^t e^{-\lambda_n \cdot D_{S_s} \cdot (t-\tau)} \cdot \frac{2}{n\pi} \frac{\mu_m}{Y_{S_s}} \cdot g(\tau) \cdot X_m \sin\left(n\pi \cdot \frac{L_p(\tau)}{L_c}\right) d\tau = \\ & \frac{2}{n\pi} \frac{\mu_m}{Y_{S_s}} \cdot g(t) \cdot X_m \cdot \sin\left(n\pi \cdot \frac{L_p(t)}{L_c}\right) \int_0^t e^{-\lambda_n \cdot D_{S_s} \cdot (t-\tau)} d\tau = \\ & \frac{\mu_m \cdot g(t) \cdot X_m}{Y_{S_s}} \cdot \frac{2}{\lambda_n \cdot n\pi} \cdot \sin\left(n\pi \cdot \frac{L_p(t)}{L_c}\right) \cdot \left(1 - e^{-\lambda_n \cdot D_{S_s} \cdot t}\right) \end{aligned}$$

Now realizing that:

$$eq. A-32 \quad OUR(t) = \frac{L_p(t)}{L_c} \cdot \frac{\mu_m g(t) X_m}{Y_{O_2}}$$

The solution for the soluble substrate concentration runs as:

eq. A-33

$$\begin{aligned} S_s(t, z) = & S_s(0) + \int_0^t k_h \cdot S_{s,t}(\tau) d\tau - \frac{Y_{O_2}}{Y_{S_s}} \int_0^t OUR(t) d\tau - \\ & \frac{Y_{O_2}}{Y_{S_s}} \frac{OUR(t)}{\frac{D_{S_s}}{L_c^2}} \sum_{n=1}^{\infty} \frac{2}{(n\pi)^2} \cdot \frac{L_c}{n\pi L_p(t)} \sin\left(n\pi \cdot \frac{L_p(t)}{L_c}\right) \left(1 - e^{-\lambda_n \cdot D_{S_s} \cdot t}\right) \cos(\sqrt{\lambda_n} \cdot z) \end{aligned}$$

Upon neglecting the transient terms evaluating the soluble substrate concentration at $z=0$ yields:

$$S_s(t, 0) = S_s(0) + \int_0^t k_h \cdot S_{s,t}(\tau) d\tau - \frac{Y_{O_2}}{Y_{S_s}} \int_0^t OUR(t) d\tau - \frac{Y_{O_2}}{Y_{S_s}} \frac{OUR(t)}{\left(\frac{D_{S_s}}{L_c^2}\right)} \cdot \frac{L_c}{L_p(t)} \sum_{n=1}^{\infty} \frac{2}{(n\pi)^3} \cdot \sin\left(n\pi \cdot \frac{L_p(t)}{L_c}\right)$$

Now if $L_p(t) \ll L_c$, the following approximation can be made

eq. A-34

$$\sin\left(n.\pi.\frac{L_p(t)}{L_c}\right) \approx n.\pi.\frac{L_p(t)}{L_c}$$

The sum term

eq. A-35

$$\sum_{n=1}^{\infty} \frac{1}{(n.\pi)^2} = \frac{1}{6}$$

One can write for the soluble substrate concentration at the gas side interface for a larger particle after some time:

eq. A-36

$$S_s(t,0) = S_s(0) + \int_0^t k_h \cdot S_{i,i}(\tau) d\tau - \frac{Y_{O_2}}{Y_{S_s}} \int_0^t OUR(t) d\tau - \frac{1}{3} \frac{Y_{O_2}}{Y_{S_s}} \frac{OUR(t)}{\frac{D_{S_s}}{L_c^2}}$$

The switch time t_s can be solved from these equation by using the equation $S(t_s,0)=0$.

5. EXPERIMENTAL VALIDATION OF THE SINGLE PARTICLE MODEL	168
5.1 INTRODUCTION	168
5.2 THE IDENTIFIABLE OUR MODEL	169
5.2.1 <i>Model equations</i>	169
5.2.2 <i>Dimensional identifiability</i>	171
5.2.3 <i>Practical identifiability analysis</i>	172
5.3 MATERIALS AND METHODS	177
5.3.1 <i>OUR-measurement device</i>	177
5.3.2 <i>Experimental setup</i>	179
5.4 RESULTS	180
5.5 DISCUSSION	187
5.6 REFERENCES	189

5. Experimental validation of the single particle model

5.1 *Introduction*

The oxygen uptake rate (OUR) is the single most important measure available to monitor the composting process. The time development of the OUR under constant environmental conditions is currently generally described as a first order process (chapter 3). In this thesis a theoretical model (chapter 3) for the OUR time course was developed together with its analytical approximation (chapter 4). The analytical approximation describes the time development of the OUR as a function of the initial state of a waste particle under constant environmental conditions. The initial state of the waste is characterised by its particle size, soluble substrate concentration, insoluble substrate concentration and initial microbial biomass concentration. Both the sensitivity analysis of the theoretical model (chapter 3) and the results of the analytical approximation (chapter 4) reveal the utmost importance of the particle size. To validate the theoretical model the effect of the particle size on the OUR time course will therefore be investigated experimentally.

The model will be supported if the observed particle size effect on the OUR time course is according to the prediction by the analytical model. To obtain a prediction knowledge of the model parameter values is necessary. As these parameter values are not all accurately known, the predictions will have a large uncertainty. Deviations of the predicted OUR time course from the measured trajectory can then be either attributed to a deficient model or to a deficient knowledge of the parameter values. Direct comparison of model prediction, using literature parameter values, with data does not give sufficient information on the appropriateness of the model.

Parameter estimation is thus necessary prior to model validation and the model parameter identifiability is therefore first investigated. Identifiability of a parameter means that it is possible to extract a unique value for each parameter from the data at hand. If no unique parameter values can be determined, physical interpretation of the parameter values is difficult. A lack of identifiability can be a result of the structure of the equation, the experimental design and/or the variance of the measurement.

Identifiability is investigated using dimensional identifiability analysis and a local identifiability analysis with a parameter derivative based method according to Reich. The latter method is

also used to investigate the required minimum duration of an experiment. All these concepts have been introduced in chapter 2.

The aim of this identifiability analysis is to obtain a model parameterisation such that all model parameters are identifiable given the data set used. The identifiable parameters may differ from the parameters originally proposed in the conceptual model. These identifiable parameters are called aggregated parameters, as they often consist of a number of unidentifiable parameters (proposed in the conceptual model).

After defining the identifiable model, (i.e. a model with all parameters identifiable) the values of the identifiable parameters can be extracted from the data by finding an optimal fit between model and data. If the model reflects reality a good fit is expected, however if a good fit is found the opposite need not be true.

The OUR time course is measured for particles with different sizes. For all experiments the aggregated parameters are estimated. As a result of this aggregation some aggregated parameter will depend on the particle size. Validation of the model is performed by comparing the measured particle dependency with the particle size dependency as predicted by the model.

5.2 *The identifiable OUR model*

5.2.1 Model equations

In the previous chapter an analytical model for the OUR time course under constant environmental conditions has been developed. The analytical model is an approximation of the theoretical model, with a bias smaller than 1% compared to the theoretical model.

Figure 5-1 shows the typical time course of the OUR. The OUR time course is characterized by two subsequent stages, the substrate saturated stage (period A+B) and the substrate limited stage (period C+D). During the substrate saturated stage, soluble substrate is abundantly present and the OUR is determined by the processes of biomass growth (period A) and oxygen diffusion (period B). During the substrate saturated stage the soluble substrate concentration decreases and eventually reaches such low levels that the availability of substrate starts determining the conversion rate. This is the onset of the substrate limited stage where the OUR is at first determined by the diffusional transport rate

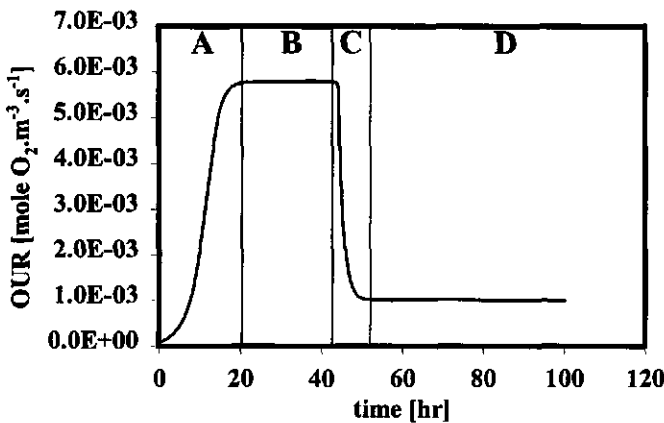


Figure 5.1: The characteristic development in time of the OUR. Four different periods are distinguished. A: OUR increase due to biomass growth; B: plateau of maximum OUR due to biofilm limitation; C: fast decrease due to limited soluble substrate availability; D: slow decrease due to hydrolysis of insoluble substrate. The periods A and B form together the substrate saturated stage, The periods C and D form together the substrate limited stage.

(period C) and eventually by the hydrolysis rate of insoluble substrate (period D). The point of time at which the substrate saturated stage ends and the substrate limited stage starts is called the switch time t_s . The analytical solution developed in chapter 4 reflects this two-stage nature of the OUR time course as follows:

eq. 5-1

$$R(t) = \begin{cases} \sqrt{\frac{\beta_{\text{eff}}}{\beta_{\text{eff}} + e^{\mu_{\text{eff}} t}}} \cdot \text{OUR}_m & t \leq t_s \\ \left(\text{OUR}(t_s) - \frac{Y_{S_i}}{Y_{O_2}} S_{i,t}(t_s) \frac{k_n \left(\frac{Y_{S_i}}{Y_{S_i} - Y_{S_s}} \right) \frac{3.D_{S_i}}{L_c^2}}{\frac{3.D_{S_i}}{L_c^2} - k_n} \right) e^{-\frac{3.D_{S_i}}{L_c^2}(t-t_s)} + \frac{Y_{S_i}}{Y_{O_2}} S_{i,t}(t_s) \frac{k_n \left(\frac{Y_{S_i}}{Y_{S_i} - Y_{S_s}} \right) \frac{3.D_{S_i}}{L_c^2}}{\frac{3.D_{S_i}}{L_c^2} - k_n} e^{-k_n(t-t_s)} & t \geq t_s \end{cases}$$

OUR(t): oxygen uptake rate at time t [mol O₂.m⁻³.hr⁻¹]

t : Time [hr]

t_s : Switch time [hr]

β_{eff} : Effective dimensionless initial biomass concentration [-]

μ_{eff} : Effective maximal biomass growth rate [hr⁻¹]

k_n	: Net hydrolysis rate constant	[hr ⁻¹]
OUR_m	: Maximal oxygen uptake rate	[mol O ₂ .m ⁻³ .hr ⁻¹]
L_c	: Characteristic particle size	[m]
D_{ss}	: Diffusion coefficient for soluble substrate	[m ² .hr ⁻¹]
Y_{ss}	: Biomass yield on soluble substrate	[mol X.mol S _s ⁻¹]
Y_{si}	: Biomass yield on insoluble substrate	[mol X.mol S _i ⁻¹]
Y_{O_2}	: Biomass yield on oxygen	[mol X.mol O ₂ ⁻¹]
$S_{i,t}(t_s)$: Total insoluble substrate at t_s	[mole S _i .m ⁻³]

In the derivation of this analytical expression the parameters t_s , μ_{eff} , β_{eff} and OUR_m are introduced, which are based on a number of basic biokinetic parameters. It is important to note that these aggregated parameters show a dependence on particle size, in contrast to the basic biokinetic parameters that are independent of particle size. Appendix A summarizes these relationships.

The net hydrolysis constant k_n gives the hydrolysis constant of the total insoluble substrate. This net hydrolysis constant is smaller than the actual hydrolysis constant k_h as part of the hydrolysed material is again converted into insoluble material in the form of biomass. The net hydrolysis rate is however no function of particle size.

5.2.2 Dimensional identifiability

Chapter 2 introduced the technique of dimensional identifiability analysis. This technique allows the selection of those parameters that are non-identifiable because they have a unit (e.g. mol biomass-C.m⁻³) that is not observed. A parameter that is dimensionally non-identifiable can form part of a parameter combination that is not non-identifiable. The technique allows the construction of the maximum number of parameter combinations that are not dimensionally non-identifiable. The technique can not give a definite answer to the question whether a specific parameter or parameter combination is identifiable, as other sources of non-identifiability exist. This question will be addressed with a practical identifiability analysis. If the available data consist of the OUR development in time, the following parameters or parameter combinations are shown to be not dimensionally non-identifiable.

$$\text{eq. 5-2} \quad OUR_m, \quad \mu_{\text{eff}}, \quad k_n, \quad \beta_{\text{eff}}, \quad t_s, \quad \frac{D_{S_i}}{L_c^2}, \quad \frac{Y_{S_i}}{Y_{O_2}} \cdot S_{i,t}(t_s), \quad \frac{Y_{S_i}}{Y_{O_2}}, \quad \frac{Y_{S_i}}{Y_{S_t}}$$

Appendix B shows the procedure in more detail. It is important to note that the switch time is treated as a parameter that has to be identified as well. To express the model in a more clear way revealing the meaning of the identifiable parameter groups the following new parameters are introduced.

$$\text{eq. 5-3} \quad k_D = 3 \cdot \frac{D_{S_i}}{L_c^2}, \quad S_{i,t,\text{ox}}(t_s) = \left(\frac{Y_{S_i}}{Y_{S_i} - Y_{S_t}} \right) \cdot \frac{Y_{S_i}}{Y_{O_2}} \cdot S_{i,t}(t_s)$$

$$k_D \quad : \text{Diffusional transport rate constant} \quad [\text{hr}^{-1}]$$

$$S_{i,t,\text{ox}} \quad : \text{Insoluble substrate concentration expressed in oxygen equivalents} \quad [\text{mole O}_2 \cdot \text{m}^{-3}]$$

The diffusion coefficient itself is not identifiable, since it is assumed that generally no size measurements are available. In that case only the parameter k_D might be identifiable. The parameter $S_{i,t,\text{ox}}(t_s)$ expresses the amount of oxygen needed for complete oxidation of the total insoluble substrate present at the switch time. The OUR model thus can be expressed as:

$$\text{eq. 5-4} \quad OUR(t) = \begin{cases} \sqrt{\frac{\beta_{\text{eff}}}{\beta_{\text{eff}} + e^{\mu_{\text{eff}} \cdot t}}} \cdot OUR_m & t \leq t_s \\ \left(OUR(t_s) - S_{i,t,\text{ox}}(t_s) \cdot \frac{k_n \cdot k_D}{k_D - k_n} \right) e^{-k_D \cdot (t-t_s)} + S_{i,t,\text{ox}}(t_s) \cdot \frac{k_n \cdot k_D}{k_n - k_n} \cdot e^{-k_n \cdot (t-t_s)} & t \geq t_s \end{cases}$$

The dimensional analysis gives the maximum set of identifiable parameters, however the identifiability of these parameter(combinations) needs to be investigated further to remove other sources of lacking identifiability.

5.2.3 Practical identifiability analysis

Local parameter identifiability means that the parameters are uniquely determined in the neighborhood of parameter set involved. Several methods are available to assess the local

parameter identifiability [1]. Practical identifiability is a somewhat broader concept related to parameter identifiability. If a parameter is identifiable it means that the data set allows the determination of a unique value, i.e. the data can be generated by one parameter set only. However, for practical applications this finding in itself is not sufficient to guarantee meaningful parameter estimation results. The sensitivity of this unique outcome to changes in the data set has to be taken into account. Widely differing parameter values may generate different outcomes that do not differ appreciably. In such a case, it is hard to obtain meaningful parameter values because the uncertainty of the parameter values will be large. Of course the choice whether differences are appreciable depends on the experimental error involved. If this error is small, smaller parameter differences may be detected.

A number of methods are based on studying the derivatives of the model equations with respect to the parameters, the so-called parameter sensitivity functions. Reich [2] introduced a dimensionless identifiability measure $|R_0|^{-1}$ that enables assessment of practical parameter identifiability given a certain experimental set up. The measure is the inverse of the determinant of a matrix, related to the sensitivity matrix. A value of $|R_0|^{-1} > 10^4$ indicates a lack of practical identifiability, a value of $|R_0|^{-1} < 10^2$ a good practical identifiability. In the range 10^2-10^4 , additional information on the variance of the measurement error and the number of parameters involved is needed to determine whether the parameters are practically identifiable. The method is introduced in more detail in chapter 2

The identifiability of the switch time t_s itself can not be investigated by this method as the first time derivative of the solution has a discontinuity at this point. However as the switch time has such a dominant role in the description it can be assumed that this parameter is identifiable if the experiment lasts long enough to include the switch time. The analysis of practical identifiability will be applied separately for the substrate saturated stage and substrate limited stage.

5.2.3.1 The substrate saturated stage.

For this phase two different parameterizations are considered. The first is the parameterization as considered up till now:

$$\text{eq. 5-5} \quad \text{OUR}(t) = \sqrt{\frac{\beta_{\text{eff}}}{\beta_{\text{eff}} + e^{-\mu_{\text{eff}} \cdot t}}} \cdot \text{OUR}_m \quad t \leq t_s$$

This form will be called the β -parameterization. A second parameterization of this equation is the following.

$$\text{eq. 5-6} \quad \text{OUR}(t) = \sqrt{\frac{1}{1 + e^{-\mu_{\text{eff}}(\Omega - \Omega)}}} \cdot \text{OUR}_m \quad t \leq t_s$$

Ω : Lag time

In this parameterization a new parameter is defined, the lag time Ω . This form is called the Ω -parameterization. The lag time Ω is related to effective dimensionless biomass concentration according to:

$$\text{eq. 5-7} \quad \Omega = -\frac{\ln(\beta_{\text{eff}})}{\mu_{\text{eff}}}$$

A decreasing initial biomass concentration leads to an increased lag time.

The identifiability measure is a function of the experimental time, the number of equally spaced data points and the parameter values. The number of equally spaced data points is expressed as the measurement frequency, i.e. the number of measurements per unit of time. Instead of the experimental time the upper observed OUR_u is used i.e. the OUR value observed at the end of the experiment. The following relation may thus be assumed to exist:

$$\text{eq. 5-8} \quad |R_\theta|^{-1} = f(\text{OUR}_u, \omega_m, \text{OUR}_m, \beta_{\text{eff}}, \mu_{\text{eff}}).$$

$|R_\theta|^{-1}$: Identifiability measure [1]

OUR_u : Upper observed OUR [$\text{mole O}_2 \cdot \text{m}^3 \cdot \text{s}^{-1}$]

ω_m : Measurement frequency [hr^{-1}]

This relationship can be rendered dimensionless using the Π -theorem. This yields the following results:

$$\text{eq. 5-9} \quad |R_\theta|^{-1} = f(\Pi_1, \Pi_2, \Pi_3).$$

In which the following dimensionless numbers are defined:

$$\Pi_1 = \frac{OUR_u}{OUR_m}$$

$$eq. 5-10 \quad \Pi_2 = \frac{\omega_m}{\mu_{eff}}$$

$$\Pi_3 = \beta_{eff}$$

The first dimensionless number ranges from approximately β to 1, as the OUR_u never can exceed OUR_m . The second dimensionless number expresses the measurement frequency relatively to the growth rate. It is assumed that we have a sufficient measurement frequency, i.e. no further improvement is expected from an increase of the measurement frequency. The parameter β_{eff} is already dimensionless, thus this shows up as the third dimensionless number. In a similar way the second parameterization (eq. 5-5) can be treated. This gives the dimensionless numbers:

$$eq. 5-11 \quad \Pi_a = \frac{OUR_u}{OUR_m}$$

$$\Pi_b = \frac{\omega_m}{\mu_{eff}}$$

$$\Pi_c = \Omega \cdot \mu_{eff}$$

It is clear that $\Pi_a = \Pi_1$, $\Pi_b = \Pi_2$ and $\Pi_c = -\ln(\Pi_3)$. Figure 5.2A shows the contour plot of $\log(|R_e|^{-1})$ as a function of Π_1 and Π_3 , while figure 5.2B shows the contour plot of $\log(R_e|^{-1})$ as a function of Π_a and Π_c . The Y-axis of figure 5.2A is logarithmic, i.e. $\log(\Pi_3)$, the Y-axis of figure 5.2B gives the values of $-\ln(10) \cdot \Pi_c$. In this way for a given OUR -curve the identifiability measure can be read for both parameterizations at the same point. Comparison of the graphs shows that the area of acceptable dimensionless number combinations (i.e. is $\log(R_e|^{-1}) < 2$) is larger for the Ω -parameterizations. It is thus easier to determine the parameter of the Ω parameterization.

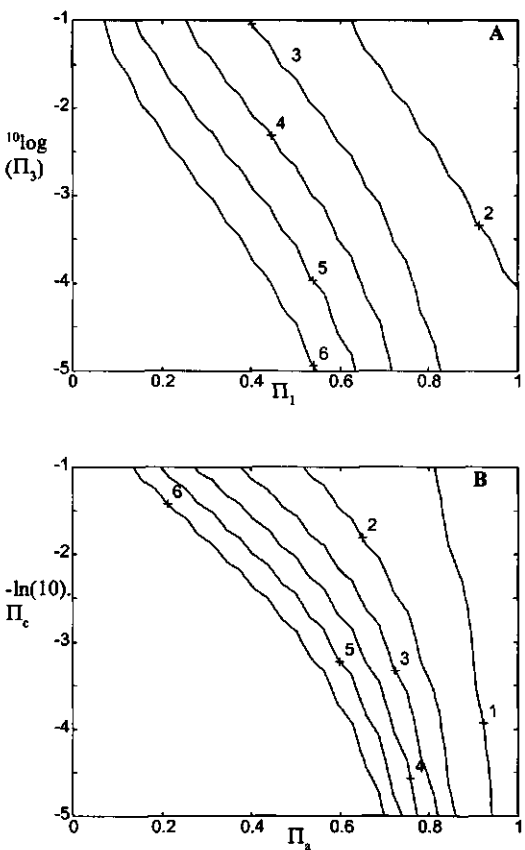


Figure 5.2: The contour plot of identifiability measure $|R_d|^{-1}$ for the β (A) and Ω (B) -parameterization. The label values give the $10\log$ values of $|R_d|^{-1}$. The plot is shown for dimensionless number Π_1 (X-axis) and Π_3 (Y-axis) for A and Π_a (X-axis) and $-\ln(10).\Pi_c$ (Y-axis) for B.

5.2.3.2 Substrate limited stage

The OUR during the substrate limited stage is described as the sum of two exponential terms. Identifiability of this type of model has been extensively studied in the literature [2], from which it can be concluded that the parameters in the substrate limited stage model are identifiable:

- (i) if the ratio of the diffusional and hydrolysis rate constant $k_D/k_n > 5$, and
- (ii) if the exponential term associated with the fast rate constant $e^{-k_D t}$ is effectively fully decayed, i.e. $k_D \cdot t > 5$, and
- (iii) if the exponential term associated with the slow rate constant $e^{-k_n t}$ is sufficiently decayed, i.e. $k_n \cdot t > 0.5$.

In practice the time scales of the two exponential terms are so different that condition i is always met. As the difference is large, the terms can be treated as originating from two independent sequential processes. To identify all parameters therefore an experimental time is needed $t_s + 5/k_D + 0.5/k_n$. The last term gives the largest contribution to the experimental time. As our interest lies here primarily in the effect of particle size, it is convenient to consider an experimental time $>t_s + 5/k_D$ and approximate the hydrolytic term with its first-order Taylor approximation. The so-called short-term model can be described as:

$$\text{eq. 5-12} \quad \text{OUR}(t) = \begin{cases} \sqrt{\frac{1}{1 + e^{-\mu_{eff}(t-\Omega)}}} \cdot \text{OUR}_m & t \leq t_s \\ \left(\text{OUR}(t_s) - A_h \right) e^{-k_D(t-t_s)} + A_h & t \geq t_s \end{cases}$$

A_h : hydrolytic activity [mole O₂.m⁻³.s⁻¹]

where $A_h = k_n S_{i,tox}(t_s)$.

Although the Ω -parametrization is used to estimate the parameter, the estimated parameters β_{eff} will be reported. This parameter has a more relevant physical interpretation, and can be calculated from the estimated value of Ω , via eq.5-7

5.3 Materials and methods

5.3.1 OUR-measurement device

Figure 5.3 shows schematically the OUR measurement system. Gas enters the system via two mass flow controllers, one controller supplying nitrogen (1) and the other oxygen (2). Both oxygen and nitrogen are technical grade gases. The reactor vessel (3) is a stainless steel cylinder with a height of 30 cm and a diameter of 14.3 cm with a working volume of 6.3 liter. The gas mixture enters the reactor via a perforated pipe along the height of the reactor. The gases leave the reactor via a similar pipe fitted at the opposite side of the entrance pipe. The reactor is closed with PE lid. The gas is recirculated over the reactor with a gas pump (4) at a rate of approximately 95 l/hr. This recirculation enables a nearly complete mixing of the gas phase, as was shown by residence time distribution

measurements (data not shown). The gas is recirculated via a glass bottle (5), containing water, to humidify the gas. The gas leaving the reactor is dried by an electro-cooler (6), after which the oxygen level is measured (7). Gas pump, water bottle and reactor are placed in a temperature-controlled cupboard (8).

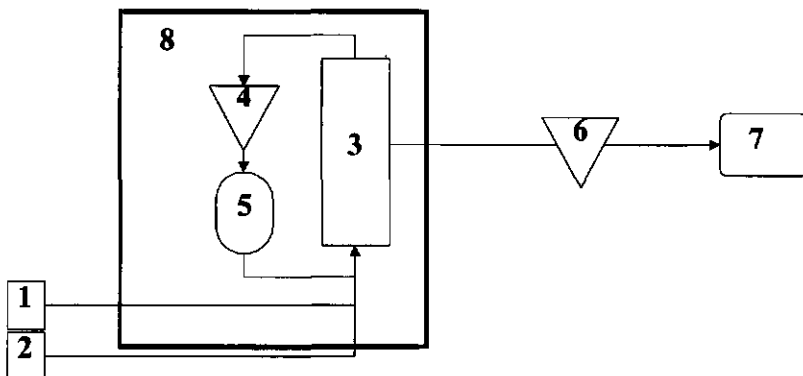


Figure 5.3: Schematic representation for OUR measurement device. Numbers are explained in the main text.

The measurement device is able to control the effluent oxygen level and the reactor temperature. The reactor oxygen level is equal to the effluent oxygen level due to the sufficient gas mixing of the reactor. The control systems consist of a MS-DOS PC using the ControlEG-software connected to an RTI-board for A/D conversion.

The OUR is measured as the difference in amount of oxygen entering and leaving a reaction vessel at a specific point of time. This estimate is exact if the oxygen level within the reactor is constant in time. To achieve this the following control algorithm is used. During a period i the flows of oxygen and nitrogen are kept constant. Assuming a respiration coefficient of 1 the OUR at the end of period i is calculated as:

$$\text{eq. 5-13} \quad \text{OUR}_R(i) = F_{O_2}(i) - F_T \cdot O_{2,e}(i)$$

in which :

$$\text{eq. 5-14} \quad F_T = F_{N_2}(i) + F_{O_2}(i)$$

$OUR_R(i)$: Reactor oxygen uptake rate	[mole.h ⁻¹]
F_T	: Total gas flow	[mole.h ⁻¹]
$F_{O_2}(i)$: Oxygen flow into the system	[mole.h ⁻¹]
$F_{N_2}(i)$: Nitrogen flow into the system	[mole.h ⁻¹]
$O_{2,e}(i)$: Effluent oxygen fraction	[1]

From this OUR value the oxygen flow for the next period is determined as follows.

$$eq. 5-15 \quad F_{O_2}(i+1) = OUR_R(i) + F_T \cdot O_{2,s}$$

$$O_{2,s} : Set\ value\ for\ effluent\ oxygen\ fraction \quad [1]$$

The nitrogen flow is set as the difference between the fixed total flow and the newly set oxygen flow.

$$eq. 5-16 \quad F_{N_2}(i+1) = F_T - F_{O_2}(i+1)$$

The duration of a single period i (the period between flow adjustments) should be sufficiently long to assure a stable control. In all experiments a fixed flow and a twenty-minute period is employed. The first period of an experiment takes always two hours.

A separate temperature control device controlled the cupboard temperature. The set temperature of this device was set via the computer. If the temperature measured in the vessel exceeded the reactor set temperature, the cupboard set temperature was lowered. However the temperature difference between the reactor and cupboard set temperature was not allowed to exceed 5°C. In this way the temperature gradient in the reactor vessel was minimized (<2°C, data not shown).

5.3.2 Experimental setup

All experiments are performed with chicken manure, collected from an experimental facility from the WAU. Each experiment is performed with a different batch of material. To obtain a specific particle size circular plates (internal diameter 10 cm), with a brim at the

edge are filled with chicken manure. The height of the brim determines the thickness of the material placed on the plate. These plates are piled in the reactor with a space of 2 cm in between. Experiments were performed with a manure thickness of 2 or 4 or 8 or 16 mm. All experiments are performed in duplicate. Tap water is added to the manure to set a dry matter content of $21\% \pm 1\%$. Using this dry matter content prevents crack formation when filling the plates. After filling the plates are leveled with a knife. In all experiments the reactor temperature is controlled at 55°C and the oxygen content at 19 vol. % on a dry air basis.

The data are fitted with the OUR-model eq. 5-12 using the least squares criterion. The parameter search is done with the so-called Simplex routine coded according to Press [3]. The organic matter content and dry matter content are analyzed at the start and the end of the experiment. The OUR is expressed on the basis of initial organic matter content, as is common in the literature.

5.4 Results

As a first step the OUR model was fitted to all data sets. This yields for each experiment a set of parameter values for the aggregated parameters. The result of the 16 mm particle size experiments were discarded, as they showed an irregular behavior. Gas, probably produced by anaerobic activity, could not leave the manure layer rapidly enough. As a result gas bubbles formed within the material, causing the material to rise and break. The space between subsequent plates was clogged, hindering the passing of the gas between the subsequent plates. The particle size changed strongly and made the result impossible to interpret with the model developed so far. Although these results can not be used to validate the model, they do show that anaerobic activity is present. This is in accordance with the results of the mechanistic model that predicts the existence of a fairly large anaerobic core inside the particle (see Chapter 3). For one experiment at 2 mm the control algorithm was after some time very unstable, this made estimation of the t_s , k_D and A_h in that case impossible.

Figure 5.4 shows the measurements and the fitted model of the material at 2 (fig. 5.4A), 4 (fig. 5.4B) and 8 mm (fig. 5.4C) thickness. The measured OUR displays oscillations, indicating a non optimal control algorithm. The curves observe the typical behavior predicted by the theoretical model, i.e. the steep ascent at the start followed by plateau,

subsequently a steep descent followed by a relative stable level. In accordance with the expectation it is found that with decreasing particle size the maximum OUR increases while the duration of the plateau becomes smaller (see Chapter 3).

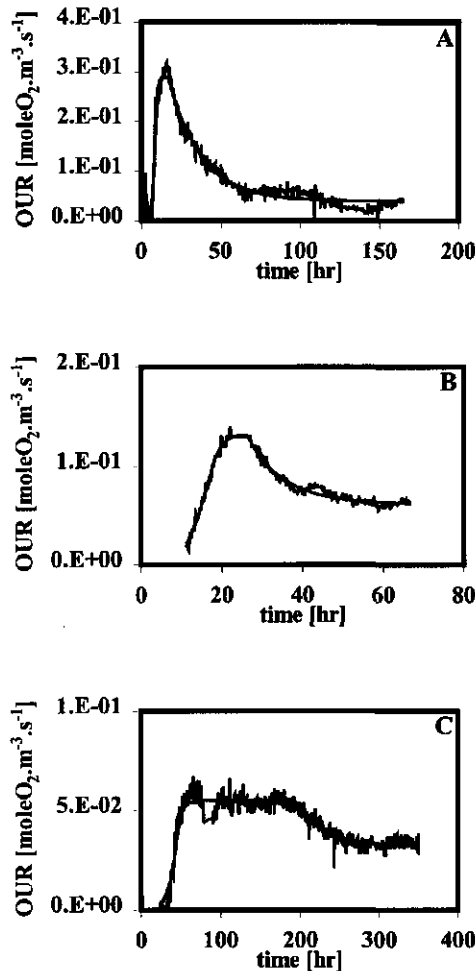


Figure 5.4: The measured OUR time course for 2 mm particle size (A), 4 mm particle size (B) and 8 mm particle size (C). The X-axis denotes time (hr) and the Y-axis OUR (mol O₂.m⁻³.s⁻¹)

As a second step the dependence of the aggregated parameters on the particle size is investigated. Table 5.1 shows the dependence of the identifiable aggregated parameters on the particle size. The first column denotes the identifiable parameter. The second column gives the particle size dependence of the aggregated parameters. The parameters A_1 , A_2 and $S_{s,0,ox}$ are newly introduced lumped parameters. The relationship between these newly introduced parameters and those introduced in the conceptual model is given in the third

column. These relationships can be straightforwardly derived from the relationships as derived in the previous chapter and summarized in appendix A.

Table 5-1: Particle size dependence of the identifiable aggregated parameters.

Aggregated parameter	Particle size dependency	Newly introduced parameters
μ_{eff}	$\frac{L_c}{L_c + A_1} \cdot \mu_n$	$A_1 = \sqrt{D_{O_2} \cdot O_{2,i} \cdot \frac{Y_{O_2}}{X_m \cdot \mu_n}}$
Ω	-	-
OUR_m	$\frac{1}{L_c} \cdot A_2$	$A_2 = \sqrt{2 \cdot D_{O_2} \cdot O_{2,i} \cdot \frac{X_m \mu_n}{Y_{O_2}}}$
A_h	-	-
k_D	$\frac{3 \cdot D_{S_s}}{L_c^2}$	-
t_s	$t_s = \left(1 - \frac{A_h}{A_2} \cdot L_c\right)^{-1} \left[\frac{S_{S,0,\text{ox}}}{A_2} \cdot L_c - \frac{\ln(4)}{\mu_{\text{eff}}} - \Omega - \frac{1}{k_D} \right]$	$S_{S,0,\text{ox}} = \frac{Y_{S_n} \cdot S_{S,0}}{Y_{O_2}}$

It is investigated to which extent the particle size dependence is according to the dependence predicted by the mechanistic model, as outlined in table 5.1. The dependence of the OUR_m on particle size is shown in figure 5.5. The data points can be reasonably fitted with the theoretical expectation. The value of the exponential parameter is -1.17 which is close to the theoretically expected -1.

During the substrate saturated stage there is first a sharp drop in OUR (period C), characterized by a time constant k_D . Based on the estimated value of k_D and the particle size the diffusion coefficient can be calculated. The average value of the diffusion coefficient compare well for the 4 ($D_{S_s} = 2.5 \cdot 10^{-10} \text{ m}^2 \cdot \text{s}^{-1}$) and 8 mm ($D_{S_s} = 2.6 \cdot 10^{-10} \text{ m}^2 \cdot \text{s}^{-1}$) experiments. At 2mm only a single diffusion coefficient could be determined ($D_{S_s} = 2.7 \cdot 10^{-11} \text{ m}^2 \cdot \text{s}^{-1}$) which is clearly much lower.

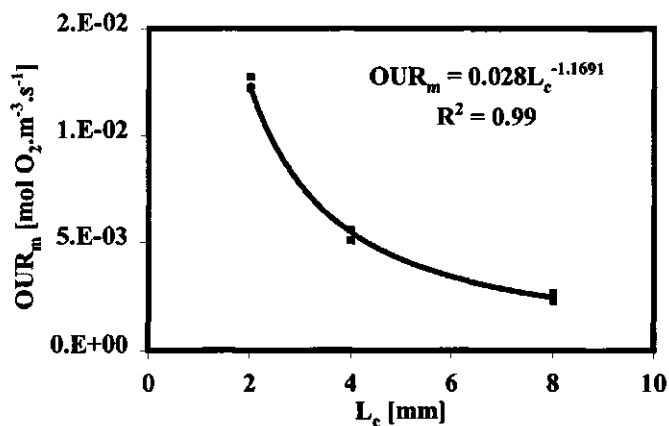


Figure 5.5: Dependence of the maximum oxygen uptake rate OUR_m (Y-axis, mol O₂.m⁻³.s⁻¹) on the particle size L_c (X-axis, mm).

The OUR eventually reaches a stable level, characterized by the hydrolytic activity A_h (period D). According to theory the hydrolytic activity shows no dependence on the particle size. The data as shown in figure 5.6 give no reason to challenge this.

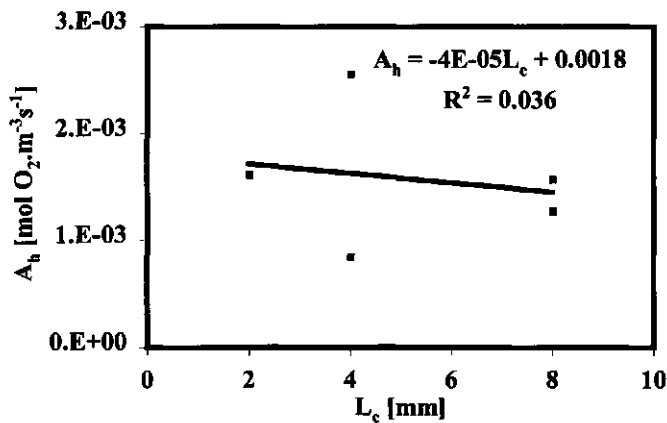


Figure 5.6: Dependence of the hydrolytic activity A_h (Y-axis, mol O₂.m⁻³.s⁻¹) on the particle size L_c (X-axis, mm).

Figure 5.7 shows the dependence of the lag time Ω on the particle size. This lag time should be independent of particle size, only at very small particle sizes (<0.05 mm), an appreciable deviation is expected (see Appendix A). However it is found that the lag time increases as a function of particles size.

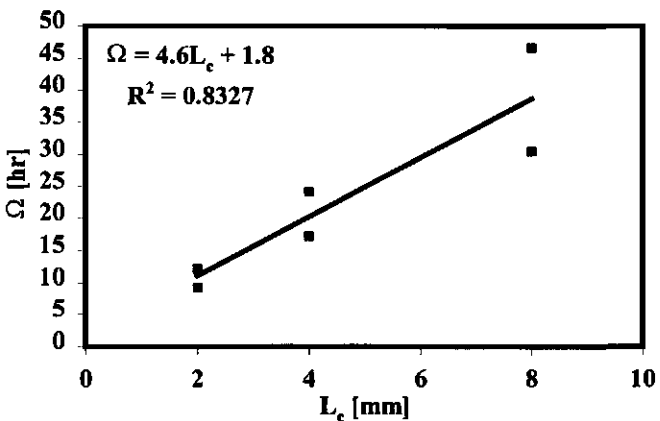


Figure 5.7: Dependence of the lag time Ω (Y-axis, hr) on the particle size L_c (X-axis, mm).

For each experiment the parameter $S_{s,0,ox}$, i.e. initial soluble substrate expressed in oxygen equivalents can be calculated (see table 5.1). Figure 5.8 shows the resulting values as a function of the particle size. As is expected, there is no relationship between particle size and initial soluble substrate. With the average value of the initial soluble substrate concentration (expressed in oxygen equivalents), the already established relationships for OUR_m , A_h , D_{ss} and Ω and the average value of μ_{eff} the switch as a function of particle size time can be calculated. Figure 5.9 shows the dependence of the switch time on particle size, together with the fitted theoretical curve. It is clear that the strong increase in the switch time t_s with increasing particle size can be explained from the theory.

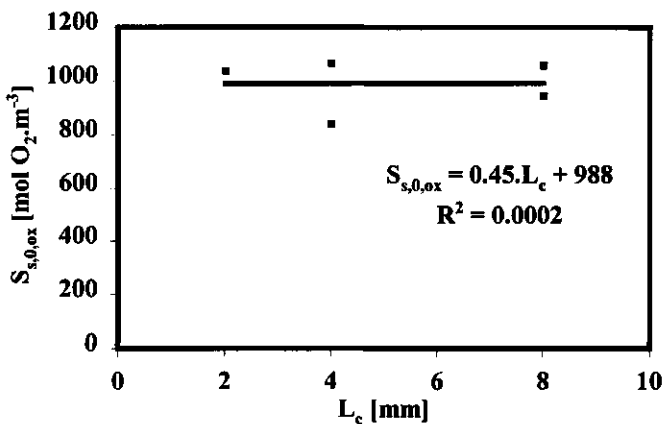


Figure 5.8: Dependence of the initial soluble substrate concentration $S_{s,0}$ (Y-axis, mol O₂·m⁻³) on the particle size L_c (X-axis, mm).

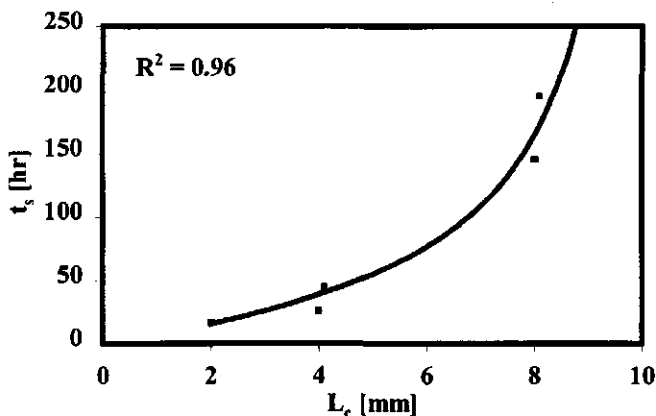


Figure 5.9: Dependence of the switch time t_s (Y-axis, hr) on the particle size L_c (X-axis, mm).

Figure 5.10 shows the dependence of the effective growth rate constant on the particle size. There is a strong increase of the growth rate constant at lower particle sizes. This relationship can be reasonably fitted with the particle size dependence relationship. As a third step the estimated parameter values will be compared with the theoretical expectation.

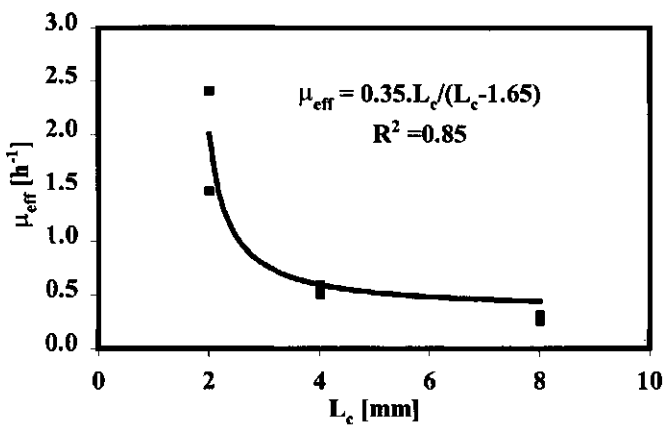


Figure 5.10: Dependence of the effective growth rate constant μ_{eff} (Y-axis, s^{-1}) on the particle size L_c (X-axis, mm)

Table 5-2 summarizes the estimated values and the theoretically expected values. The theoretically expected values are based on the parameter values listed in chapter 3. These parameter values are taken from literature. Many reported values show an appreciable scatter and comparison of the estimated and predicted values can only be an order of magnitude comparison. Therefore the last column gives the $^{10}\log$ value of the ratio of the estimated to the expected value.

Table 5-2: Estimated and expected model parameter values.

Parameter	Estimated	Theoretical	Unit	$^{10}\log(\text{ratio})^a$
A_1	$1.7 \cdot 10^{-3}$	$1.2 \cdot 10^{-5}$	m	2.2
A_2	$2.2 \cdot 10^{-5}$	$1.5 \cdot 10^{-5}$	$\text{mol O}_2 \cdot \text{m}^{-2} \cdot \text{s}^{-1}$	0.16
D_{ss}	$2.7 \cdot 10^{-10}$	$7 \cdot 10^{-10}$	$\text{m}^2 \cdot \text{s}^{-1}$	-0.41
μ_{eff}	$4.4 \cdot 10^{-4} - 7.7 \cdot 10^{-5}$	$2.10 \cdot 10^{-4}$	s^{-1}	-0.41...0.31
Ω	9-46	13	h	-0.12...0.5
$S_{s,0,\text{ox}}$	988	568	$\text{mol O}_2 \cdot \text{m}^{-3}$	0.24
A_h	$1.8 \cdot 10^{-3}$	$1.1 \cdot 10^{-3}$	$\text{mol O}_2 \cdot \text{m}^{-3} \cdot \text{s}^{-1}$	0.21

^a: ratio is estimated value over the expected value

Inspection of the table learns that except for A, the estimated values and expected values are within a half order of magnitude of each other. More can not be expected, as the theoretical values are only rough estimated for a system of which not much is yet known.

5.5 Discussion

Literature often refers to particle size as a factor influencing composting, nevertheless the amount of data proving this assertion is small. In all cases reported, reduction of the particle size, means grinding wood-type materials [4]. In such an experimental set up it is difficult to distinguish between the effect of particle size on the hydrolysis rate and on the oxygen transport. It has been well documented that increasing the surface area of solid primary particles increases the hydrolysis rate. As the material in this study has not been grinded, i.e. the surface available for hydrolysis has not been changed, any effect of particle size can be attributed the effect of particle size on oxygen and soluble substrate transport. Another complication in these reported studies is that waste consisting of particles with different particle sizes are used. Particles with different size have a different switch time and will thus reach the substrate limited period at different points of time. The OUR of the waste at a certain point of time will thus be determined both by particle in the substrate saturated period and the substrate limited period. This mixing up of phases makes data interpretation more troublesome. This is therefore the first study that allows a clear separation of the effect of particle size on mass transfer and hydrolysis on the composting rate.

Based on the analytical model an identifiable model has been presented for description of the OUR time course of a single particle. Such a model is necessary as the original theoretical model contains so many parameters that OUR time course calculations are practically impossible due the necessity to obtain all parameter values involved. Using the dimensionless numbers Π_a and Π_c it can be checked whether the parameters are practically identifiable.

In all experiments parameters showed to be well identifiable as $\Pi_a > 0.99$ and $\Pi_c > 10$. The functional dependence of the parameters μ_{eff} , OUR_{max} , k_D , A_h and t_s on the particle size can be well described by the proposed model. The only parameter that shows a deviant behavior with respect to particle size is the lag time that increase with increasing particle size. All estimated parameters except A, compare favorable with the theoretical value. The large

deviation of A_1 is an indication that the decrease of the growth rate constant with increasing particle size is the result of a process not yet accounted for in the model. Most likely this is caused by substrate inhibition of the aerobic microbial growth, as the hydrolytic activity at 4mm and 8 mm particle size is relatively high compared to the maximum oxygen uptake rate OUR_m . This leads to a temporary build-up of soluble substrate, and consequently a temporary inhibition of the growth rate. An increase of the particle size leads to an increased lag time Ω as a result of this reduction of the growth rate constant. This initial retardation has been observed by others [5-7]. The effect of this Ω increase on the overall OUR description is however small, as the switch time increases much stronger, with increasing particle size.

The proposed identifiable model thus serves as an excellent description of the OUR time course with parameters that are well identifiable and have a clear physical interpretation. This is an important feature, as it gives some confidence to prediction outside the direct domain of observation.

Waste materials are in practice composed of particles with different waste characteristics. For instance Veeken [8] gives a large spread in particle size for biowaste. As particle size is the main characteristic influencing the OUR time course, the particle size distribution needs to be taken into account for describing the time course of any practical waste. As the present model is very well able to describe the effect of particle size on the OUR time course it is an indispensable element to obtain further insight in the composting of a real waste.

5.6 References

1. Walter, E., *Identifiability of State Space Models*. 1982, Berlin: Springer.
2. Seber, G.A.F. and C.J. Wild, *Nonlinear regression*. 1989, New York: John Wiley & Sons.
3. Press, W.H., et al., *Numerical Recipes*. 1986, Cambridge: Cambridge University Press.
4. Gray, K.R., K. Sherman, and A.J. Biddlestone, *Review of composting part 2*. Process Biochemistry, 1971. 6(10): p. 22-28.
5. Wiley, J.S. *Progress report on high-rate composting studies*. in *11th Annual Purdue Industrial Waste Conference*. 1956.
6. Wiley, J.S. *Progress report on high-rate composting studies*. in *12th Annual Purdue Industrial Waste Conference*. 1957.
7. Schulze, K.L. *Rate of oxygen consumption and respiratory quotients during the aerobic decomposition of a synthetic garbage*. in *13th Purdue International Waste Conference*. 1958.
8. Veeken, A.H.M., *Removal of heavy metals from biowaste*, in *Environmental Technology*. 1998, Wageningen Aricultural University: Wageningen.

A. Appendix Basic Parameters

In chapter 4 an analytical approximation was developed for the theoretical model developed in chapter 3. A number of parameters introduced in the theoretical model formed the basis of the parameters introduced in the analytical approximation. These so-called basic parameters are:

μ_n	: Maximal net growth rate constant	$1.8 \cdot 10^{-4}$ [s ⁻¹]
X_m	: Maximal biomass density	2850 [mole X.m ⁻³]
L_c	: Particle size	2.5 m ⁻³ .[m]
D_{O_2}	: Effective diffusion coefficient of oxygen	$1.2 \cdot 10^{-9}$ [m ² .s ⁻¹]
D_{S_s}	: Effective diffusion coefficient of soluble substrate	$7 \cdot 10^{-10}$ [m ² .s ⁻¹]
k_h	: Hydrolysis rate constant	$4.9 \cdot 10^{-7}$ [s ⁻¹]
$O_{2,i}$: Oxygen content at gas side interface	0.18 [mole O ₂ .m ⁻³]
S_i	: Initial insoluble substrate concentration	4100 [mole S.m ⁻³]
$S_{s,0}$: Initial soluble substrate concentration	1200 [mole S.m ⁻³]
X_0	: Initial biomass concentration	0.5 [mole X.m ⁻³]
Y_{O_2}	: Biomass yield on oxygen	1.12 [mole X.mole O ₂ -1]
Y_{S_i}	: Biomass yield on polymeric substrate	1.0 [mole X.mole S _i -1]
Y_{S_s}	: Biomass yield on soluble substrate	0.53 [mole X.mole O ₂ -1]

Based on these basic parameters a set of new parameters is introduced in the OUR model. These new parameters can be derived from the basic parameter in the following manner:

$$\text{eq. A-1} \quad S_{i,t,0} = S_{i,0} + \frac{X_0}{Y_{S_i}}$$

$$\text{eq. A-2} \quad \alpha = 0.85$$

$$\text{eq. A-3} \quad \mu_n = \mu_m - b$$

eq. A-4

$$\beta = \frac{X_o}{X_m - X_o}$$

eq. A-5

$$OUR_m = \frac{I}{L_c} \cdot \sqrt{2 \cdot D_{O_2} \cdot O_{2,i} \cdot \frac{X_m \mu_n}{Y_{O_2}}}$$

eq. A-6

$$\lambda_{p,\min} = \frac{1}{L_c} \cdot \sqrt{2 \cdot D_{O_2} \cdot O_{2,i} \cdot \frac{Y_{O_2}}{X_m \cdot \mu_n}}$$

eq. A-7

$$\mu_{\text{eff}} = (1 - \lambda_{p,\min} \cdot \sqrt{\chi_2})^{-1} \cdot \mu_n$$

eq. A-8

$$\beta_{\text{eff}} = \beta^{(1-\lambda_{p,\min} \cdot \sqrt{\chi_2})^{-1}} \left(\frac{(\sqrt{\beta+1} + \sqrt{\beta})(2 - \sqrt{2})}{(\sqrt{\beta+1} - \sqrt{\beta})(2 + \sqrt{2})} \right)^{\frac{\lambda_{p,\min}}{(1-\lambda_{p,\min} \cdot \sqrt{\chi_2})}}$$

eq. A-9

$$t_s = \left(1 - \frac{k_h \cdot \left(\frac{Y_{S_i}}{Y_{O_2}} \cdot S_{i,t,0} + COU(t_a) \right)}{OUR_m} \right)^{-1} \left[\frac{Y_{S_i}}{Y_{O_2}} \frac{S_{i,t,0}}{OUR_m} - \frac{\ln(4 \cdot \beta_{\text{eff}})}{\mu_{\text{eff}}} - \frac{L_c^2}{3 \cdot D_{S_i}} \right]$$

eq. A-10

$$S_{i,t}(t_s) = \left(S_{i,t,0} + \frac{Y_{O_2}}{Y_{S_i}} \cdot COU(t_a) \right) e^{-k_h t_a} + \frac{Y_{O_2}}{Y_{S_i}} \cdot \frac{OUR_m}{k_h} \cdot (1 - e^{-k_h (t_s - t_a)})$$

eq. A-11

$$\Omega = - \frac{\ln(\beta_{\text{eff}})}{\mu_{\text{eff}}}$$

Under normal conditions $\beta_{\text{eff}} \ll 1$ and $\lambda_{p,\min} \ll 1$ and eq. A-8 can be written as:

eq. A-12

$$\beta_{\text{eff}} = \beta^{(1-\lambda_{p,\min} \cdot \sqrt{\chi_2})^{-1}}$$

Substituting eq. A-12 and A-7 in eq. A-11 yields the following result for Ω :

eq. A-13

$$\Omega = -\frac{\ln(\beta)}{\mu_n}$$

B. Appendix Dimensional identifiability

Again recalling the basic parameters

μ_n	: Maximal net growth rate constant	$1.8 \cdot 10^{-4} [\text{s}^{-1}]$
X_m	: Maximal biomass density	$2850 [\text{mol X.m}^{-3}]$
L_c	: Particle size	$2.5 \text{ m}^{-3} \cdot [\text{m}]$
D_{O_2}	: Effective diffusion coefficient of oxygen	$1.2 \cdot 10^{-9} [\text{m}^2 \cdot \text{s}^{-1}]$
D_{S_s}	: Effective diffusion coefficient of soluble substrate	$7 \cdot 10^{-10} [\text{m}^2 \cdot \text{s}^{-1}]$
k_h	: Hydrolysis rate constant	$4.9 \cdot 10^{-7} [\text{s}^{-1}]$
$O_{2,i}$: Oxygen content at gas side interface	$0.18 [\text{mol O}_2 \cdot \text{m}^{-3}]$
S_i	: Initial insoluble substrate concentration	$4100 [\text{mol S.m}^{-3}]$
$S_{s,0}$: Initial soluble substrate concentration	$1200 [\text{mol S.m}^{-3}]$
X_0	: Initial biomass concentration	$0.5 [\text{mol X.m}^{-3}]$
Y_{O_2}	: Biomass yield on oxygen	$1.12 [\text{mole X.mol O}_2^{-1}]$
Y_{S_i}	: Biomass yield on polymeric substrate	$1.0 [\text{mole X.mol S}^{-1}]$
Y_{S_s}	: Biomass yield on soluble substrate	$0.53 [\text{mole X.mole O}_2^{-1}]$

Based on this listing the following dimensional matrices can be devised for the parameter A and the observations O.

The vector D describes the basic dimensions used, respectively seconds (s), C-mole substrate (both soluble and insoluble) (S), C-mole of biomass (X), meter (m) and mole of oxygen (O_2).

$$D = \begin{bmatrix} s \\ S \\ X \\ m \\ O_2 \end{bmatrix}$$

The vector P describes the parameters involved.

$$P = (L_c, Y_{S_i}, X_m, D_{S_s}, D_{O_2}, \mu_n, Y_{S_s}, Y_{O_2}, k_h, S_{s,0}, S_{i,0}, X_0, O_{2,i})$$

The observation matrix \mathbf{O} with columns time and OUR has rank 2, and runs as:

$$\mathbf{O} = \begin{bmatrix} 1 & 1 \\ 0 & 0 \\ 0 & 0 \\ 0 & -3 \\ 0 & 1 \end{bmatrix}$$

The parameter matrix \mathbf{A} has rank 5 and runs as:

$$\mathbf{A} = \begin{bmatrix} 0 & 0 & 0 & -1 & -1 & -1 & 0 & 0 & -1 & 0 & 0 & 0 & 0 & 0 \\ 0 & -1 & 0 & 0 & 0 & 0 & -1 & 0 & 0 & 1 & 1 & 0 & 0 \\ 0 & 1 & 1 & 0 & 0 & 0 & 1 & 1 & 0 & 0 & 0 & 1 & 0 \\ 1 & 0 & -3 & 2 & 2 & 0 & 0 & 0 & 0 & -3 & -3 & -3 & -3 \\ 0 & 0 & 0 & 0 & 0 & 0 & -1 & 0 & 0 & 0 & 0 & 1 \end{bmatrix}$$

The maximum number of dimensionally non-redundant parameter or parameter groups is thus $13+2-5 = 10$. Combining the observation matrix \mathbf{O} and the parameter matrix \mathbf{A} and using gaussian reduction yields the following result \mathbf{Z} :

$$\mathbf{Z} = \begin{bmatrix} 1 & 0 & 0 & 0 & 0 & -1 & -1 & 0 & -1 & -1 & 0 & 0 & 0 & 1 \\ 0 & 1 & 0 & 0 & 0 & 0 & 0 & 0 & 0 & -1 & 0 & 0 & 0 & 1 \\ 0 & 0 & 1 & 0 & 0 & 2 & 2 & 0 & 0 & 0 & 0 & 0 & 0 & 0 \\ 0 & 0 & 0 & 1 & 0 & 0 & 0 & 0 & 1 & 0 & 0 & -1 & -1 & 0 & 0 \\ 0 & 0 & 0 & 0 & 1 & 0 & 0 & 0 & 0 & 1 & 0 & 1 & 1 & 1 & 0 \end{bmatrix}$$

From this matrix dimensionally non-redundant groups may be determined as:

$$\frac{D_{S_s}}{L_c^2}, \quad \frac{D_{O_2}}{L_c^2}, \quad \mu_n, \quad \frac{Y_{S_s}}{X_m}, \quad \frac{Y_{O_2}}{X_m}, \quad k_h, \quad S_{s,0} \cdot \frac{Y_{S_s}}{X_m}, \quad S_{i,0} \cdot \frac{Y_{S_i}}{X_m}, \quad \frac{X_0}{X_m}, \quad O_{2,i}$$

Listed below are the OUR model parameters as they are defined in analytical approximation, these parameters are different from the fundamental parameters used in the dimensional analysis.

OUR model parameters

β_{eff}	: effective dimensionless initial biomass concentration	[1]
D_s	: diffusion coefficient for soluble substrate	[m ² .hr ⁻¹]
L_c	: characteristic particle size	[m]
OUR_m	: maximal oxygen uptake rate	[moleO ₂ .m ⁻³ .hr ⁻¹]
$S_i(t_s)$: total insoluble substrate at t_s	[mole C.m ⁻³]
t_s	: switch time	[hr]
Y_{O_2}	: biomass yield on oxygen	[mole C.mole O ₂ ⁻¹]
Y_{Si}	: biomass yield on insoluble substrate	[mole C.mole C ⁻¹]
Y_{Ss}	: biomass yield on soluble substrate	[mole C.mole C ⁻¹]
μ_{eff}	: effective maximal biomass growth rate	[hr ⁻¹]

The relationships between these OUR model parameters and the fundamental parameters are shown in appendix A. Inspection of these relationship shows that all OUR model parameters consist of dimensional non-redundant groups, and thus the OUR model parameters are also dimensionally non-redundant.

6. DEVELOPMENT OF THE DISTRIBUTED OUR MODEL	198
6.1 INTRODUCTION	198
6.2 PARTICLE SIZE DISTRIBUTION MODEL	199
6.2.1 <i>Conceptual bed model</i>	199
6.2.2 <i>The box representation</i>	200
6.3 GAMMA DISTRIBUTION AS AN APPROXIMATE DISTRIBUTION	204
6.4 GAMMA DISTRIBUTION AND BALANCE EQUATIONS	208
6.4.1 <i>OUR model for a single particle</i>	208
6.4.2 <i>Average OUR-time relationship</i>	210
6.4.3 <i>Substrate-time relationship</i>	213
6.5 BEHAVIOUR OF THE DISTRIBUTED MODEL	213
6.6 DISCUSSION	218
6.7 REFERENCES	222

6. Development of the Distributed OUR Model

6.1 *Introduction*

In the previous chapters a theoretical model has been developed for the oxygen uptake rate (OUR) time course of a composting waste particle with a fixed size. It was shown that the particle size is the most important waste characteristic influencing the OUR time course. This was shown by a sensitivity analysis of the theoretical model (chapter 3), the results of the analytical approximation (chapter 4) and the measurements on the effect of particle size on the OUR development (chapter 5).

In practice a waste generally does not consist of particles with one specific particle size but consists of particles with different sizes (e.g.[1]). Waste is characterised by a size distribution and not by a single particle size. As the particle size is the most important waste characteristic determining the OUR, modelling a real world waste implies that the particle size distribution needs to be taken into account. In this chapter a model is derived for a waste with a particle size distribution, this model will be referred to as “the distributed OUR model”.

The particle size distribution can be an original attribute of the waste and/or the result of waste pre-treatment like screening and shredding. To compost waste it is piled in heaps up to a height of 4 m. As a result of the pressure inside the pile, waste particles may agglomerate and the resulting particle size distribution in the pile will then differ from the original particle size distribution. It is this actual in-situ particle size distribution within the pile that is determining the OUR time course.

The analysis of the distributed particle size model starts with a conceptual model of the piled bed of waste. Based on this conceptual model of the waste bed the gamma distribution function is proposed to describe the particle size distribution. Use of a conceptual model is necessary, as it allows the distribution parameters to be related to physical processes influencing the particle size distribution, like drying and compaction. This particle size distribution is combined with the analytical approximation of the OUR time course to obtain the distributed OUR model. The effect of the size distribution on the OUR time course is investigated and compared to the case of a single particle size.

6.2 Particle size distribution model

6.2.1 Conceptual bed model

The waste bed is assumed to consist of a pile of small solid organic and solid inert particles, called primary particles. Between the primary particles pores are present. Either gas or water fills the pores of this pile. Water is bound within the pores through capillary binding or by direct attachment through London-van der Waals forces. Water has a tendency to fill up first the smallest pores, as they have the biggest capillary suction. In this way areas will arise consisting solely of wetted particles connected via water filled pores. Such an area will be called a secondary particle. Gas filled pores constitute the border of the secondary particle (Figure 6.1). This set of secondary particles is assumed to be exposed to a homogenous gas phase with a constant composition. The secondary particles all have the same initial composition and the same constant temperature. There is no mass transport between the particles. The composting process occurs within the secondary particles as is described by the theoretical model (chapter 3).

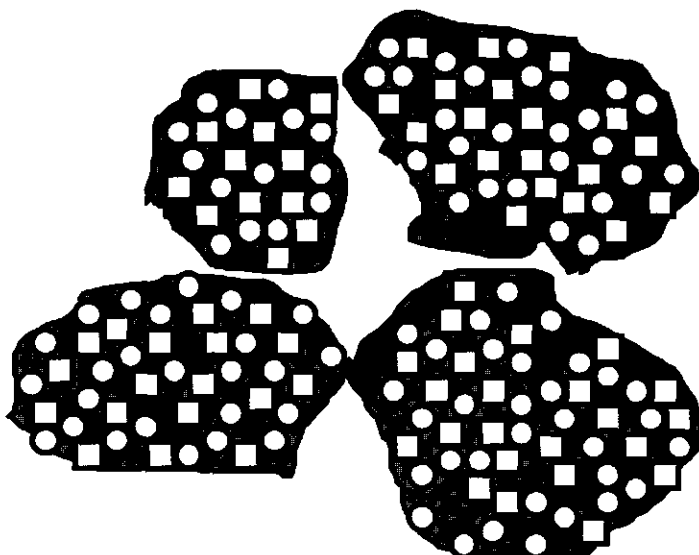


Figure 6.1: Two dimensional representation of the secondary particle. The rectangles represent the organic primary particles, circles the inert. The shaded area is the water bounded to the particles due to surface binding or capillary binding. The solid line represents the boundary between the gas phase and the secondary particle.

The conceptual model implies that the particle size is strongly influenced by the extent to which the pores are water filled. If more pores are water filled, the secondary particles will become larger. This can be understood by considering the gas filled pores. With an increase of water filled pores the number of gas filled pores will decrease. As the number of gas filled pores will decrease the average distance between the gas filled pores will increase. As the gas filled pores are the boundaries of the secondary particle this implies that the secondary particle size will increase. In this thesis the secondary particle size distribution will be derived by considering the distribution of the gas filled pores. The advantage of grounding the particle size distribution in a conceptual model is that the effect of moisture can be incorporated.

6.2.2 The box representation

As a first step to analyze the secondary particles size distribution, these particles will be represented as a box. This so-called representative box has the same specific surface area as the secondary particle and represents the secondary particle's shape best in some sense. A box is chosen to represent the secondary particle as it reflects the three dimensional aspect of the problem and remains close to the flat-plate representation used in the previous chapters. How to find a procedure for determining the representative box will not be analyzed further, as the existence of such a procedure and thus the existence of a uniquely representative box for each particle is assumed. Figure 6.2 shows a two-dimensional illustration of a secondary particle and the associated representative box. The faces of the representative box are the interface between the particle and the gas filled pores. The representative box is characterised by the distance between the opposite faces of the box in the three dimensions, denoted with L_x , L_y , L_z . The size of L_x , L_y and L_z is thus related to the distribution of the gas pores within the waste.

To determine the particle size distribution we therefore study the distribution of the gas pores. Consider first a unit length water of a water filled waste matrix. All primary particles will in this case be connected via single continuous water phase (Figure 6.3A). The presence of a pore will split this unit length in two smaller particles. The pore crossing density λ is defined as the number of pores that cross a unit distance (either x, y or z) of water connected primary particles (Figure 6.3B). Defining the crossing density in this way makes that only the presence of a gas pore determines the particle size and that the size of a gas pore does not influence the

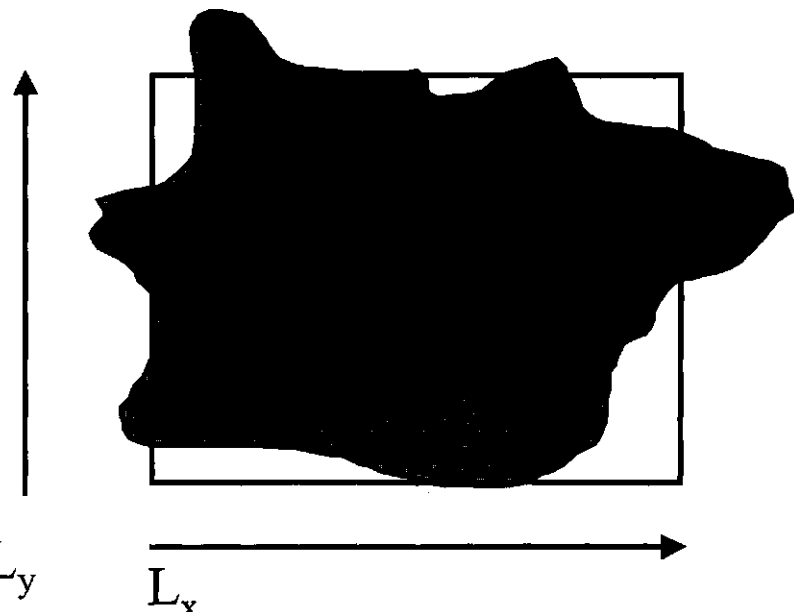


Figure 6.2 Two dimensional illustration of a secondary particle (shaded area) and the associated representative rectangle). L_x and L_y denote the length of the box edges.

particle size. The number of pores that cross a unit distance (either x, y or z) of water will determine the number and size of the particles (Figure 6.3C). In the following analysis it will be assumed that all primary particles have an equal probability to lie next to a gas filled pore in the x, y or z-direction. In other words the distribution of the pores in a certain direction is described by a uniform distribution. The uniform distribution is characterised by a uniform density, equalling the pore crossing density. A uniform distribution of the gas pores implies that the distribution of the distances between two consecutive tubes is given by a Poisson distribution function [2]. The distribution function of L_x is given by :

$$\text{eq. 6-1} \quad f_1(L_x) = \lambda_x e^{-\lambda_x L_x}$$

- | | | |
|-------------|--|------------|
| $f_1(x)$ | : Particle dimension distribution density in one dimension | $[m^{-1}]$ |
| L_x | : Box size in x-direction | $[m]$ |
| λ_x | : X-direction associated gas pore crossing density | $[m^{-1}]$ |

The expected value of L_x is equal to λ_x^{-1} . A similar equation holds for the y-direction and the z-direction, for which the tube crossing densities are given by λ_y and λ_z . The pore crossing

densities in the three different directions need not to be equal. Together these three distribution functions describe the representative box size and shape distribution (Figure 6.3D).

The OUR model for a single particle size as developed in the previous chapter was based on a flat plate representation. This representation may be used safely for differently shaped particles as long as the specific surface area is the same and the penetration depth of oxygen is relatively small [3]. Under these conditions the reaction zone is confined to a thin outer shell of the particle, and thus proportional to the surface area. The volumetric conversion rate is

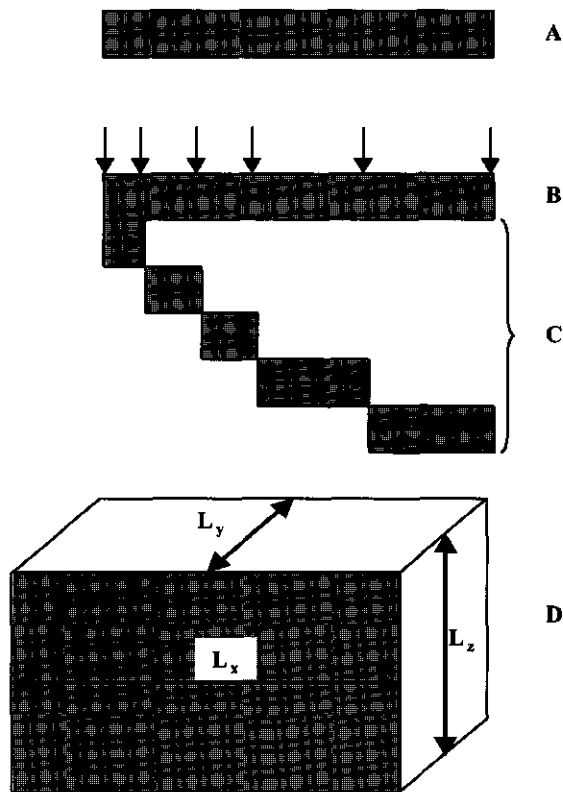


Figure 6.3 : A shows a unit length of fully water filled waste matrix, i.e. all primary particles are only connected via a single continuous water phase. If less water is present within the waste gas pores will form. B indicates the location of these gas pores, that are uniformly distributed. It is important to note that only the number of gas pores influences the particle size and that pore size itself is not of importance. C shows the particles with different size that are formed as a result of the cutting of the unit length of waste. D shows a box that is a result of the cutting process in three dimensions.

thus proportional to the specific surface area of the particle in question. This is indeed the case for a composting particle, as was shown in chapter 3 and 4.

To establish a relationship between the representative box and the single particle OUR model, a single measure, the characteristic particle size, will be associated with the representative box. The characteristic particle size is chosen such that the specific surface area of the box and the flat plate equal each other. The representative box has a specific surface A_c of :

$$\text{eq. 6-2} \quad A_c = \frac{2 \cdot L_x \cdot L_y + 2 \cdot L_x \cdot L_z + 2 \cdot L_y \cdot L_z}{L_x \cdot L_y \cdot L_z}$$

A_c : Specific surface area of the representative box [m².m⁻³]

The specific surface area of a flat plate equals:

$$\text{eq. 6-3} \quad A_s = \frac{1}{L_c}$$

A_s : Specific surface area of the flat plate system [m².m⁻³]

L_c : Characteristic particle size [m]

By equating eq. 6-2 and eq. 6-3 and linearizing the resulting equation, a linear approximation for the characteristic particle size is obtained:

$$\text{eq. 6-4} \quad L_c = \frac{L_x}{18} + \frac{L_y}{18} + \frac{L_z}{18}$$

The characteristic particle size is a weighted sum of the L_x , L_y and L_z . As the distribution functions for L_x , L_y and L_z are known, these equations are the starting point for derivation of the characteristic particle size distribution function. By an 18 fold increase of the value of the pore crossing densities, the factor 18 can be left out in the subsequent derivations. In the following of the text λ_x , λ_y , and λ_z denote these changed parameter values of the pore density. The distribution function of a weighted sum of functions can be derived in a straightforward manner (Appendix A). The distribution of the characteristic particle size is described by:

eq. 6-5

$$f_3(L_c) = \frac{\lambda_x \lambda_y \lambda_z}{(\lambda_y - \lambda_z)(\lambda_z - \lambda_x)(\lambda_y - \lambda_x)} (e^{-\lambda_x L_c} (\lambda_y - \lambda_z) + e^{-\lambda_y L_c} (\lambda_z - \lambda_x) + e^{-\lambda_z L_c} (\lambda_x - \lambda_y))$$

$$\lambda_x \neq \lambda_y \neq \lambda_z \quad \lambda_x > 0, \lambda_y > 0, \lambda_z > 0$$

The distribution function is a sum of three exponential terms. This distribution function will be referred to as the “sum-of-exponentials” distribution function. The identifiability of this type of function has been extensively investigated [4] and it can be stated that all parameters should differ with a factor 5 of each other to be well identifiable. Although the value of the pore crossing density may differ from direction to direction, it is unlikely that they will differ that dramatically. This would indicate that the identifiability of this distribution function is poor. To solve this problem the gamma distribution will be introduced as an approximating distribution function.

6.3 Gamma distribution as an approximate distribution

The distribution of the sum of independent variables distributed according to exponential functions like eq. 6-1 with a common scale factor λ can be described by the gamma distribution [5]. The probability density function of the gamma distribution runs like:

eq. 6-6

$$G(L_c, \lambda, \gamma) = \lambda^\gamma \cdot \frac{L_c^{\gamma-1}}{\Gamma(\gamma)} \cdot e^{-\lambda L_c}$$

$G(L_c, \lambda, \gamma)$: Gamma distribution

[-]

λ : Scale parameter

[m^{-1}]

γ : Shape parameter

[-]

Γ : Gamma function

[-]

For instance, if $\lambda_x = \lambda_y = \lambda_z$ then the resulting particle size distribution is described by the gamma distribution with a values of $\gamma = 3$ and $\lambda = \lambda_x$. The extent to which the sum-of-exponentials distribution function can be adequately described by the gamma distribution will be investigated for the particular case that all three pore density parameters differ from each other and all are unequal to zero. For this purpose values of γ and λ will be sought such that

the gamma distribution has the same first and second moment as the associated sum-of-exponential distribution function. These parameter values will be called the corresponding values λ_c and γ_c . Equating the moments of the gamma distribution with the moments of the sum-of-exponential distribution function and defining $\alpha = \lambda_y / \lambda_x$ and $\beta = \lambda_z / \lambda_x$, yields the following result for λ_c and γ_c as detailed in Appendix A-2.

For λ_c it is found that:

$$\text{eq. 6-7} \quad \lambda_c = \frac{\alpha \cdot \beta (\alpha + \beta + \alpha \cdot \beta)}{\alpha^2 + \beta^2 + \alpha^2 \beta^2} \cdot \lambda_x$$

λ_c : Corresponding pore crossing density. [m⁻¹]

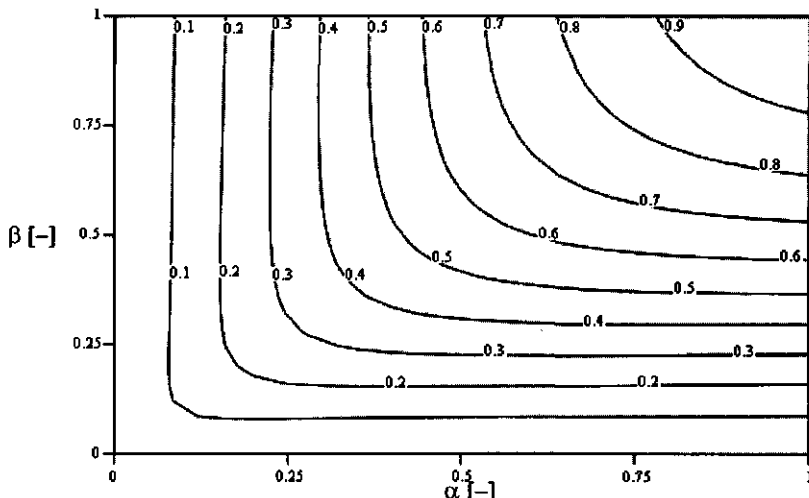


Figure 6.4: The value of λ_c/λ_x as function of α (X-axis) and β (Y-axis).

The value of λ_c/λ_x is shown as a function of α and β in figure .6.4. It is assumed that $\lambda_x > \lambda_y$ and $\lambda_x > \lambda_z$. This gives no loss of generality, in a given situation some dimension has the highest pore crossing frequency, and to this dimension the label x can be given. This implies that $0 < \alpha < 1$ and $0 < \beta < 1$. For γ_c it is found that:

$$\text{eq. 6-8} \quad \gamma_c = \frac{(\alpha \cdot \beta + \alpha + \beta)^2}{\alpha^2 \cdot \beta^2 + \alpha^2 + \beta^2}$$

γ_c : Corresponding gamma value [-]

This equation shows that the value of corresponding gamma is only determined by the ratios of the sizes of the different faces of the representative box. It is a measure of the shape of the average representative box. In this sense the shape parameter γ_c has two meanings, there is a relation to the average shape of the representative box and to the shape of the distribution curve. In figure 6-5 the dependency of the value of γ_c on the values of α and β is shown in a contourplot. This figure shows clearly that the value of γ remains in the range of 1-3. As is shown in appendix A-2, the mean of the gamma distribution, and thus the mean particle size is given by:

$$\text{eq. 6-9} \quad \Lambda = \frac{1}{\lambda_x} + \frac{1}{\lambda_y} + \frac{1}{\lambda_z}$$

Λ : Mean particle size [m]

The variance equals:

$$\text{eq. 6-10} \quad \sigma^2 = \frac{1}{\lambda_x^2} + \frac{1}{\lambda_y^2} + \frac{1}{\lambda_z^2}$$

σ^2 : Variance of particle size distribution [m²]

Appendix A-2 gives the details of the derivation.

Figure 6.6 illustrates that the gamma distribution gives an acceptable approximation to the sum-of-exponentials distribution function. The first example gives the case that the pore frequency in all three dimensions differ appreciably from each other ($\lambda_x=1$ $\lambda_y=0.5$ and $\lambda_z=0.25$). The second case illustrates the case that the pore crossing frequency in one frequency is appreciably smaller ($\lambda_x=1$ $\lambda_y=0.9$ and $\lambda_z=0.25$).

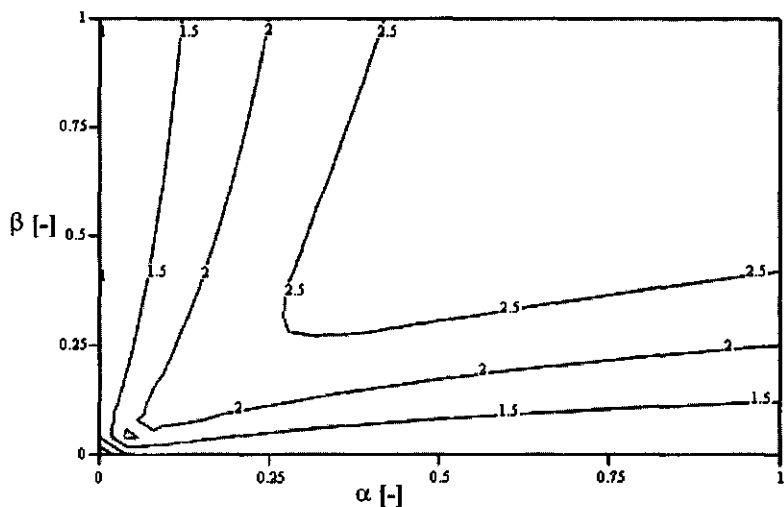


Figure 6.5 : The value of γ_c shown in a contour plot as a function of α (X-axis) and β (Y-axis).

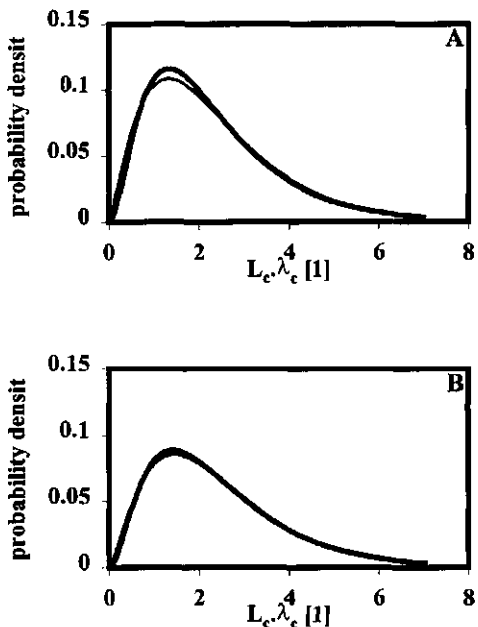


Figure 6.6: The probability density of the sum of exponential distribution curve (thin line) and the approximating gamma distribution (thick line). The upper curve A is for the case $\lambda_x=1$, $\lambda_y=0.5$ and $\lambda_z=0.25$, the lower B for the case ($\lambda_x=1$, $\lambda_y=0.9$ and $\lambda_z=0.25$).

The gamma distribution seems a good approximation of the sum-of-exponential distribution function. The gamma distribution will therefore be used as the particle size distribution model. The model parameters γ_c and λ_c still can be given a physical interpretation. If the pore crossing frequencies do not differ too strong a γ_c value in the range of 2-3 is expected.

6.4 Gamma distribution and balance equations

6.4.1 OUR model for a single particle

In chapter 4 an analytical model for the OUR time course of a single particle under constant environmental conditions was derived. The model is expressed as:

$$\text{eq. 6-11} \quad \text{OUR}(t) = \begin{cases} \sqrt{\frac{\beta_{\text{eff}}}{\beta_{\text{eff}} + e^{\mu_{\text{eff}} t}}} \cdot \text{OUR}_m & t \leq t_s \\ \left(\text{OUR}(t_s) - S_i(t_s) \frac{k_n \cdot k_D}{k_D - k_n} \right) e^{-k_D \cdot (t - t_s)} + S_i(t_s) \frac{k_n \cdot k_D}{k_D - k_n} e^{-k_n \cdot (t - t_s)} & t \geq t_s \end{cases}$$

OUR(t): OUR of a single particle [mol O₂.m⁻³.s⁻¹]

t : Time [s]

t_s : Switch time [s]

μ_{eff} : Effective maximal biomass growth rate constant [s⁻¹]

Ω : Lag time [s]

k_n : Net hydrolysis rate constant [s⁻¹]

OUR_m : Maximal oxygen uptake rate [mol O₂.m⁻³.s⁻¹]

k_D : Diffusional transport time constant [s⁻¹]

S_i : Insoluble substrate expressed in oxygen equivalents [mol O₂.m⁻³]

This model will be referred to as the analytical single particle OUR model. In the previous chapter the model has been validated. All parameters are identifiable if OUR data are taken over a sufficient long period. The lag time representation is used, as this parameter is better identifiable and does not depend as strongly on particle size as the effective initial dimensionless biomass concentration.

When a distribution model is introduced this single particle model model can be further

simplified by neglecting the diffusional term $\left(OUR(t_s) - S_{i,t,ox}(t_s) \cdot \frac{k_n \cdot k_D}{k_D - k_n} \right) e^{-k_D(t-t_s)}$. This

simplification is justified, not only because this term influences the OUR over a very short period, but more importantly because this term will show to be negligible compared to a more dominant term introduced by the size distribution. The rate constant k_D is much bigger than k_n (see chapter 3), which implies that:

$$eq. 6-12 \quad \frac{k_n \cdot k_D}{k_D - k_n} \approx k_n$$

The simplified model is then as follows:

$$eq. 6-13 \quad OUR_s(t) = \begin{cases} \sqrt{\frac{1}{1 + e^{-k_{eff} \cdot (t-\Omega)}}} \cdot OUR_m & t \leq t_s \\ k_n \cdot S_{i,0} \cdot e^{-k_n \cdot t} & t > t_s \end{cases}$$

in which :

$$eq. 6-14 \quad S_{i,0} = S_i(t_s) e^{-k_n \cdot t_s}$$

$S_{i,0}$: Apparent initial insoluble substrate [mol O₂.m⁻³]

OUR_s : Simplified analytical OUR model. [mol O₂.m⁻³.s⁻¹]

Leaving out the substrate diffusion means that the substrate saturated phase description will last until the soluble substrate is zero. From this point (t_s) on, the soluble substrate will remain zero, and the OUR will be determined by the solubilization rate. From the equation for soluble substrate given in chapter 4 the following simplified equation for the soluble substrate can be derived:

eq.6-15

$$S_s(t) = \begin{cases} S_{s,0} - \left(\frac{1}{\mu_{\text{eff}}} \cdot \ln \left(\frac{2e^{-\mu_{\text{eff}} \cdot \Omega} + e^{-\mu_{\text{eff}} \cdot t} + 2\sqrt{e^{-\mu_{\text{eff}} \cdot \Omega} (e^{-\mu_{\text{eff}} \cdot \Omega} + e^{-\mu_{\text{eff}} \cdot t})}}{2e^{-\mu_{\text{eff}} \cdot \Omega} + 1 + 2\sqrt{e^{-\mu_{\text{eff}} \cdot \Omega} (e^{-\mu_{\text{eff}} \cdot \Omega} + 1)}} \right) + t \right) \cdot \text{OUR}_m + S_{i,0} \cdot (1 - e^{-k_n \cdot t}) & t \leq t_s \\ 0 & t > t_s \end{cases}$$

S_s : Soluble substrate expressed in oxygen equivalents [mole O₂.m⁻³]

$S_{s,0}$: Initial soluble substrate expressed in oxygen equivalents [mole O₂.m⁻³]

$S_{i,0}$: Initial total insoluble substrate expressed in oxygen equivalents [mole O₂.m⁻³]

From the condition that the soluble substrate concentration becomes zero at the switch time the switch time can be determined.

6.4.2 Average OUR-time relationship

The OUR of a set of distributed particles can be calculated as the weighted average of the OUR of the individual particles. The development of the OUR in time will be named the size averaged OUR and denoted as $\text{OUR}_a(t)$. When the size distribution is described by a continuous function, such as the gamma distribution described above, the $\text{OUR}_a(t)$ can be calculated as:

$$\text{eq. 6-16} \quad \text{OUR}_a(t) = \int_0^{\infty} G(L_c, \lambda_c, \gamma_c) \cdot \text{OUR}_s(t, L_c) dL_c$$

$\text{OUR}_s(t, L_c)$: OUR_s of a single particle as function of time and particle size [mole O₂.m⁻³.s⁻¹]

$\text{OUR}_a(t)$: Size averaged OUR [mole O₂.m⁻³.s⁻¹]

The average OUR is determined as the integral over the particle size from zero to infinity of the product of the OUR of a specific particle size and the probability density of this specific particle size. As during the substrate saturated phase the OUR of a single particle depends on the particle size, this is explicitly denoted as $\text{OUR}(t, L_c)$.

As the OUR_s depends on the particle size only during the substrate saturated stage, the integral of eq. 6-16 is divided in two domains. The first is the domain of the particles, which have been fully depleted from soluble substrate. Their OUR will be solely determined by the

hydrolysis rate, and is independent of particle size. The small particles are depleted first, so the substrate depleted domain will run from particle size zero until some particle size L_s , the so-called switch particle size. All particles smaller or equal to L_s will be substrate depleted. L_s is a function of time because with increasing time larger particles will also become substrate depleted.

The larger particles will still contain soluble substrate and are still in the substrate saturated phase. The OUR_m of these particles can be written as N_m divided by L_c , in which the constant N_m is a constant that is not particle size dependent. The parameter N_m can be understood as the maximal oxygen flux through the surface of a waste particle. For the whole population one can write the equation:

$$eq. 6-17 OUR_a(t) = \int_{L_s}^{\infty} G(L_c, \lambda_c, \gamma_c) \cdot \frac{N_m}{L_c} \cdot \sqrt{\frac{1}{1 + e^{-\mu_{eff}(t-\Omega)}}} dL_c + \int_0^{L_s} G(L_c, \gamma_c, \lambda_c) k_n \cdot S_{i,0} \cdot e^{-k_n t} dL_c$$

L_s : Switch particle size [m]
 N_m : Maximal oxygen flux [mol O₂.m⁻².s⁻¹]

The first integral from L_s to infinity concerns the particles that are not yet substrate depleted. The second integral from 0 to L_s concerns the particles that are already substrate depleted and whose OUR is determined by the hydrolysis reaction. The OUR of this group is particle size independent.

For any specific time L_s can be determined as that particle size at which the available soluble substrate has just become zero. This means that for this specific particle size the switch time has been reached at that specific instant. By writing this condition out and solving it for the particle size, the following relationship is obtained:

$$eq. 6-18 L_s(t) = \frac{N_m \cdot \int_0^t \sqrt{\frac{1}{1 + e^{-\mu_{eff}(\tau-\Omega)}}} d\tau}{S_{s,0} + S_{i,0} \cdot (1 - e^{-k_n t})}$$

$L_s(t)$: Switch particle size at time t [m]

By substitution of the gamma distribution, eq. 6-6 in eq. 6-17 the following relationship can

be obtained:

eq. 6-19

$$OUR_a(t) = N_m \cdot \sqrt{\frac{1}{1 + e^{-\mu_{eff}(t-\Omega)}}} \cdot \frac{\lambda_c}{\gamma_c - 1} \int_{L_s}^{\infty} G(L_c, \lambda_c, \gamma_c - 1) dL_c + k_n \cdot S_{i,0} \cdot e^{-k_n t} \cdot \int_0^{L_s} G(L_c, \lambda_c, \gamma_c) dL_c$$

The scale factor λ_c can be combined with the maximum oxygen flux N_m into a single new parameter, the scaled maximum oxygen uptake rate defined as $N_m \cdot \lambda_c$ and denoted as $OUR_{m,\lambda}$. This new parameter has a comparable status as the maximum OUR_m in the single particle size case.

As the particle size is inversely proportional to the scale factor, the scaled particle size $\zeta = \lambda_c \cdot L_c$ is introduced. Substituting ζ / λ_c for L_c and changing the integration limits in eq. 6-19 gives:

eq. 6-20

$$OUR_a(t) = \sqrt{\frac{1}{1 + e^{-\mu_{eff}(t-\Omega)}}} \frac{OUR_{m,\lambda}}{\gamma_c - 1} \int_{\zeta_{s,0}}^{\infty} \zeta^{\gamma-2} \cdot e^{-\zeta} d\zeta + k_n \cdot S_{i,0} \cdot e^{-k_n t} \int_0^{\zeta_{s,0}} \zeta^{\gamma-1} \cdot e^{-\zeta} d\zeta$$

ζ : Scaled particle size [1]

$\zeta_{s,0}$: Scaled switch particle size [1]

$OUR_{m,\lambda}$: Scaled maximum OUR [$\text{mol O}_2 \cdot \text{m}^{-3} \cdot \text{s}^{-1}$]

Due to the change in integration limits of the integrals in eq. 6-20, a scaled switch particle size $\zeta_{s,0}$ is introduced that is given by:

$$eq. 6-21 \quad \zeta_{s,0}(t) = \lambda_c \cdot L_s = \frac{OUR_{m,\lambda} \int_0^t \sqrt{\frac{1}{1 + e^{-\mu_{eff}(\tau-\Omega)}}} d\tau}{S_{i,0} + S_{i,0} \cdot (1 - e^{-k_n t})}$$

It is important to note that $OUR_{m,\lambda}$ differs from the maximum oxygen uptake rate OUR_m of the average sized particle. Denoting $OUR_{m,\Lambda}$ as the maximum activity of the average size particle we can write :

eq. 6-22

$$OUR_{m,\Lambda} = \frac{OUR_{m,\lambda}}{\gamma_c}$$

In cases where γ_c has an integer value eq. 6-20 has an analytical solution that runs like:

$$\text{eq. 6-23} \quad \text{OUR}_a(t) = \sqrt{\frac{1}{1 + e^{\mu_{\text{eff}}(t-\Omega)}}} \cdot \frac{\text{OUR}_{m,\lambda}}{\gamma_c - 1} \cdot e^{-\zeta_c} \cdot \sum_{n=0}^{\gamma_c-2} \frac{\zeta_c^n}{n!} + k_n \cdot S_{i,0} \cdot e^{-k_n t} \left(I - e^{-\zeta_c} \cdot \sum_{n=0}^{\gamma_c-1} \frac{\zeta_c^n}{n!} \right)$$

6.4.3 Substrate-time relationship

A relationship can be derived for the average soluble substrate concentration $S_{s,a}$ in the same way as for the $\text{OUR}_a(t)$. For $S_{s,a}$ only the result will be given, as for the OUR_a this derivation has been presented in detail. By analogy one can find the following result:

$$\text{eq. 6-24}$$

$$S_{s,a} = \left(S_{s,0} + S_{i,0} \cdot (1 - e^{k_n t}) \right) \left(\int_{\zeta_s(0)}^{\infty} \zeta^{\gamma_c-1} e^{-\zeta} d\zeta - \frac{\zeta_s(t)}{\gamma_c - 1} \left(\int_{\zeta_s(0)}^{\infty} \zeta^{\gamma_c-2} e^{-\zeta} d\zeta \right) \right)$$

$S_{s,a}$: Average soluble substrate concentration [mole/m³]

Continuing the analogy with the OUR_a , for integer γ_c values one can write:

$$\text{eq. 6-25}$$

$$S_{s,a}(t) = \left(S_{s,0} + S_{i,0} \cdot (1 - e^{-k_n t}) \right) \left(\left(1 - e^{-\zeta_s(0)} \cdot \sum_{n=0}^{\gamma_c-1} \frac{\zeta_s^n(t)}{n!} \right) - \frac{\zeta_s(t)}{\gamma_c - 1} \cdot \left(1 - e^{-\zeta_s(0)} \cdot \sum_{n=0}^{\gamma_c-2} \frac{\zeta_s^n(t)}{n!} \right) \right)$$

As the insoluble substrate degradation is not influenced by particle size, the same equation can be used as for the single size case.

6.5 Behaviour of the distributed model

The effect of the presence of a particle size distribution on the time course of both the OUR and the soluble substrate concentration is investigated. The OUR_a is compared to the OUR (OUR_s) of a single particle (OUR_s) with the average particle size. For all calculations the standard parameter values used in chapter 3 and 4 are here as well used.

The gamma distribution is characterised by two parameters, λ_c and γ_c . The scale parameter λ_c is related to the average particle size and as such does not constitute a new parameter (compared to the single particle case). The shape factor γ_c describes the narrowness of the distribution, and represents the new aspect in the distributed model i.e. the distribution. The coefficient of variation (standard deviation divided by mean value) is a measure of the homogeneity of the size distribution. A low value indicates a narrow size distribution. The value of γ_c determines the coefficient of variation of the gamma distribution as:

$$\text{eq. 6-26} \quad \frac{\sigma}{\Lambda} = \frac{1}{\sqrt{\gamma_c}}$$

σ : Particle size distribution standard deviation[m]

This equation indicates that at a very high value of γ_c , the OUR_s time course will approach the OUR_s time course for a single particle, as a single particle can be understood as very narrow distribution. Based on the previously developed theoretical consideration it is expected that the value of the shape factor γ_c is in the range 1-3.

Figure 6.7 shows the OUR_s time course for $\gamma_c=3$ and $\gamma_c=9$. The value $\gamma_c=3$ is chosen as this is in the range of expected values, while $\gamma_c=9$ is chosen to show the intermediate behaviour between $\gamma_c=3$ and the single particle model ($\gamma_c=\infty$). The OUR time course of the single particle is calculated with both the analytical model (eq. 6-11) and the simplified version (eq 6-13) used to derive the average OUR. The OUR_s curves from the distributed model using both values of gamma differ strongly from the curves from the analytical model and the simplified analytical model. The difference between the curves of the two latter models is significantly smaller than the difference between these curves and those of the distributed model. This shows that the effect of the size distribution is bigger than the effect of the model simplification, even for a relative narrow distribution like $\gamma_c=9$. The shape of the OUR time course differs fundamentally from the single particle models, a distinct OUR peak with a gradual decrease instead of a plateau with a steep decrease.

Figure 6.8 shows the effect of the size distribution on the average soluble substrate concentration time course. The effect is less pronounced than for the OUR time course, the distributed model shows a more gradual decrease of the soluble substrate concentration. The

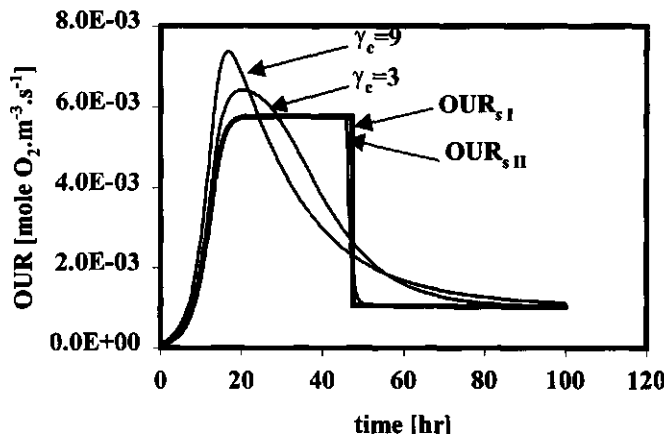


Figure 6.7: The OUR_a time course for two values of γ_c (3,9) and the OUR_s time course for a single particle with the average particle size. The OUR_s curve is calculated according the simplified analytical model (I) and the original analytical model (II). See text for additional details.

introduction of a size distribution influences the course of the OUR stronger than the average soluble substrate concentration. The effect of the size distribution is largest around the switch time for both the OUR as the average soluble substrate concentration. At the switch time the OUR is maximal and thus an effect can be easier observed than for the soluble substrate which is already low.

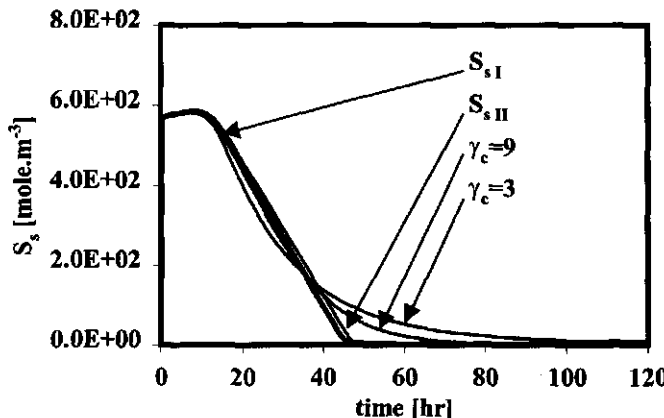


Figure 6.8: The $S_{s,a}$ time course for two values of γ_c (3,9) and the S_s time course for a single particle with the same (average) particle size. The S_s curve is calculated according the simplified analytical model (I) and the original analytical model (II). See text for additional details

In chapter 3 it was shown that initial soluble substrate concentration, initial insoluble substrate concentration, interfacial oxygen concentration and especially particle size have a strong influence on the OUR_s time course of a single particle. The effect of these factors on the OUR_a of size distributed waste will be investigated by changing the factors one by one. The soluble substrate concentration time course is not analysed further, as this does not differ so distinctly from the single particle case as the OUR_a does from the OUR_s .

For comparison both the OUR_a as the OUR_s are shown. The curves are shown for a high parameter value (the standard value times 4) in the A-figure, the low parameter value (the standard value divided by 4) in the B-figure. In both the A- and B-figure the effect of the distribution can be directly assessed by comparing OUR_s to the OUR_a . It can then be further investigated whether this effect changes as a result of the different levels of the studied factor.

Particle size (Figure 6.9)

With an increasing average particle size the maximum OUR_s value decreases, however this level is longer kept. This pattern can only be partly recognised in the OUR_a , because as a result of the distribution a distinct OUR peak has developed. While for the high average particle size value the OUR_a peak lies higher than the associated OUR_s plateau the reverse is true for the low value. The peak activity decreases with increasing particle size, however this effect is less pronounced for OUR_a than in the case of OUR_s . At a small average particle size a nearly symmetric peak arises while for a large average particle size the peak is strongly asymmetric.

Initial soluble substrate (Figure 6.10)

The effect of increasing the initial soluble substrate in case of a single particle is an extension of the substrate saturated phase. In both cases, the maximum level of the OUR_s is the same. Both for the high and low soluble substrate concentration, the presence of the distribution leads to the occurrence of distinct peak in the OUR followed by a very gradual decrease. For the high initial soluble concentration, the peak in OUR_a is higher than the maximum level of OUR_s . For the low initial soluble substrate concentration, the opposite is true, the OUR_a peak is lower than the OUR_s maximum level. The peak OUR_a has thus become dependent on the initial soluble substrate concentration, with an increasing initial soluble substrate concentration a higher peak value is expected. .

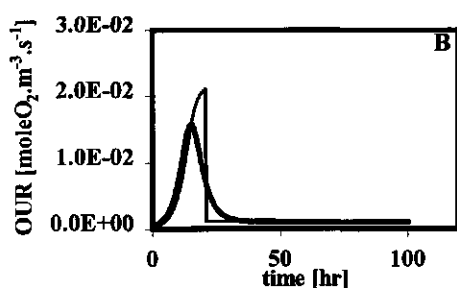
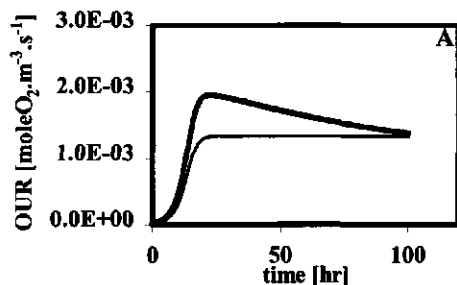


Figure 6.9: The effect of a change in the average particle size on the OUR time course. The upper curve A shows the high parameter value (standard*4), the lower curve B the low parameter value (standard/4). The thick line shows the OUR_a time course, the thin line the associated OUR_s time course.

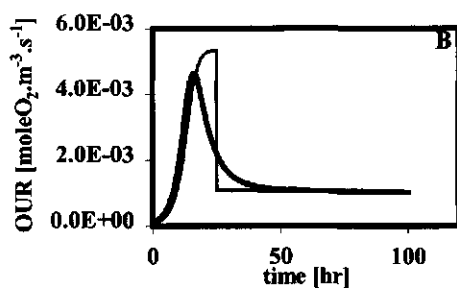
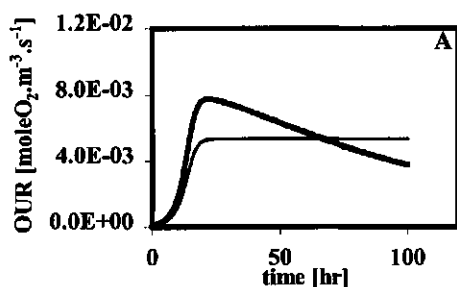


Figure 6.10: The effect of a change in the initial soluble substrate concentration on the OUR time course. The upper curve A shows the high parameter value (standard*4), the lower curve B the low parameter value (standard/4). The thick line shows the OUR_a time course, the thin line the associated OUR_s time course.

Initial insoluble substrate (Figure 6.11)

An increase in the initial insoluble substrate concentration leads to an increase of the switch time of the OUR_s when compared to the standard case. A decrease with respect to the standard case however does not lead to a decrease of the switch time. The reason lies in the fact that at the low level and the standard case the switch time is mainly determined by the initial amount of soluble substrate. Only at a very high level of insoluble substrate does the hydrolysis rate increase enough to delay the switch time. This effect is not so easily detected in the OUR_s time course. Both curves have a distinct peak with the same maximum value at the same time. An increase of the initial insoluble concentration leads to a more gradual OUR_s decrease after the peak.

Interfacial oxygen concentration (Figure 6.12)

An increase of the interfacial oxygen content leads to an increase of the maximal OUR_s value, while the switch time decreases. This effect is also seen in the OUR_n , however as in the case of the particle size the effect is diminished.

6.6 Discussion

The gamma distribution has been introduced as a description for the particle size distribution in waste. This distribution is based on a physical representation of the waste particles. This physical representation implies that the shape factor γ_c of the waste should be in the range of 1-3. Combing this distribution function with the OUR model for a single particle yields a model for the description of the OUR of a particle size distributed waste. An interesting aspect of distributed OUR model is that for γ_c approaching infinity, the distributed OUR model approaches the single particle size OUR model. The calculations show that introduction of the size distribution changes the OUR time course fundamentally. The following effects are observed.

1. Occurrence of a distinct OUR peak.

The OUR of a single particle will reach after some time a certain maximum level and remain at this level until the soluble substrate is depleted. The OUR time course of a size distributed set of particles shows no plateau but a distinct peak, that occurs around the point of time that the single particle reaches its maximum level.

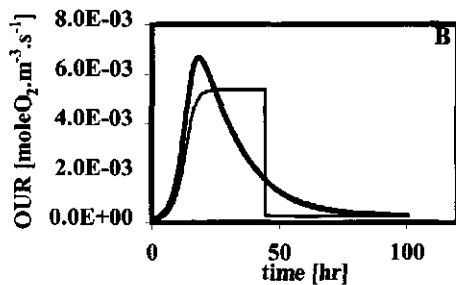
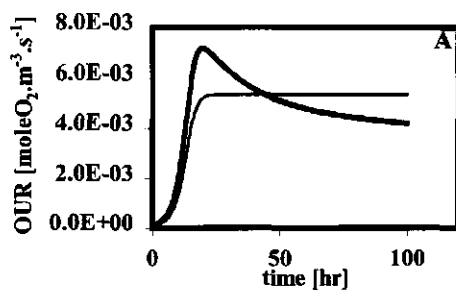


Figure 6.11: The effect of a change in the initial insoluble substrate concentration on the OUR time course. The upper curve A shows the high parameter value (standard*4), the lower curve B the low parameter value (standard/4). The thick line shows the OUR_a time course, the thin line the associated OUR_s time course.

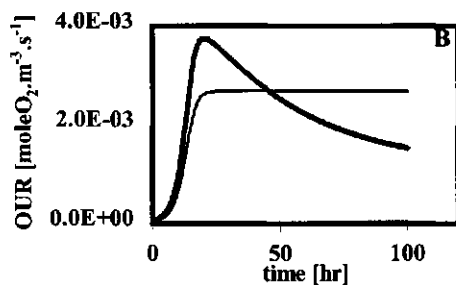
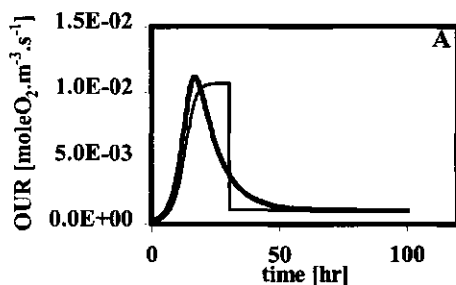


Figure 6.12: The effect of a change in the interfacial oxygen concentration on the OUR time course. The upper curve A shows the high parameter value (standard*4), the lower curve B the low parameter value (standard/4). The thick line shows the OUR_a time course, the thin line the associated OUR_s time course.

2. Introduction of a transient period

For a single particle there is a sharp transient from the maximal OUR plateau to a new lower level, which is determined by the hydrolysis rate. This sharp transient drop is caused by the diffusional soluble substrate transport from the core of the particle to the outer oxygenated zone. The time constant k_D describing this drop equals $\frac{3.D_{S_c}}{L_c^2}$. The introduction of a distribution introduces a far more slowly decreasing transient period, resulting in more gradual transient period from substrate saturation to hydrolysis limitation. In figure 6-13 this is further illustrated. Here the transient period is shown for the single particle case and the distributed model with a γ_c value of 400. This figure clearly shows that even for such a narrow distribution the transient period is more gradual in case of the distributed model.

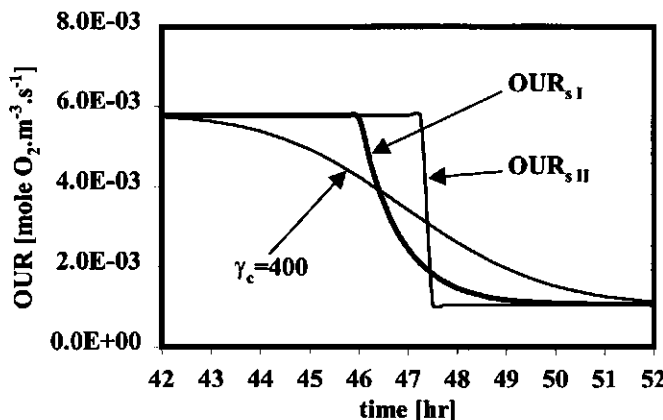


Figure 6.13: The OUR_a time course for one values of $\gamma_c = 400$ and the OUR_s time course for a single particle with the same (average) particle size. The OUR_s curve is calculated according the simplified analytical model (I) and the original analytical model (II). Only a short period around the switch time is shown because only here differences may be observed. See text for additional details

This might explain also why the diffusion coefficient as determined for 2 mm particles in the previous chapter was much lower than expected. The technique used to assure even plates may be not precise enough, to avoid the development of small uneven spots. This size distribution, how small it might be, still leads to a more gradual decrease after the switch time.

Consequently, a lower estimate of the value of k_D is obtained, that translates in a lower diffusion coefficient.

3. Introduction of maximal level OUR dependence on soluble substrate

For a single particle the maximal OUR level is not determined by the initial soluble substrate concentration. The introduction of the size distribution however introduces such dependence for the peak activity. This makes interpretation of data on maximal OUR levels more difficult, as the maximum level now depends not only on particle size and oxygen content but also initial soluble substrate concentration.

The results have shown that the OUR time course is strongly influenced by the introduction of a particle size distribution. Based on the physical underpinning of the gamma distribution model it seems plausible that for a real waste a γ_c value of 1-3 is expected. But the example of $\gamma_c = 400$ showed that even a very narrow distribution already alters the OUR time course. This means that it is anyhow necessary to introduce a size distribution to describe the OUR time of a real waste. Available measurements on the OUR time course also point in this direction. OUR measurements of different waste materials like manure, sewage sludge and biowaste all show a distinct peak and no plateau [6].

6.7 References

1. Veeken, A.H.M., *Removal of heavy metals from biowaste*, in *Environmental Technology*. 1998, Wageningen Aricultural University: Wageningen.
2. Heathcote, C.R., *Probability: elements of the mathematical theory*. 1971, London: Goerge Allen & Unwin.
3. Aris, R., *The mathematical theory of diffusion and reaction in permeable cataly*. 1975, London: Clarendon.
4. Seber, G.A.F. and C.J. Wild, *Nonlinear regression*. 1989, New York: John Wiley & Sons.
5. Shapiro, S.S. and A.J. Gross, *Statistical modelling techniques*. 1981, New York: Marcel Dekker.
6. Hamelers, H.V.M. *A Theoretical Model of Composting Kinetics*. in *Proceedings of the International Composting Research Symposium*. 1992. Columbus OH: Renaissance Publications.

A. Appendix

A.1 Derivation of the sum-of-exponentials distribution function.

The distribution function of the sum of two variables x and y is obtained [1] as:

$$\text{eq. A-1} \quad f_2(s_2) = \int_0^{s_2} f_x(u) \cdot f_y(s_2 - u) du$$

s : Sum of variables x and y [m]

$f_2(s)$: Distribution function of s. [-]

f_x, f_y : Distribution function of x and y [-1]

Taking Lx for x and Ly for y and using eq. A-1, we obtain:

$$\text{eq. A-2} \quad f_2(s) = \frac{\lambda_x \cdot \lambda_y}{\lambda_x + \lambda_y} (e^{-\lambda_y \cdot s} - e^{-\lambda_x \cdot s})$$

By combining the function $f_2(s)$ with the distribution function of the weighted variable L_c the sum of the three weighted variables can be found by as follows :

$$\text{eq. A-3} \quad f_3(L_c) = \int_0^{L_c} f_2(u) \cdot f_z(L_c - u) du$$

Evaluation of the integral in eq. A-3 yields for the distribution function of the representative particle size L_c :

eq. A-4

$$f_3(L_c) = \frac{\lambda_x \cdot \lambda_y \cdot \lambda_z}{(\lambda_y - \lambda_z) \cdot (\lambda_z - \lambda_x) \cdot (\lambda_y - \lambda_x)} (e^{-\lambda_y \cdot L_c} \cdot (\lambda_y - \lambda_z) + e^{-\lambda_z \cdot L_c} \cdot (\lambda_z - \lambda_x) + e^{-\lambda_x \cdot L_c} \cdot (\lambda_x - \lambda_y))$$

A.2 Moments of the sum of exponential distribution function.

The gamma distribution is given by:

$$\text{eq. A-5} \quad G(L_c, \lambda, \gamma) = \lambda^\gamma \cdot \frac{L_c^{\gamma-1}}{\Gamma(\gamma)} \cdot e^{-\lambda \cdot L_c}$$

The first and second moment of the gamma distribution are given by (Shapiro 1981) as :

$$\text{eq. A-6} \quad M_1(G(z, \lambda, \gamma)) = \frac{\gamma}{\lambda}$$

$$\text{eq. A-7} \quad M_2(G(z, \lambda, \gamma)) = \frac{\gamma}{\lambda} + \frac{\gamma^2}{\lambda}$$

According to a theorem given by Heathcote [1] the moments of the general particle size distribution can be found by applying the following relationship:

$$\text{eq. A-8} \quad M_n(f(x)) = (-I)^n \cdot \frac{d^n}{ds^n} L(f(x))|_{s=0} = 0$$

$M_n(f(x))$: n-th moment of function f(x)

$L(f(x))$: Laplace transform of function f(x)

By evaluating eq. A-8 for n=1 the first moment for the representative particle size can be found as:

$$\text{eq. A-9} \quad M_1(f_3) = \frac{1}{\lambda_x} + \frac{1}{\lambda_y} + \frac{1}{\lambda_z}$$

$M_1(f_3)$: first moment of $f_3(x)$

[m^{-1}]

By evaluating eq. A-8 for n=2 the second moment for the representative particle size can be found as:

eq. A-10

$$M_2(f_3) = \frac{2}{(\lambda_x \cdot \lambda_y \cdot \lambda_z)^2} (\lambda_x^2 \cdot \lambda_y^2 + \lambda_x^2 \cdot \lambda_z^2 + \lambda_y^2 \cdot \lambda_z^2 + \lambda_x^2 \cdot \lambda_y \cdot \lambda_z + \lambda_y^2 \cdot \lambda_x \cdot \lambda_z + \lambda_z^2 \cdot \lambda_x \cdot \lambda_y)$$

$M_2(f_{xy})$: second moment of $f_{xy}(x)$ [m⁻²]

Equating the moments of the gamma distribution with moments of representative particle size and defining $\alpha = \lambda_y / \lambda_x$ and $\beta = \lambda_z / \lambda_x$ one obtains:

$$\text{eq. A-11} \quad \lambda_n = \frac{\alpha \cdot \beta (\alpha + \beta + \alpha \cdot \beta)}{\alpha^2 + \beta^2 + \alpha^2 \beta^2} \cdot \lambda_x$$

λ_c : characteristic pore density [m⁻¹]

The value of γ_c equals:

$$\text{eq. A-12} \quad \gamma_c = \frac{(\alpha \cdot \beta + \alpha + \beta)^2}{\alpha^2 \cdot \beta^2 + \alpha^2 + \beta^2}$$

The mean of the gamma distribution is given by eq. A-9.

$$\text{eq. A-13} \quad \mu = \frac{1}{\lambda_x} + \frac{1}{\lambda_y} + \frac{1}{\lambda_z}$$

The variance can be derived to equal:

$$\text{eq. A-14} \quad \sigma^2 = \frac{1}{\lambda_x^2} + \frac{1}{\lambda_y^2} + \frac{1}{\lambda_z^2}$$

1. Heathcote, C.R., *Probability: elements of the mathematical theory*. 1971, London: George Allen & Unwin.

7. VALIDATION OF THE DISTRIBUTED OUR MODEL.....	228
7.1 INTRODUCTION	228
7.2 THE DISTRIBUTED OUR MODEL	229
7.3 PRACTICAL IDENTIFIABILITY	232
7.3.1 <i>Experimental time</i>	233
<i>Effect of Π_1 and Π_2</i>	236
7.4 MATERIALS AND METHODS	238
7.5 RESULTS	239
7.6 DISCUSSION.	243
7.7 REFERENCES.....	246

7. Validation of the distributed OUR model

7.1 *Introduction*

The OUR is the most important measurement available to characterize the composting process rate. A mathematical model has been developed for the OUR of a single waste particle, the so-called single particle model (see Chapter 3 and 4). For a single particle it was found that the particle size is the most important factor influencing the composting rate. This was found, both theoretically (see Chapter 3,4) and experimentally (see Chapter 5).

A real waste consists of an ensemble of particles with different particle sizes. To investigate how this particle size distribution influences the OUR time course the so-called "distributed OUR model" has been developed (see Chapter 6). This distributed model is based on the single particle OUR model and the gamma distribution model. It was found theoretically that the presence of a size distribution significantly influences the OUR. This finding implies that the OUR time course of a waste can be only adequately described if the particle size distribution is taken into account.

The shape parameter γ_c is a characteristic parameter of the distributed OUR model. The shape parameter describes the range of the gamma distribution. With an increasing γ_c value the particle size distribution becomes narrower. For a γ_c value approaching infinity the outcome of distributed model therefore coincides with the outcome of the single particle model.

The objective of this paper is to validate this distributed OUR model, i.e. to determine whether incorporation of a waste particle size distribution is necessary to understand the OUR time course. Unfortunately there are no practical means available to measure the particle size in-situ in a waste. This means that the effect of the waste particle size distribution can be only assessed from the measurement of the OUR-time course. Therefore this paper investigates whether it is possible to infer the extent of the size distribution from the OUR time course.

In chapter 5 the OUR time course of a single particle has been studied experimentally for chicken manure. By studying the OUR time course of the same material reconfigured as a solid state matrix with a range of particle sizes, the effect of the size distribution can be investigated experimentally. As the same material is used basically all differences can be attributed to the particle size distribution.

The distributed OUR model is fitted to the data and the γ_c value is established. If a low value

is found this indicates that there is an appreciable particle size distribution and that indeed a distributed model is necessary to understand the OUR of real waste.

Before the model is used to fit the data the identifiability of the distributed model is investigated. Emphasis will be given to the effect of the shape parameter γ_c on the parameter identifiability, as the single particle OUR model has already been extensively investigated.

7.2 The distributed OUR model

The distributed OUR model, as derived in the previous chapter, is based on the single particle OUR model and a particle size distribution model. The waste particle size distribution is described by the gamma distribution, which is expressed as:

$$G(L_c, \lambda_c, \gamma_c) = \lambda_c^{\gamma_c} \cdot \frac{L_c^{\gamma_c - 1}}{\Gamma(\gamma_c)} \cdot e^{-\lambda_c \cdot L_c} \quad \text{eq. 7-1}$$

L_c	: Particle size	[m]
λ_c	: Scale parameter	[m ⁻¹]
γ_c	: Shape parameter	[-]
Γ	: Gamma function	[-]

The gamma distribution is defined for $L_c \geq 0$, $\lambda_c \geq 0$ and $\gamma_c > 0$. The mean of this distribution is given by:

$$\text{eq. 7-2} \quad L_{c,a} = \frac{\gamma_c}{\lambda_c} \quad L_{c,a} : \text{Average particle size.} \quad [\text{m}]$$

The variance of the distribution is given by:

$$\text{eq. 7-3} \quad \sigma^2 = \frac{\gamma_c}{\lambda_c^2}$$

$$\sigma^2 : \text{Variance of the gamma distribution} \quad [\text{m}^2]$$

The coefficient of variation is thus given by:

$$\text{eq. 7-4} \quad \frac{\sigma}{L_{c,a}} = \frac{1}{\sqrt{\gamma}}$$

The parameter γ_c may be thus be interpreted as describing the spread of the distribution, independent of the average particle size. A large value of γ_c indicates a small particle size stretch, a small γ_c value a large stretch.

In the previous chapter a relation has been established between the gamma distribution and the particle size distribution based on the presence of uniformly distributed pores. Under these circumstances a value of γ_c in the range 1-3 is expected. Although this was a "thought experiment" it did show that it is possible to establish a link between the gamma distribution and a simple physical model of the waste. Using this distribution model and the single particle OUR model, the following OUR model for a matrix of variably sized particles was derived:

eq. 7-5

$$OUR_a(t) = \sqrt{\frac{1}{1 + e^{\mu_{eff}(t-\Omega)}}} \frac{OUR_{m,\lambda}}{\gamma_c - 1} \int_{\zeta_c(t)}^{\infty} \zeta^{\gamma-2} \cdot e^{-\zeta} d\zeta + k_n \cdot S_{i,0} \cdot e^{-k_n t} \int_0^{\zeta_c(t)} \zeta^{\gamma-1} \cdot e^{-\zeta} d\zeta$$

$OUR_a(t)$: Oxygen uptake rate at time t for a matrix with variably sized particles $[\text{mol O}_2 \cdot \text{m}^{-3} \cdot \text{h}^{-1}]$

μ_{eff} : Effective maximal biomass growth rate $[\text{h}^{-1}]$

$OUR_{m,\lambda}$: Scaled maximum OUR of the mean sized particle $[\text{mol O}_2 \cdot \text{m}^{-3} \cdot \text{h}^{-1}]$

Ω : Lag time $[\text{h}]$

ζ : Scaled particle size $[-]$

ζ_c : Scaled switch particle size $[-]$

γ_c : Characteristic shape factor $[-]$

k_n : Hydrolysis rate constant $[\text{h}^{-1}]$

$S_{i,0}$: Initial insoluble substrate expressed in oxygen equivalents $[\text{mol O}_2 \cdot \text{m}^{-3}]$

The first term on the right hand side of the equation describes the rate of those larger particles

that are in the substrate saturated phase, while the second part describes the smaller particles that have already depleted the soluble substrate. The scaled particle size is defined as:

$$\text{eq. 7-6} \quad \zeta = \lambda_c L_c$$

λ_c : Characteristic scale factor [m]

The scaled particle size that at time t has just become substrate depleted, is called the scaled switch particle size ζ_s . It is given by:

$$\text{eq. 7-7} \quad \zeta_s(t) = \frac{\text{OUR}_{m,\lambda} \int_0^t \sqrt{\frac{1}{1+e^{-\mu_{\text{eff}}(\tau-\Omega)}}} d\tau}{S_{i,0} + S_{i,0} \cdot (1 - e^{-k_n t})}$$

The background and properties of this model are extensively discussed in the previous chapter. In many cases adequate parameter values are not available in the literature. The parameter values need to be estimated from experiments. The parameters $S_{i,0}$ and k_n are only identifiable from long term experiments, i.e. $k_n \cdot t > 1$. If the OUR_a is measured over a relatively short period, $k_n \cdot t \ll 1$, than the OUR model must be altered to allow parameter estimation. This can be done by introduction of the hydrolytic activity A_h defined as:

$$\text{eq. 7-8} \quad A_h = k_n \cdot S_{i,0}$$

A_h : hydrolytic activity [mol O₂.m⁻³.hr⁻¹]

The OUR_a is then:

$$\text{eq. 7-9}$$

$$\text{OUR}_a(t) = \sqrt{\frac{1}{1+e^{-\mu_{\text{eff}}(t-\Omega)}}} \frac{\text{OUR}_{m,\lambda}}{\gamma_c - 1} \int_{\zeta_s(0)}^{\infty} \zeta^{\gamma_c-2} \cdot e^{-\zeta} d\zeta + A_h \int_0^{\zeta_s(t)} \zeta^{\gamma_c-1} \cdot e^{-\zeta} d\zeta$$

The scaled switch particle size ζ_s is then given by:

$$\text{eq. 7-10} \quad \zeta_s(t) = \frac{\text{OUR}_{m,\lambda} \int_0^t \sqrt{\frac{1}{1 + e^{-\mu_{eff}(\tau-\Omega)}}} d\tau}{S_{s,0} + A_h t}$$

Only this altered model will be used in the following, and therefore no notational difference has been made between general (eq.7-8) and altered model (eq 7-10). Modelling the hydrolysis rate as a zero order means that the altered model is only applicable during a relatively short period of the hydrolytic phase.

Figure 7.1 illustrates the OUR time course according to the single particle model and the distributed particle model for the case of $\gamma_c = 3$. The introduction of a size distribution leads to a different OUR time course, a distinct peak is present instead of a plateau and a more gradual OUR decrease after the peak appears. The parameter values used are based on the nominal values used in chapters 3 and 4. The OUR is here expressed per kg of initial volatile solids (VS), using an average mole weight of 26 g per C-mole of organic matter.

7.3 Practical identifiability

Dimensional analysis can be used to construct a model with aggregated parameters that are not dimensionally-non-identifiable (see Chapter 2). The dimensional analysis removes in this way an important source of non-identifiability. The dimensional analysis of the single particle OUR model revealed that a number of aggregated parameter could be defined that were not dimensionally-non-identifiable. The distributed model contains only a single new dimensionless parameter the scale parameter γ_c . As a dimensionless parameter is always not dimensionally-non-identifiable it follows directly that all parameters in the distributed model are not dimensionally-non-identifiable.

Practical identifiability investigates to what extent it is possible to infer a unique parameter set with reasonable accuracy from an ideal error-free data set. The identifiability measure of Reich (see Chapter 2) was employed to determine the practical identifiability. This is a local identifiability method, which is preferred over other methods as it is relatively simply to implement and it offers the possibility to gain information on experimental design. The identifiability is expressed by the value of the inverse of the determinant of a matrix, the latter constructed from the sensitivity matrix. The value of this measure indicates whether under the given conditions a parameter set is identifiable. A value of 100 or smaller indicates that the parameter set will be identifiable. A value higher than 10,000 implies that the model in

general will be non-identifiable.

The identifiability measure is a function of the model parameters, the observation period T_{exp} and the measurement frequency. As in this study an on-line measurement system with a high measurement frequency is used, the measurement frequency may safely be assumed to be unimportant. The 6 model parameters and the observation period thus determine the identifiability. As the identifiability measure is dimensionless, rendering the equation dimensionless reduces the number of independent influencing factors, so that only 5 dimensionless numbers need to be investigated. The parameters $\text{OUR}_{m,\lambda}$ and μ are used to give the following set of dimensionless groups:

$$\begin{aligned} \Pi_1 &= \frac{S_{s,0} \cdot \mu_{\text{eff}}}{\text{OUR}_{m,\lambda}} \\ \Pi_2 &= \frac{A_h}{\text{OUR}_{m,\lambda}} \\ \Pi_3 &= \Omega \cdot \mu_{\text{eff}} \\ \Pi_4 &= \gamma \\ \Pi_5 &= \mu_{\text{eff}} \cdot T_{\text{exp}} \end{aligned} \quad \text{eq. 7-11}$$

Π_i : Dimensionless group i [-]

T_{exp} : Duration of the experiment [h]

The first dimensionless group is the dimensionless period needed to deplete the initial soluble substrate with the scaled maximum oxygen uptake rate, the second is the dimensionless hydrolytic activity, the third is the dimensionless lag period, the fourth describes the spread of the particle size distribution and the fifth is the dimensionless experimental time.

7.3.1 Experimental time

The case of $\gamma_c = 2$ will be analyzed more in depth to determine the necessary experimental time. At a value of $\gamma_c = 2$, the OUR takes the longest time to achieve the stable period, and thus an experimental time that is sufficient for $\gamma_c = 2$ certainly will be sufficient for higher γ_c values. For $\gamma_c = 2$ the OUR is described by :

$$\text{eq. 7-12} \quad \text{OUR}_a(t) = \text{OUR}_{m,\lambda} \cdot \sqrt{\frac{1}{1 + e^{-\mu_{\text{eff}} \cdot (t - \Omega)}} \cdot e^{-\zeta_s(t)} + A_h \left(1 - e^{-\zeta_s(t)} \right) \left(1 + \zeta_s(t) \right)}$$

The OUR_a time course consists generally of three periods, the rapid ascension of the OUR_a , the slow descent and the stable period (Figure 7.1). These periods can be recognized in the structure of eq. 7-12. During the first period the scaled switch particle size is much smaller than 1 and the term $e^{-\zeta s(t)}$ is nearly 1, and thus the OUR will be mainly determined by the root logistic relation. Once the root logistic approaches 1, the scaled switch particle size will increase strongly (eq. 7-12) and the term $e^{-\zeta s(t)}$ determines the course of the OUR . After the peak there will be a drop in activity, as in general $\text{OUR}_{m,\lambda} > A_h$. At the same time the second term describing the hydrolytic activity increases as $e^{-\zeta s(t)}$ decreases.

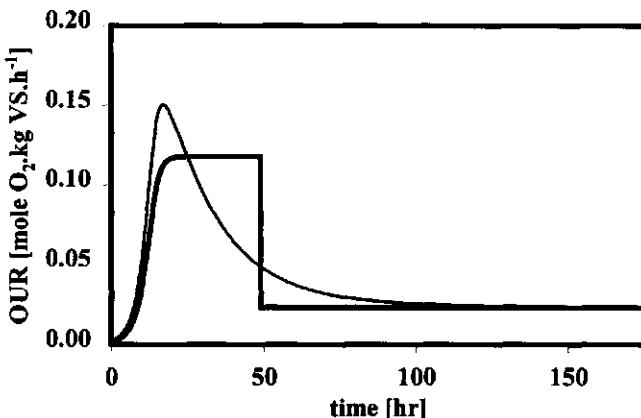


Figure 7.1 *The OUR time course according to the single particle model (thick line) and the OUR time course according to the distributed particle model with a γ value of three. The other parameter values are the same i.e. the averaged maximum oxygen uptake rate equals the maximum oxygen uptake rate in case of the single particle model.*

Without further proof it is assumed that the parameters are only then potentially identifiable if the experiment lasts long enough to reach the stable period. The minimal experimental time can thus be determined as the sum of the time needed to achieve the maximum observed OUR peak and the time needed from this point on to reach the stable period.

By setting the first derivative with respect to time of eq. 7-12 equal to zero, neglecting the hydrolytic activity in 7-10 and assuming that the root logistic function has approached 1, the time needed to reach the peak OUR is found to be:

$$\text{eq. 7-13} \quad T_p = \Omega - \frac{1}{\mu_{eff}} \cdot \ln \left(2 \left(\frac{OUR_{m,\lambda}}{S_0 \cdot \mu_{eff}} \right)^2 + 2 \cdot \frac{OUR_{m,\lambda}}{S_0 \cdot \mu} \sqrt{\left(\frac{OUR_{m,\lambda}}{S_0 \cdot \mu_{eff}} \right)^2 + 1} \right)$$

This equation expresses that the time at which the peak is reached is determined by the dimensionless substrate depletion time, the growth rate constant and the lag phase constant. As at $t=T_p$ the root logistic term has approaches 1 the OUR_a during the remaining time can be described by:

$$\text{eq. 7-14} \quad OUR_a(t) = OUR_{m,\lambda} \cdot e^{-\zeta_s(t)} + A_h \cdot (1 - e^{-\zeta_s(t)} \cdot (1 + \zeta_s(t))) \quad t > T_p$$

If now the end point of the experiment is determined by the occurrence of the event that $OUR_a(t)/A_h = \alpha$, the following relationship is found for the experimental time

$$\text{eq. 7-15} \quad T_{exp} = \Omega - \frac{1}{\mu_{eff}} \cdot \ln \left(2 \left(\frac{OUR_{m,\lambda}}{S_0 \cdot \mu_{eff}} \right)^2 + 2 \cdot \frac{OUR_{m,\lambda}}{S_0 \cdot \mu_{eff}} \sqrt{\left(\frac{OUR_{m,\lambda}}{S_0 \cdot \mu_{eff}} \right)^2 + 1} \right) + \\ - \ln \left(\frac{\alpha \cdot A_h}{OUR_{m,\lambda}} + e^{-\frac{A_h}{OUR_{m,\lambda}}} \right) \cdot \frac{S_0}{\ln \left(\frac{\alpha \cdot A_h}{OUR_{m,\lambda}} + e^{-\frac{A_h}{OUR_{m,\lambda}}} \right) \cdot A_h + OUR_{m,\lambda}}$$

In this equation the first term describes the time needed to achieve the peak, and the second the time needed to achieve α . The desired value of this factor α is determined by calculation in the following way. For the nominal case the value of the identifiability measure is calculated for different values of the total experimental time. The results of these calculations are shown in figure 7.2. With increasing experimental time the identifiability measure decreases indicating an improved identifiability. Using a threshold value of 100 as threshold of good identifiability it can be seen that this situation is reached in the nominal case at $t=160$ hr. At this point of time the value of α is 1.01. This strict value of the identifiability measure is used to assure that a value of α is chosen that is also valid for other parameter sets.

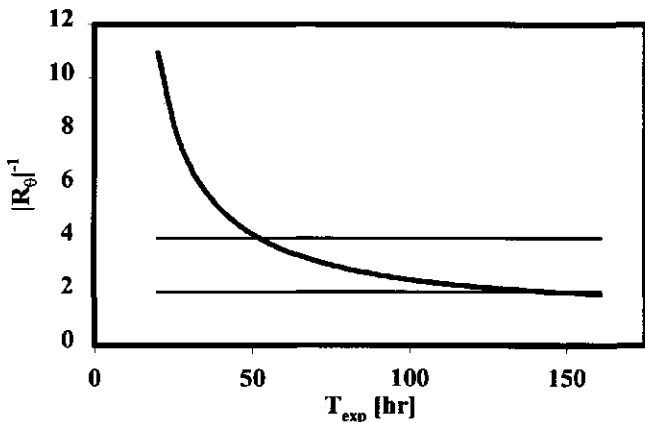


Figure 7.2: The identifiability measure $|R_\theta|^{-1}$ (thick line) as a function of the experimental time for the standard case. Note that the Y-axis is logarithmic. The straight lines indicate the levels of 10000 and 100, used as threshold values.

7.3.2 Effect of Π_1 and Π_2

The influence of the dimensionless numbers Π_1 and Π_2 on the identifiability measure is investigated for different values of gamma. For each considered parameter set, first the experimental time is determined according to eq. 7-15, using $\alpha=1.01$. Using this experimental time the identifiability measure is calculated as explained in chapter 2.

Figure 7.3 shows the contour plot for $\gamma_c = 2$, $\gamma_c = 3$ and $\gamma_c = 10$. The contour plot for $\gamma_c = 2$ shows that (threshold value of 1000) the parameters are only identifiable for higher values of the dimensionless substrate concentration $\Pi_1 > 8$, with increasing hydrolytic activity a higher soluble substrate concentration is needed.

The plot for $\gamma_c = 3$ shows that the parameters are identifiable for values of the dimensionless substrate concentration $\Pi_1 > 6.5$. With a high hydrolytic activity a somewhat higher soluble substrate concentration is needed. For $\gamma_c = 10$, nearly all combinations are identifiable. Together these plots show that with increasing gamma the identifiability increases.

The dimensionless lag period Π_3 appears to have no big effect of the identifiability, changes up to a factor 10 do not influence the identifiability appreciably (Figure not shown). The absence of an effect on identifiability is probably due to the fact that a change in lag time is accounted for in the experimental time.

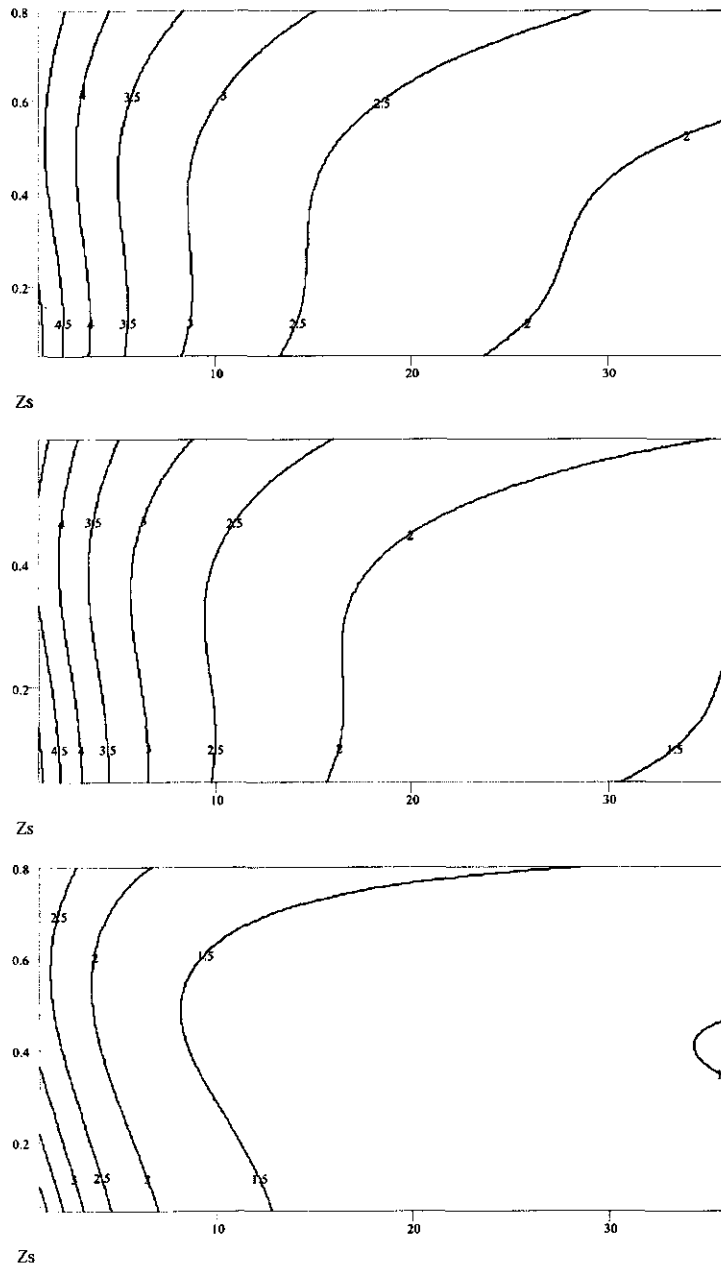


Figure 7.3: Contour plot of the identifiability measure $|R_\theta|^{-1}$ in the Π_1 (X-axis) versus Π_2 (Y-axis) plane. The upper curve shows the results for $\gamma=2$, the middle for $\gamma=3$ the lower for $\gamma=10$. All other parameters have their standard values. Label values report the $^{10}\log$ of $|R_\theta|^{-1}$

7.4 Materials and methods

Materials

All experiments were performed with chicken manure, which was supplied by an experimental facility of the WAU. The manure was collected from a belt that was emptied every two days. The manure was sampled when the belt was emptied. To enhance porosity the chicken manure was mixed with foam chips, which are commonly used as packaging material. The foam chips (approx. $0.8 \times 1.8 \times 2.6$ cm) are biologically non-degradable and have a water impermeable surface. The specific surface area was estimated as 15.8 m^2 per gram of foam chips.

Methods

The OUR time course of the manure -foam mixtures was measured with the OUR measuring device described in chapter 4. During the experiment a temperature of 55°C and an oxygen content on dry gas basis of 19% by volume was maintained. Analyses of dry matter and organic matter were performed according to standard methods [1].

Experimental set-up

The manure was transported to the lab and directly used for experiments i.e. no storage period was applied. The chicken manure was mixed with foam chips, either 1% or 3% chips on a fresh manure weight basis. After mixing the manure was mainly attached to the foam chips, it was therefore assumed that the average particle size is inversely proportional to the total chips surface in the mixture. Using the average dry matter (23%) and OM content (87%) and an average density of 1070 kg.m^{-3} , the average particle size $L_{c,a}$ was estimated as 2 mm for the 3% amendment and 6 mm for the 1% amendment. Each experiment was performed with a different batch of manure. Four experiments were conducted with 1% chips, labeled A,B,C,D the four experiments with 3% chips are labeled E,F,G,H.

Estimation procedure

Eq. 7-9 and eq. 7-10 were used to estimate the parameters μ_{eff} , Ω , $\text{OUR}_{m,\lambda}$, γ_c , A_h and $S_{s,0}$ using a conventional residual sum of squares (RSS) minimization with the simplex routine as coded by Press [2]. The identifiability analysis showed that depending on the value of γ_c the possibility exists that the parameter set is not well identifiable. This can give problems when estimating the parameter set from the measured data. The parameter set is therefore estimated with a fixed γ_c value. The parameter set that minimises the RSS is calculated for all integer values of γ_c ranging from 2 to 20. The parameter set that yields the lowest RSS in this range is reported. Also the range of γ_c values that have a RSS smaller than 1.12, the minimal RSS will

be presented. This value coincides with the 95% confidence interval assuming the ratio of variances to be described by the F-distribution and a number of 50 independent measurement points. In all experiments at least 250 measurements were present. However a lower number of observations was chosen as the measurements are correlated due to oscillations induced by the control algorithm.

7.5 Results

The measured OUR time course for an experiment with 1% chips is shown in figure 7.4 while for 3% chips in figure 7.5. Both the measurements and fitted curve are shown. Both curves show the same general behavior, an increase of activity to a maximum followed by a gentle slope. The curve is nearly symmetrical around the peak. In both cases the gentle slope downwards is followed by a relatively stable level as is expected.

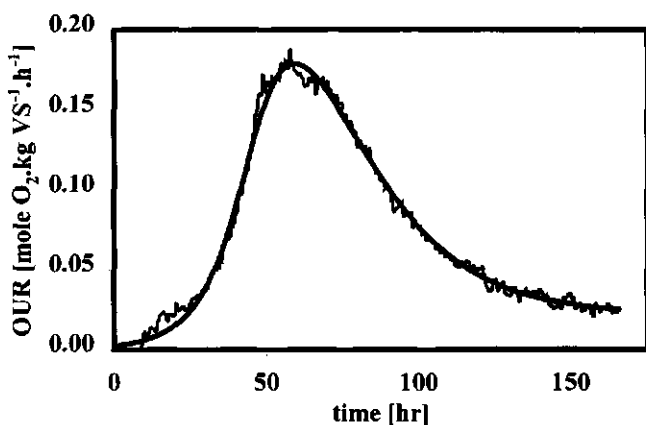


Figure 7.4: Measured (thin line) and fitted (thick line) OUR time curve of experiment A (see table 7-1)

The results of the parameter estimation are all presented in table 7-1. The first column denotes the experimental number. For each individual experiment the following results are given: the minimum value of the residual sum of squares (MRSS), the maximum OUR of the average sized particle ($OUR_{m,A}$), the maximal oxygen flux (N_m), the effective growth rate (μ_{eff}), the lag time (Ω), the initial soluble substrate concentration ($S_{s,0}$), the hydrolytic activity (A_h), the optimal γ_c value, the lower value of γ_c -range and the upper value of the γ_c -range. The maximum OUR of the average sized particle $OUR_{m,A}$ is derived from the equation

$$\frac{OUR_{m,A}}{\gamma_c} \quad (\text{see chapter 6, eq. 6-21}). \quad \text{The value of } N_m \text{ is the maximal oxygen flux per m}^2 \text{ of}$$

Table 7-1: Estimated parameter values.

Experiment	γ_c	MRSS	OJR _{m,A}	N _m	μ_{eff}	Ω	S _{s,0}	A _h	lower	upper
-	-	(mol O ₂ kg VS ⁻¹ .hr ⁻¹) ²	mol O ₂ kg VS ⁻¹ .hr ⁻¹	mol O ₂ m ⁻² .s ⁻¹	s ⁻¹	hr	mol O ₂ kg VS ⁻¹	.hr ⁻¹	-	-
A	2	5.40E-05	1.53E-01	4.15E-05	4.72E-05	59	12.4	NA	2	4
B	6	2.30E-05	1.66E-01	4.50E-05	5.28E-05	47	8.3	0.022	3	8
C	9	3.60E-05	1.18E-01	3.20E-05	3.06E-05	83	5.9	0.025	3	13
D	3	1.70E-05	1.09E-01	2.96E-05	2.78E-05	71	12.3	NA	2	6
mean	5	3.25E-05	1.37E-01	3.7007E-05	3.96E-05	65	9.7	0.024		
std	3	1.64E-05	2.73E-02	7.4098E-06	1.23E-05	15.49193	3.2	0.002		
cv	0.55	0.50	0.20	0.20	0.31	0.24	0.32	0.09		
E	8	3.23E-04	4.74E-01	1.29E-04	3.06E-05	61	7.1	0.087	2	15
F	4	1.00E-04	3.30E-01	8.95E-05	4.72E-05	48	10.1	0.007	2	8
G	3	2.30E-05	2.40E-01	6.51E-05	3.89E-05	70	7.8	0.026	2	6
H	2	7.30E-05	1.86E-01	5.04E-05	8.06E-05	39	11.6	0.028	2	4
Mean	4	1.30E-04	3.08E-01	8.3367E-05	4.93E-05	54.5	9.2	0.037	3	4
Std	2	1.33E-04	1.26E-01	3.4131E-05	2.19E-05	13.72346	2.1	0.035		
Cv	0.54	1.02	0.41	0.41	0.44	0.25	0.23	0.94		

particle surface. It's determined as the product $OUR_{m,\lambda} \cdot L_{c,a}$ in which $L_{c,a}$ is the average particle size. The latter parameter is determined as described in the materials and methods section. For each group of four experiment the mean value, the standard deviation and the coefficient of correlation of each parameter is also given

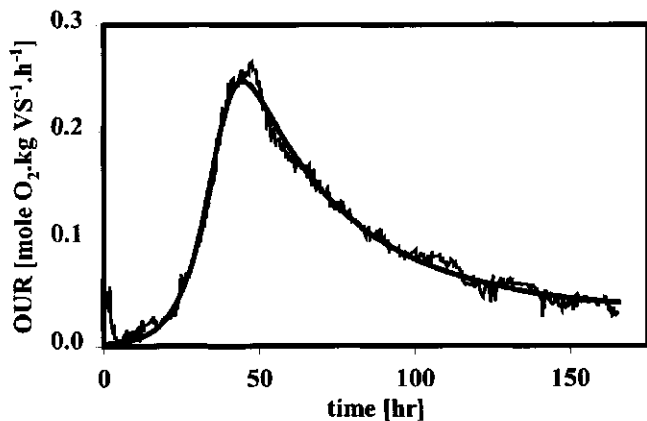


Figure 7.5: Measured (thin line) and fitted (thick line) OUR time curve of experiment E (see table 7-1)

Based on the theory as developed in chapter 5 (table 5.1) it is expected that the parameters μ_{eff} , Ω , γ_c , A_h and $S_{s,0}$ are independent of the particle size. The parameter $OUR_{m,\lambda}$ is inversely proportional to the particle size, implying that N_m is independent of particle size.

To test whether the parameters N_m , μ_{eff} , Ω , γ_c , A_h and $S_{s,0}$ are indeed independent of the particle size, the mean values of the estimated parameters will be compared by reporting the P-value using a two sided Students t-test for independent samples with unequal variance [3].

The experiments with 1% chips (A,B,C,D) clearly have a lower MRSS than the 3% group (E,F,G,H). The MRSS is significantly affected by oscillations in the measurements due to an inadequacy of the control algorithm. This phenomenon was more pronounced in the 3% group as the OUR was higher and thus the disturbances were bigger.

The 1% groups has as expected a lower $OUR_{m,\lambda}$ than the 3% group. The ratio between the average values is 2.25. Assuming the manure to be smeared out over the surface of the chips, an $OUR_{m,\lambda}$ ratio of 3 would be expected, as three times the surface area is available. The observed ratio is lower than the expected factor 3, however the values have a large spread and a factor of 3 can not be ruled out. In any case, the factor of three might be an overestimate of the theoretical factor, as part of the manure is not attached to the chips but is dispersed as

small particles between the chips. It is interesting to note that the ratio for the observed peak values of the OUR curves is only 1.7. This shows that the presence of distribution tends to diminish the effect of particle size.

The values of N_m differ, however this difference is not significant ($P=0.23$). The growth rate constant μ_{eff} is somewhat higher for the 3% group than for the 1% group. Again this difference is not significant ($P=0.46$). The lag time (Ω) also shows a difference but this is not very big and is again not significant ($P=0.36$). For the initial soluble substrate $S_{s,0}$ again no difference could be detected between both groups ($P=0.76$), the same applied to the hydrolytic activity (A_h , $P=0.54$). That all these parameters do no differ significantly is in accordance with the theory.

For some experiments, the difference between lower and upper limit of the γ_c -range shows is appreciable. For each experiment the relative dimensionless substrate concentration Π_1 was calculated from the estimated parameters. In figure 7.6 the estimated gamma range i.e. upper minus lower value is plotted against the calculated Π_1 . This figure shows that with decreasing Π_1 an increasing gamma span is found. This is in accordance with the findings of the identifiability analysis, that with decreasing Π_1 the identifiability becomes poorer.

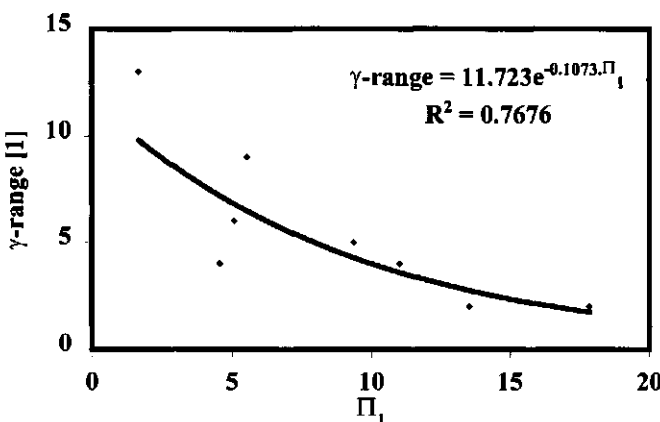


Figure 7.6: Relationship between the estimated γ -range and the value of the dimensionless depletion time Π_1 .

All experiments have the γ_c -range 3-4 in common. For $\gamma_c = 3.5$ calculation shows that Π_1 should be at least 8, to assure sufficient identifiability. Accepting this γ_c value, figure 7.6 shows that four out of eight experiments have a too low Π_1 .

7.6 Discussion.

Chicken manure was mixed with an inert foam amendment and the OUR time curve of this mixture was measured. The OUR time course of this material has previously been established for single-sized particles in chapter 5. As the amendment is inert, it can be safely assumed that the differences in OUR time course between the foam-manure mixture and the single size particles can solely be attributed to the particle size distribution.

Of the estimated parameters only the $\text{OUR}_{m,A}$ shows a strong dependency on the particle size. From the definition of the $\text{OUR}_{m,A}$ this is clearly in accordance with the model. The other parameters show no obvious dependency on the particle size, as expected on theoretical considerations. In case of a single particle a dependency of the growth rate constant on the particle size was found. In the distributed case no clear dependence is found, but this can be explained as a result of the distribution of the particles. Big particles that have a weak particle size growth rate dependence are present in both groups, and thus diminish the effect. The lack of effect of particle size on the initial soluble substrate concentration and the hydrolytic activity is according to expectation.

Overall a γ_c -value of 3-4 is found to be adequately describing the particle size distribution. The fact that such a wide distribution is found shows that incorporation of a particles size distribution in the model is indeed necessary, otherwise a much higher γ_c would have been found.

Table 7-2 compares the average of the estimated parameters found in this study with the parameters determined in chapter 5 using the single particle size model. There is an acceptable agreement between the two experiments. The N_m value is somewhat higher in the current study, however this could partly be attributed to the fact that the estimate of $L_{c,a}$ is relatively coarse. The value of $L_{c,a}$ is determined using the assumption of smearing of all material, while part is present as distinct particles.

The growth rate constant is found to be lower than in the previous study, this is in accordance with the higher lag time Ω found. A possible reason for this lower growth rate and higher lag time might be the higher initial soluble substrate concentration. The hydrolytic activity is comparable considering the large variance in both studies.

In 4 of the 8 experiments the identifiability was poor, resulting in a problematic large spread of the γ_c value. Although this is troublesome it also points to a realistic physical phenomenon. The effect of a distribution is that compared to single particle the different processes no longer occur in phase. For instance after the OUR peak value has been reached some of the

particles are in the substrate saturated phase, while others are already in the substrate depleted phase. The particle size distribution thus mixes up the information of the different phases, making it more difficult to separate between the information from the substrate saturated phase and the substrate limited phase. In this respect, the single particle size model has probably the best identifiability because the switch time in this model indicates very clearly the transition from the substrate saturated phase to the substrate limited phase. With a distribution present such a clear-cut distinction is not possible. This explains why with increasing γ_c values the parameters have a better identifiability.

Table 7-2 : Comparison of parameters estimated using the single particle size model (chapter 5) and the distributed model (this chapter).

		Mean-d ¹⁾	Min-s ²⁾	Max-s ³⁾
N_m	mol O ₂ .m ⁻² .s ⁻¹	3.2E-05	2.2E-05	
μ_{eff}	s ⁻¹	4.4E-05	4.4E-04	7.7E-05
Ω	hr	60	46	9
$S_{s,0}$	mol O ₂ . kg VS ⁻¹	9.4	6.2	
A_h	mol O ₂ . kg VS ⁻¹ .hr ⁻¹	0.033	0.041	

- 1) Mean-d: mean value of the estimated parameters using the distributed model
(this chapter)
- 2) Min-s: minimum value of the estimated parameters using the single particle model
(chapter 5)
- 3) Max-s: maximum value of the estimated parameters using the single particle model
(chapter 5)

Superficially looking the identifiability issue may be considered a disadvantage of the distributed model, it must be emphasised that it is a property of the system that the distribution causes an attenuation of the signal. The identifiability analysis showed that reconstruction of the underlying process is only possible under certain conditions i.e. a sufficient high value of Π_1 and Π_2 . These prerequisites are not met in all cases, resulting in larger parameter estimation variance. As this is a property of the system it seems unlikely that there will exist a reparameterized model with better identifiability properties.

The distributed particle size model is thus well able to describe the measurements, and yield parameter values with a physical interpretation. The dimensionless groups give clear conditions for identifiability. If these conditions are not met in practical situations, this is indicating a physical situation in which the distribution attenuation is stronger than the signal. A possible solution might be addition of soluble substrate to the waste, as in this way the low value of Π_1 can be increased to a sufficient level.

For the chicken manure $\gamma_c=3$ described all cases well. It would be interesting to investigate whether this is true also for other types of waste, as this value is close to the value derived from the theoretical model presented in the previous chapter. In this respect it would be interesting to use the factor three as a default value in those cases where there is a poor identifiability. Using the parameter estimation procedure outlined here it is always possible to see whether this value is compatible with the data.

7.7 References

1. APHA, *Standard Methods for the Examination of Water and Wastewater. 18th ed., part 2540D.* 1992, Washington DC.: American Public Health Association.
2. Press, W.H., et al., *Numerical Recipes.* 1986, Cambridge: Cambridge University Press.
3. Steel, R.G.D. and J.H. Torrie, *Principles and procedures of statistics: with special reference to the biological sciences.* 1980, New York: McGraw-Hill.

8 SIGNIFICANCE OF THE NEW DISTRIBUTED OUR MODEL FOR COMPOSTING REACTOR DESIGN	248
8.1 INTRODUCTION	248
8.2 OUR BASED DESIGN	249
8.2.1 <i>Novel composting system</i>	249
8.2.2 <i>Design quantities</i>	251
8.2.3 <i>Aeration requirement</i>	252
8.2.4 <i>Product quality</i>	254
8.2.5 <i>Product quantity</i>	256
8.3 OUR MODELS.....	256
8.3.1 <i>The first-order model</i>	256
8.3.2 <i>The distributed model</i>	258
8.4 MATERIALS AND METHODS.....	259
8.4.1 <i>Experimental</i>	259
8.4.2 <i>Parameter estimation</i>	260
8.4.3 <i>Predictions</i>	260
8.5 RESULTS	261
8.5.1 <i>Parameter estimation</i>	261
<i>Time prediction</i>	262
8.5.3 <i>Oxygen prediction</i>	264
8.5.4 <i>Oxygen effect</i>	268
8.6 DISCUSSION	270
8.7 REFERENCES.....	275

8 Significance of the new distributed OUR model for composting reactor design

8.1 Introduction

Current design approaches for composting reactors are based on a first order description of the solid matter degradation rate. Keener [1] uses the degradable solid matter as the prime state variable while Haug [2] uses the biodegradable organic matter as the prime state variable. The effect of environmental factors (e.g. temperature, oxygen content) is modeled by a multiplicative effect of the individual factors on the first-order rate constant. The first order model is an empirical model, e.g. it describes the data without physical interpretation of the parameters involved.

In this thesis the so-called distributed OUR model has been developed that describes the time course of the oxygen uptake rate (OUR) under constant environmental conditions. This distributed model is based on a mechanistic conceptual model (see Chapter 6) and has been successfully validated (see Chapter 7). A major advantage of the distributed model over an empirical model is that more insight in the process is obtained.

There is one important question that remains to be discussed: “does it matter for reactor design which type of model (first order or distributed) is used?”. To address this question, the distributed OUR model (see Chapter 7) and the first-order model (see Chapter 1) will be compared using the example of a novel composting system. This novel composting system aims at composting pig faeces with a reduced off-gas flow and ammonia emission. The composting system as described here forms an integral part of a sustainable pig production system, the so-called Hercules system [3]. This pig production system is being developed to cope with current difficulties facing traditional systems.

A characteristic of this novel composting system is that it operates at lower gas phase oxygen levels, typically ≤ 10 vol.%. Current temperature controlled composting systems run at high oxygen levels, typically 15-20 vol.%. As the operational conditions of this composting system differ strongly from conventional systems it is necessary to test it with a pilot scale facility. Kinetic data on the effect of low oxygen levels are scarce and are difficult to obtain experimentally. This is a challenge for prototype design, as one can not rely on previous data only and it is necessary to use a model to predict the OUR development at low oxygen levels. Similar challenges would arise with other new system designs or whenever data are not available for feedstocks or control situations.

It is useful to distinguish between interpolating and extrapolating predictions. An extrapolating prediction aims at predicting the system behavior outside the measurement range. For prototype design, this is the most common situation as data on the systems performance are still scarce. The model comparison will therefore focus on their ability to make sensible extrapolating predictions.

Two types of extrapolating predictions will be distinguished, time extrapolation and oxygen extrapolation. Time extrapolation means that a prediction is made outside the time domain of the measurements while an oxygen extrapolation is a prediction outside the measured oxygen level domain.

The objective of this chapter is thus to compare the first-order model and the distributed model with respect to their capability of making predictions with respect to time and oxygen for the purpose of design.

This chapter is structured as follows. First the novel composting system is introduced, together with the equations for the main design quantities. The two OUR models that will be compared, the distributed model (see Chapter 7) and the first-order model (see Chapter 1), are briefly introduced. The materials and methods section describes the experiments, parameter estimation and design quantity prediction for both models. The result section presents and compares the prediction by both models. The results will be discussed and the findings will be generalized with respect to composting system design.

8.2 *OUR based design*

8.2.1 Novel composting system

Large quantities of diluted pig manure are produced in traditional pig production systems, leading to high treatment and transport costs. Valorisation and application of pig manure is only possible if specific products are produced in an economical way without negative environmental impacts. One new approach to addressing this challenge is the separate collection of faeces and urine by a convex conveyer belt [3]. The separation creates options for separate treatment of the liquid and solid fraction into a nitrogen rich liquid fertiliser (containing 60-70% of total N) and a stabilised organic fertiliser (containing 95-98% of the total P), respectively. In this way pig manure can become a highly valuable resource through the recycling of nutrients and organic matter to soil systems, thus reducing the use of artificial fertilisers and peat.

Faeces can be converted into a stabilised organic fertiliser through composting. Composting will result in breakdown and stabilisation of organic matter, mass reduction, and removal of pathogens and weeds. However, composting of N-rich and poorly structured substrates such as pig faeces results in high ammonia emission and production of odours. Porosity and compatibility of less structured substrates can be improved through mixing with a bulking agent such as straw or wood chips. While some addition of bulking agent is necessary in this system to achieve aerobic conditions, adding enough amendment to reduce odour and ammonia emissions to acceptable levels would greatly increase the size and costs of the system. Ammonia and odour emissions can be reduced by the application of absorbing materials such as zeolite or peat [3] or treating waste-gases with biofilters [4, 5]. However these approaches are too expensive to give an economically feasible composting process for this agricultural application.

A composting system is proposed, composed of a conventional tunnel reactor and a gas cooler, to reduce total waste-gas flow and ammonia emissions during composting (see Figure 8.1). The tunnel recirculation air passes a cooler that removes the heat from the system. The cooled air can be reused, and there is no longer the need to supply fresh outside air for cooling purposes. The system thus uncouples the cooling function and the oxygen supply of the air. Fresh air is only needed to supply sufficient oxygen for aerobic degradation, resulting in a considerable off-gas flow reduction.

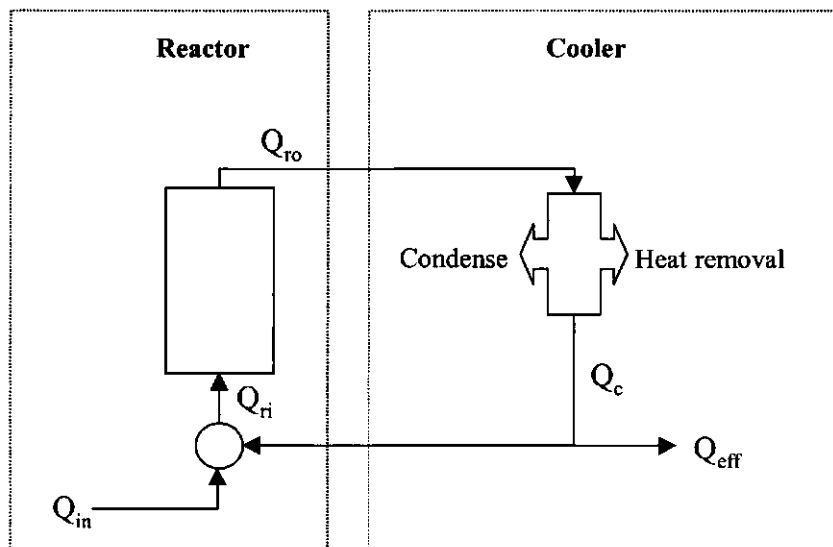


Figure 8.1: Representation of the integral system model for reactor-cooler system.

The proposed system could help in managing ammonia emissions in three ways:

1. The effluent air flow is reduced, decreasing the cost of odour treatment
2. Part of the emitted ammonia may be removed in the cooler with the condensate, lowering the total ammonia emission.
3. As the effluent gas flow is independent of the composting temperature, it is possible to run the composting process at mesophilic temperatures without the excessive effluent gas flows needed in conventional systems. The importance of the latter point is that nitrification might be introduced. Autotrophic nitrification is generally considered a mesophilic process that does not occur at thermophilic temperatures. Of course a thermophilic phase remains necessary to assure pathogen destruction.

8.2.2 Design quantities

A full (prototype) composting plant design has to take many aspects (process, material handling and storage, environmental, safety, marketing etc.) into account. A good reactor design is essential for a proper operation of the composting plant as a whole (see chapter 1). Therefore this chapter will focus on three essential elements of the reactor design.

1. Aeration requirement.

Aeration is necessary to supply oxygen and remove heat. As composting is generally operated as a batch process, both the maximum aeration requirement and the average aeration requirement are needed. The maximum value is important as it determines the capacity of the ventilator(s) needed to be installed in the process. Too small a ventilator will result in an inadequate temperature and/or oxygen control, a too big ventilator gives a low energy efficiency and unneeded costs. Inadequate process control gives a less stabilised product and increases the odour emission strongly.

A composting plant often consists of a large number of separately controlled composting reactors. The total plant off-gas can be calculated as the average flow of a single reactor multiplied by the number of reactors. The average aeration requirement is needed to size the off-gas treatment, a too low estimate gives an undersized gas treatment resulting in unacceptable emission. A too high prediction yields an oversized gas treatment and thus unnecessary investments.

2. Compost quality

Given sufficient aeration, the sizing of the reactor should be such that a specific product quality is achieved. To achieve this specific product a certain Solids Retention Time (SRT)

in the reactor is needed. A too small SRT leads to an unstable product, a too large SRT to an unnecessary investment of reactor volume. To obtain a properly sized reactor all predictions of compost quality must be made in relationship with the SRT.

3. Compost quantity

During composting a mass reduction takes place due to evaporation of water and oxidation of organic matter. A prediction of this mass reduction is needed to estimate the amount of composts that needs to be handled and marketed. For some application mass reduction is the main objective of the process and insight in the relationship SRT and compost quantity is then need for reactor design.

8.2.3 Aeration requirement

Figure 8.1 shows a schematic representation of the reactor-cooler system where the main mass and energy flows are indicated. A gaseous flow is characterised by its flow rate Q (mole/s), the temperature T ($^{\circ}\text{C}$) and its composition, i.e. nitrogen fraction (N_2), oxygen fraction (O_2), carbon dioxide fraction (CO_2) and water vapour fraction (H_2O). All gaseous flows are expressed on a molar dry gas basis (leading to more clear and simple formula's). A molar dry gas flow can be transformed to the total volumetric flow by:

$$\text{eq. 8-1} \quad Q_v = Q(1 + Z_w) \frac{P}{R.T}$$

Q_v	: Volumetric gas flow	$[\text{m}^3 \cdot \text{h}^{-1}]$
Q	: Dry gas flow	$[\text{mole} \cdot \text{h}^{-1}]$
Z_w	: Water vapour to dry gas ratio at saturation	$[\text{mole} \cdot \text{mole}^{-1}]$
P	: Total gas pressure	[Pa]
R	: Gas constant	$[\text{J} \cdot \text{mole}^{-1} \cdot \text{K}^{-1}]$
T	: Gas temperature	[K]

The concentration of all gases, except water, are expressed as fraction of the dry gas. These fractions are denoted by their chemical formula, and its subscript indicating the location (e.g. $\text{O}_{2,\text{in}}$ is the oxygen fraction of the influent gas).

The reactor temperature and effluent oxygen level are assumed to be controlled perfectly, i.e. the actual temperature and oxygen content of the reactor exhaust gas are always at the

set value. This yields a significant simplification of the model, although it means that the initial heating phase and the finishing cooling down phase can not be modelled. However, for our present objective this is no significant problem as the main part of the process takes place under controlled conditions. The model aims at developing the steady-state relationships between current OUR, the oxygen set-point and the reactor temperature set point on the one hand, and the influent flow, effluent flow and cooler flow on the other hand.

In solving the mass and energy balances the following additional assumptions are used:

- the composition of the substrate is such that on a molar basis, 1 mole of oxygen is replaced by 1 mole of carbon dioxide produced.
- the amount of carbon dioxide removed by the cooling liquid can be neglected with respect to the total carbon dioxide balance.
- the amount of ammonia present in the gas phase within the reactor can be neglected with respect to the overall gas balance.
- there is no gas hold-up in the system.
- all gas streams except the incoming stream are saturated with respect to water vapour; the incoming stream is assumed to be completely dry.
- heat production is proportional to the oxygen consumption with a proportionality constant (H_{ox}) equal to 473 kJ/mole oxygen.
- the enthalpy of a gas stream (E) is approximated by the molar specific heat capacity of the gas C_p (assumed equal for all gases and water vapour) and the latent heat from water evaporation (H_{vap}): $E = (1 + Z_w) \cdot (T - T_{in}) \cdot C_p + Z_w \cdot H_{vap}$, in which dry influent air is chosen as the reference state.

The following relationships can be derived on basis of the mass and heat balances and preceding assumptions. The influent and effluent gas flows are equal and related to the OUR by:

$$\text{eq. 8-2} \quad Q_{in}(t) = Q_{eff}(t) = \frac{\text{OUR}(t)}{O_{2,in} - O_{2,eff}}$$

OUR : Oxygen Uptake Rate [mol O₂.kg VS⁻¹.h⁻¹]

$O_{2,in}$: Influent gas oxygen fraction [mol O₂.mol dry gas⁻¹]

$O_{2,eff}$: Effluent gas oxygen fraction	[mol O ₂ .mol dry gas ⁻¹]
Q_m	: Influent gas flow	[mol dry gas.kg VS ⁻¹ .h ⁻¹]
Q_{eff}	: Effluent gas flow	[mol dry gas.kg VS ⁻¹ .h ⁻¹]

As the OUR is expressed per kilogram of initial organic matter expressed as kg volatile solids (VS), all related variables are expressed per kilogram of initial organic matter. From the enthalpy values, the flow needed to cool equals:

$$eq. 8-3 \quad Q_c(t) = \frac{H_{ox} - \frac{E_{eff}}{O_{2,in} - O_{2,eff}}}{E_{ro} - E_c} . OUR(t)$$

Q_c	: Cooler effluent gas flow	[mol.kg VS ⁻¹ .h ⁻¹]
E_{ff}	: Effluent gas enthalpy	[J.mol ⁻¹]
E_{ro}	: Reactor effluent gas enthalpy	[J.mol ⁻¹]
E_c	: Cooler effluent gas enthalpy	[J.mol ⁻¹]

It must be noted that the condition $Q_c \geq Q_{eff}$ must apply, as this latter flow is part of the cooling flow. The reactor flow equals the cooler flow, as the same amount of dry gas enters and leaves the system.

As all flow rates are proportional to the OUR value, all average flows will be proportional the cumulative oxygen uptake.

8.2.4 Product quality

The amount of organic matter is reduced as a result of oxidation. The disappearance rate of organic matter is assumed to be linearly related to OUR. Using the constant M_{om} , defined as the amount of organic matter degraded per amount of oxygen consumed the change in the organic matter amount can be described as.

$$eq. 8-4 \quad \frac{dm}{dt} = -\frac{1}{M_{om}} . OUR(t)$$

m	: Amount of organic matter per kg of initial organic matter	[kg VS.kg VS ⁻¹]
M_{om}	: Organic matter degradation per unit of oxygen consumed	[kg VS.mol O ₂ ⁻¹]

Note that the organic matter amount is expressed per unit amount of initial organic matter. From this equation the organic matter content of the material can be calculated as:

$$\text{eq. 8-5} \quad OM(t) = OM_0 \cdot \frac{1 - COU(t) \cdot M_{om}}{1 - OM_0 \cdot COU(t) \cdot M_{om}}$$

OM : Organic matter fraction on dry matter basis [kg VS.kg⁻¹]

OM₀ : Initial organic matter content on dry matter basis [kg VS.kg⁻¹]

COU : Cumulative oxygen uptake [mol O₂.kg VS⁻¹]

Note that the organic matter fraction is expressed as fraction of the total dry matter. Keener proposed the degradation extent as a measure of compost stability. The degradation extent can be calculated as:

$$\text{eq. 8-6} \quad DE(t) = \frac{COU(t)}{COU_m}$$

DE : Degradation extent [-]

COU_m : Maximum cumulative oxygen uptake i.e at $t \rightarrow \infty$ [mol O₂.kg VS⁻¹]

The COU_m is the amount of oxygen needed for complete bio-oxidation of the waste. Based on the water balance and the relationships for the cooler gas flow and exit gas flow, the dry matter content of the material can at any time be calculated as:

$$\text{eq. 8-7} \quad DM(t) = DM_0 \cdot \frac{1 - OM_0 \cdot COU(t) \cdot M_{om}}{1 + OM_0 \cdot DM_0 \cdot COU(t) (B - \Delta - M_{om})}$$

DM : Dry matter content [kg.kg⁻¹]

B : Amount of water produced per mole O₂ consumed [kg.mol O₂⁻¹]

DM₀ : Initial dry matter content [kg.kg⁻¹]

in which:

$$\text{eq. 8-8} \quad \Delta = \left(\left(1 - \frac{H_{ox} - \frac{E_{eff}}{O_{2,in} - O_{2,eff}}}{E_{r,0} - E_c} \right) (Z_{w,r} - Z_{w,c}) - \frac{Z_{w,c}}{O_{2,in} - O_{2,eff}} \right) M_w$$

H_{ox}	: Heat production per consumed mole of oxygen	[J.mol O ₂ ⁻¹]
$E_{r,0}$: Reactor effluent gas enthalpy per mole [J.mole ⁻¹]	[J.mol O ₂ ⁻¹]
E_c	: Cooler effluent gas enthalpy per mole [J.mole ⁻¹]	[J.mol O ₂ ⁻¹]
$Z_{w,r,0}$: Reactor effluent water vapour to dry gas ratio at saturation	[mol H ₂ O.mol dry gas ⁻¹]
$Z_{w,c}$: Cooler effluent water vapour to dry gas ratio at saturation	[mol H ₂ O.mol dry gas ⁻¹]
M_w	: molar weight of water	[kg.mol ⁻¹]

8.2.5 Product quantity

Based on a total mass balance the product quantity can be calculated. This product quantity will be expressed as the Relative Product Quantity (RPQ) i.e. is product quantity as a fraction of the incoming waste amount.

$$\text{eq. 8-9} \quad RPQ(t) = 1 + OM_0 \cdot DM_0 \cdot COU(t)(B - \Delta - M_{om})$$

RPQ : Relative Product Quantity [kg.kg⁻¹]

8.3 OUR models

8.3.1 The first-order model

Following the work of Keener [1] the following equation can be set up for the degradation rate of organic matter during composting.

$$\text{eq. 8-10} \quad \frac{dm}{dt} = -k \cdot f(O_2)(m - m_e)$$

m_e : Equilibrium organic matter i.e at $t \rightarrow \infty$ [kg VS.kg VS⁻¹]

k : Standard first order rate constant, i.e. under standard oxygen conditions [hr⁻¹]

Keener [1] originally defined m as the amount of dry matter, however interpreting m as organic material makes no principal difference as only organic matter disappears. Eklind [6] estimated k and m_e values based on both dry matter and organic matter and found no significant differences.

The effect of oxygen is generally described with a Monod-type of dependency. This gives the following correcting function for oxygen [7], relative to standard oxygen conditions.

$$\text{eq. 8-11} \quad f(O_2) = \frac{O_2}{K_{O_2} + O_2} \cdot \frac{K_{O_2} + O_{2,s}}{O_{2,s}}$$

$f(O_2)$: Oxygen effect correcting function [-]

$O_{2,s}$: Oxygen standard level [vol.%]

K_{O_2} : Oxygen half-saturation constant [vol.%]

Integration of equation 8-10 gives as a result:

$$\text{eq. 8-12} \quad m = m_e + (m_0 - m_e)e^{-k \cdot f(O_2) \cdot t}$$

m_0 : Initial organic matter, equals 1 by definition [kg VS.kg VS⁻¹]

By multiplying both sides by -1 and adding m_0 to both sides, equation 8-12 can be rewritten as:

$$\text{eq. 8-13} \quad m_0 - m = -(m_0 - m_e)e^{-k \cdot f(O_2) \cdot t} + (m_0 - m_e)$$

By integration of eq. 8-4 it can be found that:

$$\text{eq. 8-14} \quad COU(t) = \int_0^t OUR(\tau) d\tau = \frac{1}{M_{om}}(m_0 - m)$$

COU : Cumulative Oxygen Uptake [mol O₂.kg VS⁻¹]

Substituting 8-14 in 8-13 gives as result :

$$eq. \ 8-15 \quad COU_f(t) = COU_m \cdot (1 - e^{-k \cdot f(O_2) \cdot t})$$

COU_f : COU according to the first order model [mol O₂.kg VS⁻¹]

By differentiating eq. 8-15 the following result for the development of OUR_f in time is found:

$$eq. \ 8-16 \quad OUR_f(t, O_2) = k \cdot COU_m \cdot f(O_2) e^{-k \cdot f(O_2) \cdot t}$$

OUR_f : OUR according to the first order model [mol O₂.kg VS.hr⁻¹]

A first order model predicts the maximum OUR at t=0. By setting t=0 in the previous equation it becomes clear that:

$$eq. \ 8-17 \quad OUR_{f,0} = COU_m \cdot k \cdot f(O_2)$$

$OUR_{f,0}$: Initial OUR [mol O₂.kg VS.hr⁻¹]

8.3.2 The distributed model

A preliminary data analysis (not shown) showed that the distributed model for experiments with a constant hydrolytic activity can be used. The distributed OUR model for this case as introduced in the previous chapter is described as:

$$eq. \ 8-18$$

$$OUR_d(t, O_2) = \sqrt{\frac{1}{1 + e^{-\mu_{eff}(t-\Omega)}}} \frac{OUR_{m,\lambda}(O_2)}{\gamma_c - 1} \int_{\zeta_{s(\theta)}}^{\infty} \frac{\zeta^{\gamma_c-2}}{\Gamma(\gamma_c-1)} e^{-\zeta} d\zeta + A_h \int_0^{\zeta_{s(\theta)}} \frac{\zeta^{\gamma_c-1}}{\Gamma(\gamma_c)} e^{-\zeta} d\zeta$$

OUR_d : OUR as predicted by the distributed model [mol O₂.kg VS⁻¹.hr⁻¹]

μ_{eff} : Effective maximal biomass growth rate constant [hr⁻¹]

Ω : Lag time [hr]

$OUR_{m,\lambda}$: Scaled maximum OUR [mol O₂.kg VS⁻¹.hr⁻¹]

A_h : Hydrolytic activity [mol O₂.kg VS⁻¹.hr⁻¹]

ζ	: Scaled particle size	[1]
ζ_s	: Scaled switch particle size	[1]
γ_c	: Shape parameter of gamma distribution	[1]
Γ	: Gamma function	[1]

The scaled switch particle size equals:

$$\text{eq. 8-19} \quad \zeta_s(t) = \frac{\text{OUR}_{m,\lambda}(O_2) \int_0^t \sqrt{\frac{1}{1+e^{-\mu_{eff}(t-\tau)}}} d\tau}{S_{s,0} + A_h t}$$

The scaled switch particle size is a dimensionless measure of the size fraction that has been depleted of soluble substrate. Oxygen effects only the scaled maximum $\text{OUR}_{m,\lambda}$. At a specific oxygen content the $\text{OUR}_{m,\lambda}$ can be calculated as:

$$\text{eq. 8-20} \quad \text{OUR}_{m,\lambda}(O_2) = \text{OUR}_{m,\lambda}(O_{2s}) \sqrt{\frac{O_2}{O_{2s}}}$$

8.4 Materials and methods

8.4.1 Experimental

The pig faeces were obtained from an experimental facility of the research institute ILOB-TNO (Lelystad, the Netherlands). Straw was used as an amendment, 5% of straw (w/w) was added and mixed by hand. The OUR development over time was measured with the measurement system as described in chapter 5. Oxygen level was controlled at set levels of 1 vol. % and 15 vol. % oxygen. Due to probably some kind of controller offset and non-perfect mixing, the actual oxygen content differed from the set levels. At set level 15 vol. % the actual level was 14.6 vol. %, at set level 1 vol. %, the actual level was 1.6 vol. %. These levels were measured in the dried off-gas flow. This means that the levels within the reactor were lower as the reactor gas phase is water saturated. Correction for the water vapor pressure gives actual levels of 1.5 % and 13.4%. The temperature was controlled at 38 °C and remained within a ± 1 °C range. Dry matter (DM), organic matter (OM) of the

compost samples were determined in duplicate according to standard methods [8]. Dry matter of the mixture was 32% and organic matter 79%.

8.4.2 Parameter estimation

The parameters of the distributed model were estimated by minimizing the sum of squares of the OUR residuals, i.e. the difference between estimated and measured OUR value. Minimization was performed using the Minerr algorithm of the MathCad 2000 software (Mathsoft, Cambridge).

Two approaches can be distinguished in the literature for estimating the first order model parameters. Either both parameters (k_s , COU_m) are estimated from the COU data or either an independently determined COU_m value is used and only the time constant k , is estimated from the COU data.

Parameters for both types of first order models were estimated minimizing of the sum of squares of the COU-residuals. The COU data are used because cumulative data are commonly used to estimate first order parameters. By conferring to this practice, a better comparison with current design practice is possible. Minimization was performed using the genfit algorithm of the MatCad 2000 software (Mathsoft, Cambridge). The COU data were obtained by numerical integration of the same OUR data as used to estimate the distributed OUR model parameters. The numerical integration routine of MathCad 2000 software was used..

For the k -only-estimation the COU_m was evaluated from literature data. Based on literature data the maximum oxygen uptake COU_m was estimated as $28 \text{ mol O}_2 \cdot \text{kg VS}^{-1}$. This estimate is based on literature data and methods as proposed by Keener [1, 9].

8.4.3 Predictions

The model based predictions are determined using a reactor model (structure), reactor model parameters, an OUR model structure and the OUR model parameters. The OUR model parameters are either estimated using OUR data or derived from literature. It may thus be said that a prediction is based on the reactor model (structure), reactor model parameters, the OUR model structure, literature derived parameters and the data underlying the parameter estimation. In this chapter the same reactor model and reactor model parameters are used for all predictions and as such the reactor model and its parameters will

not influence the comparison. The data set used for parameter estimation and the OUR model will be however varied. The prediction of design variable Y at time t and oxygen content O_2 with model M , data D and literature derived parameters P will be expressed as $Y(t, O_2 | M, D, P)$. The sign $|$ is used to underline the conditional nature of a prediction. If a certain element, M , D or P is not needed for prediction, it will be left out of the list. For instance, if sufficient OUR data are available, the predictions can be based on the reactor model with its parameters and the OUR measurements, such a prediction will be expressed as $Y(t, O_2 | D)$.

Three models are distinguished, the distributed OUR model, M1, the first order model with both k and COU_m estimated, M2 and first order model with k -only-estimation, M3. The data set determined at 15% oxygen level is indicated as D_H , the data set obtained at 1% oxygen level is called D_L . For some calculation only the first half part ($0 \text{ hr} < t < 265 \text{ hr}$) of D_H is used, this specific set is indicated as D_s . Oxygen levels will be indicated in the text by 1% and 15%, in all calculations however the actual levels in the reactor gas phase are used.

8.5 Results

8.5.1 Parameter estimation

The fitted model M1 coincides almost completely with the OUR measurements as shown in Figure 8.2. This is reflected in the R^2 value of 0.99. The models M2 and M3 are fitted to the COU data as shown in Figure 8.3. The model M2 coincides almost completely with the data ($R^2 = 0.99$) while the model M3 shows some deviations. ($R^2 = 0.96$)

Using the parameters obtained from the COU data the OUR time course was calculated for the models M2 and M3. Figure 8.1 shows that the first order models M2 ($R^2 = 0.62$) and M3 ($R^2 = 0.26$) are not able to describe the OUR time course well. Direct fitting of the first order model to the OUR data gives the same result. Figure 8.3 shows that using the parameters estimated from the OUR data the model M1 gives a good description of the COU data ($R^2 = 0.99$)

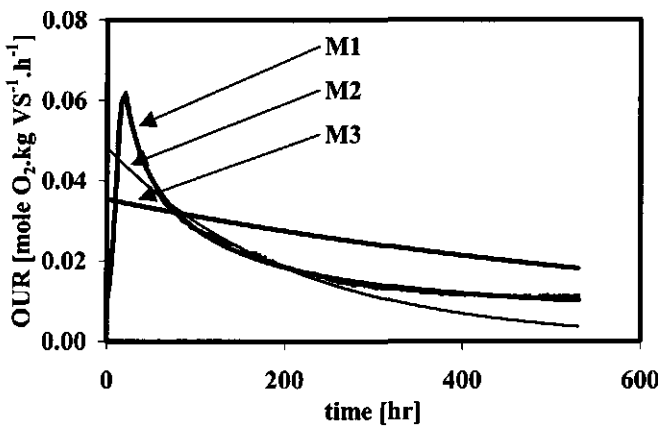


Figure 8.2: *OUR development of the faeces-straw mixture at 15% oxygen as fitted by the models M1, M2 and M3. The measurements are given by the wavy line, that however nearly coincides with the fit of M1.*

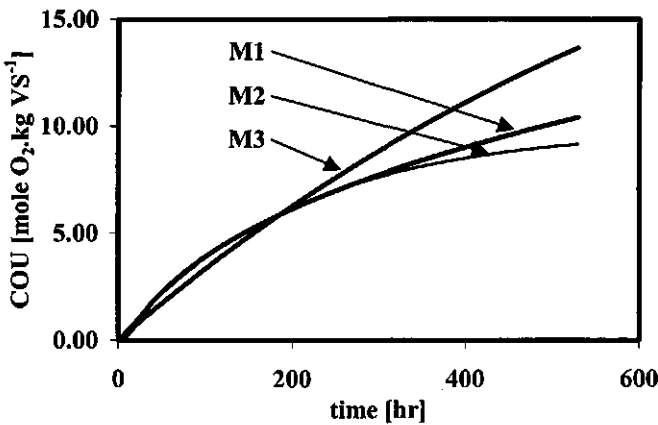


Figure 8.3.: *COU time course of the faeces-straw mixture at 15% oxygen as fitted by the models M1, M2 and M3. The measurements completely coincide with the fit of M1*

8.5.2 Time prediction

The predictions of the different design quantities at different points of time will be compared for data obtained at 15%. This experiment has the biggest cumulative oxygen uptake, and is thus most suitable for investigation of the time prediction. To obtain insight in both interpolation as extrapolation the parameter estimation for all models is based on

the first half of the data set \mathbf{D}_S . The prediction error is calculated for M1 and M2 in the following way:

$$\text{eq. 8-21} \quad E(Y, M_i, t, 15\%) = |1 - Y(t, 15\% | M_i, \mathbf{D}_S) / Y(t | \mathbf{D}_H)|$$

E	: Prediction error	[-]
Y	: Design quantity	
t	: Time	[hr]
M _i	: M1 or M2	
D _H	: OUR data set obtained at 15% O ₂ .	
D _S	: First half of data set D _H .	

The prediction error of M3 is calculated as:

$$\text{eq. 8-22} \quad E(M3, t, 15\%) = |1 - Y(t, 15\% | M3, \mathbf{D}_S, COU_m) / Y(t | \mathbf{D}_H)|$$

The prediction error of M1 and M2 are based on the same information sources, and the prediction error values can be directly compared. For model M3 one has to take into account that additional information is supplied, one might expect a lower prediction error.

The flow rates Q_{in}, Q_{ieff} and Q_c are all proportional to OUR, this means that the relative error in the design quantity maximum flow rate of Q_{in} is thus also applicable off-gas flow Q_e, and the cooler flow rate Q_c. The design quantity, maximum of the flow rate Q_{in}, is denoted as Q_{max}.

The design quantity, average of the flow rate Q_{in} is denoted as Q_{avg}. As all average flow rates are proportional to the COU, they have the same prediction error. As DE is proportional to the COU, this design quantity has the same prediction error as Q_{avg}.

Predictions for all design quantities were evaluated at three points of time, at t=265 hr, t=530 hr and t=795 hr. As t= 265 hr is the upper time of the time range of the data set D_S, the error at this point of time is an interpolation error. The error at t= 530 and t= 795 hr are extrapolation errors. The predictions at t= 795 hr could not be compared to the data as these are not available. The predictions were however compared to the prediction of M1 using kinetic parameters calculated from the whole data set, thus using Y(t, 15% | M1, D_H) for comparison.

Fig 8.4 shows the errors for the DE and the Q_{avg} . This figure shows that M1 and M2 have a negligible error at $t=265$ hr, while the error of M3 is clearly higher. At $t= 530$ hr, the error in M2 and M3 have strongly increased, while for M1 it remains small. The error in M3 is substantially bigger than for M2. The same trend is observed for $t =795$ hr. Similar trends can be observed for DM as shown in figure 8.5 and RPQ as shown in figure 8.6. As figure 8.7 shows the error for Q_{max} increases in the sequence of M1<M2<M3.

The prediction for OM showed in all cases for all three models a negligible error, i.e. smaller than 0.1%.

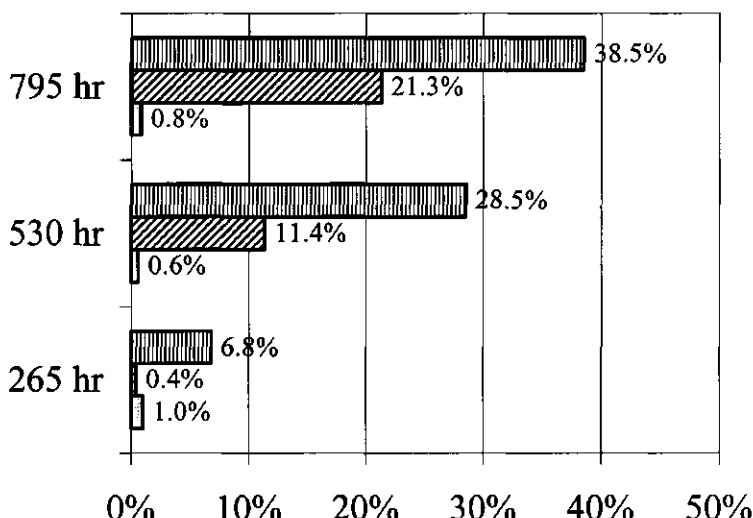


Figure 8.4: The time prediction error (X-axis, %) for DE and Q_{avg} at different points of time for model M1 (grey), M2(diagonal hatch) and M3 (vertical hatch).

8.5.3 Oxygen prediction

The oxygen prediction error for M1 is calculated as :

$$\text{eq. 8-23} \quad E(M1,t,1\%) = |1 - Y(t,1\%| M1, D_S) / Y(t,1\%| D_L)|$$

The oxygen prediction error for M2 is calculated as :

$$\text{eq. 8-24} \quad E(M2,t,1\%) = |1 - Y(t,1\%| M2, D_S, K_{O_2}) / Y(t,1\%| D_L)|$$

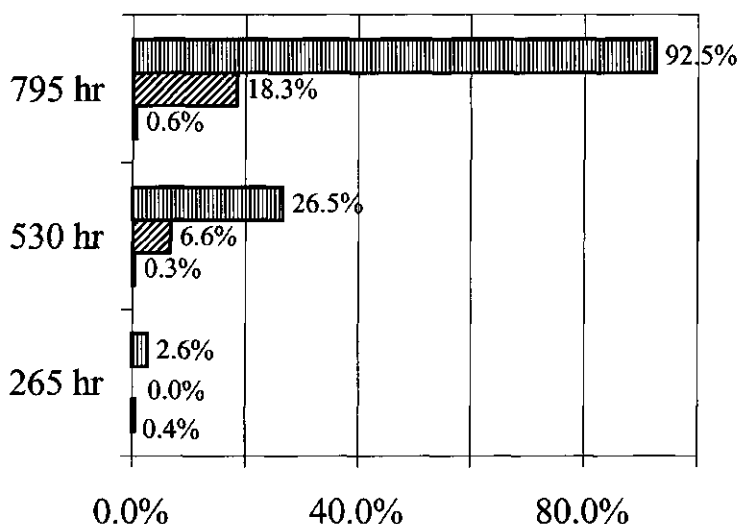


Figure 8.5: The time prediction error for DM (X-axis, %) at different points of time for model M1 (grey), M2(diagonal hatch) and M3 (vertical hatch).

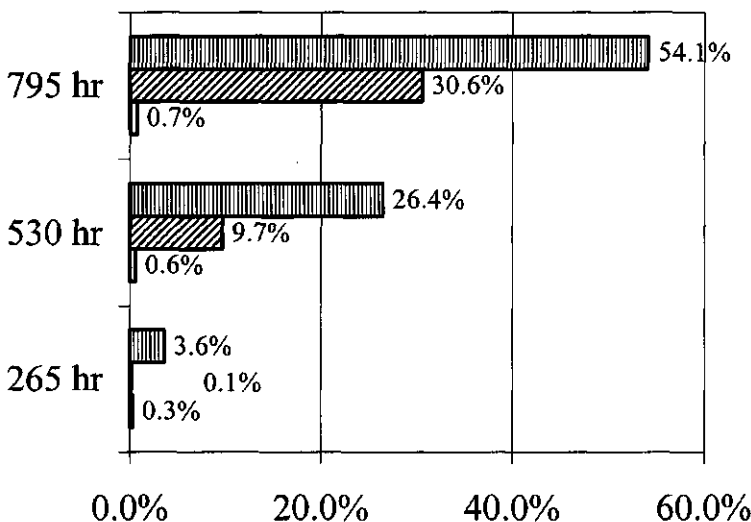


Figure 8.6: The time prediction error for RPQ (X-axis, %) at different points of time for model M1 (grey), M2(diagonal hatch) and M3 (vertical hatch).

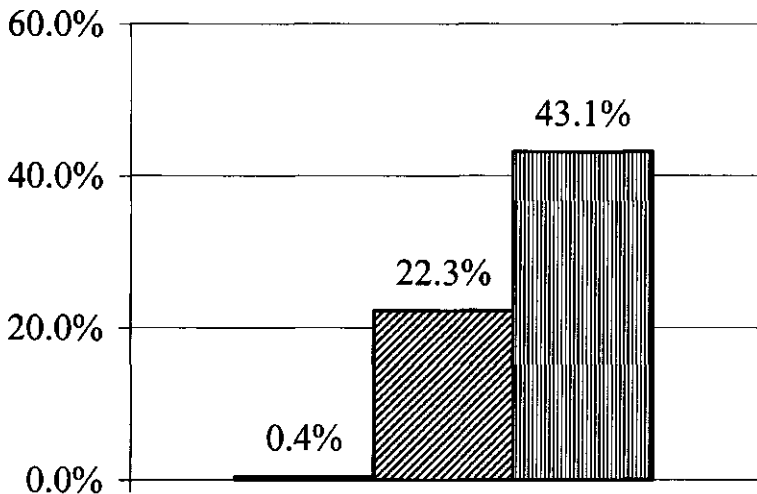


Figure 8.7: The time prediction error for Q_{max} (Y-axis, %) for model M1 (grey), M2 (diagonal hatch) and M3 (vertical hatch).

The oxygen prediction error for M3 is calculated as :

$$\text{eq. 8-25} \quad E(M3,t,1\%) = |1 - Y(t,1\%| M3, D_s, COU_m, K_{O2}) / Y(t,1\%| D_L)|$$

These predictions are made for $t=265$ hr and $t= 530$ hr. As the data analysis showed that A_h as such was not identifiable from D_L a sensible extrapolation for $t=795$ was not possible. Using the estimated parameter values the OUR at 1% oxygen can be predicted, both with the distributed and the first order model. For the first order model a value of K_{O2} of 2.8 % was used in eq. 8-11. The oxygen standard level was chosen as 15 vol.%, enabling to directly use the k_s value derived from the 15% experiment as the standard value. The K_{O2} value is based on a relationship given by Richard that gives the dependence of K_{O2} on temperature and moisture content [7].

Figure 8.8 shows the error of the DE and Q_{avg} . The errors of M1 and M2 are comparable, but compared to the case of 15 % oxygen substantially bigger. The error of M3 is again bigger than that of M1 and M2. At $t=530$ hr the errors of all three models are comparable. This is also true for DM (Figure 8.9) and RPQ (Figure 8.10). The errors increase for $M1 < M2 < M3$, but do not differ substantially.

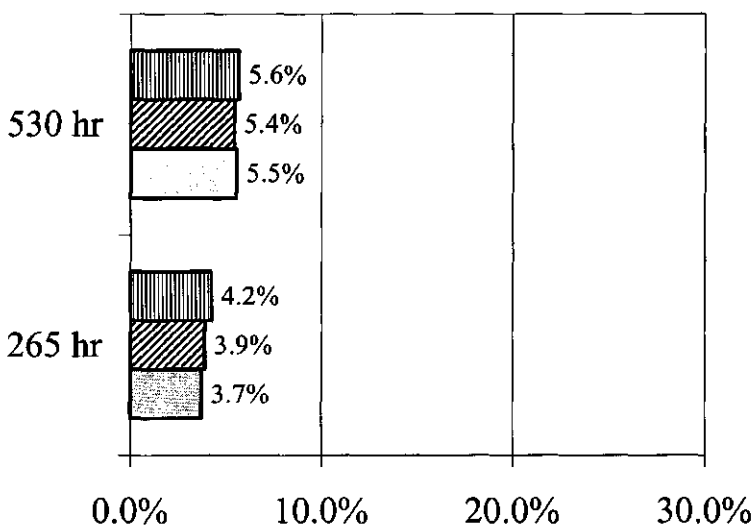


Figure 8.8: The oxygen prediction error for DE and Q_{avg} (X-axis, %) at different points of time for model M1 (grey), M2(diagonal hatch) and M3 (vertical hatch).

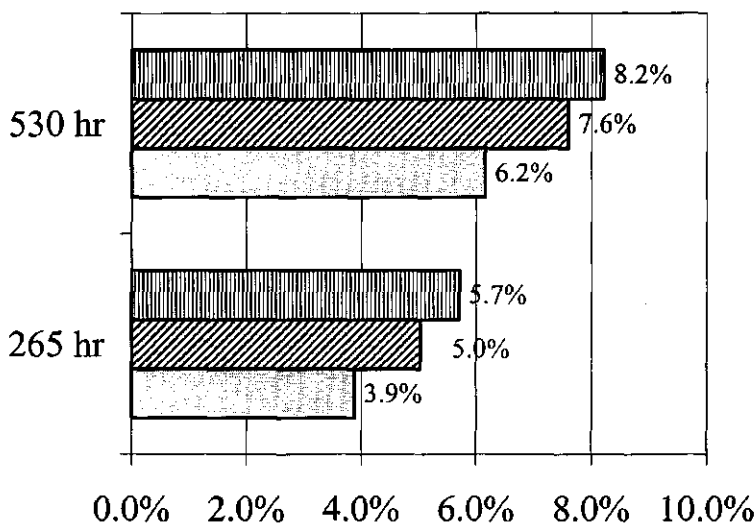


Figure 8.9: The oxygen prediction error for DM (X-axis, %) at different points of time for model M1 (grey), M2(diagonal hatch) and M3 (vertical hatch).

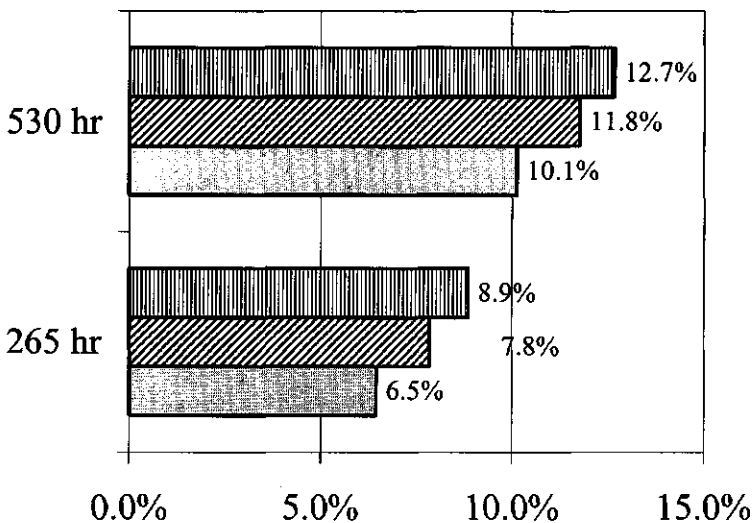


Figure 8.10: The oxygen prediction error for RPQ (X-axis, %) at different points of time for model M1 (grey), M2(diagonal hatch) and M3 (vertical hatch).

The only substantial difference is Q_{\max} , in which case M1 has a substantially lower error (figure 8.11). The error for M1 is however bigger than was the case for an oxygen level of 15%.

The error for OM was again in cases very small, i.e. smaller than 0.5%.

8.5.4 Oxygen effect

As both 1% and 15% data are available it is possibly to directly determine the effect of oxygen on the OUR. According to the first order model the ratio of OUR values observed at different oxygen levels, is constant if the COU of these observations is the same. This constant value gives the reduction of the k_s value as a result of oxygen limitation. Consider the OUR value at time t for an experiment performed at oxygen level O_2 , and the OUR value at time t' with associated oxygen levels $O_{2,s}$. According to the first-order model the following relationship should hold:

$$\text{eq. 8-26} \quad \frac{\text{OUR}(t, O_2)}{\text{OUR}(t', O_{2,s})} = \frac{O_2}{K_{O_2} + O_2} \cdot \frac{K_{O_2} + O_{2,s}}{O_{2,s}}$$

if

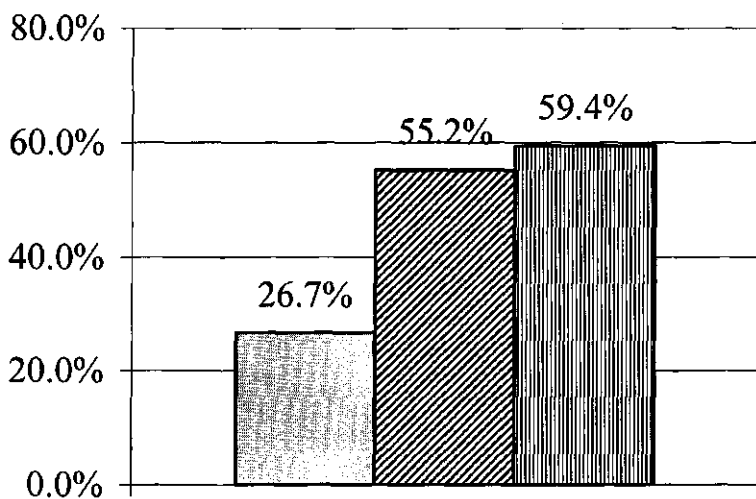


Figure 8.11: The oxygen prediction error for Q_{\max} (Y-axis, %) for model M1 (grey), M2(diagonal hatch) and M3 (vertical hatch).

eq. 8-27

$$COU(t, O_2) = COU(t^*, O_{2,s})$$

In this equation t^* is thus the time at which the COU of experiment at $O_{2,s}$ equals the COU of the experiment at oxygen level O_2 at time t . This equation is a direct consequence of the (assumed) multiplicative interaction of substrate and oxygen on the OUR. The oxygen effect is thus quantified as the ratio of OUR values at the same COU value.

This oxygen effect is calculated based on the data obtained at $O_2=1\%$ and $O_{2,s} = 15\%$. Spline interpolation was used to interpolate the OUR value. In the same way the oxygen effect was determined for model M1, based on the predictions at 1% and 15%. The parameters used for the predictions are estimated from the data set D_S . For model M2 and M3, the oxygen effect can be directly calculated from the Monod value, using the earlier mentioned value of K_{O_2} .

The results are shown in figure 8.12. It shows that initially the measured oxygen effect is approximately 1 and decreases to a stable level at $COU = 0.9 \text{ mol O}_2 \cdot \text{kg VS}^{-1}$, the average of the stable period is 0.47. The model M1 predicts a similar shape, i.e. a decrease of the oxygen effect, followed by a stable period. The Monod model predicts a stable period over

the whole COU range. The distributed model and the Monod model both predict a somewhat lower value of 0.37 for the oxygen effect.

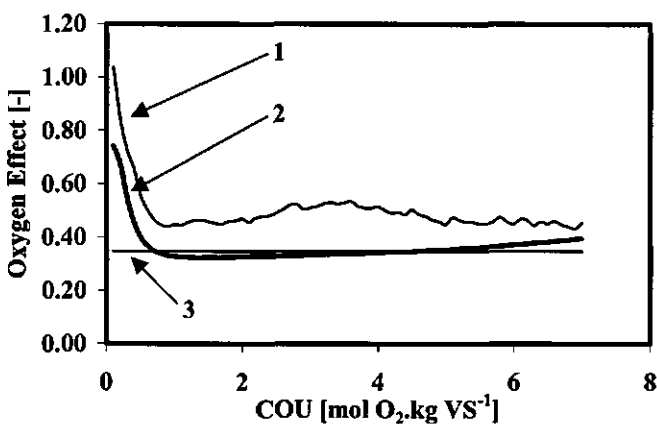


Figure 8.12: The oxygen effect as a function of COU error as measured (1), as predicted by model M1 (2) and as predicted by the Monod-model (3)

8.6 Discussion

The distributed model M1 and the first order models M2 and M3 have been compared in their capability of predicting certain design quantities. Part of the data set acquired at 15% has been used to estimate parameters for the models involved. Based on these parameter estimates prediction have been made for the design quantities RPQ, OM, DM, DE, Q_{avg} and Q_{max} at different points of time and at a different oxygen content.

For the time prediction it was shown that both M1 and M2 predict equally well the DM, RPQ, DE and Q_{avg} at $t=265$ hours, indicating that both the mechanistic model M1 as the empirical model M2 are able to interpolate the data well. It is in this respect surprising that the prediction of Q_{max} by M2 is poor, as the maximum OUR value occurs within the time range of the data set D_s used to estimate the parameters. The explanation lies in the fact that the first-order model is able to describe the COU data well ($R^2 = 0.99$) but describes the OUR data poorly ($R^2 = 0.63$). This does not change if the first-order model is directly fitted to the OUR data, almost the same parameter values with the same low R^2 value are found. The new model M1 developed in this thesis gives with the same parameter set a good description of both the OUR data ($R^2 = 0.99$) and COU data ($R^2 = 0.99$).

These results show that a good description of the COU data does not automatically lead to a good description of the OUR data. It is thus possible that a model is able to describe some part of the system well while a closely associated variable is predicted poorly. This stresses that a model must be validated for the intended purpose.

The prediction of OM is illustrative in this respect, for in all models this design quantity is predicted with less than 0.1 % error, while the prediction error for the other design quantities differs strongly between the different models. This shows clearly that an excellent performance for the design quantity OM gives no information whatsoever on the prediction performance for the other design quantities. That all models have a small OM prediction error is caused by the fact that the OM changes only little over the considered period and differences between the models can be hardly detected.

The newly developed model M1 predicts the design quantities clearly better outside the measurement time range compared to M2 and M3. The case of M2 shows that a good description of the prediction within the measurement range yields no information on the correctness of the predictions outside the measurement range.

The parameter estimation using model M2 gives an estimate of $\text{COU}_m = 11.8 \text{ mol O}_2 \cdot \text{kg VS}^{-1}$ which is an unrealistic low prediction of the long-term cumulative oxygen uptake [1]. The model M3 is supplied with a sensible value of the COU_m parameter, however M3 performs poor compared to model M2 and M1. This is an indication of the empirical nature of the first-order model, the parameters have no physical interpretation.

For the oxygen prediction it was shown that M1 performs best, however the differences in design quantities estimate errors of RPQ, OM, DM, DE, Q_{avg} are not as substantial as in the time prediction case. The value of Q_{max} is again much better predicted by M1, however the error is larger than in the time prediction case.

This result can be better understood by considering the estimated oxygen effect (Figure 8.12). Initially the oxygen effect is better predicted by M1, however soon, at $\text{COU} = 0.9 \text{ mol O}_2 \cdot \text{kg VS}^{-1}$, M1 and the Monod model give the same prediction. The fact that oxygen prediction errors of all models for RPQ, OM, DM, DE, Q_{avg} do not differ strongly is a result of the fact that the error is mainly determined by the oxygen effect prediction, which is the same for both the model M1 as the Monod model.

At $t = 530 \text{ h}$ one would expect that the effect of time extrapolation as seen for the data at 15% would influence the prediction errors at 1% much stronger. That the oxygen prediction error at $t = 530 \text{ hr}$ has not strongly increased is because the COU at this point of time at 1% O_2 ($\text{COU} = 7.0 \text{ mol O}_2 \cdot \text{kg VS}^{-1}$) is actually smaller than the COU at $t = 265 \text{ hr}$ at 15% O_2 .

(COU = 7.3 mol O₂.kg VS⁻¹). Thus with respect to the COU the oxygen prediction at 530 hr at 1% O₂ is still an interpolation. This is in line with the oxygen prediction of Q_{max}, here the difference between the models has remained substantial, because the models M2 and M3 fail to describe the OUR curve accurately.

The status of the prediction of the oxygen effect by the model M1 and the Monod model is different. The selection of the Monod model and the saturation parameter is a result of parameter estimation, using an extensive data set. The prediction of the oxygen effect by the mechanistic model M1 is a consequence of the assumed model fundamentals. The fact that both predictions coincide is a confirmation of the soundness of the fundamentals underlying the mechanistic model M1.

Both models tend to predict a stronger oxygen limitation, than is measured. Whether this is an effect of the variability of the material or indicates some systematic deviations, can not be decided on, with only one experiment.

The findings might be summarized as that the first order model M2 is able to describe the COU development sufficiently accurate but fails to describe the OUR development. As a result the interpolative predictions of COU based design quantities RPQ, OM, DM, DE, Q_{avg} are performed well. Interpolation of the OUR based design quantity Q_{max} is however poor. Extrapolation in time showed to be poor, while extrapolation to another oxygen content is only possible if an adequate empirical model for the oxygen effect is available. The distributed model is able to describe both the OUR development and COU time course well, and consequently interpolates all design quantities well and gives better time extrapolations. The distributed model needs no additional information to predict the low oxygen effect equally well.

Of course, only two data sets and of one type of waste are not really enough to generalize the findings to other types of wastes Yet the analysis gives sufficient confidence to expect the following generalized picture:

1. It is expected that under all conditions the newly developed model M1 will describe at least equally well the COU data, as the model M1 can be simplified to a first-order model.
2. The better behavior of the distributed model M1 relative to the first order model M2 can be explained from the presence of a peak in the OUR course. Of course the initial increase in the OUR followed by a decrease can not be handled well by a first order model. This type of model only can describe either a decreasing or increasing curve. The peak is

generally present in composting kinetics [10] and thus the distributed is expected to be superior in most cases to the first order model.

3. Thoroughly tested empirical models for the effect of environmental conditions are only available for oxygen and temperature. It would be interesting to compare the temperature effect as predicted by distributed model with these empirical models. For other factors like moisture and porosity that are strongly correlated with the structure of the waste the distributed model is expected to be very helpful, and in fact almost indispensable.

4. Even if an empirical function is present that describes the effect of environmental conditions it remains to be seen whether this function can be extrapolated. For instance a simulation of the oxygen effect using the parameters for the faeces straw mixture, changing only the distribution parameter from 1.1 (measured) to 3., gives a different picture (see Figure 8.13) for the oxygen effect. At a COU from 6 and up we see a dramatic change in the oxygen effect. This indicates that limitation may exist to the empirical functions.

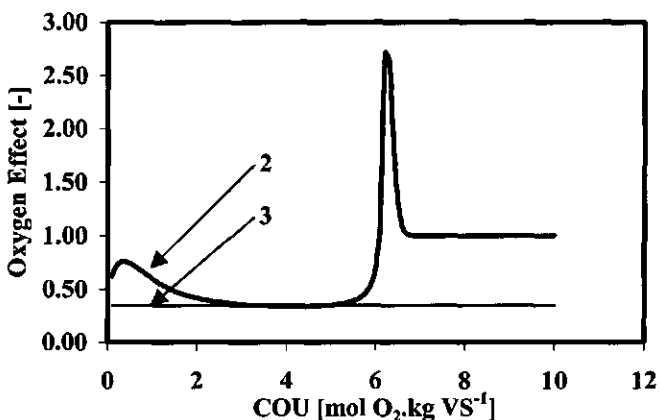


Figure 8.13: The predicted oxygen effect for a less distributed waste as a function of COU error, as predicted by model M1 (2) and as predicted by the Monod-model (3)

The fundamental reason why the distributed model performs better is because it is able to model the different processes that occur within the composting particles. This makes it possible to retrieve more information from the data. It may be concluded that the distributed model M1 is to be preferred over the first order models M2 and M3, not only scientifically because of the enhanced insight but also practically because of possibility to improve

composting reactor designs. It is believed that the advantage using the distributed model will only grow as more environmental factors are taken into account.

8.7 References

1. Keener, H.M., et al. *Optimizing the efficiency of the composting process.* in *Proceedings of the International Composting Research Symposium.* 1992. Columbus OH: Renaissance Publications.
2. Haug, R.T., *Compost Engineering: Principles and Practice.* 1980, Ann Arbor: Ann Arbor Science.
3. Kroodsma, W., et al. *A technique for direct separation of pig excrements followed by on-farm treatment of the components.* in *International conference on Agricultural Engineering.* 1998. Oslo, Norway.
4. Walker, J.M. *Control of composting odors.* in *Proceedings of the International Composting Research Symposium.* 1992. Columbus OH: Renaissance Publications.
5. Williams, T., O. and F.C. Miller. *Composting facility odor control using biofilters.* in *Proceedings of the International Composting Research Symposium.* 1992. Columbus OH: Renaissance Publications.
6. Eklind, Y. and H. Kirchman, *Composting and storage of organic household waste with different litter amendments. I: carbon turnover.* Bioresource Technology, 2000. 74: p. 115-124.
7. Richard, T.L., *The kinetics of solid-state aerobic biodegradation.* 1997, Cornell University.
8. APHA, *Standard Methods for the Examination of Water and Wastewater. 18th ed., part 2540D.* 1992, Washington DC.: American Public Health Association.
9. Marugg, C., et al., *A kinetic model of the yard waste composting process.* Compost Science & Utilization, 1993. 1(1): p. 38-51.
10. Hamelers, H.V.M. *A Theoretical Model of Composting Kinetics.* in *Proceedings of the International Composting Research Symposium.* 1992. Columbus OH: Renaissance Publications.

Summary

Composting plays an important role in waste management schemes and organic farming, as it enables reuse of organic matter and nutrients. The compost produced can be beneficially used in agriculture as a soil conditioner or as an ingredient for container growing media. To compete with comparable products the compost should have a high quality and a fair price. A composting plant must comply with strict environmental regulations, especially concerning odor nuisance. The need to control odor emissions has led to the development of so-called closed composting systems, enabling collection and treatment of the off-gases. The construction costs for a closed composting facility are much higher than for an open system, and to remain efficient a closed composting process must operate at a much higher production rate compared to open composting systems. A modern plant should thus produce fairly priced high quality compost at a high rate with minimal odor emissions.

Current design strategies for composting plants are mainly based on practical experience and rules of thumb. Optimization of the plant takes place during operation. This more or less trial-and-error design and optimization is a (too) costly approach as any error will result in a full scale facility producing a poor compost and/or odor problems for the surroundings.

A more rational approach to design and plant optimization is needed to realize better composting plants. Mathematical reactor models are a useful, if not necessary, tool in rational design. All reactor models developed so far are based on empirical kinetics, which restricts their generality and thus applicability. To obtain a more general model for composting reactors a more general model for composting kinetics is needed.

Current kinetic models are inductive models, i.e. they are inspired by the measured data. It is argued that the inductive model strategy has reached its practical potential. No further progress is expected, as certain important variables like biomass and particle size can not (yet) be adequately measured. Incorporation of new variables in the inductive model needs an ever-increasing massive experimental effort, as the number of interactions strongly increases.

In this thesis the deductive strategy has been used to develop a more general kinetic model. A central problem in mechanistic modeling in environmental systems is the incongruence between the (presumed) complexity of the systems and the available measurements on the

system. This sets a limit on the predictive power of the developed models, as these models can not be fully validated.

In this thesis a modified deductive strategy is proposed that aims at identifying the limitation arising from the incongruence between model complexity and available measurements. The principal tool used to detect these limitations is investigation of parameter identifiability. A parameter is identifiable if one can uniquely determine its value from the data at hand. Only if all model parameters are identifiable, the model can be sensibly validated. **The objective of this thesis is thus to develop a mechanistic kinetic model for the composting process with all parameters identifiable.**

The thesis can be structured in three main parts. The first part, "dimensional identifiability analysis", is concerned with the use of dimensional analysis for identifiability analysis. Together with the proposed deductive modeling strategy it is a methodological contribution to modeling of relatively complex systems with limited available measurements.

The second part, "the single particle model", is concerned with the development and validation of a theoretical model for the aerobic degradation of a single waste particle. This theoretical model gives insight in the processes occurring within a composting waste particle. An analytical solution containing only identifiable parameters is derived and validated.

The third part, "the distributed model", deals with the development, validation and application of a kinetic model for a waste consisting of size distributed waste particles. The model is based on a distribution function describing the particle size distribution and the developed analytical identifiable single particle model. The distributed model is validated and is used to design of a new composting concept. This model application shows the advantages the distributed model for reactor design.

Dimensional identifiability analysis. (Chapter 2)

Dimensional analysis is a tool widely used in mathematical modeling and (chemical) engineering. Central to dimensional analysis is the principle of dimensional homogeneity, which states that the description of a relation between a number of physical quantities should be independent of the system of units involved to measure these quantities. Dimensional analysis allows for model simplification by grouping of variables and parameters into dimensionless numbers.

In the case of parameter estimation direct construction of dimensionless number is not possible. The measurements can not be made dimensionless beforehand, as the parameters

needed to do so are yet unknown. Dimensional analysis is however still a useful tool for parameter estimation purposes if a different starting point is chosen for the analysis.

The unit of a parameter consists of one or more basic units. The basic units constitute together the basis of the unit system employed. It is shown that a parameter will be non-identifiable if it contains a basic unit that is not part of the unit of the observations. Such a parameter is called dimensionally-non-identifiable. It is shown that if some parameters are dimensionally-non-identifiable, these parameters can be transformed to a set of aggregated parameters that are not dimensionally-non-identifiable. This type of dimensional analysis can be easily performed, and as it removes a source of non-identifiability it is advised to use the technique prior to any other technique for identifiability analysis.

Dimensional analysis may also show relationships between parameter identifiability of different models that are otherwise not so easily detected. This is illustrated by analyzing the microbial growth in batch culture. For four different models the identifiability can be proven, while only for one model the tedious calculations to prove the identifiability have to be performed. Practical identifiability can be greatly facilitated by using dimensional analysis. This is especially true if a dimensionless identifiability measure is used.

The single particle model; development, derivation and validation (Chapter 3-5)

The Oxygen Uptake Rate (OUR) is the amount of oxygen that is taken up by a unit sample of waste in a unit period of time. It is the most important composting process rate indicator as it is directly linked to the composting reaction. The OUR is linearly linked to heat production independent of molecular substrate composition and is a direct measure of compost stability. The OUR depends strongly on the state of the waste, e.g. temperature and moisture content influence the OUR. To predict the OUR a kinetic model is needed that relates the rate determining factors to the OUR. Kinetic models developed so far are empirical multiplicative models.

Chapter 3 introduces a theoretical model for composting kinetics. The basis of the model is the waste particle whose volume is made up of water, insoluble organic material, insoluble inert material and aerobic biomass. Soluble substrate and oxygen are dissolved in the water and are consumed by the aerobic biomass. The oxygen is transported from the gas phase surrounding the particle to the water phase inside the particle. Soluble substrate is initially present and is produced through microbial hydrolysis from insoluble organic material. Within the water phase both the soluble substrate and oxygen are transported via diffusion.

Two microbial processes are taken into account: aerobic heterotrophic growth and hydrolysis.

Due to the low oxygen solubility, oxygen will penetrate the particle only partially. Aerobic microbial growth will occur only in the outer edge of the particle. The core of the particle is anaerobic and hydrolysis of insoluble material will take place. As a result of the fact that microbial growth only takes place locally a convective mass flow occurs within the particle. Based on a mathematical description of microbial reactions (biomass growth, hydrolysis), diffusional transport of oxygen and soluble substrate and convective transport of biomass, inert material, organic insoluble material and water, mass balances describing the system are set up. The resulting equations are solved numerically. The properties of the model are investigated via a sensitivity analysis.

The OUR time course can be divided in four distinct phases depending on the dominant process involved. During the first phase the OUR rapidly increases as a result the growth rate of the aerobic biomass. After a biofilm has been formed at the gas-particle interface the OUR stabilizes at its maximal value, at a constant level. During this phase the OUR is determined by the biofilm activity. After the soluble substrate has been nearly depleted the OUR drops rapidly during the short third phase. The OUR enters then the fourth phase during which the OUR is determined by the hydrolysis rate.

The model enables to investigate the effect of different waste characteristics and oxygen levels on the OUR. It showed that the particle size is the most influential single waste property influencing the OUR. Surprisingly the initial biomass density had almost no effect on the OUR time course. The model is able to explain a number of phenomena that can not be explained by conventional empirical models.

An analytical solution for the OUR time course is found based on the theoretical model (Chapter 4). This so-called single particle model gives more insight in the parameter dependence of the OUR time course. The single particle model is based on a simplification of the balances derived in the previous chapter. Comparison of the numerical results and the analytical calculation showed an excellent agreement.

The single particle model was validated, for which purpose the parameter identifiability was investigated (Chapter 5). Two dimensionless numbers were determined that can be used to check the practical identifiability of the parameters in the analytical model. To validate the analytical model an experimental system has been developed to assess the effect of particle size on the OUR time course. The material used was chicken manure and was composted at 55°C with 19 vol.-% of O₂. Particle sizes of 16, 8, 4 and 2 mm were studied.

The results at 16 mm were discarded as the material swelled and cracked as a result of gas formation. The parameters of the single particle model were estimated for each measured OUR time curve. The dependence of the parameters on the particle size showed in all but one case an excellent agreement to the expected dependence. The parameter values were in accordance with the expected values. An indication for temporary substrate inhibition of the aerobic microbial growth was found.

The distributed model; development, validation and application (Chapter 6-8)

Waste is made up of a mix of particles with different particle sizes. Because the particle size is the most important factor influencing the OUR, the size distribution should be taken into account.

The gamma distribution function is used to describe the particle size distribution of the particles within the waste (Chapter 6). The gamma function can be derived from the assumption that the gas-filled pores are homogeneously distributed within the waste matrix. The so-called gamma parameter describes the width of the distribution. With increasing gamma values the distribution becomes narrower and eventually approaches a single particle size. Based on theoretical considerations, a gamma value in the range 1-3 is expected.

This distribution function is combined with the single particle model to derive the so-called distributed model. The OUR of a distributed set of particles shows to be determined by two classes of particles, those that still have soluble substrate and those that are depleted of substrate. The rate of the latter class is determined by the hydrolysis rate, which is independent of particle size. The rate of the class of particles containing soluble substrate is inversely proportional to the particle size. In time the substrate depleted class will grow as more and more substrate saturated particles become depleted.

This OUR time course as described by the distributed model has been compared to the single particle model. The main difference is that the distributed model shows a clear OUR peak followed by a gradual decrease, while the single particle model has a distinct constant OUR level for some time, followed by an almost instantaneous drop.

The identifiability of the distributed model has been investigated (Chapter 7). Given a sufficiently long measurement period with a sufficiently high measurement frequency the identifiability is mainly determined by the width of the distribution and the amount of soluble substrate. It showed that under some practical conditions, i.e. a wide distribution and a relative low initial soluble substrate concentration, problems with parameter

identifiability could not be ruled out. This lack of identifiability is a result of the fact that the OUR of the waste is a mixture of the OUR of the two classes with different behavior with respect to particle size, oxygen etc. This mixing up of signals makes the interpretation of the resulting signal more difficult.

The distributed model was validated with the same waste material and environmental conditions as have been used for the validation of the single particle model. This material has been mixed with an inert amendment. This set-up enabled a direct experimental comparison of the outcome of both experiments, as the same material was used. It showed that the OUR time course runs as predicted by the distributed model. This clearly shows that a distribution is a necessary element in the description of real waste.

The distributed model has been used for design of a new composting system (Chapter 8). The new composting system consists of tunnel reactor with a cooled recirculation flow, enabling a substantial reduction of the off-gas flow. As a result of cooling and reuse of the recirculation flow the oxygen level in the gas phase of the composting matrix is low (<10 vol.%) compared to conventional composting systems (>15 vol.%).

The distributed model has been used to predict a number of design quantities like flow rates, compost composition and amount. Some design quantities are depending on the OUR while others depend on the cumulative amount of oxygen consumed (COU). Two types of prediction were distinguished, interpolative predictions and extrapolative predictions. Interpolative predictions are predictions in the range of the measurements underlying the model parameters, while extrapolative prediction are outside this range. All predictions by the distributed model were compared to predictions made by the currently used empirical models and data based predictions.

The distributed model has a smaller interpolative prediction error than the currently used models for the design quantities based on the COU. For the OUR based quantities the prediction error of the distributed model was substantially smaller, by a factor of 2. The distributed model showed to better describe the effect of oxygen on the OUR than the empirical model.

It may be concluded that the distributed model predicts the design quantities much better than the empirical models. It is expected that this is also true in other situations, i.e with different types of waste and different rate determining factors, like temperature, porosity, etc. It is argued that for factors like particle size, porosity and moisture content, the distributed model is indispensable as the effect of these factors is closely connected to the structure of the waste matrix, an element that is explicitly modeled in the distributed model.

The distributed model is an almost essential tool for the design of composting system, it gives insight in the process and gives better predictions of design quantities.

Samenvatting

Composting van reststoffen maakt het mogelijk om nutriënten en organische stof in de vorm van compost op een nuttige wijze te hergebruiken. In de landbouw kan compost gebruikt worden als bodemverbeteraar en als ingrediënt voor potgrond. Om deze reden heeft compostering een belangrijke functie zowel in de afvalverwerking als in de biologische landbouw. Om te kunnen concurreren met vergelijkbare producten zoals veen moet de compost een goede kwaliteit en een redelijke prijs hebben.

Composteringsinstallaties moeten voldoen aan strikte milieu-eisen, vooral wat betreft geur. De noodzaak om de geur emissies te reduceren heeft geleid tot de ontwikkeling van gesloten composteringssystemen. Deze gesloten systemen maken verzameling en reiniging van de afgassen mogelijk. De constructiekosten voor een gesloten systeem zijn veel hoger dan voor open systemen. Om efficiënt te produceren dient een gesloten composteringsinstallatie een veel hogere volumetrische verwerkingscapaciteit te hebben. Een moderne composteringsinstallatie dient dus een hoge capaciteit te hebben en een goede compost tegen een concurrerende prijs met minimale emissies te produceren.

Huidige ontwerpstrategieën voor composteringsinstallaties zijn voornamelijk gebaseerd op ervaring en op vuistregels. Na het ontwerp vindt optimalisatie plaats gedurende het inbedrijf-zijn van de installatie. Deze “trial and error” strategie is een kostbare methode, omdat elke fout resulteert in een installatie, die compost van onvoldoende kwaliteit produceert en/of geurhinder veroorzaakt.

Een meer rationele strategie voor ontwerp en optimalisatie is nodig om betere composteringsinstallaties te realiseren. Wiskundige reactor-modellen zijn hiervoor een bijna noodzakelijk instrument. De tot nu toe ontwikkelde modellen zijn gebaseerd op een empirische modelbeschrijving van de kinetiek. Dit beperkt de algemeenheid en dus de bruikbaarheid van de reactormodellen. Om een meer algemeen reactormodel te krijgen is een meer algemeen kinetisch model nodig.

De huidige kinetische modellen zijn inductieve modellen. Dit betekent, dat ze uitsluitend gebaseerd zijn op gemeten data. Het gebruik van inductieve modellen voor de composteringkinetiek heeft zijn grens van praktische mogelijkheden bereikt. Geen verdere vooruitgang wordt verwacht, omdat bepaalde belangrijke variabelen zoals biomassa en deeltjesgrootte (nog) niet goed gemeten kunnen worden. Het toevoegen van nieuwe

variabelen aan inductieve modellen leidt tot een gigantische experimentele opzet, omdat het aantal interacties sterk toeneemt.

In dit proefschrift wordt de deductieve modelstrategie gebruikt voor het opstellen van een meer algemeen kinetisch model. Een centraal probleem in de mechanistische modellering van de milieu systemen is de onbalans tussen de (aangenomen) complexiteit van het systeem en de beschikbare metingen. Dit stelt een grens aan de voorspellende waarde van de mechanistische modellen, omdat deze niet volledig gevalideerd kunnen worden.

Een gemodificeerde deductieve strategie wordt voorgesteld, die bedoeld is om de effecten van de onbalans tussen metingen en modelcomplexiteit te identificeren. Om deze effecten in kaart te brengen wordt de zogenaamde parameter-identificeerbaarheidsanalyse toegepast. Een parameter is identificeerbaar, als een unieke waarde vastgesteld kan worden op basis van de beschikbare gegevens. Alleen als alle parameters in het model identificeerbaar zijn, kan het model op een zinvolle wijze gevalideerd worden.

De doelstelling van dit proefschrift is het ontwikkelen van een mechanistisch kinetisch model met identificeerbare parameters voor het composteringsproces.

Het proefschrift is opgebouwd uit drie delen. Het eerste deel “ dimensie-analyse van identificeerbaarheid” behandelt het gebruik van dimensie-analyse om de identificeerbaarheid van parameters te bepalen. Samen met de voorgestelde model strategie is dit de methodologische bijdrage tot het modelleren van relatief complexe systemen met beperkte metingen.

Het tweede deel “ het enkel deeltje model” behandelt de ontwikkeling en validatie van een theoretisch model voor de aerobe afbraak van een enkel afval deeltje. Het theoretische model geeft inzicht in de processen, die zich afspeLEN in een composterend afvaldeeltje. Een analytische oplossing met identificeerbare parameters is afgeleid en gevalideerd.

Het derde deel “ het gespreide model “ behandelt de ontwikkeling, validatie en toepassing van een kinetisch model voor het totale afval bestaande uit een verzameling afvaldeeltjes met een deeltjesgroottespreiding. Het model is gebaseerd op een verdelingsfunctie voor de deeltjesgrootte en het reeds ontwikkelde kinetisch model voor het enkele deeltje. Het gespreide model is gevalideerd en toegepast voor het ontwerpen van een nieuw composteringsproces. Deze model-toepassing toont het voordeel van het gespreide model voor het reactorontwerp.

Dimensie-analyse van identificeerbaarheid. (Hoofdstuk 2)

Dimensie-analyse wordt veel gebruikt voor wiskundige modellering en in de chemische technologie. Centraal staat het concept van dimensionele homogeniteit. Dit principe zegt dat de beschrijving van een fysiek systeem onafhankelijk dient te zijn van het stelsel van eenheden dat gebruikt wordt voor de metingen. Dimensie-analyse maakt model vereenvoudiging mogelijk door het groeperen van een aantal parameters in een kleiner aantal dimensieloze getallen.

In het geval van parameter-bepaling uit metingen is een directe constructie van de dimensieloze getallen niet mogelijk. De metingen kunnen niet dimensieloos gemaakt worden, doordat de parameters die hier voor nodig zijn, niet vorhanden zijn.

Dimensie-analyse blijkt echter toch een bruikbaar instrument te zijn, als een ander startpunt wordt gekozen voor de analyse. Aangetoond wordt, dat een voorwaarde voor parameter-identificeerbaarheid is dat de eenheden van de parameter op de juiste wijze voorkomen in de eenheden van de metingen. Parameters die niet aan deze voorwaarde voldoen zijn niet-identificeerbaar. Een dergelijke parameter heet dimensioneel niet-identificeerbaar. Parameters die dimensioneel niet-identificeerbaar kunnen altijd gegroepeerd worden tot een kleiner aantal parameters die niet langer dimensioneel niet-identificeerbaar zijn.

Dimensie-analyse kan verbanden aantonen tussen modellen die anders moeilijker opgemerkt worden. Dit wordt geïllustreerd aan het voorbeeld van microbiële groei. Voor vier verschillende modellen is de identificeerbaarheid aangetoond, terwijl maar voor één model uitgebreide berekeningen uitgevoerd hoefden te worden om dit aan te tonen. Met hetzelfde voorbeeld wordt aangetoond dat dimensie-analyse ook de zogenaamde praktische identificeerbaarheidsanalyse vereenvoudigt.

Het enkel deeltjes model: ontwikkeling, afleiding en validatie (Hoofdstuk 3-5)

De zogenaamde zuurstofopnamesnelheid, aangeduid met de engelse afkorting OUR (Oxygen Uptake Rate) is de hoeveelheid zuurstof, die per tijdseenheid door een eenheid afval wordt opgenomen. Het is de meest belangrijke processnelheids-indicator, omdat deze direct gekoppeld is aan de composteringsreactie. De OUR is lineair gekoppeld aan de warmteproductie, nagenoeg onafhankelijk van de samenstelling van de organische stof. De OUR is tevens een directe maat voor de stabiliteit van de compost. De toestand van het afval (temperatuur, zuurstof etc.) bepaalt in sterke mate de OUR.

Hoofdstuk 3 introduceert een theoretisch model voor de composteringskinetiek. De basis van het model is het afvaldeeltje, dat bestaat uit water, onopgelost organisch materiaal,

onopgelost inert materiaal en aërobe biomassa. Opgelost substraat en zuurstof zijn opgelost in het water en worden geconsumeerd door de aërobe biomassa. Het zuurstof wordt aangevoerd vanuit de gasfase om het deeltje heen naar de waterfase in het deeltje. Opgelost substraat is initieel aanwezig en wordt verder geproduceerd door microbiële hydrolyse uit onopgelost organisch materiaal. Zuurstof en opgelost substraat worden beiden via diffusie door de waterfase getransporteerd. Twee microbiële processen worden in het model onderscheiden, de heterotrofe microbiële groei en de hydrolyse.

Als gevolg van de lage oplosbaarheid van zuurstof zal zuurstof het deeltje slechts gedeeltelijk binnendringen. Aërobe microbiële groei zal slechts in de buitenste schil van het deeltje plaatsvinden. De kern van het deeltje is zuurstofloos en daar zal slechts hydrolyse plaatsvinden. Omdat microbiële groei alleen in de buitenste schil plaatsvindt, zal er convectief massa-transport optreden in het deeltje. Gebaseerd op een wiskundige beschrijving van de microbiële processen, diffusie en convectief transport worden de massabalansen die de toestand van het systeem beschrijven opgesteld. De vergelijkingen worden numeriek opgelost. De kenmerken van het model worden onderzocht via een gevoeligheidsanalyse.

Op basis van het dominerende snelheidsbepalende proces kan het verloop van de OUR in de tijd opgedeeld worden in vier fasen. Gedurende de eerste fase neemt de OUR sterk toe als gevolg van de biomassagroei. Gedurende deze fase vormt zich een biofilm. Wanneer deze eenmaal ontwikkeld is, begint de tweede fase, gedurende welke de OUR constant is. Is het opgeloste substraat bijna uitgeput dan daalt de OUR sterk, dit is de derde fase. Daarna begint de vierde fase, gedurende welke de activiteit bepaald wordt door de hydrolysesnelheid.

Het blijkt dat de deeltjesgrootte verreweg de belangrijkste grootheid is, die het verloop van de OUR beïnvloedt. Het model voorspelt het effect van interacties, die niet door de huidige empirische modellen kunnen worden verklaard.

Een analytische oplossing is gevonden voor het theoretische model. (Hoofdstuk 4) De analytische oplossing is mede gebaseerd op een aantal vereenvoudigingen van het theoretische model. Desondanks wordt er een uitstekende overeenkomst gevonden tussen de uitkomsten van het theoretische en analytische model.

Na een onderzoek van de parameter-identificeerbaarheid is het analytische model gevalideerd (Hoofdstuk 5). Twee dimensioze getallen zijn geïdentificeerd, die gebruikt kunnen worden om de praktische identificeerbaarheid van de parameters te controleren. Om het analytische model te valideren is een experimenteel systeem ontworpen, dat het

mogelijk maakte het effect van deeltjesgrootte op de OUR te meten. Als afvalstof werd kippemest gebruikt, die gecomposeerd werd bij 55 °C met 19 vol.-% zuurstof in de gasfase. Het tijdsverloop van de OUR van deeltjes met groottes van 16, 8, 4 en 2 mm is bestudeerd. De parameters in het analytische model zijn voor elke experiment afzonderlijk bepaald. De invloed van de deeltjesgrootte op de waarde van de diverse parameters zijn, uitgezonderd in één geval uitstekend te beschrijven door het model. De parameterwaarden zijn in redelijke overeenkomst met wat verwacht mag worden op basis van literatuurgegevens. Een aanwijzing voor een tijdelijke remming van het proces door de ophoping van opgelost substraat is gevonden.

Het gespreide model; ontwikkeling, validatie en toepassing (Hoofdstuk 6-8)

Afval bestaat uit een mengsel van deeltjes met verschillende deeltjesgrootte. Omdat gebleken is dat de OUR het sterkst door de deeltjesgrootte bepaald wordt, moet de deeltjesspreiding betrokken worden in een kinetisch model voor de compostering van afval. De zogenaamde gamma functie is gebruikt als spreidingsmodel. Deze functie kan afgeleid worden uit de aanname, dat de met gas gevulde poriën in het afval homogeen verdeeld zijn. De zogenaamde gamma parameter beschrijft de breedte van de spreiding. Met toenemende gamma-waarde wordt de spreiding smaller en bereikt uiteindelijk een verzameling deeltjes met gelijke deeltjesgrootte. Op theoretische gronden wordt een gamma-waarde in het bereik van 1 tot 3 verwacht.

Het spreidingsmodel is gecombineerd met het analytische model voor een enkel deeltje, waardoor het zogenaamde “gespreide model” kan worden afgeleid. De OUR van een verzameling deeltjes met gespreide deeltjesgrootte blijkt bepaald te worden door twee klassen van deeltjes, de deeltjes met voldoende opgelost substraat en de opgelost substraat uitgeputte deeltjes. De afbraaksnelheid van de laatste klasse wordt bepaald door de hydrolyse, die onafhankelijk is van de deeltjesgrootte. De afbraaksnelheid van de klasse “deeltjes met voldoende opgelost substraat” is omgekeerd evenredig met de deeltjesgrootte. Gedurende de tijd zal de “substraat uitgeputte” klasse groeien, daar steeds meer deeltjes uitgeput raken.

Het tijdsverloop van de OUR zoals beschreven met het gespreide model wijkt wezenlijk af van de beschrijving volgens het enkel deeltjes model. Dit toont aan dat de deeltjesspreiding een wezenlijk deel is van een kinetisch model.

De identificeerbaarheid van het gespreide model is onderzocht, waarna het model gevalideerd is (Hoofdstuk 7). De identificeerbaarheid wordt voornamelijk bepaald door de

breedte van de spreiding van de deeltjesgrootte en de hoeveelheid opgelost substraat. Aangetoond is, dat onder bepaalde praktijkomstandigheden (brede spreiding en lage opgelost-substraat concentratie) problemen met de identificeerbaarheid kunnen ontstaan. De basis van het probleem is het gegeven dat de meting bestaat uit een mengsel van signalen van deeltjes, die een verschillend gedrag hebben afhankelijk van de klasse waartoe ze behoren. Deze menging van signalen maakt interpretatie van het gemengde signaal moeilijker.

Het gespreide model is gevalideerd aan hetzelfde materiaal onder dezelfde omgevingscondities als het-enkel-deeltje model is gevalideerd. Het materiaal is gemengd met een kunststof-toeslag om een spreiding in deeltjesgrootte te verkrijgen. De resultaten tonen duidelijk aan, dat de spreiding een ander verloop van de OUR te zien geeft. Het gespreide model geeft een goede voorspelling van het verloop.

Het gespreide model is gebruikt voor het ontwerp van een nieuw composteringsysteem (Hoofdstuk 8). Het nieuwe systeem bestaat uit een tunnel-reactor met gekoelde recirculatiestroom. Door koeling van de recirculatiestroom is een grote reductie van de afgashoeveelheid mogelijk. Als gevolg van de gereduceerde verversing van de gasfase zal de het zuurstofgehalte in het composterende materiaal aanzienlijk lager zijn dan in conventionele systemen.

Het gespreide model is gebruikt om een aantal ontwerpgrootheden zoals gasdebieten, compost samenstelling en hoeveelheid te voorspellen. Sommige grootheden hangen af van de actuele zuurstofopnamesnelheid (OUR), sommige van de cumulatieve zuurstofopname (COU). Twee typen voorspellingen worden onderscheiden, nl. interpolerende voorspellingen en extrapolerende voorspellingen. Interpolatorende voorspellingen liggen in het bereik van de uitgevoerde metingen, extrapolerende daarbuiten. Alle voorspellingen met het gespreide model zijn vergeleken met voorspellingen via een conventioneel model en voorspellingen gebaseerd op metingen.

Het gespreide model heeft een kleinere fout wat betreft interpolerende voorspellingen van grootheden, die op de COU gebaseerd zijn. Wat betreft de OUR gebaseerde voorspellingen heeft het gespreide model een substantieel kleinere fout, een factor 2. Het gespreide model is beter in staat het effect van zuurstof te voorspellen.

Geconcludeerd mag worden, dat het gespreide model de ontwerpgrootheden veel beter voorspelt dan de empirische modellen. Verwacht wordt, dat dit ook geldt voor andere situaties, bijvoorbeeld een ander afval of andere omstandigheden van temperatuur, vocht e.d. Voor processnelheidsbepalende factoren zoals vocht en porositeit, die een duidelijke

samenhang vertonen met de structuur van het afval is het gespreide model noodzakelijk om tot goede kinetische modellen te komen. Het gespreide model is een noodzakelijk instrument voor het ontwerp van een effectieve composteringsinstallatie. Het combineert inzicht in het proces met betere voorspellingen.

Dankwoord

Aan het eind van dit proefschrift rest mij nog een dankwoord. Dit is hier zeker op zijn plaats, zonder steun van velen was dit boekje een zachte dood gestorven.

In de eerste plaats de promotoren Wim Rulkens en Gerrit van Straten, die mij de gelegenheid gaven te promoveren. Wim, bedankt voor je continue zorg voor de grote lijn, “wat is de boodschap van dit hoofdstuk” en daarnaast je soms pijnlijk nauwkeurig checken van formules. Gerrit, bedankt voor het introduceren en meedenken op jouw vakgebied. Dit heeft mij een grote meerwaarde aan mijn denken over modellen gegeven. Hopelijk reflecteert zich dit in het proefschrift.

Als docent heb ik veel studenten mogen begeleiden tijdens hun afstudeerwerk. Alhoewel allen gewerkt hebben aan de biologische verwerking van vast afval, is slechts een zeer klein gedeelte hiervan terug te vinden in het proefschrift. Echter allen hebben hun bijdrage gegeven aan het opperen, vormgeven en toetsen van ideeën, waardoor dit proefschrift is wat het is.

De collegae van de vakgroep zijn in al die jaren belangrijk geweest voor een inspirerende werksfeer. Discussies tijdens werkbesprekingen maar ook tijdens koffie en lunch vormen een belangrijke inspiratiebron. Daarnaast zijn de collegae steeds bereid geweest bij het overnemen van taken opdat ik tijd had om het werk af te ronden.

Iman Koster, Harry Hoitink, Harold Keener, Joop van Tubergen, Tom Richard en Adrie Veeken zijn in verschillende fasen van mijn werk van groot belang geweest door hun overtuiging dat het werk in dit proefschrift er toe doet voor het veld “composting”. Wat betreft de modellering waren de kritische beschouwingen van Gatze Lettinga “ik ben niet tegen modelleren, alleen tegen zinloos modelleren” steeds een aansporing om die zin te zoeken.

Geen onderzoek zonder gegevens, en in mijn geval geen gegevens zonder Vinnie de Wilde. Zonder zijn technisch kunnen en inzet voor het vlekkeloos laten verlopen van proeven zou er niet zo'n uniek experimenteel systeem werken.

Geen proefschrift zonder thuisfront, zonder het geloof van mijn moeder en Erna had ik dit proefschrift niet op deze manier kunnen invullen.

Curriculum Vitae

De auteur, Hubertus Victor Marie (Bert) Hamelers, werd op 1 augustus 1958 geboren te Maastricht. In 1976 behaalde hij het Atheneum-B diploma aan het Henric van Veldeke College te Maastricht. In datzelfde jaar werd de studie Milieuhygiëne begonnen aan de toen geheten Landbouw Hogeschool. In januari 1987 werd de studie met lof afgerond met als specialisatie Waterzuivering. Afstudeervakken waren Waterzuivering, Microbiologie en Wiskunde. De stage werd doorgebracht bij het Institut für Siedlungswasserwirtschaft und Abfalltechnik te Hannover in Duitsland, waar hij zich bezig hield met de anaërobe zuivering van brouwerij afvalwater.

In 1987 was hij werkzaam voor de firma Paques bij de licentiehouder Ahlström in Finland. Het werk omvatte onderzoek naar de anaërobe zuivering van pulp en papier afvalwater, en training van de werknemers van Ahlström op het gebied van de anaërobe zuivering.

In 1988 begon hij als toegevoegd onderzoeker bij de vakgroep Waterzuivering van de LandbouwUniversiteit Wageningen te werken aan een project op het gebied van de mestcomposting. In 1991 werd hij Universitair Docent aan dezelfde vakgroep, met de nieuwe naam Milieutechnologie. Zijn functie omvat onderwijs en onderzoek op het gebied van de biologische verwerking van vast organisch afval.